University of Alberta
Department of Civil & Environmental Engineering

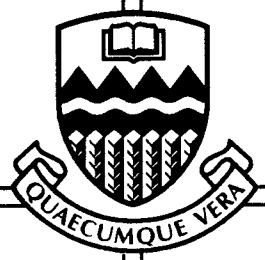

Structural Engineering Report No. 221

REPAIR OF CRACKED STEEL ELEMENTS USING COMPOSITE FIBRE PATCHING

by

GAYLENE D. KENNEDY

and

J.J. ROGER CHENG

May 1998

Structural Engineering Report No. 221

REPAIR OF CRACKED STEEL ELEMENTS USING COMPOSITE FIBRE PATCHING

by

Gaylene D. Kennedy

and

J.J. Roger Cheng

Department of Civil & Environmental Engineering
University of Alberta
Edmonton, Alberta, Canada
T6G 2G7

May 1998

ABSTRACT

Composite fibre patching techniques are being considered as alternatives to traditional methods of strengthening and fatigue crack repair in steel structures. As a step towards the development of effective patching techniques, this investigation focused on the flow of load through a cracked steel plate repaired with a bonded patch.

An experimental program measured strain distributions and bond strength of joints between carbon fibre/epoxy composite patches and steel tabs. A numerical model was developed to further the strain distribution study, and to study the effects of patch geometry and material properties on joint behaviour. A second experimental program studied the strain distributions in ten 6.35 mm steel plates with internal cracks, nine of which were repaired with carbon fibre/epoxy composite patches. A three-dimensional, elastic finite element model of the test plates was also developed. Experimental and numerical results were used to determine patterns of stress flow, and to study the effects of patch size, stiffness and edge conditions on strain distributions at the crack tip and the patch edge. Guidelines for patch design were developed and a case study was considered to illustrate their application.

ACKNOWLEDGEMENTS

The authors would like to acknowledge financial support provided by the Natural Sciences and Engineering Research Council of Canada, the Alberta Heritage Scholarship Fund, Petro-Canada, the Jean Isabel Soper Memorial Graduate Scholarship in Science, and the Canadian Federation of University Women, Edmonton.

Larry Burden and Richard Helfrich of the I.F. Morrison Structural Laboratory at the University of Alberta assisted with the experimental testing. Mal Carroll and Mike Lipsett of Syncrude Canada, Ltd. provided background information and assistance with the case study concerning the draglines at the Syncrude mines. Heng Aik Khoo assisted with preparation and testing of the first experimental series. Dr. Alaa Elwi of the University of Alberta provided guidance for the numerical modeling of the project. Mitsubishi Canada supplied materials used in the experimental studies. These contributions are gratefully acknowledged.

TABLE OF CONTENTS

Page

LIST OF TABLES

LIST OF FIGURES

Page

LIST OF SYMBOLS

a	crack size, for an internal crack total length = 2a
A_p	cross-sectional area of the patch
C	material constant used in the Paris equation
e	eccentricity of centroid of plate and the line of action of the resultant load on the patched cross-section
E	modulus of elasticity
E_C	modulus of elasticity of carbon fibre composite
E_G	modulus of elasticity of glass fibre composite
E_p	modulus of elasticity of the patch material
E_pt_p	stiffness of patch
E_s	modulus of elasticity of steel
E_st_s	stiffness of adherend
G	shear modulus
K_I	stress intensity
L	patch length, for an internal crack repair total patch length = 2L
ℓ_{min}	minimum required bond length
M_p	moment required to keep the patched cross-section in equilibrium
MPC	multipoint constraints
n	material constant used in the Paris equation; number of layers of composite
N	number of load cycles
P	applied load
q	shear flow in the bond
t_C	thickness of carbon fibre composite
t_G	thickness of glass fibre composite
T_p	resultant load on a patched cross-section
t_p	thickness of the composite patch
t_s	thickness of the steel adherend
T_u	resultant load on an unpatched cross-section
w	patch width, for an internal crack repair, total patch width = 2w
z	initial deflection from plane of the horizontal centerline of a test plate
β	geometry coefficient used to define stress intensity range
ΔK_I	stress intensity range

$\Delta\sigma$	applied stress range
ε	strain
ε_p	strain in the patch
ν	Poisson's ratio
σ	stress
σ_o	far field applied stress
σ_{pk}	peak stress observed
σ_{ult}	tensile strength
τ	shear stress in bond
τ_y	shear yield stress of bond

1 INTRODUCTION

Composite materials are providing new options for repair and strengthening of structural elements. Bonded composite patches are lightweight and easy to apply, and offer high chemical and corrosion resistance, fatigue resistance, and design flexibility (Karbhari and Shulley 1995). While composite patching techniques have been successfully used in the aircraft industry (Baker 1987), their use in repair/rehabilitation of steel structures is relatively unproven.

Patching an element aims to redirect load so the resulting stress distribution is more favourable. In crack repair, the goal is to reduce crack tip stresses and alter the fatigue mechanisms at work, ultimately slowing crack propagation. As an initial step towards development of effective composite patching methods for steel elements, this investigation aims to describe the flow of load in a cracked steel adherend repaired with a bonded composite fibre patch. Transfer of load is considered for both a bonded joint and a bonded crack repair. Experimental testing and numerical analysis are used to define relationships between load flow and material properties and geometry. Consideration is given to minimizing stress concentrations in the steel base material, both at the crack tip and at the patch edge.

1.1 Principles of Crack Repair by Patching

In a predominantly linear elastic material, crack growth rate under fatigue loading can be described by the Paris equation (Barsom and Rolfe 1987):

$$\frac{da}{dN} = C(\Delta K_I)^n \qquad [1.1]$$

where a is a measure of crack size, and C and n are material constants. N is the number of load cycles applied, limited by the fatigue life of the cracked element. ΔK_I is the stress intensity range, generally defined as

$$\Delta K_I = \beta \Delta \sigma \sqrt{a} \qquad [1.2]$$

where β is a function of specimen geometry, and $\Delta\sigma$ is the applied stress range. Patching aims to reduce crack growth by reducing stress intensity at the crack tip. This is done by bridging the stresses across the crack, which reduces the effect of the applied stress range, and by constraining the crack from opening, which effectively reduces the geometry factor β.

1.1.1 Traditional Crack Repair

Traditionally, crack repair has been accomplished by drilling holes to blunt the crack tips and attaching steel plates over the damaged areas by welding or mechanical fasteners. These methods are somewhat effective, but offer disadvantages such as residual stresses due to welding, damage due to drilling and bolting, newly introduced local stress raisers, and additional weight added to the structure (Karbhari and Shulley 1995).

1.1.2 Composite Patching

Composite fiber/epoxy patches are providing a new medium for crack repair in structures. Layers of fiber are impregnated with epoxy and bonded to the surface of a damaged structure, stiffening the area and restricting crack opening. Carbon, glass, and aramid fibre composites offer high strength and stiffness, light weight, and superior long term properties, including fatigue resistance (Konur and Matthews 1989). They also permit the distribution of stresses over a large area, lowering fatigue effects in the base metal adherend (Alawi and Saleh 1992).

Adhesively bonded patches of advanced fibre composites are used extensively in the repair of metallic aircraft components cracked due to fatigue or to stress corrosion (Baker 1987). The concept was pioneered in the early 1970's and has been successfully applied in a range of repair programs for both military and commercial aircraft applications (Baker 1987; Barthlomeusz et al. 1993). These applications, along with numerical (Chue et al. 1996; Paul et al. 1994; Siener 1992) and analytical (Rose 1988) investigation, have

demonstrated the effectiveness and efficiency of composite patch repairs for thin aluminum alloy components.

Schubbe and Mall (1997) compared experimental and numerical results for post-repair fatigue crack growth in thick (6.35 mm) aluminum panels repaired with a boron/epoxy composite patch. The results showed that the repair technique was effective on the thick panel, and that the modeling technique could accurately predict crack growth in the repaired section.

Bonded repairs to cracked steel elements have not been as thoroughly investigated as repairs to aluminum components. Alawi and Saleh (1992) showed that steel patches bonded to a cracked steel adherend were effective in retarding fatigue growth. Roberts (1995) investigated bond behaviour and fatigue performance of a carbon fibre patch bonded to a thick steel adherend and showed that this patching technique was also effective in retarding fatigue growth. Applications to steel elements are unique because of the high stiffness of the base material and the thickness of the adherends commonly under consideration.

1.2 Scope and Objectives

The primary objective of this program was to develop a picture of the stress distributions in a steel element with a bonded composite patch. Three aspects of the stress flow were considered. Stresses due to the transfer of load from the steel adherend to the patch and back were investigated first through a study of bonded joints. Stresses in the steel through the patched area, and in particular at the crack tip, were considered second. The final area of interest was the stress concentrations in the steel at the patch edge. The investigation focused on repair of steel elements using unidirectional fibre composite. The effects of patch and adherend stiffness and repair geometry were considered, with the goal of establishing guidelines for patch design. At the conclusion of the program, the

results were applied to a case study. Future work may adopt the stress distribution information gained through this program as a basis for investigating fatigue behaviour.

Several factors affect bond strength and consequently patch performance, but it is not feasible for a single investigation to explore all these factors. For constructional practicality, room temperature cured epoxy was used in the program, and all specimens were prepared and cured at room temperature. The surface of the steel adherend had to be cleaned in preparation for bonding of the composite patch. Sandblasting has been proven effective (Roberts 1995) and was used for all specimens in this study.

1.2.1 Bonded Joints

Bonded joints were studied to develop an understanding of the load transfer between a patch and the base metal adherend. This load transfer is a function of the component material properties and the geometry of the bond. A series of experimental tests were conducted, supplemented by a two-dimensional finite element analysis. Strain distribution through the bonded components was investigated, first to determine general behaviour, then as the basis for a parametric study. Consideration was given to the effect of patch parameters on stress concentrations in the base material.

1.2.2 Bonded Patch Assembly

There were two objectives to the study of strain distribution in a bonded patch assembly: to determine the effects of patching on stresses responsible for crack propagation, and to determine the minimum requirements for an effective patch. Experimental tests studied the strain distributions in a cracked plate and nine similar plates with internal cracks repaired by composite patching. A three-dimensional finite element model was also developed to more clearly define strain distributions and to perform a parametric study.

The analysis of experimental and numerical results first aimed to define the general patterns of strain distribution through a patched area. This involved load transfer between and through the patch and base metal, and the bending that resulted from the asymmetrical patch assembly. Particular attention was paid to the strains at the crack tip, which have the most significant influence on crack growth.

The strain distributions were then used to develop guidelines for patch design. Maximizing the dimensions of the patch will improve its effectiveness (Chue et al. 1996); however, an over-designed patch may not be practical in terms of space restrictions or cost. Therefore, patch design must satisfy minimum dimensions to develop full strength. Patch stiffness is also a key parameter for patch design. Ideally, the stiffness of the patch would equal the stiffness of the cracked base metal (Rose 1988); however, this is impractical and unnecessary when working with thick steel adherends. The effect of changing patch stiffness on stress distribution was estimated, but further fatigue studies are required to develop stiffness design guidelines.

1.2.3 Stress Conditions at the Patch Edge

Due to changes in load distribution and cross-sectional dimensions, patching induces stress concentrations in the base metal around a patch that were not present in the unpatched element. These stresses may cause new crack development in elements subjected to fatigue loading. The objective of this study was to examine possible methods of reducing the stresses in the base metal at the patch edges. Tapering the patch edges and the use of an elliptical patch in place of a rectangular one were two methods considered, and both were studied experimentally and numerically. The experimental study was incorporated into the bonded patch assembly tests, and the numerical studies used models developed for the bonded joint and bonded patch assembly studies.

1.3 Thesis Outline

This research looks at three aspects of the stress distribution in a bonded patch assembly, and then at a practical application of the results. Chapter 2 considers the general behaviour of a bonded joint. Chapters 3 and 4 focus on the stress transfer and load sharing in a one-sided patch repair of a plate with an internal crack. This includes stresses through the patched area and at the crack tip. Chapter 5 discusses the stress concentrations that develop away from the repaired area, at the patch edge. In Chapter 6, the results of the stress distribution study are applied to the example of fatigue crack repair of dragline booms at the Syncrude mining site in Fort McMurray, Alberta. A suggested patch design is presented for the given application.

1.4 References

Alawi, H. and I.E. Saleh. 1992. "*Fatigue Crack Growth Retardation by Bonding Patches.*" Engineering Fracture Mechanics, Vol. 42, No. 5, pp. 861-868.

Baker, A.A. 1987. "*Fibre Composite Repair of Cracked Metallic Aircraft Components - Practical and Basic Aspects.*" Composites, Vol. 18, No. 4, pp. 293-308.

Barsom, John M., and Stanley T. Rolfe. 1987. Fracture and Fatigue Control in Structures. Prentice-Hall, Inc., New Jersey.

Barthlomeusz, R.A., J.J. Paul, and J.D. Roberts. 1993. "*Application of Bonded Composite Repair Technology to Civil Aircraft - B747 Demonstration Programme.*" Aircraft Engineering, Vol. 65, No. 4, pp. 4-7.

Chue, Ch.-H., W.-Ch. Chou, and Th. J.-Ch Liu. 1996. "*The Effects of Size and Stacking Sequence of Composite Laminated Patch on Bonded Repair for Cracked Hole.*" Applied Composite Materials, Vol. 3, No. 6, pp. 335-367.

Karbhari, V.M., and S.B. Shulley. 1995. "*Use of Composites for Rehabilitation of Steel Structures—Determination of Bond Durability*". Journal of Materials in Civil Engineering, Vol.7, No. 4, ASCE, pp. 239-245.

Konur, O. and F.L. Matthews. 1989. "*Effect of the Properties of the Constituents on the Fatigue Performance of Composites: A Review.*" Composites, Vol. 20, No. 4, pp. 317-328.

Paul, J., R.A. Bartholomeusz, R. Jones, and M. Ekstrom. 1994. *"Bonded Composite Repair of Cracked Load-Bearing Holes"*. Engineering Fracture Mechanics, Vol. 48, No. 3, pp. 455-461.

Roberts, Pamela D. 1995. *"Crack Growth Retardation by Carbon Fibre Composite Patching: An Application to Steel Pressure Vessel Repair."* Master of Science Thesis, University of Alberta, Department of Mechanical Engineering.

Rose, L.R.F. 1988. *"Theoretical Analysis of Crack Patching."* Bonded Repair of Aircraft Structures, ed. A.A. Baker and R. Jones. Martinus Nijhoff Publishers, Dordrecht, pp. 49-76

Schubbe, J. and S. Mall. 1997. *"Fatigue Crack Growth Behaviour of Thick Aluminum Panels Repaired with Composite Patch."* 42nd International SAMPE Symposium, pp. 197-207.

Siener, M.P. 1992. *"Stress Field Sensitivity of a Composite Patch Repair as a Result of Varying Patch Thickness."* Composite Materials: Testing and Design (Tenth Volume), ASTM STP 1120, Glen C. Grimes, Ed. American Society of Testing and Materials, Philadelphia, pp. 444-464.

2 BONDED JOINTS

The behaviour of a patch is highly dependent on the transfer of load between the patch and adherend. This load transfer is best analyzed using bonded joints, where a known load must transfer through a bond of known area, and extraneous effects such as out-of plane bending are removed. A series of experimental tests was conducted to study the strain distribution in a carbon fibre composite joint of steel adherends. The study was supplemented by the development of a numerical model. Both experimental and numerical results were also used to define the effects of material properties and geometry on joint strength and behaviour.

2.1 Background

2.1.1 Bond Length

There is a non-linear shear stress distribution between bonded adherends as a result of strain compatibility (Hart-Smith 1987). Consider a long bonded lap joint of two identical tabs, shown in Figure 2.1(a). At both A and B, the full load is in one element, with none in the other, and consequently there is an incompatibility of displacements. This results

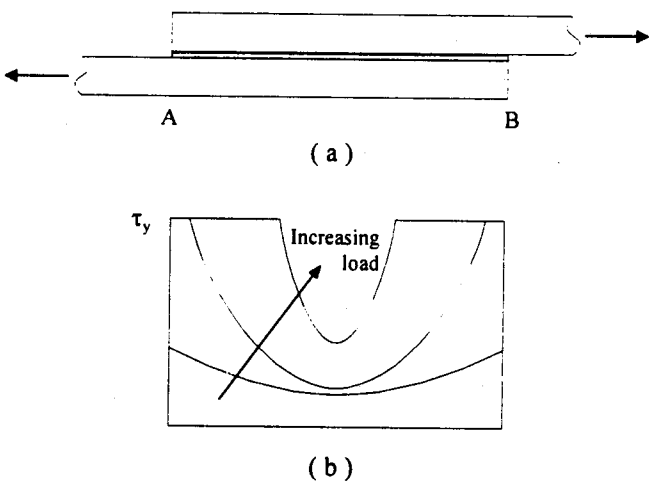

Figure 2.1 Shear stress distribution in the bond between two identical tabs (adapted from Hart-Smith 1987)

in an increase in bond shear stresses at these points. At some intermediate point between A and B, the bonded elements act as a homogeneous unit: the stress is distributed across the section according to relative stiffness of the components, the strains are compatible, and the bond shear stress approaches zero.

The bond can be thought of as a thin layer of epoxy between the two adherends. As the load increases, shear stresses in the bond increase until the ends of the bond reach the yield point. Under further applied load, shear stresses in the bond are distributed inward, causing additional yielding. This concept is shown in Figure 2.1(b).

Figure 2.2 shows the relationship between joint strength and bond length, along with the shear stress distribution in the bond at failure of the joint. For short bond lengths, the joint reaches fully plastic shear before onset of failure in the patch or base metal adherend. For intermediate bond lengths, an elastic trough is present in the stress distribution and failure may include some fibre breakage in the patch laminae. For long overlap lengths, the length of the elastic region in the center of the bond increases with bond length. The area of the bond involved in load transfer may be a small portion of the

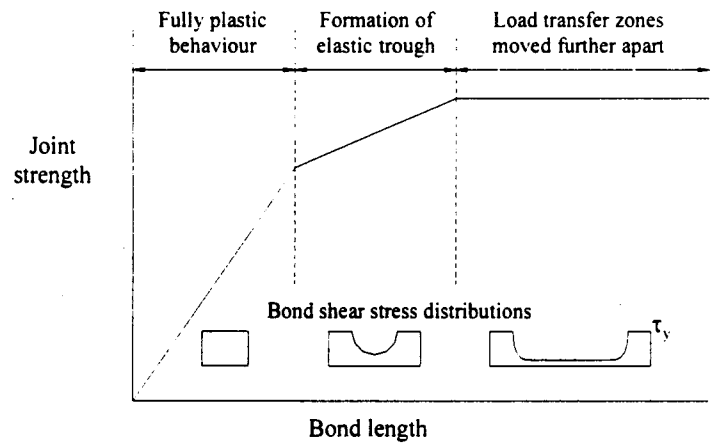

Figure 2.2 Influence of bond length on joint strength and bond shear stress distribution (adapted from Hart-Smith 1987)

total bond. Since failure in these specimens is dictated primarily by the strength of the adherends, the strength of the joint is relatively insensitive to bond length in this region.

The presence of an elastic region in a long bond also helps to minimize creep and increase durability of a bond: creep that occurs at the ends of the bond cannot accumulate because the stiff, elastic adherends push the adhesive back to its original position when the joint is unloaded.

2.1.2 Patch Stiffness

In a bonded joint, strain incompatibility, and consequently shear stress distribution, is a function of the relative stiffness of the patch and adherend. Figure 2.1 depicts the strain distribution for a bonded joint of two identical tabs. For a composite patch on a steel adherend, symmetry of the stress distribution about the center of the bond length is lost. The expected shear stress distribution is shown in Figure 2.3. In the figure, curve S_1 is for a patch and adherend of equal stiffness, while curve S_2 is for a patch that is less stiff than the adherend. A lower stiffness patch reduces the shear stresses in the bond at the edge of the patch, and increases them at the edge of the steel.

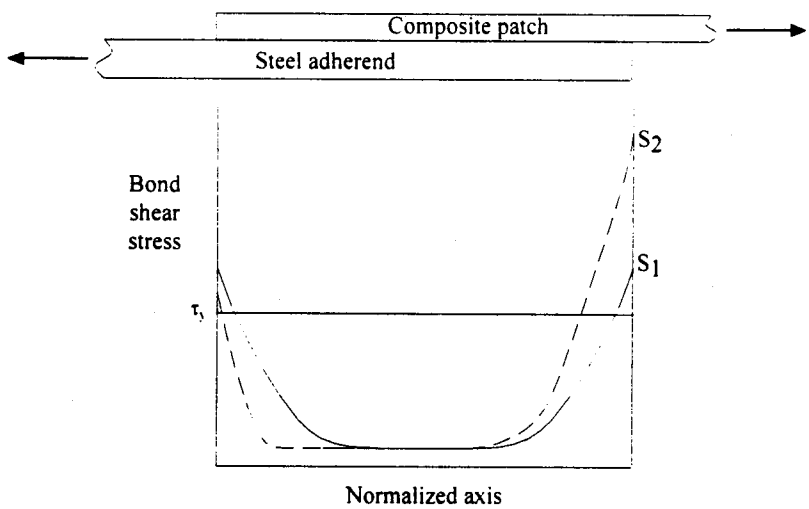

Figure 2.3 Bond shear stress distribution as a function of the relative stiffness of patch and adherend (adapted from Roberts 1995)

2.1.3 Patch Strain and Bond Shear Stress

In a bonded joint, the shear flow in the bond, q, can be estimated from the strain in the patch. Consider the free body diagram of a segment of bond, Δy, in Figure 2.4.

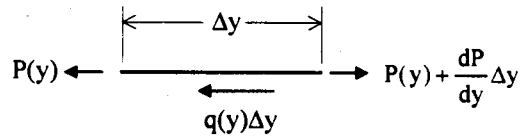

Figure 2.4 Free body diagram of patch element

From equilibrium,

$$q(y)\Delta y + P(y) = P(y) + \frac{dP}{dy}\Delta y$$

$$q(y)\Delta y = \frac{dP}{dy}\Delta y \qquad [\,2.1\,]$$

From elasticity,

$$\frac{P}{t_p} = \varepsilon_p E_p \qquad [\,2.2\,]$$

where t is the cross sectional thickness, ε is the strain, and E is the elastic modulus. The subscript "p" designates values for the patch. Differentiating [2.2],

$$\frac{dP}{dy} = E_p t_p \frac{d\varepsilon_p}{dy} \qquad [\,2.3\,]$$

Combining [2.1] and [2.3],

$$q(y) = E_p t_p \frac{d\varepsilon_p}{dy} \qquad [\,2.4\,]$$

which is the desired relationship between the strain and bond shear flow for a unit width element. Expected distributions of patch strain and bond shear stress are shown in Figure 2.5. The bond yields when the shear stress exceeds the shear strength of the bond, τ_y.

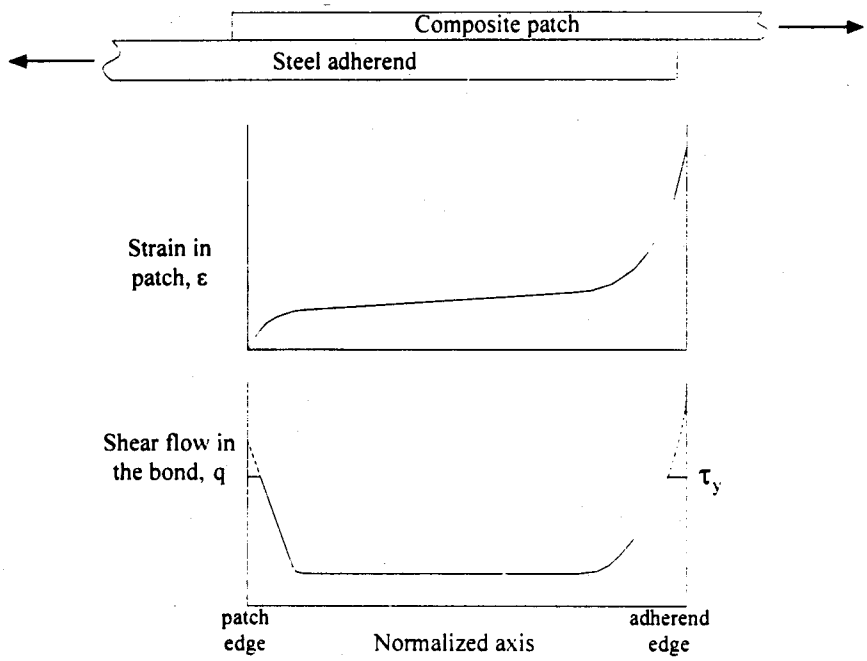

Figure 2.5 Expected distribution of strain in patch and corresponding bond shear stress

2.2 Experimental Program

An experimental program was designed to study the load transfer behaviour and bond strength for carbon fibre composite patches bonded to steel adherends.

2.2.1 Test Specimens

Five double butt joint specimens were fabricated for this experimental program. Figure 2.6 illustrates one of the test specimens.

Two sandblasted steel tabs, each 12.7 mm (0.5 in.) thick and 25.4 mm (1in.) wide, were bonded together using unidirectional carbon fibre composite. The number of layers of composite was the same on each side of the joint, but varied among specimens. The composite was applied using a hand lay-up procedure, first applying a two-part epoxy compound to the steel, then a layer of carbon fibre, followed by epoxy. This sequence

was repeated, smoothing each layer with hand pressure, until the desired patch thickness was reached. The patch was topped with a layer of epoxy. The assembly was allowed to cure at room temperature for a minimum of seven days.

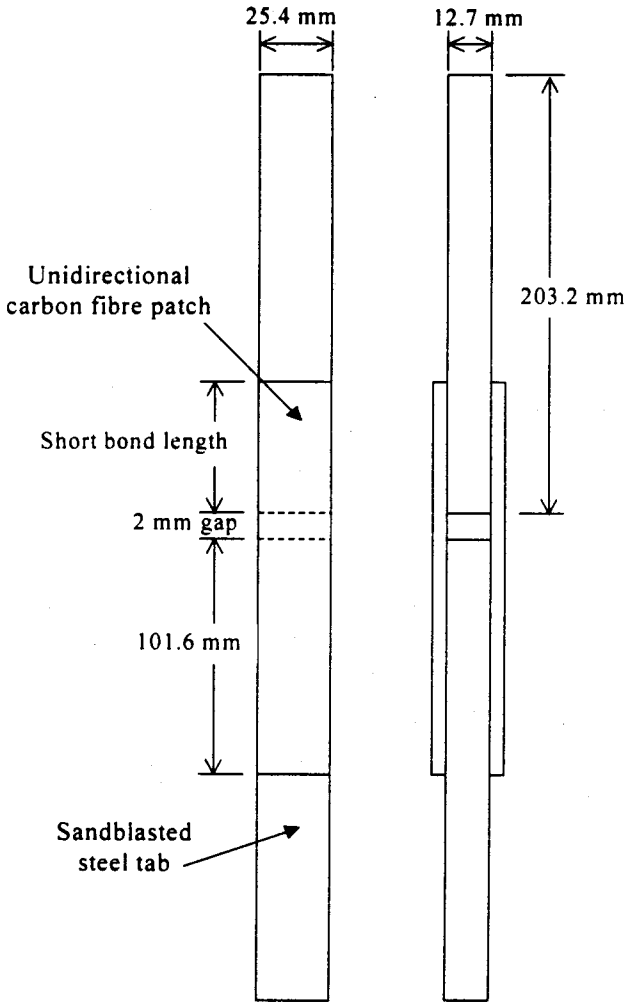

Figure 2.6 Experimental test specimen, bonded joint

All specimens had a 101.6 mm (4 in.) bond length on one end of the joint. The bond length on the second end varied among specimens, but was always less than 101.6 mm and is referred to as the short bond length. It was intended that the joint would fail in the short bond length first, if the length was less than that required for full strength.

Table 2.1 summarizes the parameters for each of the test specimens. The specimens were designated CM *n-l*, where CM stood for carbon fibre on mild steel, *n* was the number of layers on each side of the joint, and *l* was the length of the short bond in inches.

Table 2.1 Summary of bonded joint test specimens

Specimen	No. of layers per side	Short bond length
		mm (in.)
CM 6-3	6	76.2 (3)
CM 4-3	4	76.2 (3)
CM 2-3	2	76.2 (3)
CM 2-2	2	50.8 (2)
CM 2-1	2	25.4 (1)

2.2.2 Instrumentation and Test Protocol

Strain gauges were applied along the surface of the patch to monitor the strain distribution in the patch as loading progressed. Gauges were applied primarily to one face of the element, referred to as the *front face*. A single gauge was applied to the *back face*. For specimens with a short bond length of 76.2 mm (tests CM 2-3, CM 4-3, and CM 6-3), gauges were applied on both the 101.6 mm and short bond lengths. The other tests were gauged on the short bond length only. On each specimen, gauges were centered over the gap on both faces of the joint. Figure 2.7 shows the layout of gauges for the specimens.

Specimens were tested in tension under stroke-controlled loading at a rate of .02 mm/min to failure in two of the four bonds.

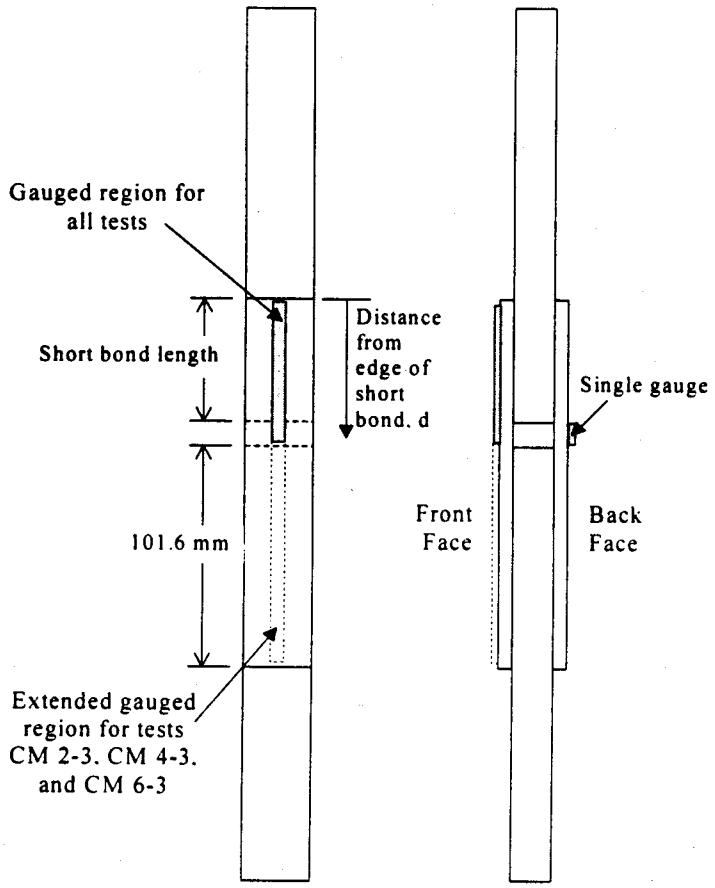

Figure 2.7 Strain gauge layout for bonded joint tests

2.2.3 Material Properties

The elastic modulus of the steel was assumed to be E = 200 000 MPa. For the carbon fibre composite, 11 tension coupons were fabricated and tested according to ASTM Standard D3039/D3039M-95a (1995). The coupons were four or six layers of unidirectional fibre composite, with all fibres aligned parallel to the axis of loading. An additional layer of fibre was bonded on each side and at both ends of the test coupons to act as gripping tabs. One strain gauge was attached near the center of each coupon for the calculation of material properties.

Because of the hand lay-up procedure used in patch fabrication, the thickness of the resulting composite is highly variable. The epoxy is not believed to carry a significant

portion of the applied load, yet it is this portion of the composite that is most responsible for variations in thickness. This implies that the thickness of the composite layer assumed in calculations has a significant effect on the calculated composite material behaviour.

Five thickness measurements were taken at approximately equal intervals along the length of each test coupon and the results divided by the number of layers of fibre used for the given coupon. This resulted in an average composite thickness of 0.23 mm/layer with a coefficient of variation of 4.0%. All stress calculations were based on this patch thickness, and the resulting elastic modulus values are shown in Table 2.2.

Table 2.2 Summary of tension coupon test results for composite elastic modulus

6-layer coupons		4-layer coupons	
	Elastic modulus, E MPa		Elastic modulus, E MPa
6a	122638	4a	134998
6b	114754	4b	114413
6c	130757	4c	129691
6d	154379	4d	136348
6e	115213	4e	131178
		4f	124650
Average		128093 MPa	
Standard Deviation		11826 MPa	
Coefficient of Variation		9.2 %	

Tensile strength of the composite was also calculated from the coupon tests, as summarized in Table 2.3. The composite exhibited a linear stress versus strain relationship to failure, which was generally sudden and complete. The tensile strength, σ_{ult}, was calculated as the peak load achieved divided by the cross sectional area of the coupon, based on a thickness of 0.23 mm/layer.

The results of the six-layer tests were not used for estimating tensile strength, since at high loads the gripping mechanism appeared to affect the coupon performance: two of the tests failed at the edge of the grip and two others failed only on inside layers of the coupon, instead of through the thickness. With the exception of coupon 4c, the four-layer

tests failed more consistently, with fibre breakage occurring evenly across the coupon width and thickness. The initial portion of the loading curve for test 4c was linear, but it dropped sharply and began to carry an increasing load again. The test was stopped before visible failure was obtained and the load reported in Table 2.3 was the first peak in load. The results of test 4c were not included in the average strength calculation.

Table 2.3 Summary of tension coupon test results for composite ultimate strength

4-layer coupons	
	Tensile strength, σ_{ult} MPa
4a	813
4b	1038
4c	*470**
4d	1161
4e	1212
4f	1093
Average	1063 MPa
Standard Deviation	155 MPa
Coefficient of Variation	14.5 %

* Value neglected in calculation of average

2.2.4 Test Results

2.2.4.1 Behaviour of Test Specimens

Figure 2.8 shows the results of test CM 2-2. The figure shows the MTS load versus MTS stroke curve for the test, along with the patch strain distribution measured by strain gauges along the front face at selected loading points designated A-E.

At low loads, patch strains on the front face were compressive, while the strain in the single back face gauge was tensile. This suggests there was some misalignment of the steel tabs during fabrication, and when the specimen was gripped in the MTS machine, realignment caused some bending of the joint. As the load was applied, strains from gauges centered over the gap on both the front and back faces increased at about the same rate, until the load reached 20.0 kN. At that point, strains in the back face started to plateau in spite of increasing MTS stroke.

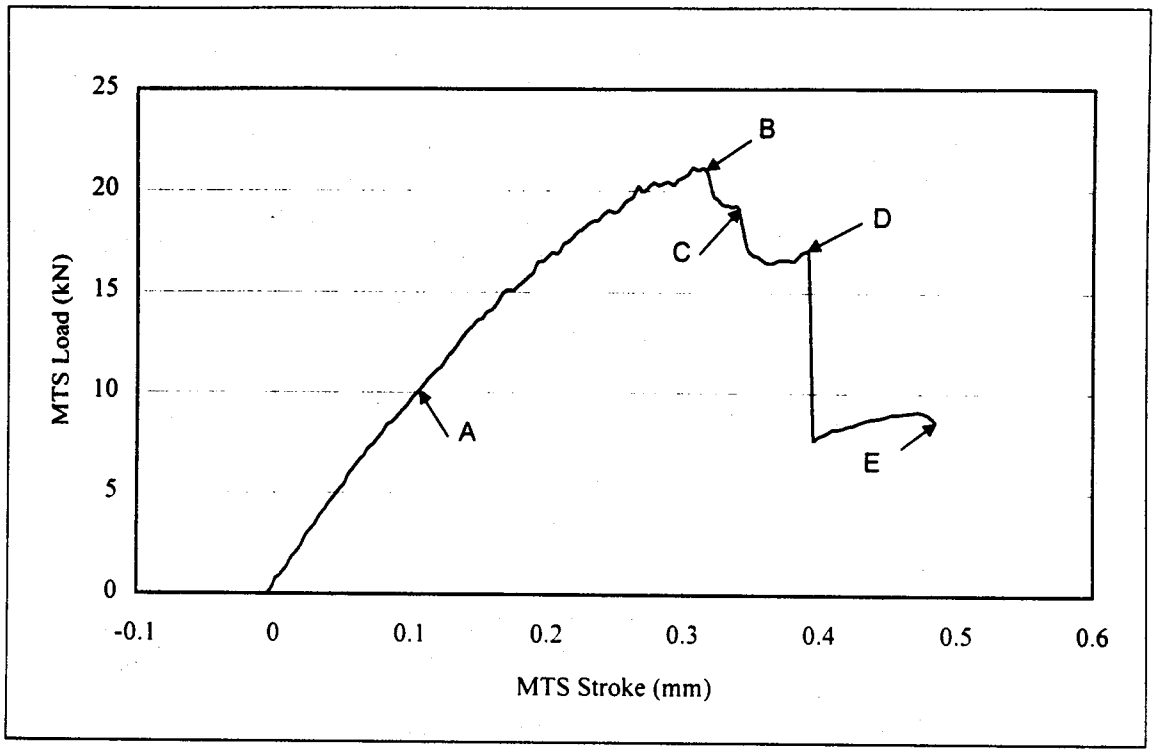

(a) MTS Load versus MTS Stroke curve

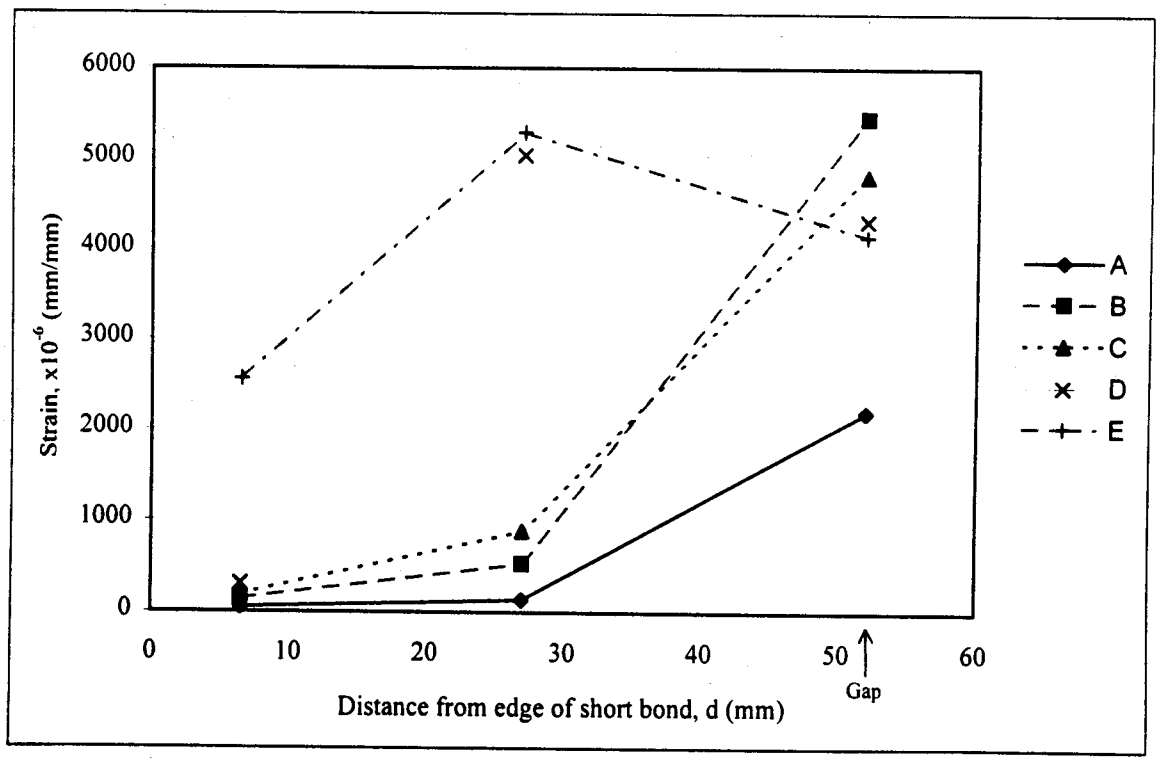

(b) Strain distribution

Figure 2.8 Results of Test CM 2-2

A strain plateau at a point in the patch while the joint is subjected to increasing MTS stroke is indicative of delamination or *yielding* of the bond. It was established through tension coupon tests that the composite strain responds linearly to increasing load until failure, and for the loads applied in this test series the steel does the same. Thus any non-linearity of the strain response of the specimen must be a result of the behaviour of the bond. Yielding of the bond shows up in the load versus stroke curve as a decreasing slope. In the strain distribution, it shows up as increasing strain along the bond at points progressively further from the gap.

As the back face bond yielded, its stiffness relative to the front face decreased and the front face received an increased portion of the load. As the load in the front bond exceeded its resistance, it began to yield as well. The first bond began to fail at 21.1 kN applied load, at point B. In the region of decreasing load that followed, some fibre breakage and bond failure occurred. The strain distributions for load points C and D showed relatively constant strain in the patch near the gap and increasing strain near the center of the bond, suggesting yielding along the bond. (Recall the strain distribution shown is for the front face.)

At point D, when the applied load was 17.0 kN, the short bond on the back face failed completely in a combination of shear within the patch and fibre breakage. A sharp drop in load accompanied this failure, again because the test was stroke-controlled. The front bond continued to carry increasing load, and continued to yield as seen in the strain distribution profile. The front bond failed at 9.1 kN, 43 % of the first failure load, also in the short bond length. At this point, yielding had occurred some distance along the bond, but the strain at the edge of the patch was not as high as that in the middle, suggesting the bond was not completely yielded. The second bond failure was also a combination of shear and fibre breakage.

The other four tests exhibited similar behaviour to CM 2-2. The variations in this behaviour are discussed individually below.

CM2-1 : Test results shown in Figure 2.9

Front and back strains near the gap were very close until the applied load reached 6.5 kN. Yielding in the back face likely began at this point as the back face strain increased more slowly than the corresponding front face strain from that point until failure. The short bond on the back face failed at 12.1 kN. The remaining bond carried increasing load to a maximum of 10.2 kN, followed by a decrease in load to complete failure in the long bond at 8.8 kN. The decrease in slope of the load versus stroke curve suggested some yielding occurred prior to failure of the second bond. This yielding was likely in the long bond, as it was not apparent in the strain distribution shown for the short bond.

CM 2-3: Test results shown in Figure 2.10

As for specimen CM 2-2, the strains after gripping and at low loads suggest loading induced additional tensile stresses in the back face due to misalignment of the steel tabs. Again the strains increased uniformly with increasing load until bond yielding began and the load versus stroke curve reached a plateau. The back face failed in the short bond at an applied load of 21.8 kN. The load in the second bond increased to 11.3 kN before decreasing to 10.4 kN prior to failure. Both failures were a combination of shear and fibre breakage. The valley shown in the strain distribution adjacent to the gap at load points D and E may have been a result of bending due to asymmetry of the element after failure of the first bond.

CM 4-3: Test results shown in Figure 2.11

The front face was initially under higher load than the back, likely due to misalignment of steel tabs. The drop in load at point A was likely the result of some form partial bond failure, since the strains on the two faces evened out at point B and

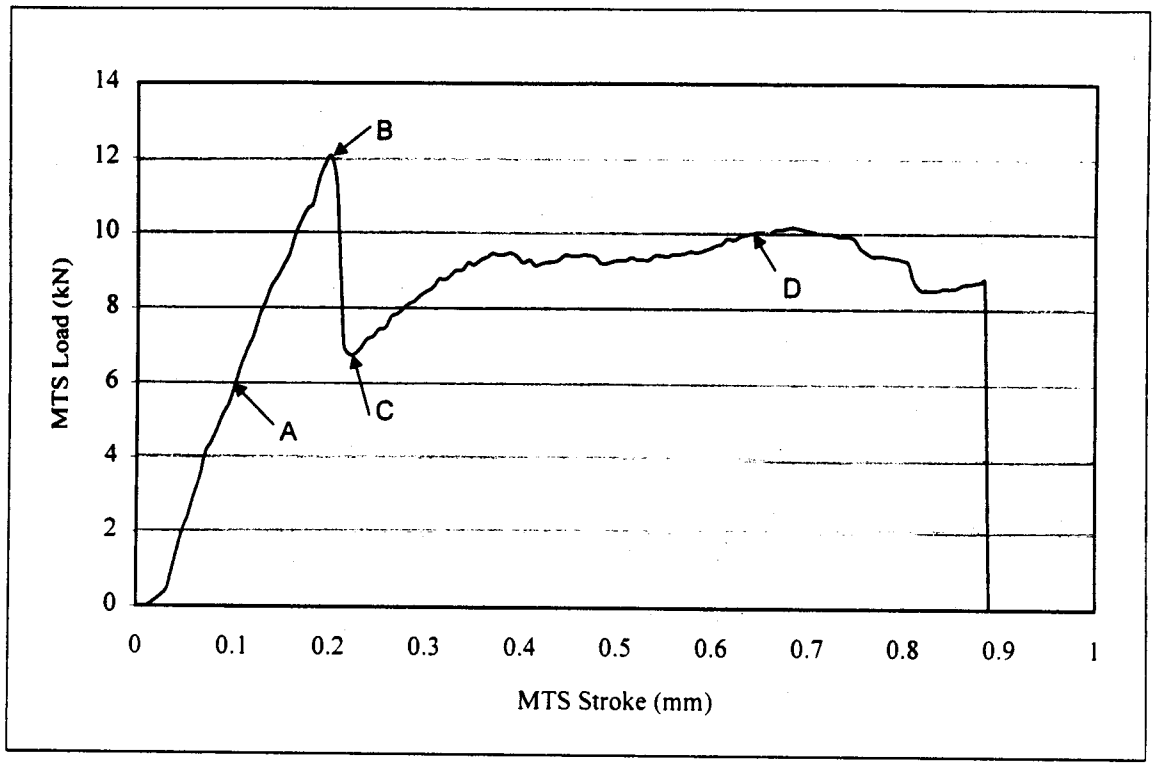

(a) MTS Load versus MTS Stroke curve

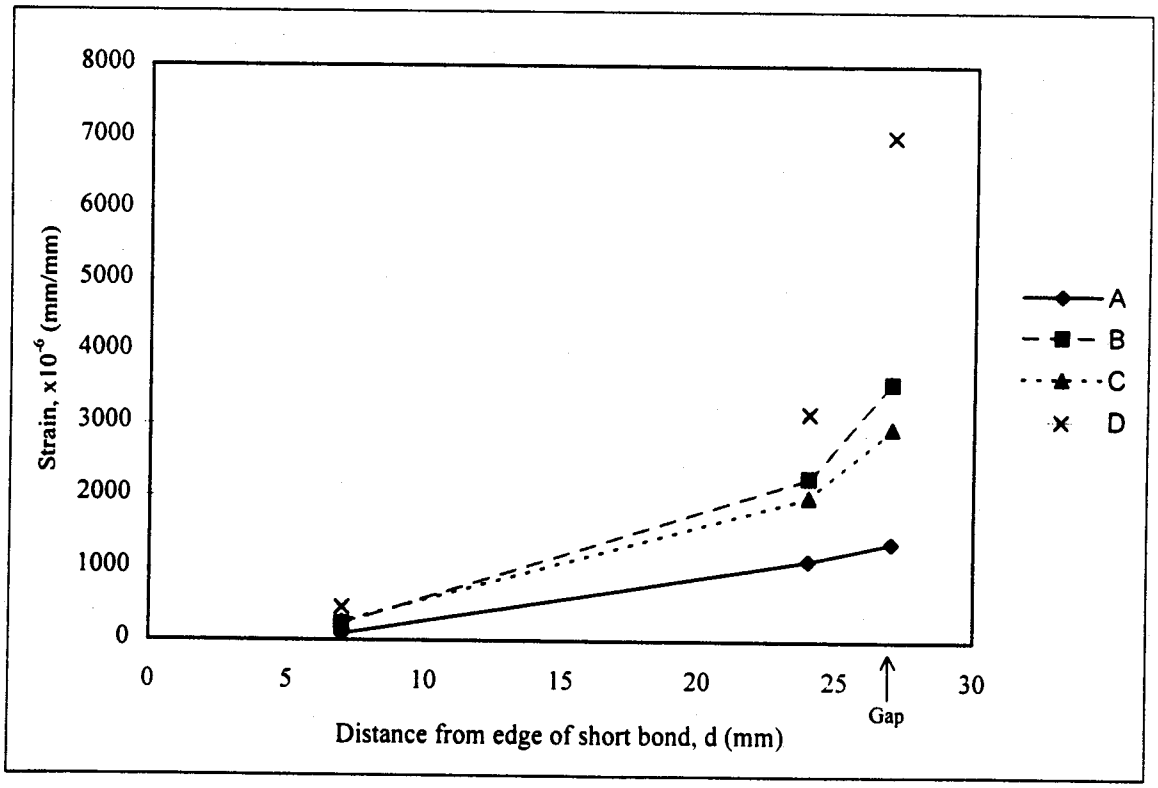

(b) Strain distribution

Figure 2.9 Results of Test CM 2-1

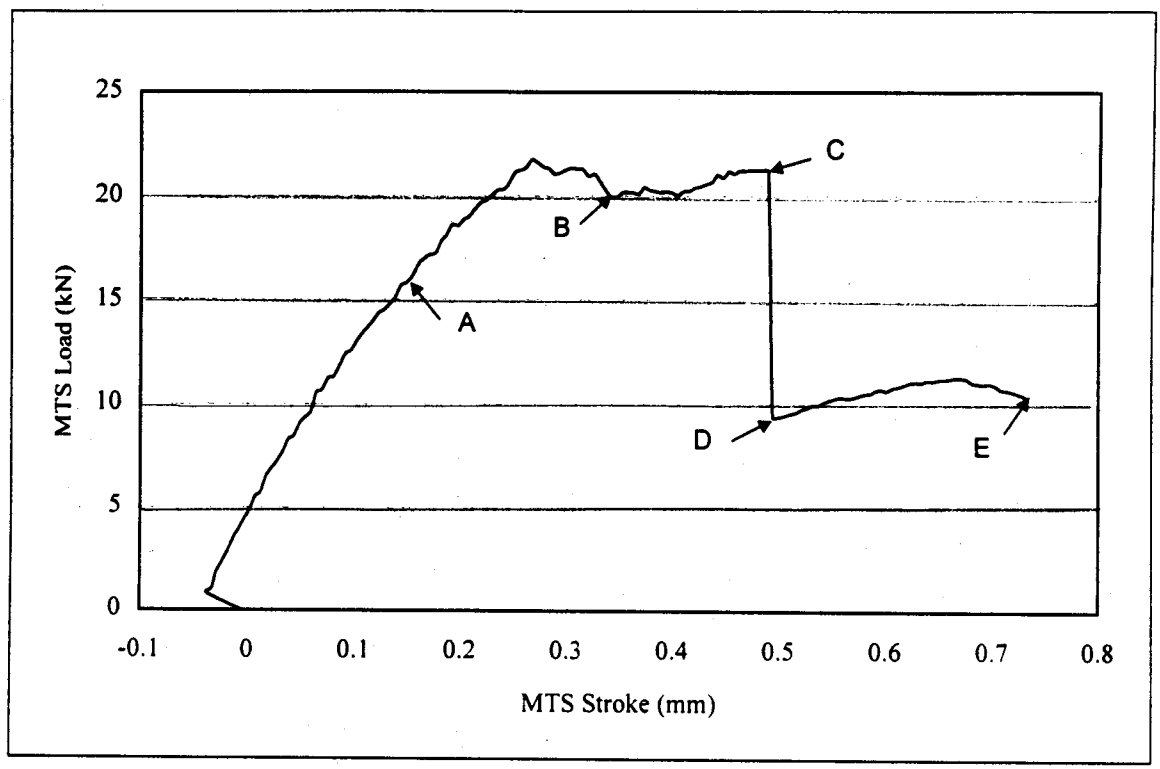

(a) MTS Load versus MTS Stroke curve

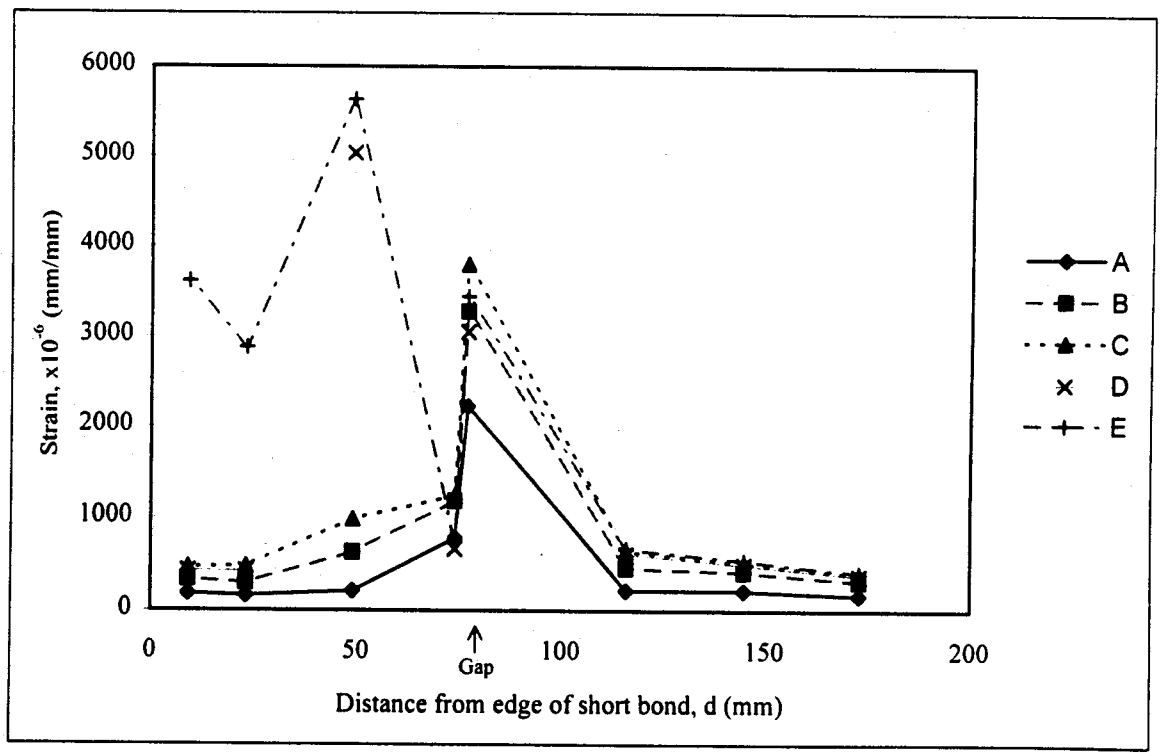

(b) Strain distribution

Figure 2.10 Results of Test CM 2-3

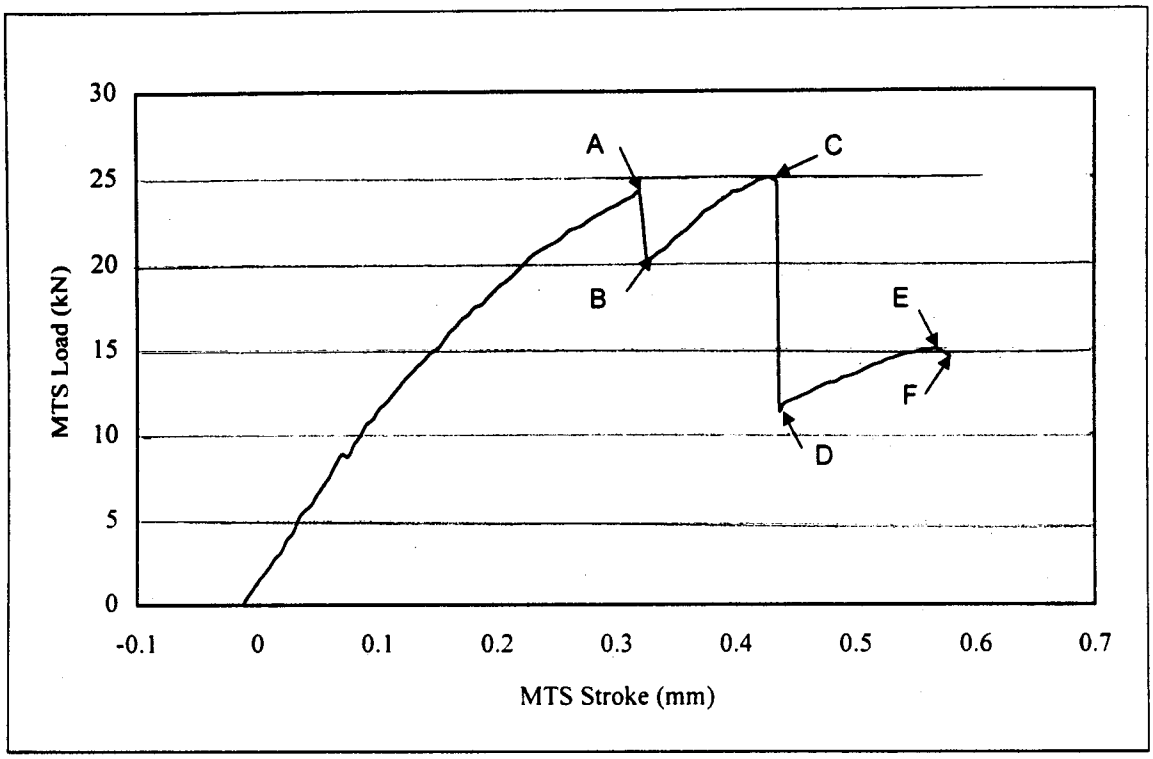

(a) MTS Load versus MTS Stroke curve

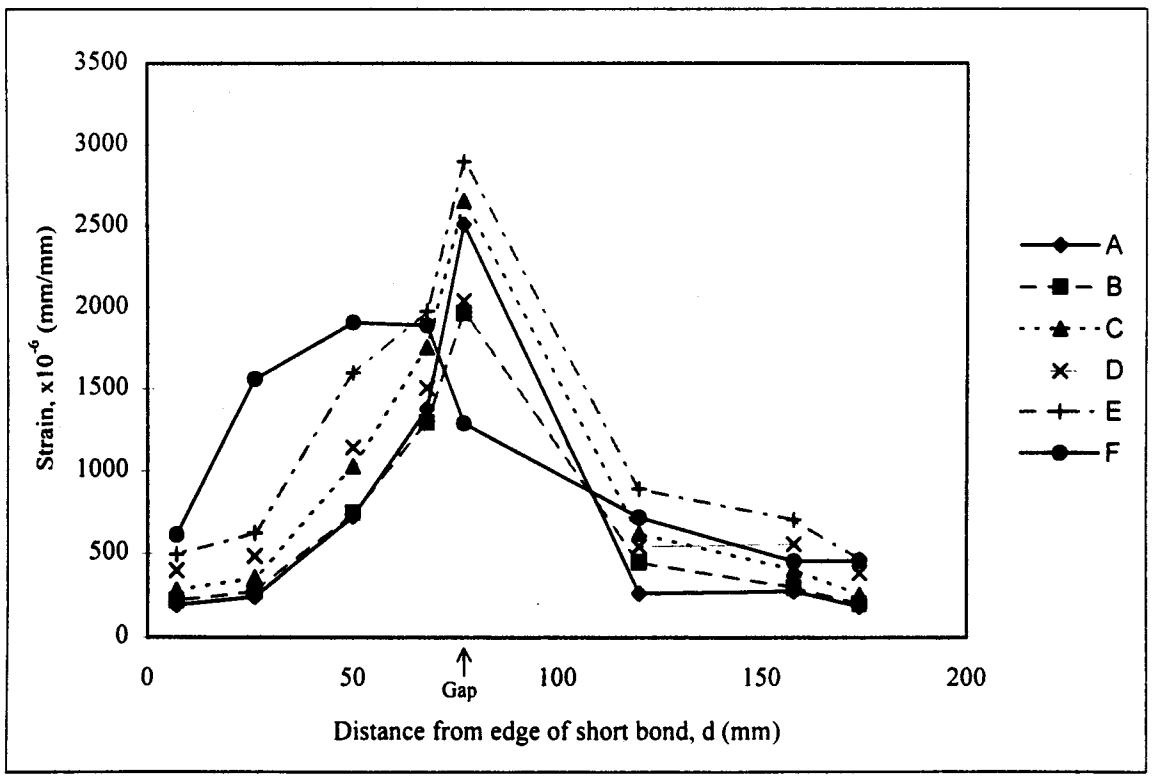

(b) Strain distribution

Figure 2.11 Results of Test CM 4-3

increased together under further applied load. The strain in the back face began to plateau, suggesting yielding, at an applied load of 24.0 kN. This yielding was also indicated by a short plateau in the load versus stroke curve prior to failure in the long back bond at 25.0 kN. Following the first bond failure, some yielding was seen in the short bond on the front face, but the second bond failure was also in the long bond, at 15.0 kN. Both failures were in the bond between the adherend and the steel with no fibre breakage.

CM6-3: Test results shown in Figure 2.12

Strains near the gap increased similarly on the front and back faces until the applied load reached about 21 kN. After this, the front strain across the gap appeared to increase slightly faster than the corresponding back face strain. At 40.1 kN, yielding increased on the front face, as reflected in both the load versus stroke and the strain distribution curves. The short front bond failed completely at 39.5 kN in a combination of bond shear and fibre breakage.

The progression of yielding of the bond under increasing applied load can be clearly traced in the strain distribution diagram. At load point A, the load was low, the elastic plateau was well defined, and the steep strain profile near the gap indicated there was little yielding in the bond. At B and C, it appeared the bond was yielding from approximately 50 to 75 mm from the edge of the short bond, since strain readings in that area were increasing. At D, the load versus stroke curve suggested some yielding, and the gauge at 50 mm showed increasing strain. Finally at E, immediately prior to failure, the gauge at the patch edge was carrying more load and the strains had increased along the length of the bond.

Following the first bond failure, the load versus stroke curve showed a similar slope to that prior to the failure, suggesting yielding on the back face was similar to that in

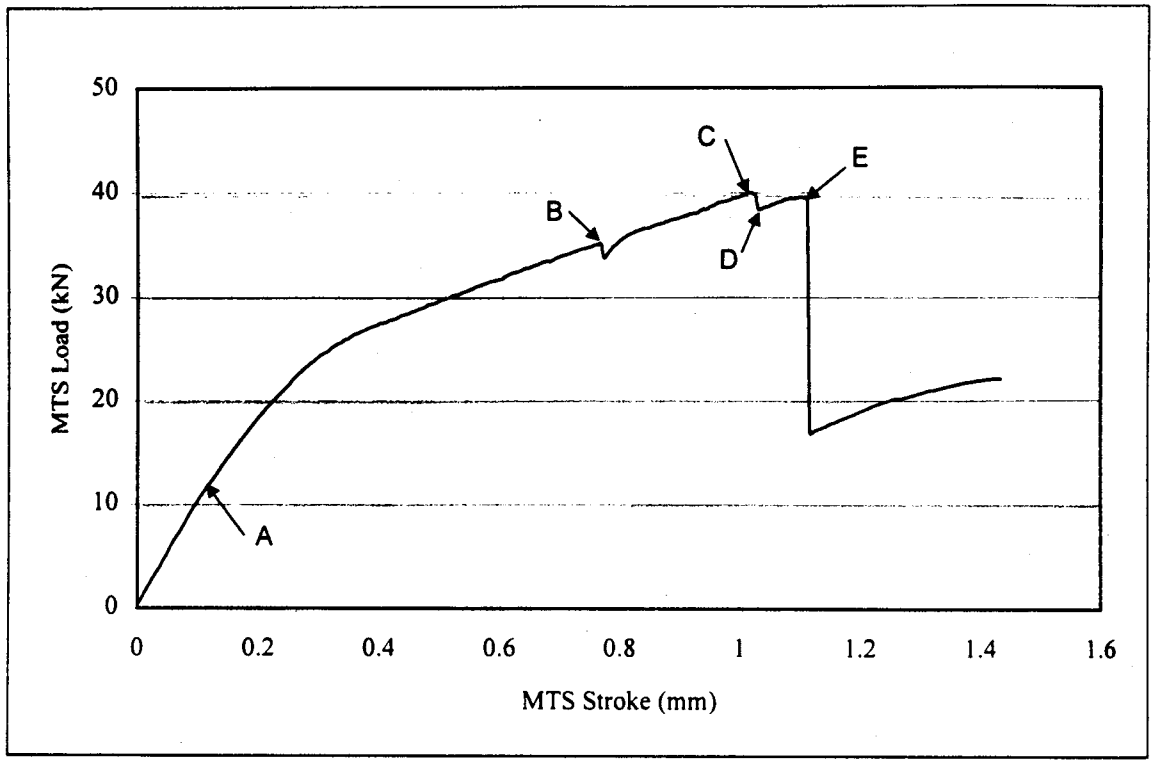

(a) MTS Load versus MTS Stroke curve

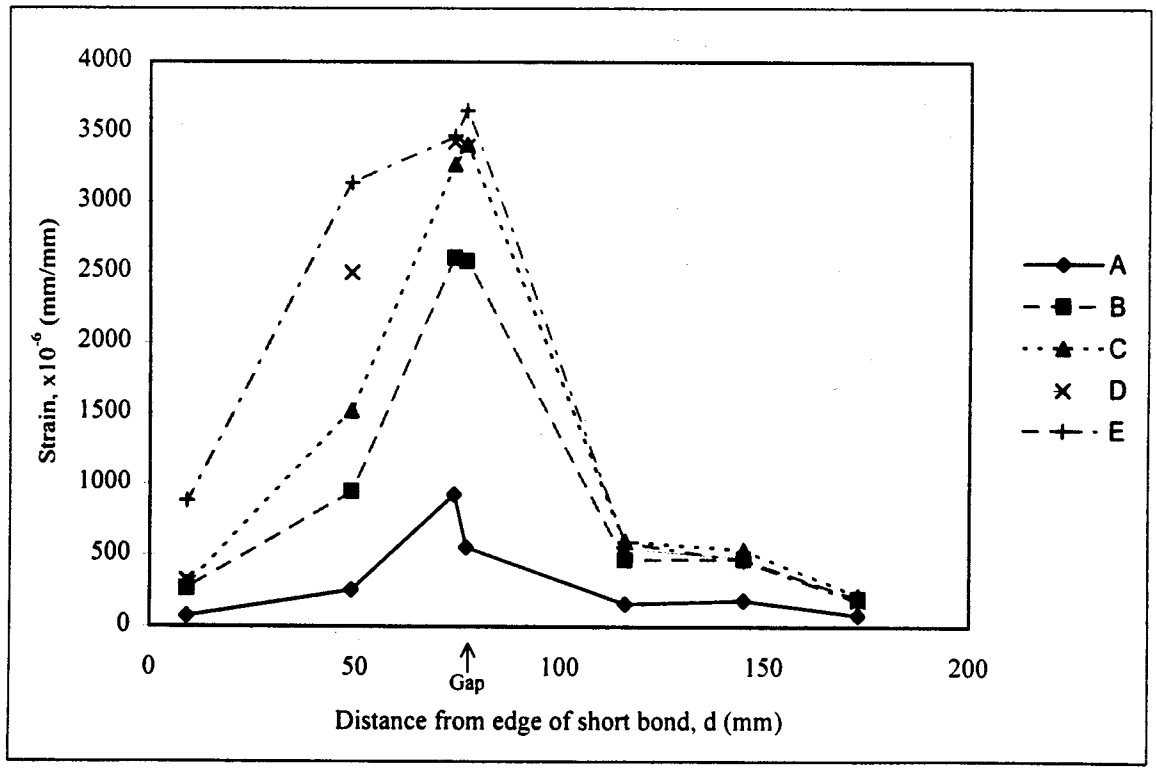

(b) Strain distribution

Figure 2.12 Results of Test CM 6-3

the strain distribution profile for the front face. The back face failed in the long bond at 22.1 kN, also in bond shear and fibre breakage.

2.2.4.2 Failure Modes

With the exception of CM 4-3, the specimens failed in a combination of shear within the patch and some fibre breakage, as shown in Figure 2.13. As discussed in section 2.1.1, this failure indicates a portion of the bond remained elastic until failure. Strain distributions also showed an elastic region in all gauged bonds prior to failure.

While test CM 2-1 did fail in a combination of shear and fibre breakage, it may have failed prematurely. The other two layer tests, CM 2-2 and CM 2-3, showed some yielding in both faces prior to failure of the first bond, while CM 2-1 did not show any yielding on the front face. This may have been the result of a weak bond on the back face, possibly due to poor fabrication.

Both joint failures for test CM 4-3 were in the interface between the patch and the steel, with no fibre breakage. Very little yielding was observed, suggesting the failure was not a result of complete yielding of the bond. As well, the failures were in the long bond in both cases; if the failure were a result of yielding it would be expected to occur first in the short bond. The results suggest some irregularity of the joint was responsible for the failure: for example, the steel may have been dirty when the patch was applied. It is likely that the joint did not reach its full capacity.

Strain distribution data was not available for test CM 6-3 following failure of the first bond because the first failure was on the front face. The load versus stroke curve did not show any irregularities, however, and it is accepted that the second bond was able to achieve its peak load before failing in a combination of shear and fibre breakage.

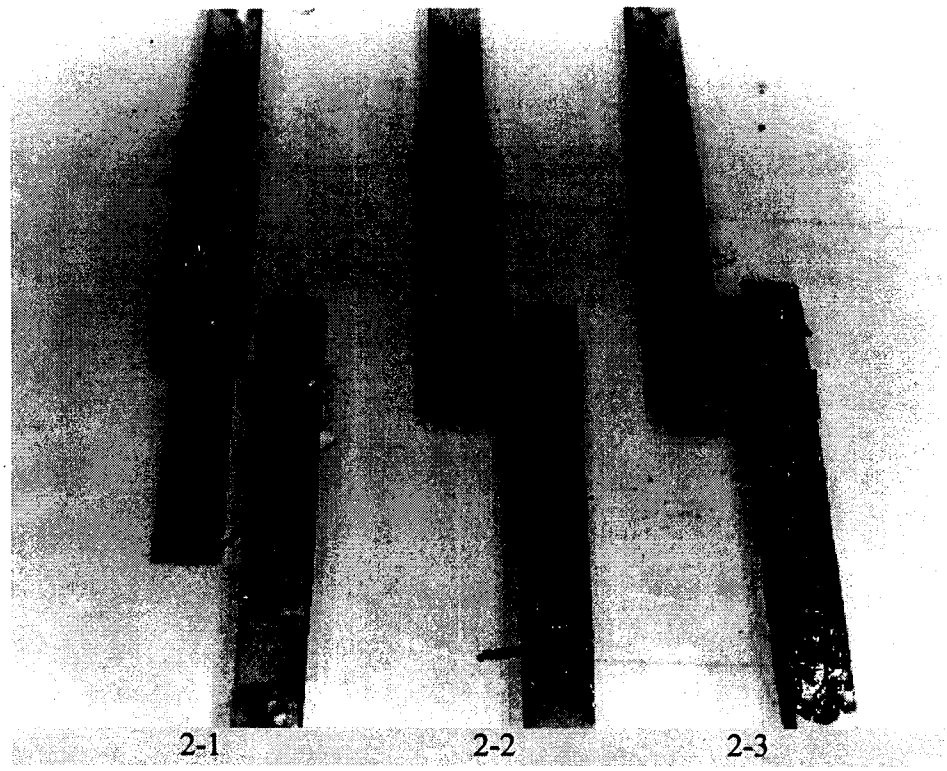

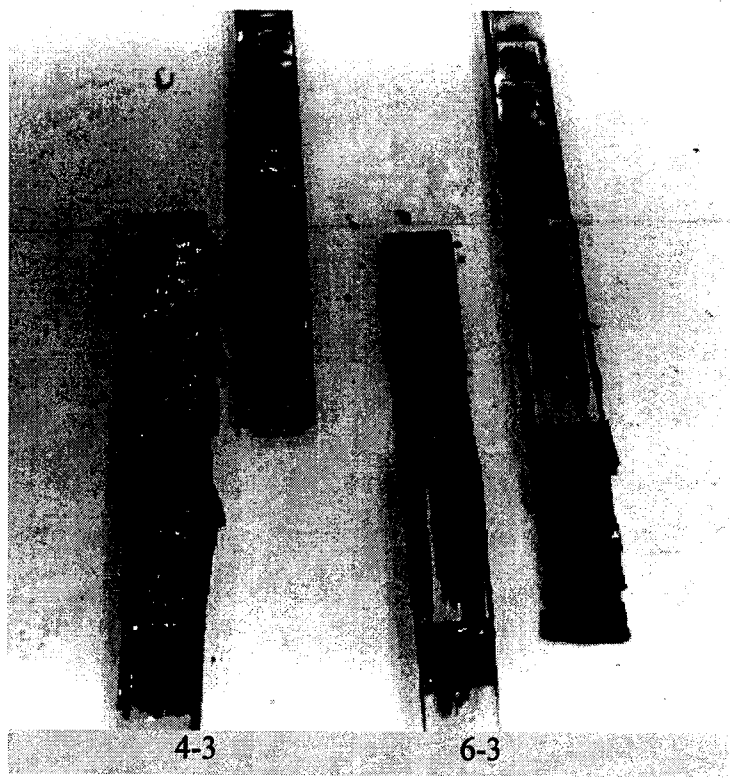

Figure 2.13 Bonded joint specimens after testing

For all tests, the test specimens were subjected to asymmetric loading following the failure of the first bond. The effects of this loading are unknown, although the test results do not suggest severe consequences. The asymmetry may have been responsible for low strains recorded near the gap in some tests, and possibly for premature failure in the second bond due to peel-off stresses, although this cannot be confirmed.

2.2.4.3 Bond Strength

Table 2.4 summarizes load results for the five tests. The first bond failure loads are the peak loads achieved during the test. Complete failure of the bond was typically at a slightly lower load than the peak load. The second bond failure load is the peak load recorded following complete failure of the first bond.

Table 2.4 Summary of bonded joint test results

Test	1st bond failure		2nd bond failure	
	Bond	Load (kN)	Bond	Load (kN)
CM 2-1	short	12.1	long	10.2
CM 2-2	short	21.1	short	9.1
CM 2-3	short	21.8	short	11.3
CM 4-3	long	25.0	long	15.0
CM 6-3	short	40.0	long	22.1

Joint strength is expected to increase with bond length until sufficient bond length is provided to retain an elastic region in the bond to the point of failure of the fibre. The maximum strength a joint can achieve is then restricted by the strength of the fibre. Figure 2.14 shows the relationship between bond length and peak load for specimens with two layers of composite per side. This figure suggests a minimum bond length for formation of an elastic trough in this configuration is less than 50.8 mm. The figure also shows the relationship between the bond length and failure load of the second bond for the same specimens. In this case, it appears the minimum bond length is less than 25.4 mm.

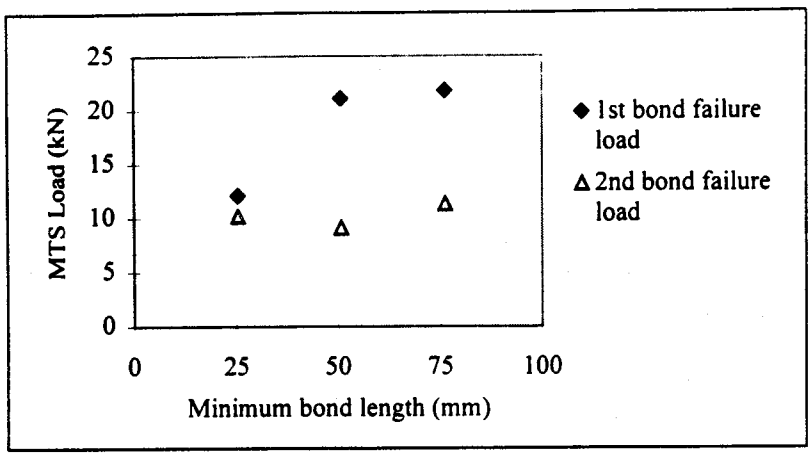

Figure 2.14 Peak load as a function of minimum bond length, bonded joint tests

In addition to the reasons outlined above, the strength data suggests that the first bond failure in CM 2-1 was premature. For the other two-layer specimens and the six layer specimen, which are believed to have reached their peak strength, the second bond failed at about half the load of the first bond; for CM 2-1 the failure of the second bond was at 84% of the load achieved prior to failure of the first bond.

Figure 2.15 shows the relationship between patch thickness and peak and failure loads for specimens with a short bond length of 76.2 mm. The results show bond strength increased as the stiffness of the patch approached the stiffness of the adherend. Due to

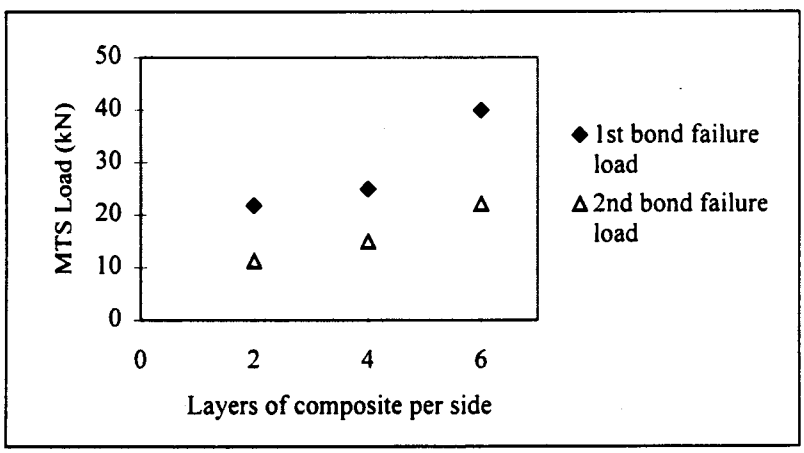

Figure 2.15 Peak load as a function of number of layers of composite per side, bonded joint tests

the observed failure modes, it is suspected that neither bond reached its full capacity in the four-layer test.

2.2.4.4 Strain and Ductility

The peak strain in the butt joint assembly was in the patch across the gap between the steel tabs. This was the least stiff area of the assembly and all load had to pass through the patch to flow across the gap.

The strain values recorded at gauges centered over the 2 mm gap did not report the theoretical peak strain value for most tests. For test CM 2-2, 5 mm strain gauges were used, so the center gauge extended beyond the gap, overlapping the start of the bond with both tabs. All other tests used 2 mm strain gauges, which may or may not have been entirely between the steel tabs, depending on the accuracy of the alignment. Table 2.5 summarizes the strains in the gauges centered over the front and back faces of the gap, both at 10kN applied load and at the onset of failure in the first bond.

Table 2.5 Strains recorded by gauges centered over the gap for bonded joint tests

	At 10 kN applied load				At failure of the first bond				
	Front face		Back face			Front face		Back face	
	Strain	Calculated Load	Strain	Calculated Load	Failure Load	Strain	Calculated Load	Strain	Calculated Load
	(με)	(kN)	(με)	(kN)	(kN)	(με)	(kN)	(με)	(kN)
CM 2-1	2453	7.3	1735	5.2	12.1	3635	10.9	2074	6.2
CM 2-2	1885	5.6	2544	7.6	21.1	5537	16.6	5665	16.9
CM 2-3	1060	3.2	1840	5.5	21.8	3093	9.3	5159	15.4
CM 4-3	755	4.5	432	2.6	25.0	2726	16.3	2630	15.7
CM 6-3	284	2.5	381	3.4	40.0	3370	30.2	2605	23.4

The calculated loads in Table 2.5 were determined by multiplying the recorded strain value by the composite elastic modulus and the total cross-sectional area of the patch, including both sides of the joint. The calculated load is less than the applied load in all

cases. The consistently low values are indicative of how quickly the strain in the patch dropped at the start of the bond. Low values may also have resulted from shear lag through the thickness of the patch: higher strains may have been present on the inside of the patch and lower strains on the outside, leading to an underestimation of the load being carried when using strains on the outside of the patch. Shear lag is expected to be highest in thicker patches, which would explain the greater discrepancy between applied and calculated loads for those tests (CM 4-3 and CM 6-3).

From the load versus stroke results for the five tests, it is noted that the 6-layer test sustained considerably higher stroke before failure than others did. For this stiffer joint, the total strain should have been lower under a given load, resulting in a lower stroke. Table 2.6 summarizes stroke data at 10 kN applied load and shows that this is the case. The table also gives the stroke to onset of failure of the first bond - at that point test CM 6-3 shows much higher results than the other tests. All stroke values are much higher than those estimated from the strain calculated as the applied stress divided by the elastic modulus of the adherends. These high stroke values may have been the result of yielding of the bond, which would allow high strains in the patch over a distance longer than the width of the gap. As well, high shear strains may have been present in the bond or the patch.

Table 2.6 MTS stroke at selected load points, bonded joint tests

	At 10 kN applied load	At failure of the first bond	
	Stroke	Failure Load	Stroke
	(mm)	(kN)	(mm)
CM 2-1	0.164	12.1	0.201
CM 2-2	0.104	21.1	0.306
CM 2-3	0.100	21.8	0.266
CM 4-3	0.086	25.0	0.427
CM 6-3	0.096	40.0	1.015

2.3 Numerical Program

2.3.1 Model Review

A two dimensional, plane strain model of a bonded joint was developed and run in the finite element analysis package ABAQUS 5.6 (Hibbitt, Karlsson & Sorenson, Inc., 1996a). The model represented one quarter of an experimental specimen, taking advantage of symmetry. Boundary conditions restrained the assembly from out-of-plane motion.

All material properties used in the model were linear elastic. Tensile tests of the composite showed linear stress/strain behaviour, and for the loads being applied here the steel was expected to remain elastic as well. John (1994) conducted numerical and experimental studies of adhesively bonded joints and found an elastic model to be a reasonable approximation.

The mesh used for the model began as three rows of steel elements and four rows of patch elements, all 8-node quadrilaterals with reduced integration. The patch was "bonded" to the steel by the sharing of nodes. The patch and adherend were each 1.5 times the bond length, which was 16 steel elements. To model a four-layer patch, the thickness of each patch layer was set at 0.23 mm; this limited the bond length to 22 mm to maintain a minimum aspect ratio of 1:6. Because this bond length limit was unacceptable, the number of patch elements was doubled along the length of the bond, and the adjacent elements on the bond face of the steel were divided into four. Quadratic Multipoint Constraints (MPC) (Hibbitt, Karlsson & Sorenson, Inc., 1996b) were used along the interface of mesh refinement areas to ensure continuity between elements. The resulting mesh is shown in Figure 2.16. This mesh was restricted to bond lengths of 44 mm when using a patch element thickness of 0.23 mm.

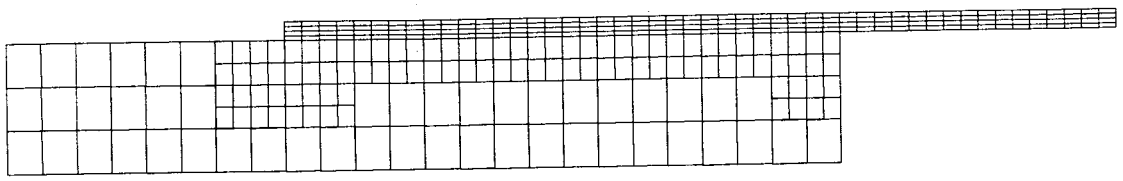

Figure 2.16 Original mesh for ABAQUS 5.6 model of a bonded joint

Elements along the bond and in areas of high strain gradient were refined once again. All patch elements were divided in half along the length of the bond, and steel elements adjacent to the bond and at bond ends were quartered. The refined mesh is shown in Figure 2.17. This model was capable of bond lengths of 2.5 mm to 88 mm for patch elements 0.23 mm thick.

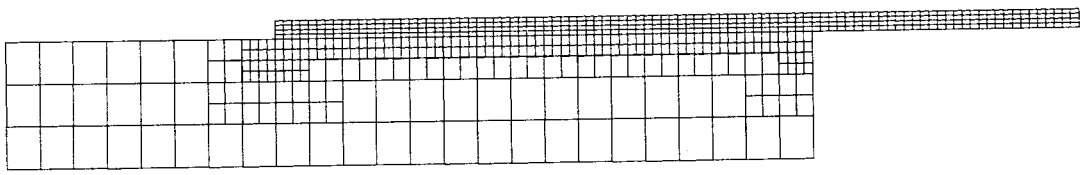

Figure 2.17 Refined mesh for ABAQUS 5.6 model of a bonded joint

The strain distribution from the element integration points along the top of the steel is shown in Figure 2.18 for both models with a 24 mm bond length. The stress concentration in the steel at the patch edge was 8.5 % higher in the more refined model, largely due to that model having integration points closer to the patch edge. The strain distributions were also different near the end of the steel, with the refined model showing much higher strains in that area. The refined model was chosen for further use. Further refinement of the mesh was not investigated because it may have interfered with the modeling of short bond lengths, and it was not expected to improve accuracy significantly.

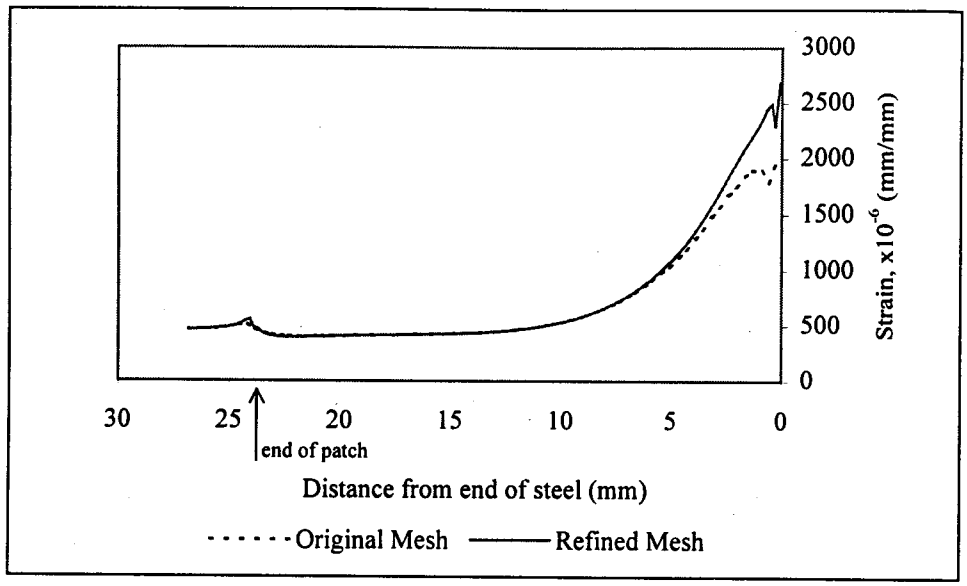

Figure 2.18 Strain distribution along top of steel for original and refined ABAQUS 5.6 models of bonded joints

2.3.2 General Analytical Results

The primary application of the numerical model was the determination of load transfer patterns in bonded joints. Figure 2.19 shows the strain distributions in the bottom of the patch and the top of the steel along a 16 mm bonded joint. All strain distributions are shown at 100 MPa far field applied stress unless stated otherwise. The model represented a four-layer patch (t_p = 0.92 mm, E_p = 70 GPa) bonded to a 6.35 mm steel adherend.

The high gradient in the patch strain distribution near the end of the steel indicates most of the load transfers out of the patch and into the stiffer material, the steel, immediately. Load continues to be transferred out of the patch at a decreasing rate along the bond until the profile plateaus, indicating strain compatibility. The load retained in the patch for strain compatibility is transferred quickly to the steel at the patch edge.

Figure 2.19 also shows the strains in the top of the steel adherend. At the end of the steel, the strain is zero, but increases immediately as a large portion of the load is transferred from the patch. The strain drops along the bond as load is distributed through the

thickness of the steel. In a long enough bond, the strain plateaus at the level of strain compatibility. Near the end of the patch, the strain in the steel increases again as the load remaining in the patch is transferred and the total stiffness of the cross-section decreases.

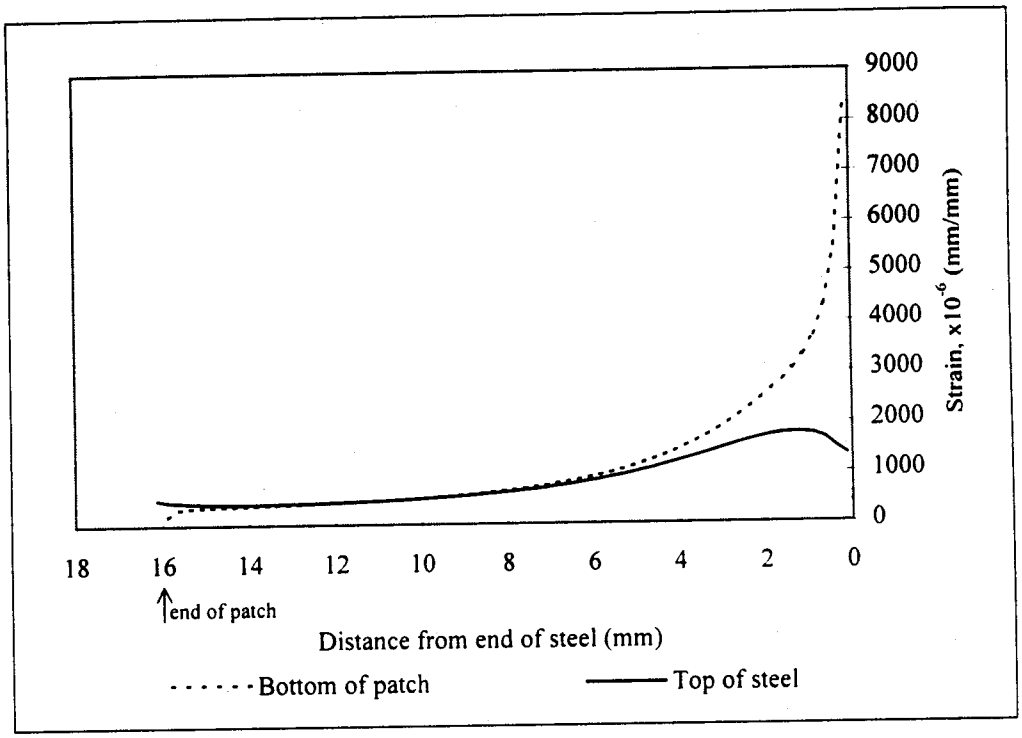

Figure 2.19 Strain distribution in bottom of patch and top of steel along a bonded joint

There is also a stress concentration in the steel near its end, where a large portion of the load from the patch is initially transferred. Because this is an area of high bond shear stress, the bond will likely yield in this region and the transfer of load to the steel will not be as quick; thus, the stress concentration in the steel will not be as high as indicated in the elastic model. Bond yielding is discussed further in section 2.4.1.2.

Figure 2.20 compares the strain in the top row of patch elements to the strain in the bottom row for a 0.92 mm thick patch with an elastic modulus of 70 GPa, bonded to a 6.35 mm steel adherend. The strain on the bottom of the patch decreases quickly as load is transferred to the steel; since the top of the patch is not as closely linked to the steel, and strains do not decrease as quickly. The distance required for load transfer through the

patch thickness is not very long, however. Both profiles reach the same plateau, indicating a constant through-thickness strain distribution in the region of strain compatibility.

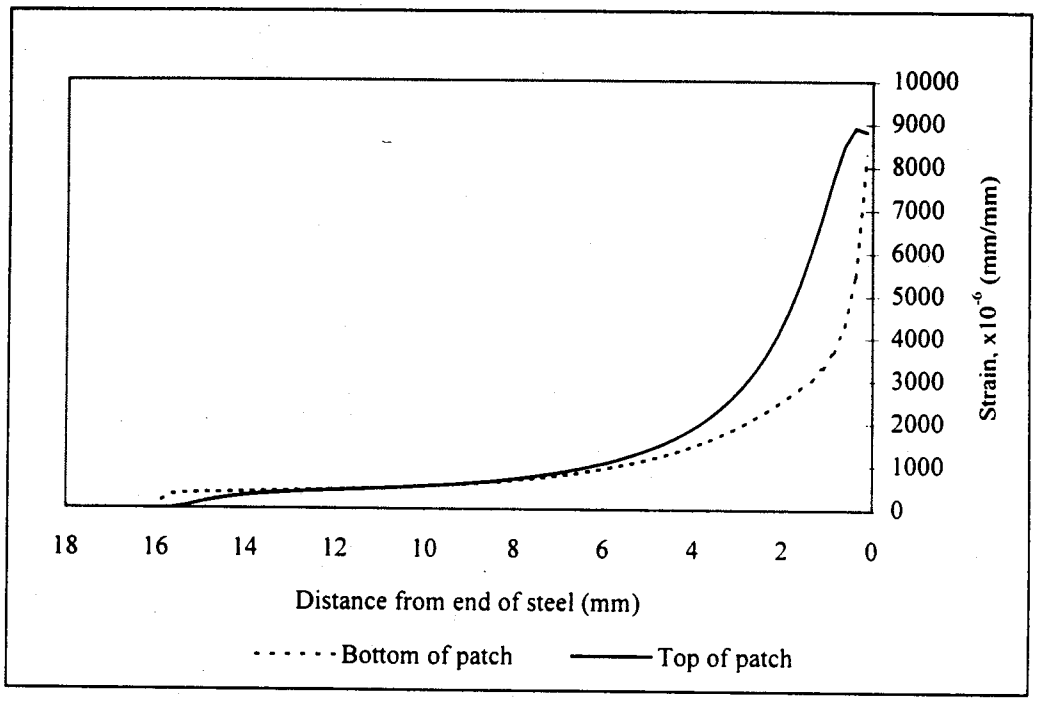

Figure 2.20 Strain distribution on the top and bottom of the patch in a bonded joint

Equation [2.4] relates the shear stress in the bond to the strain gradient in the patch. The equation was derived based on the resultant strain on the patch cross-section, as discussed in section 2.1.3. For shear stress calculations in the presentation of the numerical results, the strain along the bottom of the patch was used in place of the resultant strain. For experimental results, strains along the top of the patch were used. This neglected shearing within the patch, but appeared to provide reasonable results.

Figure 2.21 shows typical strain contours in the base metal and patch near the edge of the patch for the original model. The stress concentration at this location may cause cracking in an element subjected to fatigue loading.

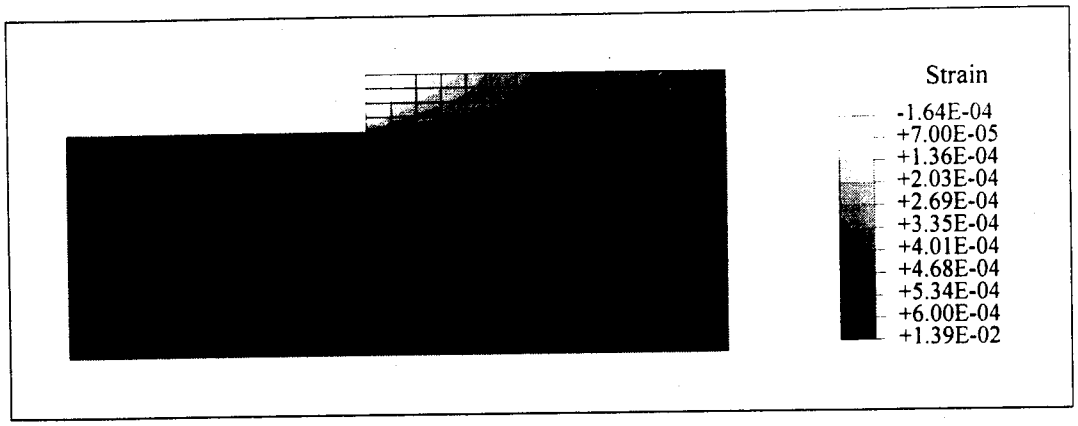

Figure 2.21 Typical strain contours at the patch edge

2.4 Comparison of Numerical and Experimental Results

2.4.1 Strain Distribution

2.4.1.1 Modeling of Test Series

Because the numerical model was not designed to account for yielding, comparisons between numerical and experimental data are performed at low applied loads. Strain distributions along the top of the patch from the numerical model are plotted in Figure 2.22 along with the experimental data at the corresponding loads. Because a strain gauge measures an average strain over its length, experimental values in areas of high strain gradient are not expected to be accurate compared with the numerical model.

In all cases, the general shape of the numerical and experimental results is the same: a plateau is evident over the center and near the end of the bond, with a sharp increase in strains near the end of the steel. Figure 2.22(a) shows the comparison plot for specimen CM 2-1, which is acceptable. The agreement for specimen CM 2-2, in Figure 2.22(b), is not as good. At the load under consideration, gauges on opposite sides of the specimen at the gap measured 487 με and 688 με on the front and back faces respectively. This suggests the two steel tabs were slightly misaligned, causing some compressive strain in the front face when subjected to loading, which may account for the low strain readings.

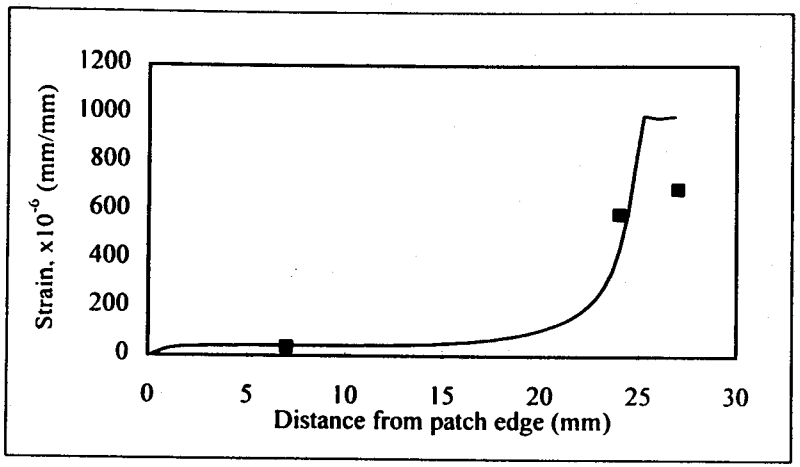

(a) Specimen CM 2-1 at 10 MPa far field stress

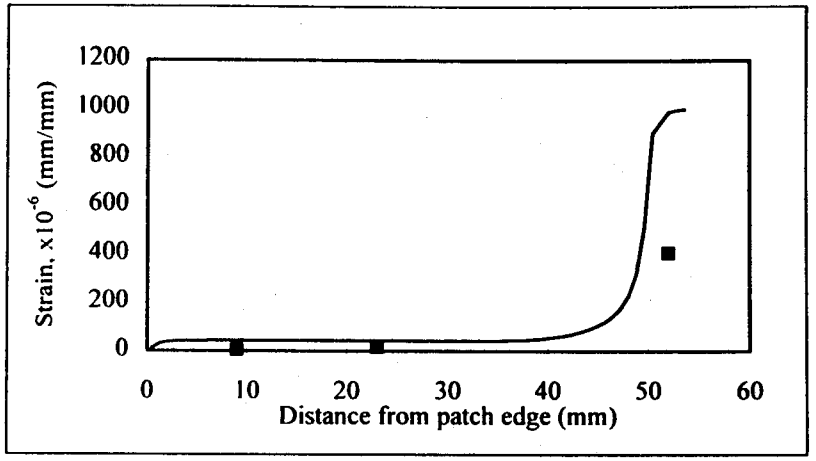

(b) Specimen CM 2-2 at 10 MPa far field stress

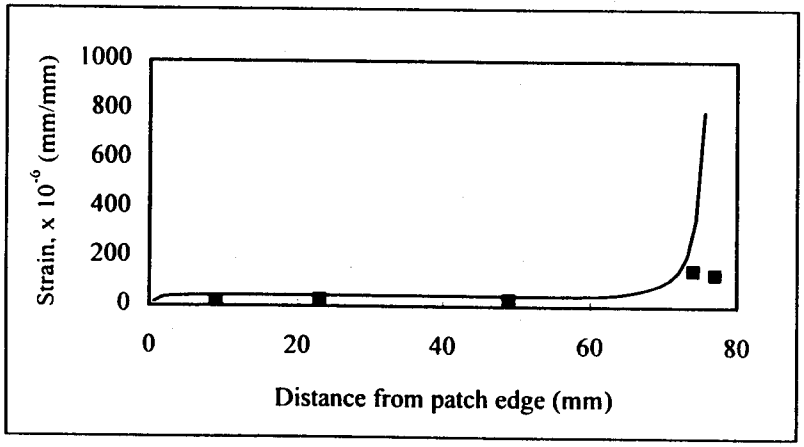

(c) Specimen CM 2-3 at 10 MPa far field stress

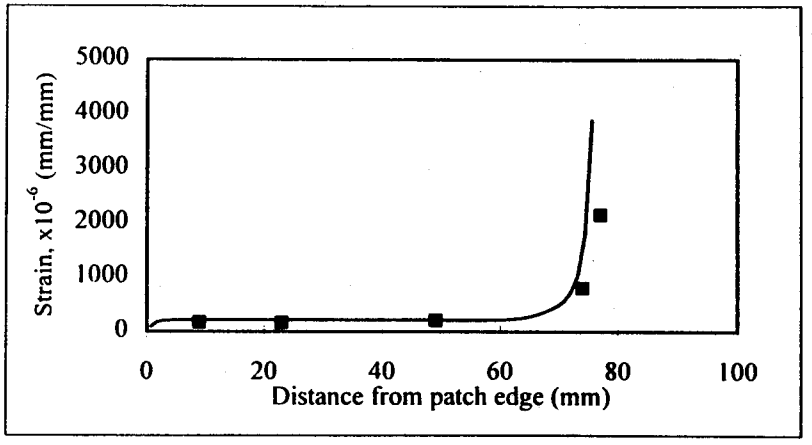

(d) Specimen CM 2-3 at 50 MPa far field stress

—— Model prediction ■ Experimental values

Figure 2.22 Comparison of numerical and experimental results for CM 2-1, CM 2-2, and CM 2-3

Specimen CM 2-3 exhibited some of this same misalignment, with gap strain readings of 133 με and 535 με on the front and back faces respectively at 10 MPa far field stress, the loading point represented in Figure 2.22(c). Although a difference in center strains was still observed at 50 MPa far field stress, the agreement of the numerical and experimental data is better (Figure 2.22(d)). This may be due to some yielding in the bond that relieved bending stresses from the length of the joint and localized them in the yielded area.

2.4.1.2 Yielding of the Bond

Because bond shear stresses at the ends of the joint are high, some yielding of the bond is expected in these areas. The bond can be thought of as a thin layer of epoxy between the patch and steel adherend, so bond yielding is largely a function of the epoxy properties. Hart-Smith (1987) states the material properties of the epoxies used in composite repair are best described using an elastic-plastic model.

Figure 2.23(a) is a conceptual sketch of the effects of yielding on bond shear stress distribution. The first curve assumes unlimited elastic behaviour of the bond, as was the case for the numerical model. The second curve shows the modified stress distribution for a bond with elastic-plastic behaviour. Because the shear stress in the bond at the end of the steel cannot exceed the shear yield value, the curve is truncated at that value. The bond must still transfer the entire applied load along its length, so the area under the shear stress curve must be the same, and the bond stresses increase along the length of the bond.

From [2.4], the slope of the strain distribution curve is directly proportional to the shear stress in the bond. Therefore, integrating the shear stress curves results in Figure 2.23(b). Yielding has the effect of decreasing strain gradients, causing higher patch strains near the end of the steel, and lower strains near the patch edge.

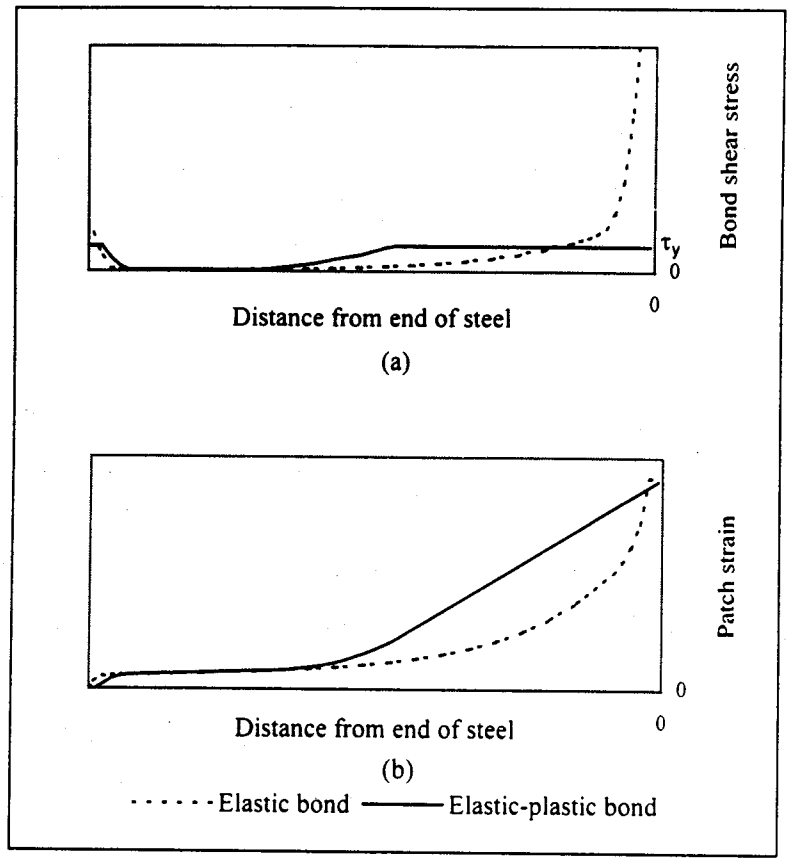

Figure 2.23 Conceptual sketch of the effect of bond yielding on patch strain

There are two major implications of bond yielding. If the shear stresses are high enough, the bond may yield at the patch edge, slowing the transfer of strain compatibility load out of the patch and reducing the magnitude of the stress concentration in the steel. It is therefore possible that there is a maximum stress concentration that would occur at a patch edge. Second, an increased bond length may be required to maintain an elastic region in the center of the bond. Figure 2.23(a) shows an elastic region in the elastic-plastic bond, but it is much shorter than for the elastic model.

The experimental and numerical results for tests CM 4-3 and CM 6-3 are shown in Figure 2.24. The results suggest yielding was present in the bond, as the experimental strains follow profiles that are more suggestive of the elastic-plastic bond model than the elastic bond model as shown in Figure 2.23(b).

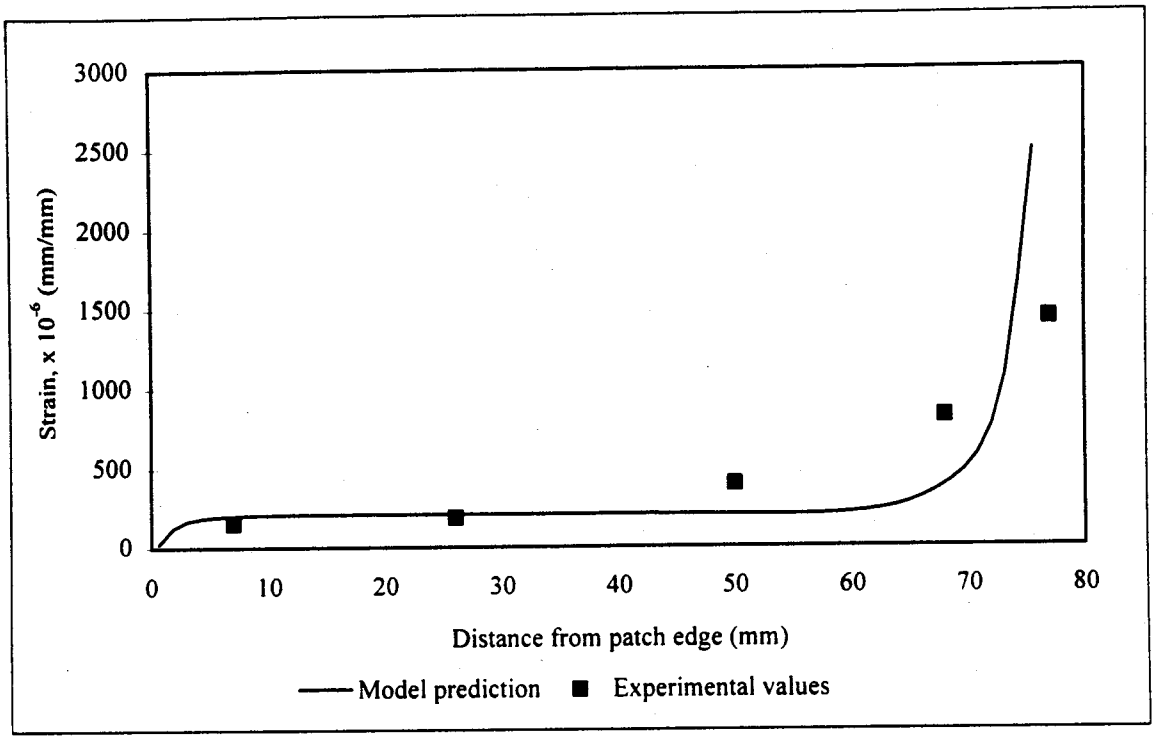

(a) Specimen CM 4-3 at 50 MPa far field stress

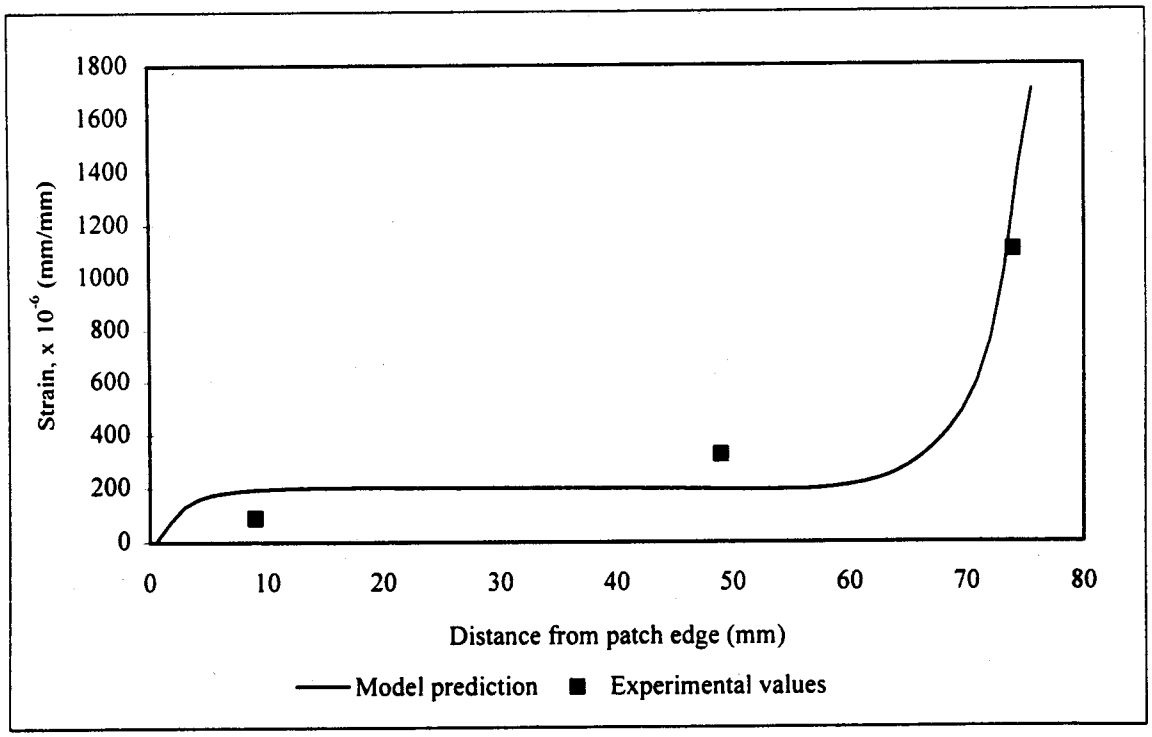

(b) Specimen CM 6-3 at 50 MPa far field stress

Figure 2.24 Comparison of numerical and experimental results for CM 4-3 and CM 6-3

2.4.2 Bond Length

2.4.2.1 Defining Minimum Bond Length

The minimum bond length is the length required to maintain an elastic trough in the adhesive shear stress distribution until failure of the joint. An elastic trough indicates strain compatibility has been established, and the shear flow in the bond, q, approaches zero. For this analysis, the minimum bond length is defined as:

> *The minimum bond length is the length required to reach q less than 0.1 N/mm under 10 MPa applied stress in the steel, plus an additional 20% to allow transfer of the strain compatibility load out of the patch at its edge.*

For a four-layer patch on a 6.35 mm steel tab, each patch layer 0.23 mm thick with an elastic modulus of 70 GPa, this minimum bond length is 15.6 mm.

From the finite element analysis corresponding to specimen CM 2-3, the minimum bond length was calculated to be 14.5 mm. Figure 2.25 shows the shear flow calculated from experimental results immediately prior to failure for specimens with two layers of composite fibre on each side (CM 2-1, CM 2-2, and CM 2-3). It appears that the shear flow was approximately zero at 20 mm distance from the gap in all three cases, suggesting a minimum bond length slightly higher than that estimated from the elastic model.

A minimum bond length of 20 mm implies that even specimen CM 2-1, with a short bond length of 25.4 mm, had sufficient length to retain an elastic trough to failure. Results of test CM 2-1 are discussed in detail in section 2.2.4, but to summarize, the failure mode and strain distribution of specimen CM 2-1 support the theory that the minimum bond length is less than 25.4 mm.

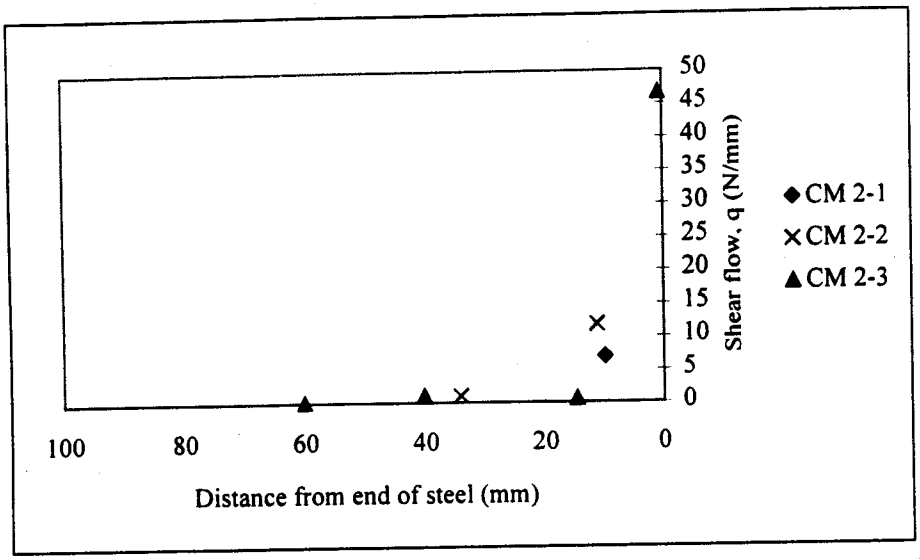

Figure 2.25 Shear flow in the bond at failure for tests CM 2-1, CM 2-2, and CM 2-3

2.4.2.2 Joint Configuration and Bond Length

For the repair of cracked steel elements, a patch is less stiff than the steel adherend, or at most of equal stiffness. As the patch stiffness, $E_p t_p$, approaches the base metal stiffness, $E_s t_s$, the strain incompatibility near the end of the steel decreases. Because this incompatibility is the driving force behind load transfer, a decrease in the incompatibility reduces the rate of load transfer and the minimum required bond length increases.

Figure 2.26 shows numerical model results to support this concept. Plots of patch strain and shear flow distribution, calculated from [2.4], are shown for 0.92 mm patches on 6.35 mm thick steel adherends. The plots show the initial load transfer is higher for a lower modulus patch. Further, recall that for equilibrium (from [2.1]), the area under each shear flow curve of Figure 2.26(b) must equal the applied load:

$$\int q dx = P$$

Since the area under the lower stiffness curve is greater at the end of the steel, the stiffer patch must have a greater area under the remainder of the bond, implying a more gradual

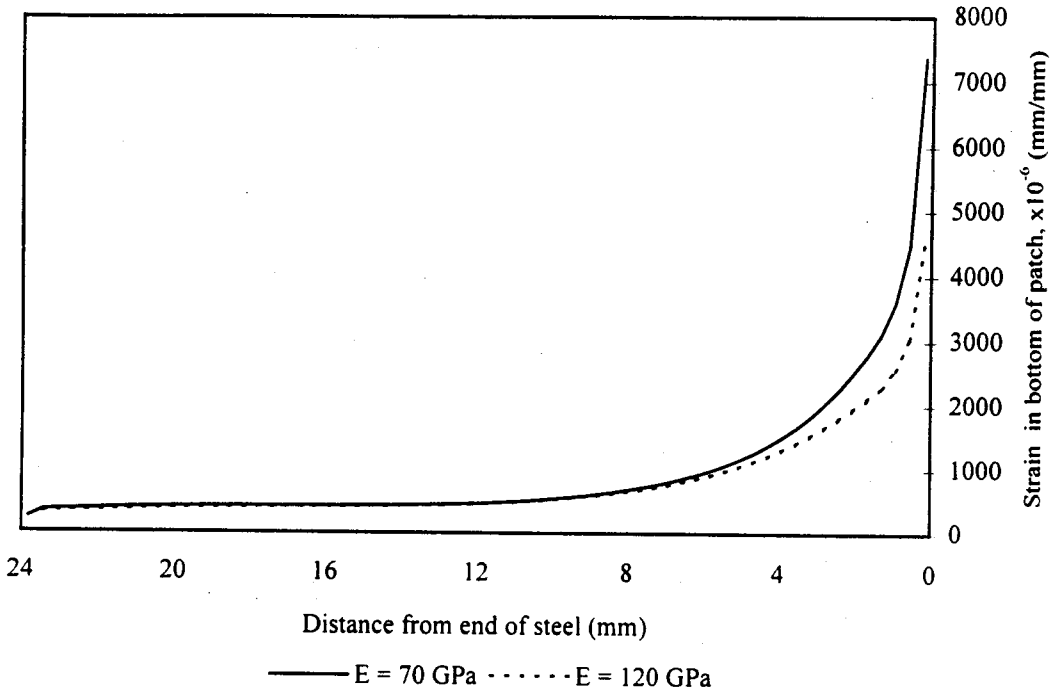

(a) Strain in patch along bond length for different patch stiffness

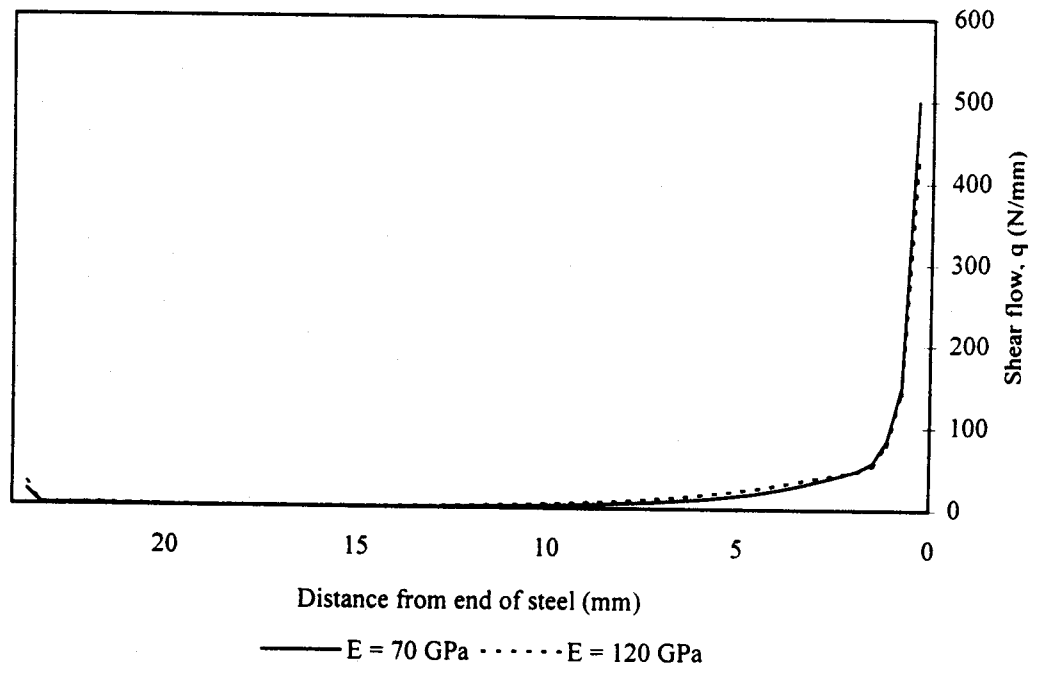

(b) Shear flow in the bond for different patch stiffness

Figure 2.26 Effect of patch stiffness on patch strain and bond shear stress distributions

transfer of load and a longer distance to attain zero shear stress. This assumes the amount of load transferred at the end of the patch is small for the patch stiffness properties being considered.

The experimental results also support the idea of stiffer patches resulting in more gradual load transfer along the bond. Figure 2.27 shows a comparison of shear flow in the bond for tests CM 2-3 and CM 4-3 at 50 MPa far-field applied load, prior to any signs of yielding. The two-layer test showed higher shear flow in the start of the bond, and the four-layer test showed a more gradual decrease in shear flow along the length of the bond. Baker (1987), in his design approach for bonded composite repairs to aircraft components, and Hart-Smith (1987) provide slightly different guidelines for required bond length but the results are the same - a stiffer patch requires a longer minimum bond length.

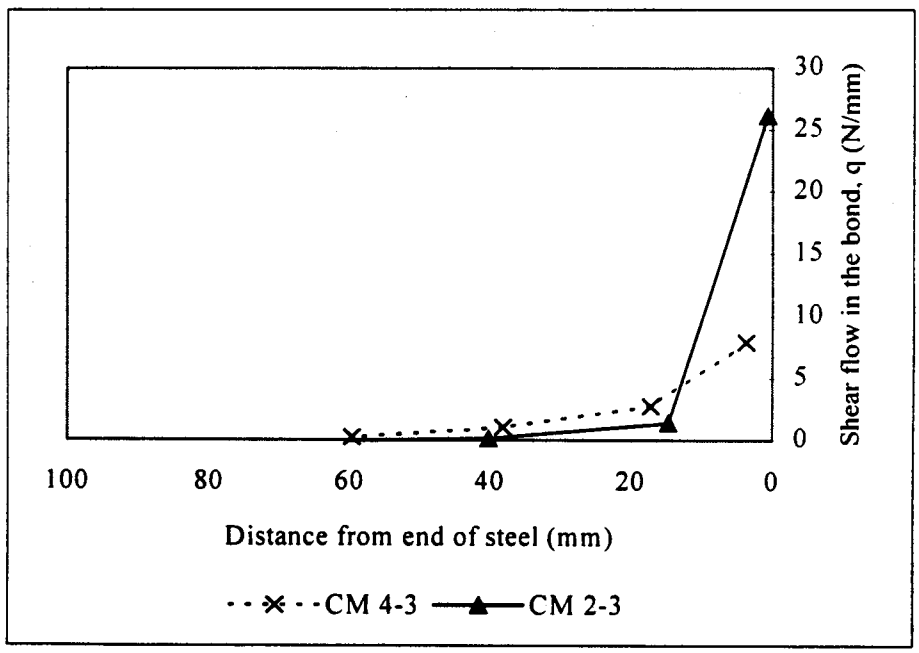

Figure 2.27 Shear flow in the bond at failure for tests CM 2-3 and CM 4-3

2.4.2.3 *Model for Estimating Minimum Bond Length*

Figure 2.28 shows the minimum required bond length as a function of the relative stiffness of patch and adherend from a series of numerical models. From a simple linear best fit, the minimum required bond length can be estimated as

$$\ell_{min} = 29.2\frac{E_p t_p}{E_s t_s} + 14.4$$

where ℓ_{min} is in mm. The equation was developed for $E_p t_p / E_s t_s$ less than 0.25. This is a non-conservative estimate, and a greater length should be used to account for yielding and error in the best fit line. The 95% confidence limit for the data suggests (Miller et al. 1990)

$$\ell_{min} = 30\frac{E_p t_p}{E_s t_s} + 17 \qquad [2.5]$$

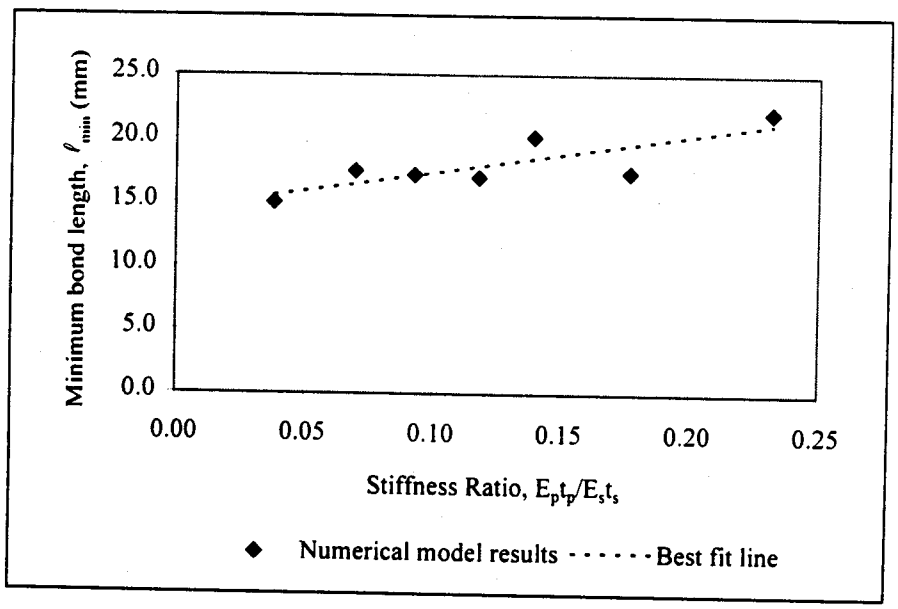

Figure 2.28 Minimum bond length as a function of the relative stiffness of patch and adherend

Substituting the parameters for the test specimens, [2.5] gives minimum bond lengths of 17.7 mm for two layers of composite per side (CM 2-1, CM 2-2, and CM 2-3), 18.4 mm for four layers (CM 4-3), and 19.1 mm for six layers (CM 6-3). Considering the small

contribution of the stiffness term of the equation, it may be best to simply specify a minimum bond length of

$$\ell_{min} = 30(0.25) + 17 \approx 25\text{mm}$$

for $E_p t_p / E_s t_s$ less than 0.25.

2.4.2.4 Bond Length, Joint Configuration, and Joint Strength

Joint strength is expected to increase with increasing bond length until the minimum bond length is reached and the bond maintains an elastic region at its center until failure. Beyond this point, the strength of the joint is governed by the strength of the composite and does not increase further.

The first bond failures for tests CM 2-2 and CM 2-3 occurred at 21.1 kN and 21.8 kN respectively. If we accept that these two specimens had more than the minimum required bond length, the average of the two results, 21.5 kN, is taken as the peak joint strength for the particular patch to adherend stiffness ratio.

In general, it is thought that as $E_p t_p$ approaches $E_s t_s$, the joint efficiency improves and the bond strength increases (Siener 1992). Figure 2.29 shows the relationship between peak joint strength and the $E_p t_p / E_s t_s$ ratio for tests performed as part of this investigation and by

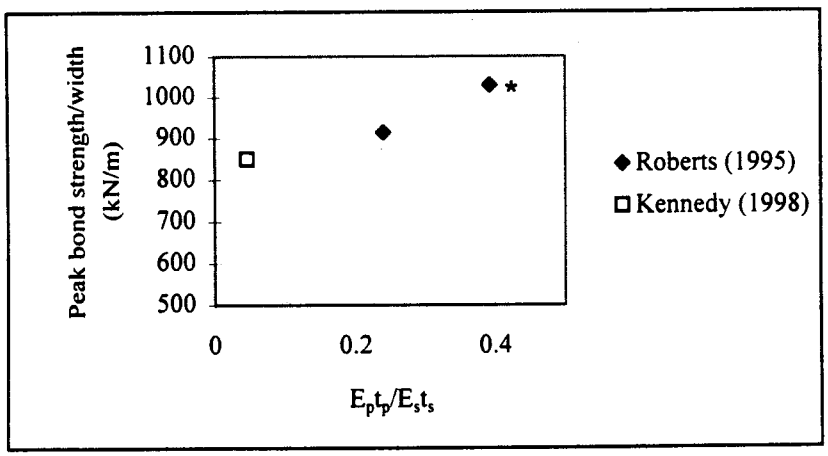

Figure 2.29 Bond strength as a function of the relative stiffness of patch and adherend

Roberts (1995), all for carbon fibre composite patches on steel adherends. The data point marked with a star had a stiffer patch than base metal adherend so the strength is plotted against the inverse ratio ($E_s t_s / E_p t_p$). Results for four- and six-layer patches from this study are not shown because there was only one test of each configuration and the repeatability of results is not known.

2.5 Parametric Study

A parametric study was conducted to investigate the effects of variations in material properties and geometry on the performance of a bonded joint. Figure 2.21 shows the stress contours at the patch edge, indicating a high stress concentration in the steel. Minimizing this stress concentration is of primary concern in preventing the formation of new cracks at a patch boundary, and was the basis for comparison in this parametric study. The stress concentration factor was calculated by dividing the peak stress of this concentration by the applied far field stress in the steel (σ_{pk}/σ_o).

2.5.1 Bond Length

Figure 2.30 shows that for an otherwise constant patch configuration, the stress concentration factor at the end of the patch is highest when the bond length is short. The

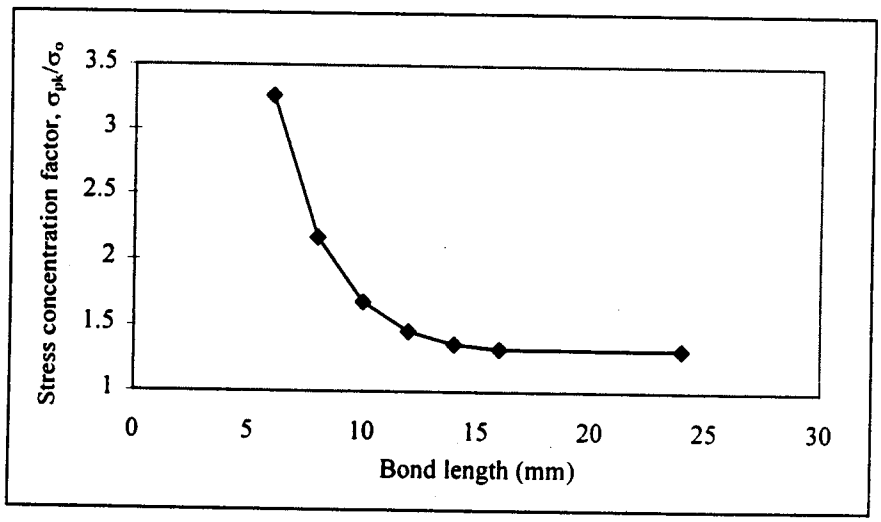

Figure 2.30 Effect of bond length on the stress concentration in the steel at the patch edge

stress concentration approaches a constant level as the bond length is increased and the bond develops a region of strain compatibility. Patches should be designed with sufficient bond length to reduce the stress concentration to the level of the plateau seen in the figure. The data shown is for a 0.92 mm thick patch with an elastic modulus of 70 GPa, on a 6.35 mm thick steel adherend.

Figure 2.31 shows the shear stress distribution in bonds of varying length, with the same material specifications as Figure 2.30. If the patch is not long enough to reach the strain compatibility region, there is still considerable shear stress in the bond at the patch edge, and the patch is carrying more load than that required for strain compatibility. This higher load is transferred to the steel at the patch end, causing a higher stress concentration.

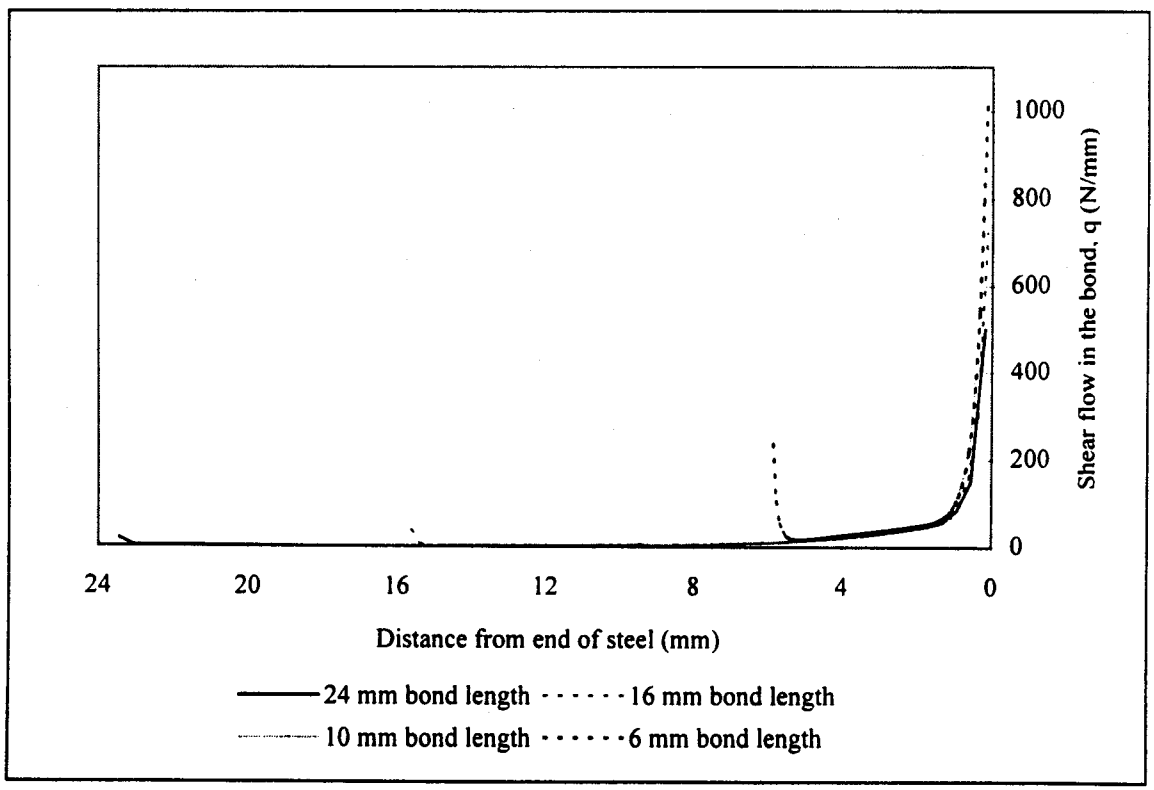

Figure 2.31 Shear flow in the bond for varying bond lengths

2.5.2 Patch Stiffness

Finite element analysis allows the variation of the stiffness of patch and adherend, where stiffness implies the product E_pt_p or E_st_s respectively. Figure 2.32 shows the stress concentration factor in the steel at the patch edge as a function of the patch to adherend stiffness ratio for a number of numerical analyses. The results show a linear trend with minimal scatter, suggesting the stress concentration at the patch edge is largely a function of the load required in the patch for strain compatibility. Separating the effects of thickness and elastic modulus, as shown in Figure 2.33, it appears the material properties have a slightly greater effect than component thickness on stress concentrations in the steel.

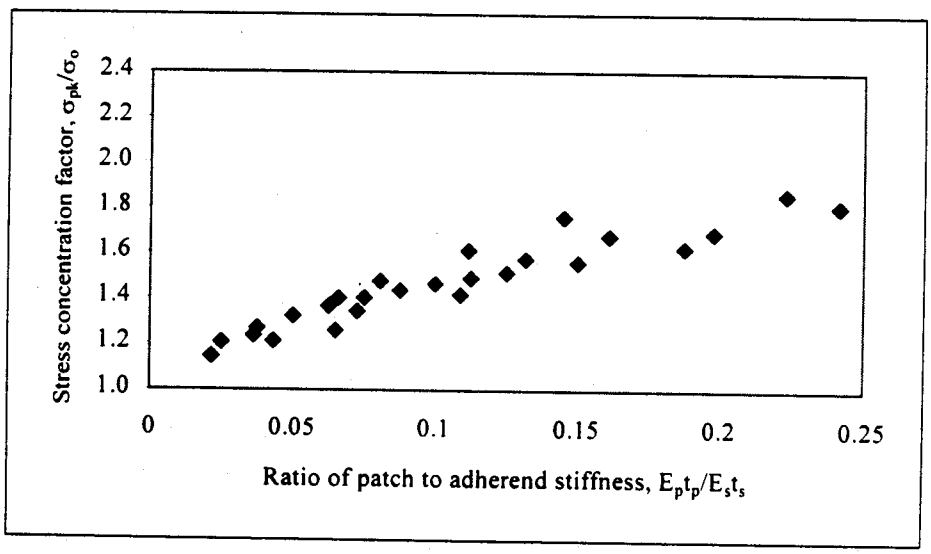

Figure 2.32 Effect of the patch to adherend stiffness ratio on the stress concentration in the steel at the patch edge

2.5.3 Use of Combined Fibre Types

Using a combination of fibre types in a patch lay-up may improve durability and fatigue performance. Karbhari and Shulley (1995) suggested that a reliable patch might be S-glass under carbon fibre. This combination would exhibit more durability than a single fibre patch, and decreased potential for long-term degradation due to galvanic potential between carbon and steel. Konur and Matthews (1989) stated that fatigue performance

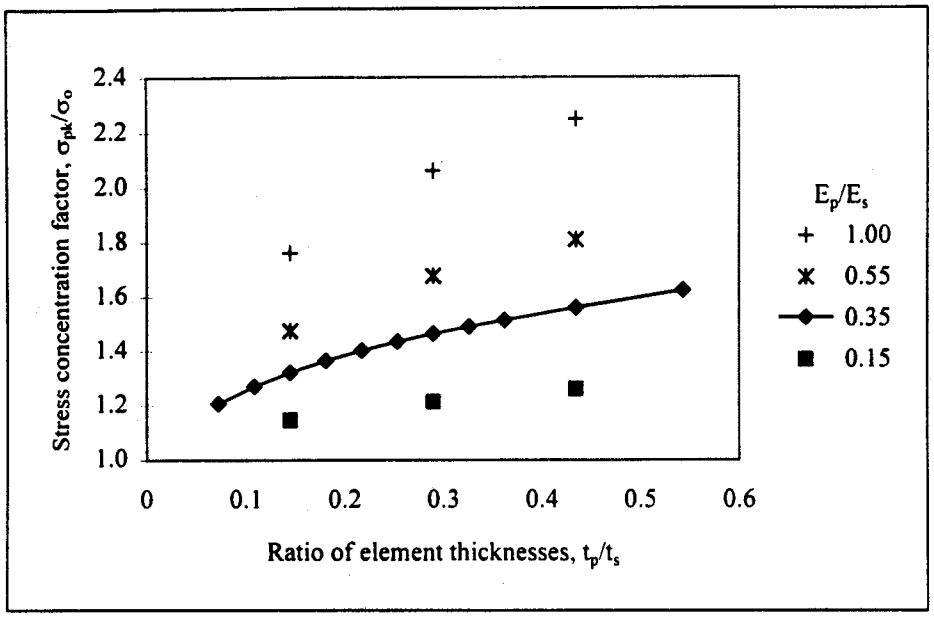

Figure 2.33 Effect of the patch to adherend thickness and elastic modulus ratios on the stress concentration in the steel at the patch edge

varies with fibre type, and that the fatigue performance of glass and aramid fibres can be improved with hybridization with carbon.

Having a lower stiffness fibre underneath a higher one, such as glass under carbon, may also benefit stress distribution. A stiffer outer layer may decrease shear lag through the patch and reduce inter-laminar shear strains. As well, it was shown that a lower stiffness patch helps to reduce the stress concentration at the patch edge. Layering of fibre types may help to achieve a similar stress reduction while maintaining the same overall patch stiffness, thus the same crack repair effectiveness.

Table 2.7 shows the results of analyses for a four-layer carbon fibre composite patch, and for a patch with glass composite under carbon composite. For the latter, the ratio of composite thickness was three carbon to one glass, with a hypothetical composite thickness calculated to give the same overall patch stiffness. This theoretically ensured similar load distribution between patch and adherend for strain compatibility, so the stress concentration factor was approximately constant with respect to that parameter. The

stress concentration factors obtained from the analysis suggest this may be an effective way to reduce edge stress concentration factors, in addition to durability merits.

Another alternative to the unidirectional patch is changing fibre orientation for different plies. Since patch ductility changes with fibre orientation, variable ply orientation may be a means of reducing stress concentrations at the patch edge. Variable or multi-directional loading may also require mixed fibre orientation (Chue et al. 1996).

Table 2.7 Numerical analysis of patch layering

Patch Description	Carbon fibre		Glass fibre		Overall patch stiffness	Resulting stress concentration
	Thickness	Assumed elastic modulus	Thickness	Assumed elastic modulus		
	t_C(mm)	E_C(GPa)	t_G(mm)	E_G(GPa)	$\Sigma E_i t_i$ (GPa-mm)	
Pure carbon	0.92	130			119.6	1.545
Glass under carbon	0.84	130	0.28	35	119	1.383

2.5.4 Adhesive Layer

Models for bonded patches frequently incorporate a three-layer approach, representing the base metal, the patch, and a layer of adhesive between the two. In cases where a tape-adhesive is used, this may be necessary because of the increased thickness of the adhesive layer. Various methods have been used to model the adhesive numerically, including shear springs, plate elements, and brick elements, with varying accuracy and model size as a result (Naboulsi and Mall 1996).

In the experimental tests conducted here, the adhesive layer was very thin. An unbonded carbon sheet has a thickness of 0.11 mm and an elastic modulus of 230 000 MPa, according to manufacturer specifications. Since the measured thickness of a bonded layer was 0.23 mm, the difference (0.23-0.11=0.12) can be attributed to the epoxy. The epoxy

does impregnate the fibres of the composite, so the increased layer thickness is due in part to spreading of the fibres and in part to the addition of an epoxy layer between layers of composite.

Numerically determined strain distributions along the top of the steel are shown in Figure 2.34 for two finite element models. The first model assumed a homogeneous patch with an elastic modulus of 128 000 MPa and a thickness of 0.23 mm/layer. This was the basic model discussed to this point in the study. The second model assumed the extreme case of a single patch layer consisting of a 0.06 mm layer of epoxy, a 0.11 mm layer of carbon fibres with an elastic modulus of 230 000 MPa, and a second 0.06 mm layer of epoxy. The epoxy was given an elastic modulus of 3000 MPa as estimated by the manufacturer. Both models used a two-layer patch on a 6.35 mm steel adherend.

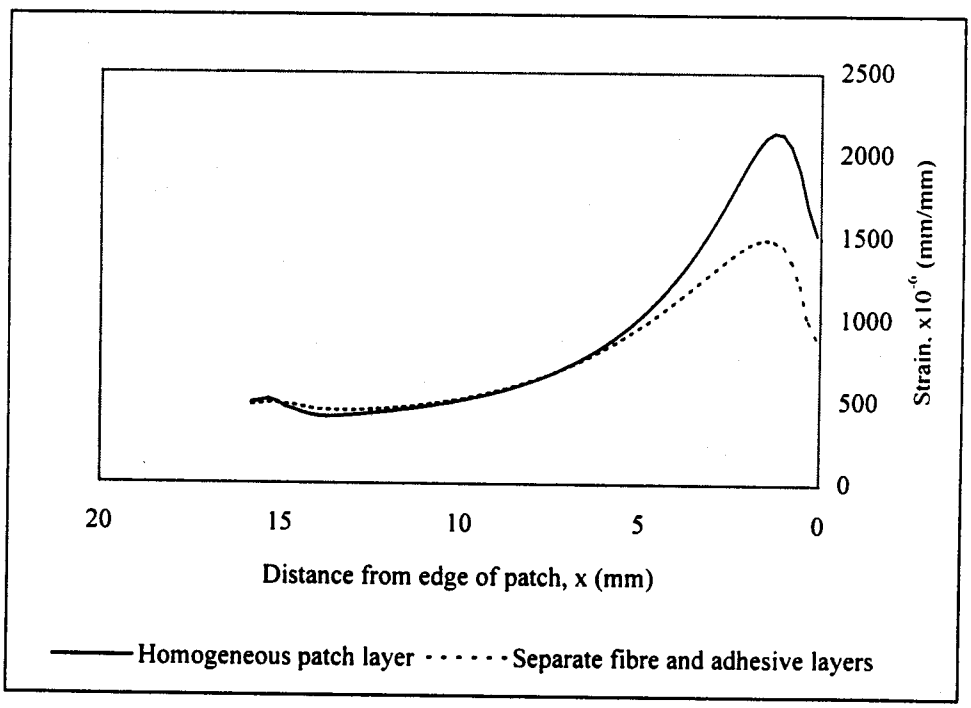

Figure 2.34 Strain distribution along top of steel for bonded joint models with and without a separate adhesive layer

The effect of the adhesive layer is to flatten the strain distribution, implying more gradual transfer of load. This results in lower stress concentrations in the steel both near the end

and at the patch edge. With this apparent ability of a low-modulus adhesive to slow load transfer, the use of stiffer patches, even bonded steel patches, may be considered. As long as sufficient bond length is provided, the stress concentrations at the patch edge could be minimized while capitalizing on the ability of a stiffer patch to reduce crack tip stresses.

2.6 References

ASTM D3039/D3039M-95a. 1995. "*Standard Test Method for Tensile Properties of Polymer Matrix Composite Materials.*" American Society for Testing and Materials, West Conshohocken, PA, U.S.A.

Baker, A.A. 1987. "*Fibre Composite Repair of Cracked Metallic Aircraft Components - Practical and Basic Aspects.*" Composites, Vol. 18, No. 4, pp. 293-308.

Chue, Ch.-H., W.-Ch. Chou, and Th. J.-Ch. Liu. 1996. "*The Effects of Size and Stacking Sequence of Composite Laminated Patch on Bonded Repair for Cracked Hole.*" Applied Composite Materials, Vol. 3, No. 6, pp. 335-367.

Hart-Smith, L.J. 1987. "*Joints.*" Engineered Materials Handbook, Volume 1: Composites, ASM International, pp. 479-495.

Hibbitt, Karlsson & Sorenson, Inc. 1996. "*ABAQUS Version 5.6.*" ABAQUS/Standard User's Manual Volumes I and II, Pawtucket, Rhode Island, USA.

Hibbitt, Karlsson & Sorenson, Inc. 1996. "*General Multi-point Constraints.*" ABAQUS/Standard User's Manual Volume II, ABAQUS Version 5.6, Pawtucket, Rhode Island, USA, pp. 20.2.2-1-20.2.2-30.

John, S.J. 1994. "*Predicting the Strength of Bonded Carbon Fibre/Epoxy Composite Joints.*" Composites Bonding, ASTM STP 1227, Ed. Dennis J. Damico, Thomas L. Wilkinson, Jr., and Sandra L.F. Niks. American Society for Testing and Materials, Philadelphia, pp. 45-59.

Karbhari, V.M., and S.B. Shulley. 1995. "*Use of Composites for Rehabilitation of Steel Structures—Determination of Bond Durability*". Journal of Materials in Civil Engineering, Vol.7, No. 4, ASCE, pp. 239-245.

Konur, O. and F.L. Matthews. 1989. "*Effect of the Properties of the Constituents on the Fatigue Performance of Composites: A Review.*" Composites, Vol. 20, No. 4, pp. 317-328.

Miller, Irwin, John E. Freund, and Richard A. Johnson. 1990. Probability and Statistics for Engineers, Fourth Edition. Prentice-Hall, Inc., Englewood Cliffs, New Jersey.

Naboulsi, S., and S. Mall. 1996. "*Modeling of a Cracked Metallic Structure With Bonded Composite Patch Using the Three Layer Technique.*" Composite Structures, Vol. 35, pp. 295-308.

Siener, M.P. 1992. "*Stress Field Sensitivity of a Composite Patch Repair as a Result of Varying Patch Thickness.*" Composite Materials: Testing and Design (Tenth Volume), ASTM STP 1120, Glen C. Grimes, Ed. American Society of Testing and Materials, Philadelphia, pp. 444-464.

3 STRESS DISTRIBUTION IN A BONDED PATCH - EXPERIMENTAL PROGRAM

In a cracked element, all stresses must flow around the crack, inducing high stress concentrations at the crack tip that are responsible for crack propagation. When a patch is applied to the cracked area, the stress flow patterns change, affecting the mechanisms of crack growth. New stress concentrations are also introduced by patching; these may cause new crack formations when subjected to fatigue loading. An experimental program was conducted to study the stress distribution in a patched element, and the effect of varying patch dimensions and stiffness on that stress distribution. A numerical program was also conducted, the results of which are presented in Chapter 4.

3.1 Experimental Design

3.1.1 Test Specimens

Eleven tests were performed to study the effects of patching on stress distribution through a cracked plate. All specimens were 6.35 mm (1/4 in.), 300 MPa steel plate, 400 mm wide by 750 mm long outside dimensions. The gripping mechanism consisted of a narrow, 31.75 mm (1 ¼ in.) thick plate gripped by the MTS machine, which was spliced to the specimen by two 12.7 mm (1/2 in.) plates at each end. The system, shown in Figure 3.1 attempted to provide a uniform stress distribution across the end of the plate.

A through-thickness saw cut 80 mm wide was made in the center of each plate, representative of a crack. The saw cut radiated from an 8 mm diameter hole drilled in the center of the plate. Ten of the "cracked" plates were then patched on one side with carbon fibre composites prior to testing. The final plate was tested without a patch for reference. A schematic diagram of a test specimen is shown in Figure 3.2. Note that for the internal crack being considered, the total patch width is 2w, the patch length is 2L, and the total crack length is 2a, but reference to patch dimensions is commonly to the

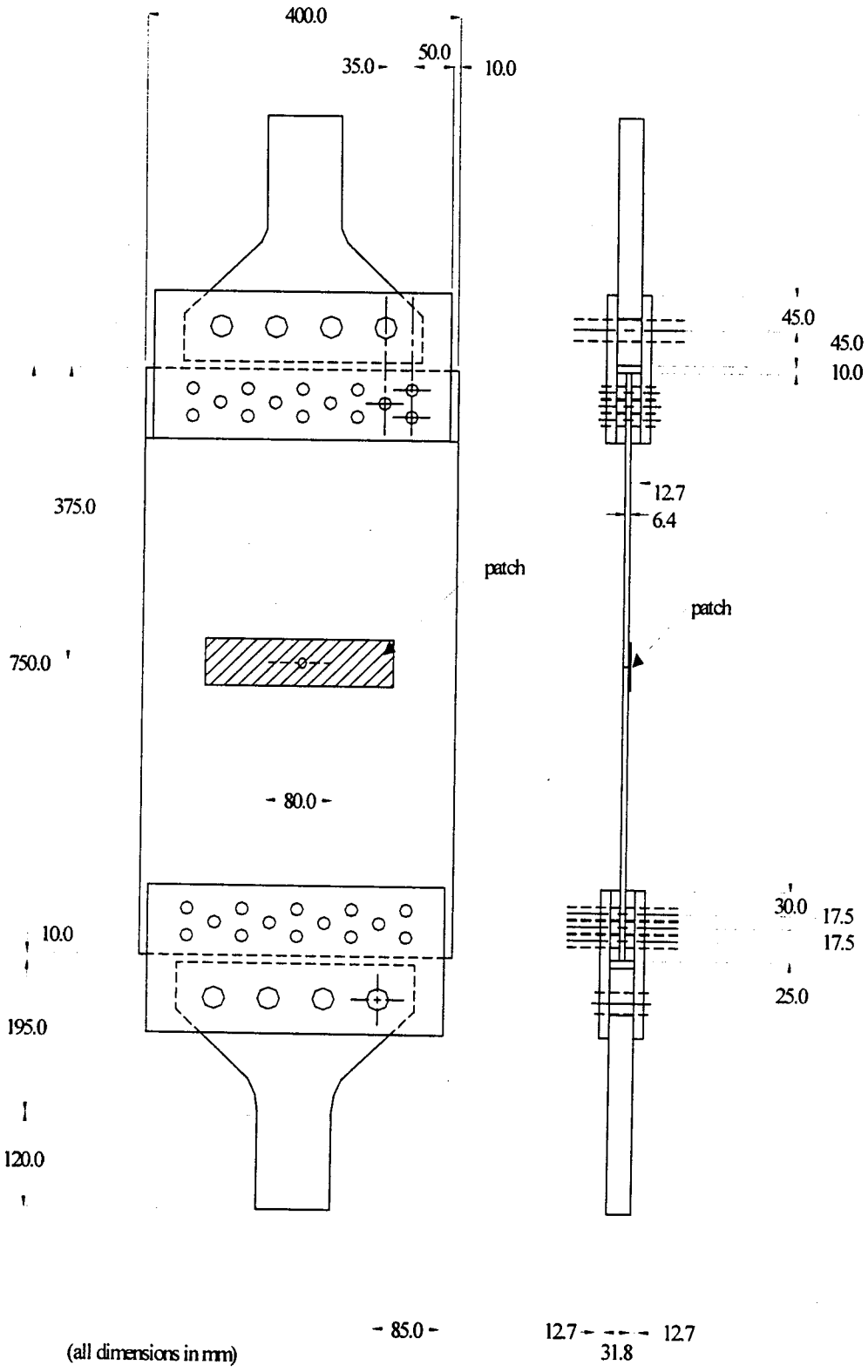

Figure 3.1 Experimental setup, bonded patch tests

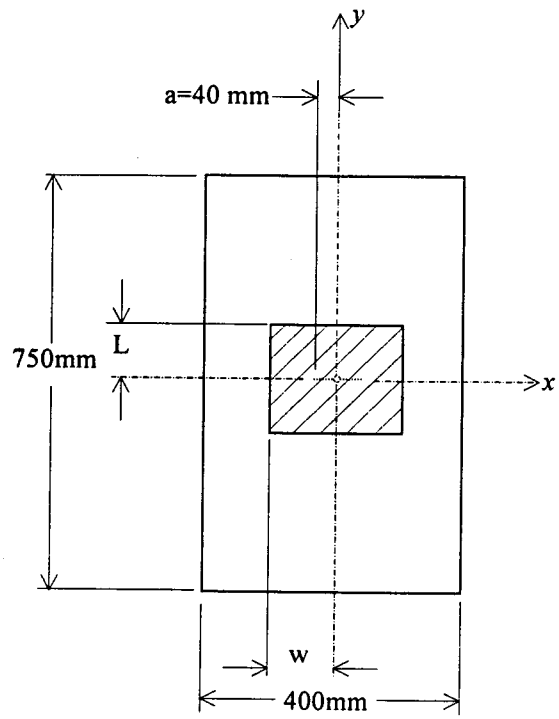

Figure 3.2 Schematic diagram of bonded patch test specimens

"half-parameters" L, w, and a. The *x*-axis represents the horizontal centerline of the plate, and the *y*-axis the vertical centerline.

Six layers of fiber were applied to the majority of the specimens, providing a patch to adherend stiffness ratio, $E_p t_p / E_s t_s$, of 0.16. To obtain results for a different stiffness ratio, some were patched with only four layers of fibre. Three different bond lengths, L, were tested: 20 mm, 30 mm, and 100 mm. The first two lengths were chosen to be near the anticipated minimum bond length based on the bonded joint study, and the third long enough to ensure a strain compatibility plateau would be developed and could be observed with strain gauge readings. Three patch widths, w, were also tested: 80 mm, 120 mm, and 160 mm.

All investigations reviewed in the references used a tapered patch. Baker (1987) suggested that a 5° taper angle should be used. On tests with three layers of composite

fibre, Roberts (1995) staggered the end of each layer by 5 mm, equivalent to a taper angle of 2.9°. Schubbe and Mall (1997), in testing thick patches and adherends, tapered the patches over 18 mm, 1 mm/layer (7.2° taper angle). For this test series, eight of the test patches had 5 mm/layer (2.6°) taper on both edges perpendicular to the applied load. The remaining two specimens had a 3 mm/layer (4.4°) taper on one of these edges and a 20 mm/layer (0.7°) taper on the other. Taper results are discussed in Chapter 5.

Rectangular patches were used for six tests, while the remaining four had patches that were rectangular above the crack and elliptical below. Patch shape results are also discussed in Chapter 5.

Table 3.1 summarizes the patches used for each test specimen. Tests were designated with a four character name: R*wln* or M*wln* where R or M indicated a rectangular or mixed shape patch; *w* was a number 1-3 indicating which width was used, 1 being the widest; *l* was a number 1-3 indicating which length was used, 1 being the longest; and *n* was 4 or 6 depending on the number of layers of composite applied.

Table 3.1 Summary of test specimen variables for bonded patch specimens

Specimen	Length, L (mm)	Width, w (mm)	Layers, n	Taper (mm)		Shape
				top	bottom	
R116	100	160	6	5	5	Rectangular
M216	100	120	6	5	5	Mixed
M214	100	120	4	5	5	Mixed
M316	100	80	6	5	5	Mixed
M314	100	80	4	5	5	Mixed
R226	30	120	6	3	20	Rectangular
R224	30	120	4	5	5	Rectangular
R326	30	80	6	5	5	Rectangular
R324	30	80	4	3	20	Rectangular
R336	20	80	6	5	5	Rectangular

The carbon fibre sheet and the epoxy used in this test series were the same as for the bonded joint tests. Tensile coupon test results and the calculated material properties for the composite material were presented in Table 2.2.

3.1.2 Instrumentation and Test Protocol

The tests were conducted in the MTS 1000 machine at the I.F. Morrison Structures Lab, University of Alberta. Each specimen was loaded at a stroke-controlled rate of 1 mm/min, and the tests were stopped when the applied load reached approximately 650 kN, equivalent to a far field stress of about 250 MPa. At this point the load-stroke curve from the MTS machine began to reflect some yielding (see Figure 3.3).

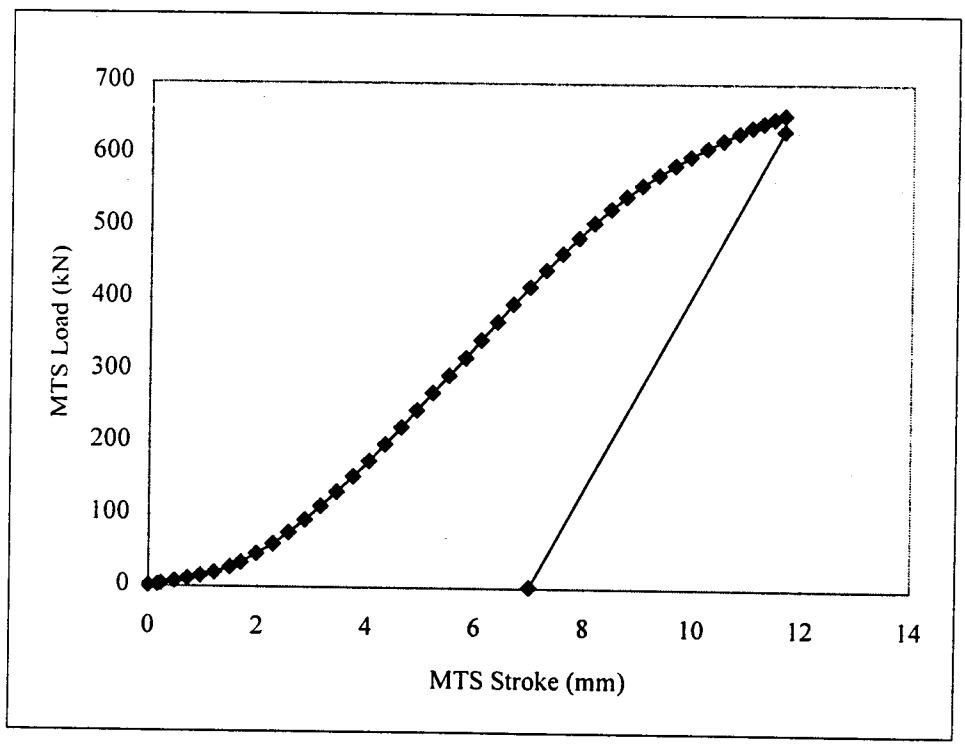

Figure 3.3 Typical load versus stroke curve for bonded patch test

A Fluke data acquisition system was used to measure strains from gauges applied to the specimen. Eighteen to twenty-five gauges were applied to each specimen, on the both the patched and unpatched surfaces. The locations of strain gauges for each specimen are

presented in section 3.2 (Figures 3.6-3.16). Gauges were either 2 mm or 5 mm, corresponding to regions of suspected high strain gradient or relatively constant strain respectively. Figure 3.4 shows a gauged test plate.

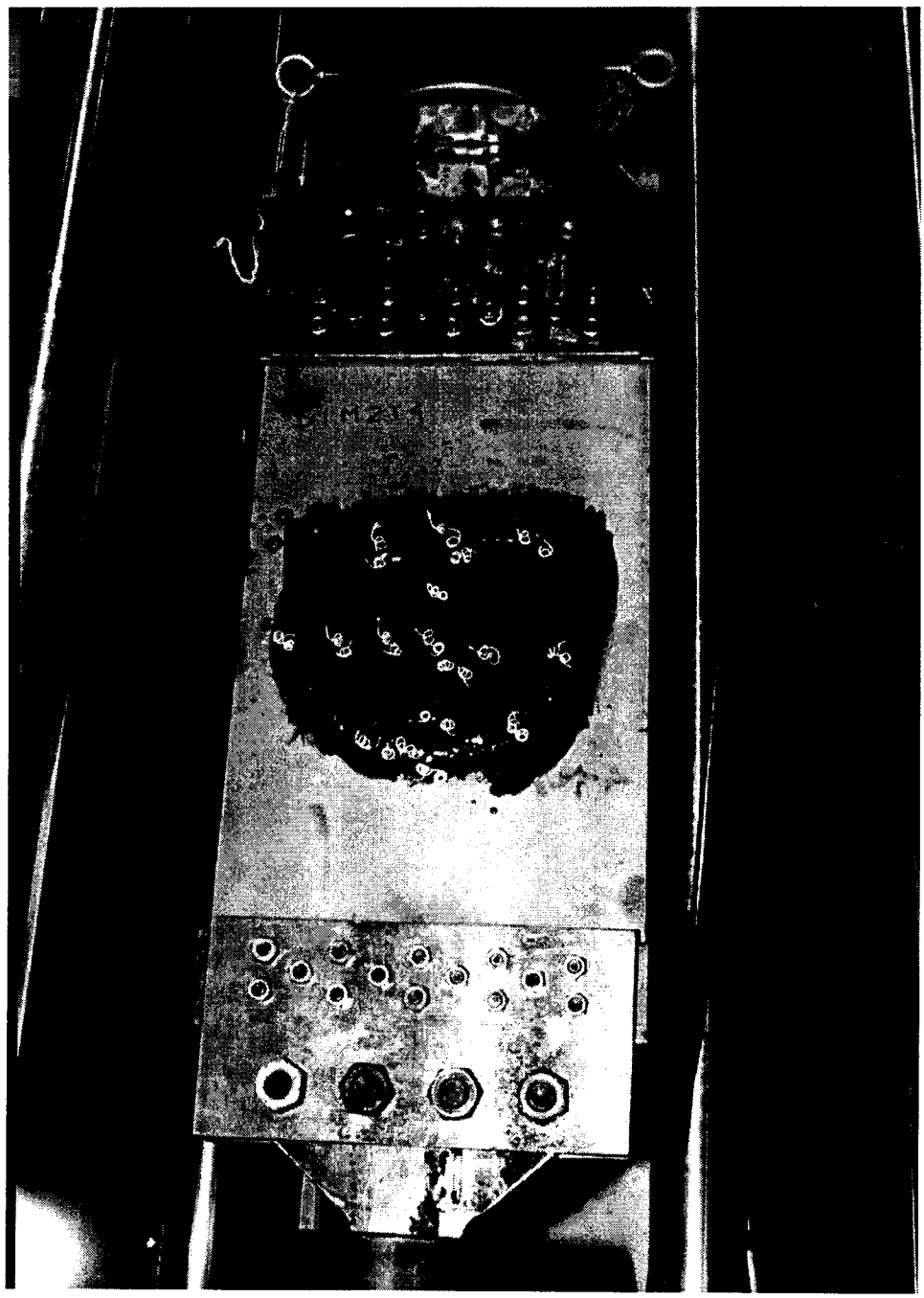

Figure 3.4 Typical gauged specimen, bonded patch test

An electronic demec gauge mechanism was also used for each test. Demec points were attached to the unpatched face of the plate along the vertical centerline. The points were centered across the crack at a gauge length of 98 mm. A modified demec gauge equipped with an LVDT was held in place by a compressed spring, mounted in a wooden frame that was clamped to the test specimen. Readings were taken electronically throughout the test. Figure 3.5 shows a sketch of the demec apparatus and a photo taken during a test.

3.2 Experimental Results

A typical plot of applied load versus stroke as recorded by the MTS machine is shown in Figure 3.3. The plot initially showed a low slope, while the bolted connections were seating and the plate was being straightened. This was followed by a region of linear elastic response to increasing load, and finally by a decreasing slope as yielding began. The smallest net cross-section in the plate was through the bolted connection, so it was anticipated that this would be the area to yield first and it would not be possible to test the plates to failure in the patched crack. Examination of the specimens after testing and low measured strains over most of the patched region confirmed the yielding was in the bolted connection.

In all cases, loading produced no visible damage to the patch. Yielding was seen in the plate at the bolt holes, and some flaking of the scale on the unpatched surface was noted. This flaking did not constitute notable yield line patterns, but was generally observed within a 25 mm to 50 mm radius around both crack tips. No signs of applied load were visible on plates with a painted unpatched surface, or on the sandblasted surfaces of the plates.

Specimen R336 was the only test with a patch length, L, of 20 mm. While this dimension was chosen to test the effects of a short patch length, it was found that a patch this short cannot be applied accurately. Because the composite is unidirectional, the only shear resistance in the fibre direction of the carbon fibre sheet is due to friction between fibres.

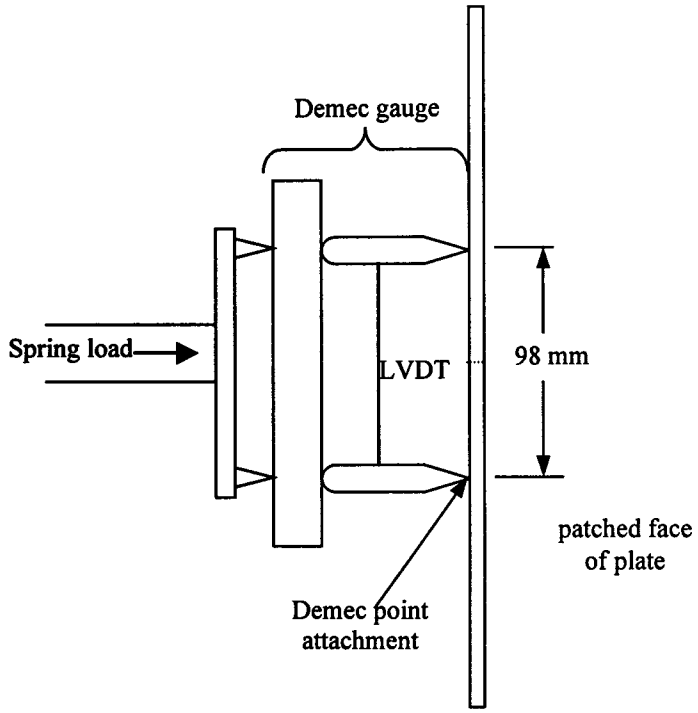

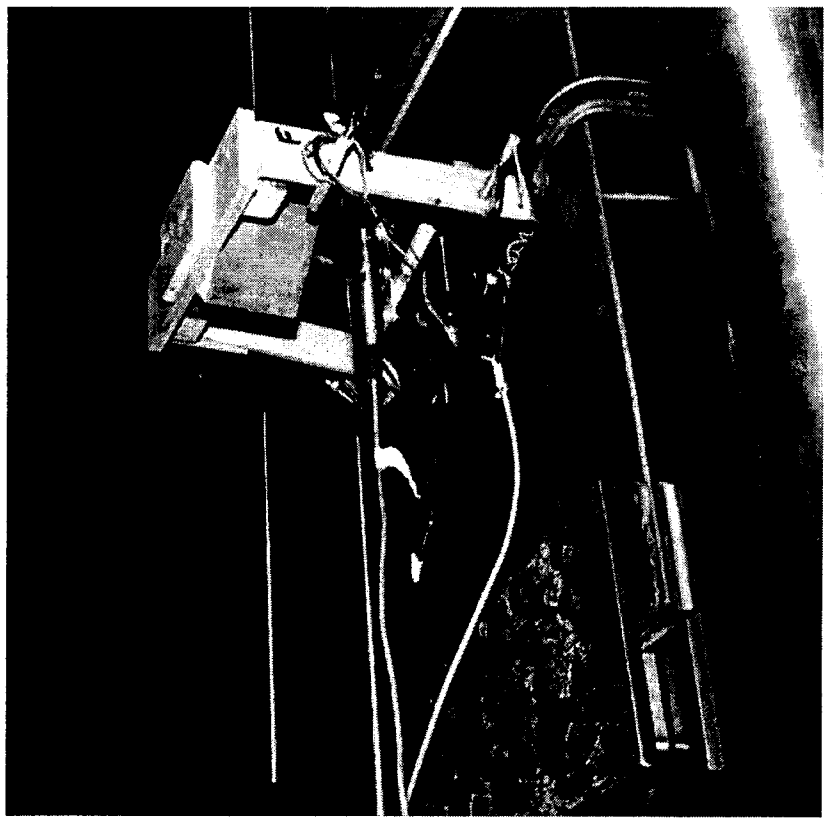

Figure 3.5 Electronic demec gauge apparatus

This lack of resistance was a problem when applying a short patch, as application of the epoxy tended to split the composite in the longitudinal direction. This caused discontinuities within individual patch layers and misalignment both within a patch layer and between layers. The strain gauge readings for R336 were erratic and difficult to interpret as the patch was not symmetrical as planned, and the results from this specimen were rejected. It is not recommended that a patch length shorter than 30 mm be used for practical fabrication reasons, regardless of the minimum required bond length.

3.2.1 Strain Gauge Results

An applied load of 254 kN, which corresponds to a far field stress of 100 MPa, was chosen as the basis for manipulation and comparison of test data. Figure 3.3 indicates the overall response of the patched plate is linear at this point.

Figure 3.6 shows the experimental strains for test R116 at 100 MPa far field applied stress. Part (a) of the figure shows the results for the patched face and has three parts: the strains as measured at the pictorially represented gauge locations, the strain distribution across the width of the plate, and the strain distribution along the plate length.

In the upper left part of the figure, strain gauge output is shown in italics adjacent to the marked gauge locations. The values shown are in microstrain ($x10^{-6}$ mm/mm). Only half of the plate is shown to take advantage of symmetry–while gauges may have been on either side of the vertical centerline, they are all represented as being in the positive x quadrants. All gauges measured strain in the longitudinal or loading direction. The crack location is shown and dimensions of the patch from Table 3.1 can be related to the variables shown in the figure.

On the right hand side of the figure, the strain distribution along the plate length is shown. Because of the difficulty in placing strain gauges very close together, a band 40 mm wide was used for the placement of gauges to define behaviour along the centerline.

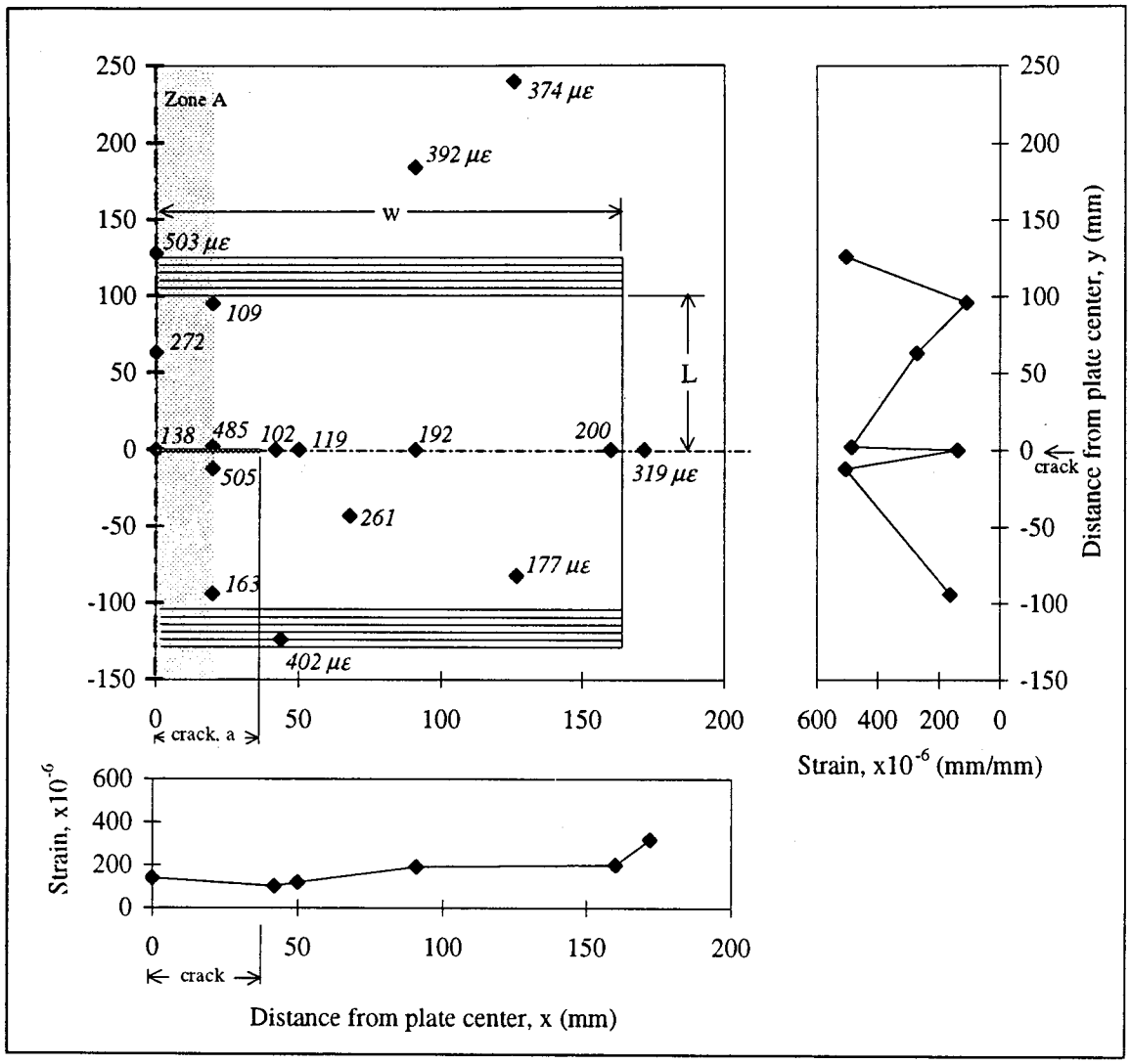

(a) Strain data for patched face

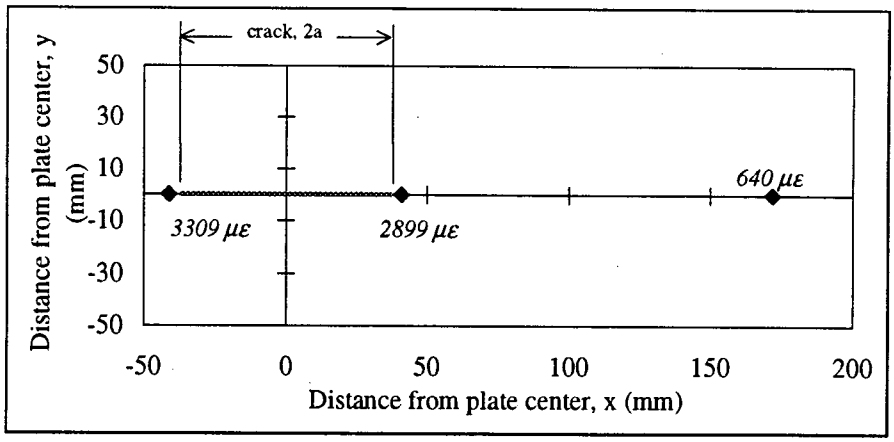

(b) Strain data for unpatched face

Figure 3.6 Experimental strain data for R116 at 100 MPa far field stress

This band is indicated as Zone A on the figure, and all gauges within this zone were used to generate the strain distribution plot along the plate length, neglecting their horizontal location.

The final portion of part (a) of the figure, on the bottom, shows the change in longitudinal strain across the plate width. Only gauges located on the horizontal centerline were used for this plot.

Figure 3.6(b) shows the strain output for gauges on the unpatched face of the plate. Gauges were mounted at both crack tips, so the plot does not incorporate symmetry in order to show both results. While these gauges were placed as close as possible to the crack tip, the distance from the end of the crack to the centerline of the gauge varied from 1 to 2 mm.

Output for all other patched tests is shown in Figure 3.7 to Figure 3.14. Where two output values are shown separated by a comma and adjacent to a single gauge marker (Figure 3.11 and Figure 3.14), gauges were installed at the same relative location on both sides of the vertical centerline.

Figure 3.15 shows the results for the unpatched test. In this figure, the front face refers to the face with the majority of the gauges; the back face had the electronic demec gauge. The plate was bi-symmetrical about both the horizontal and vertical centerlines, so only one quarter of the plate is shown. Again output separated by a comma indicates gauges at the same absolute coordinate location.

To illustrate the difference in strains with a change in load, Figure 3.16 presents the data for R116 at 200 MPa far field stress. Comparing this figure with Figure 3.6, in particular the strain distributions of part (a), it is seen that the shape of the distribution changed very little. This suggests the response was mostly elastic in the range of 100 MPa to 200 MPa

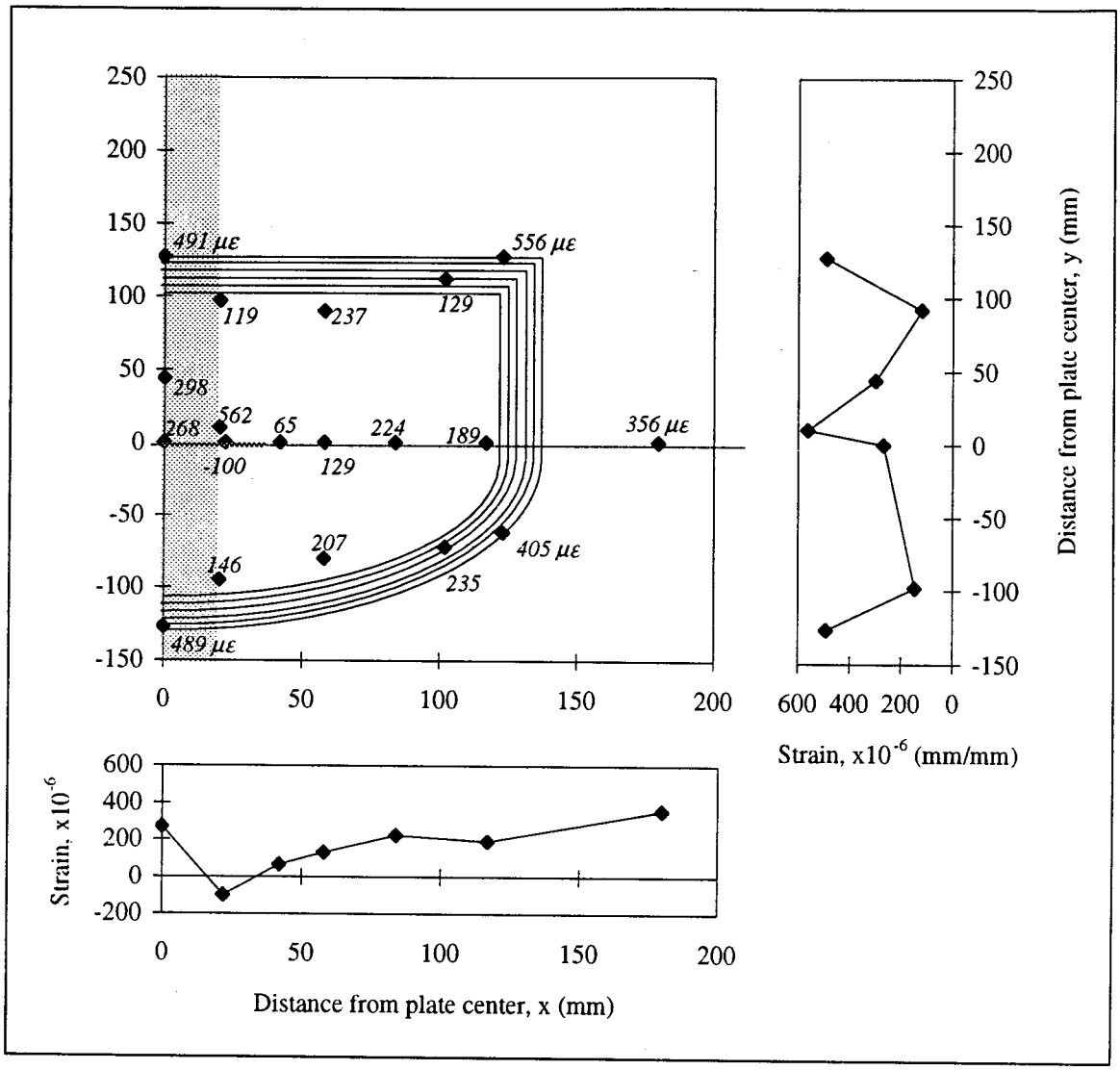

(a) Strain data for patched face

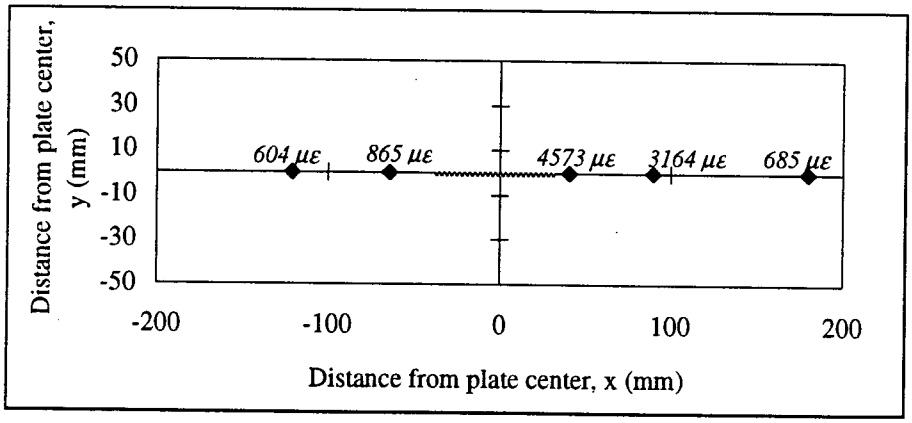

(b) Strain data for unpatched face

Figure 3.7 Experimental strain data for M216 at 100 MPa far field stress

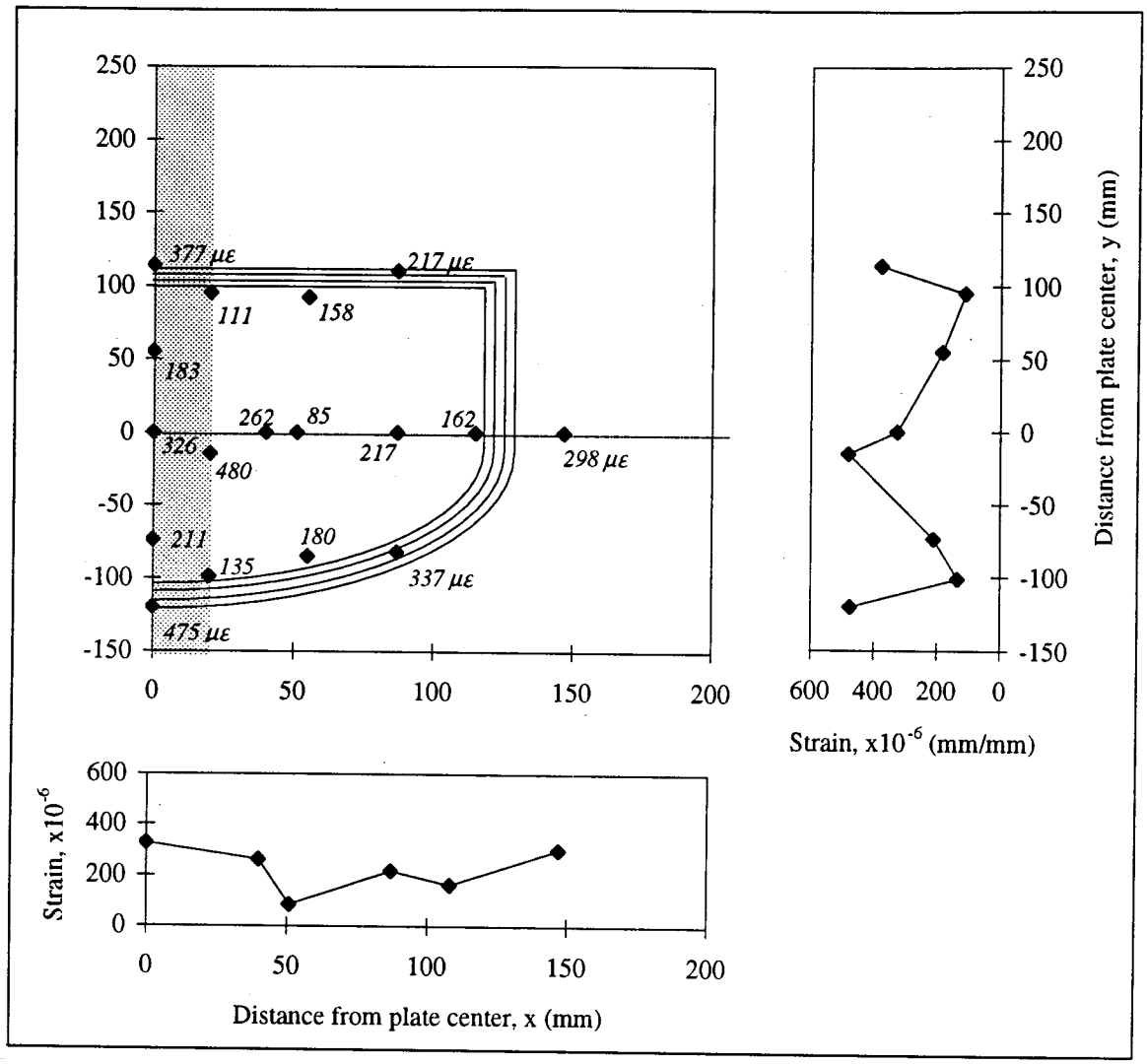

(a) Strain data for patched face

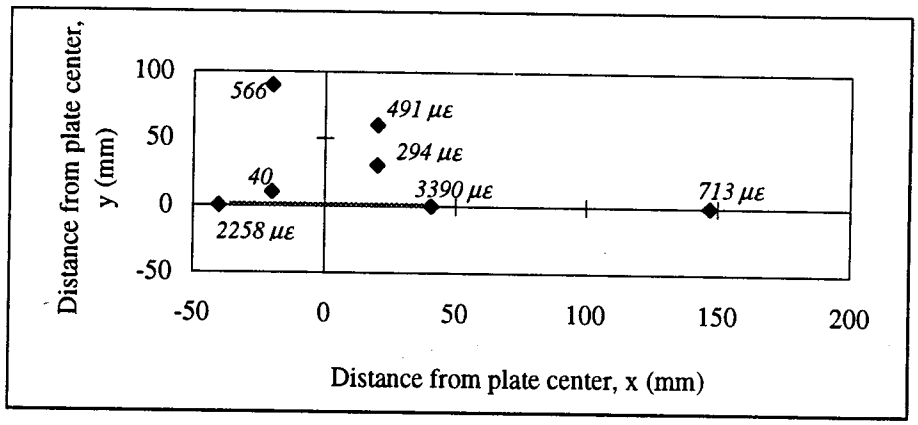

(b) Strain data for unpatched face

Figure 3.8 Experimental strain data for M214 at 100 MPa far field stress

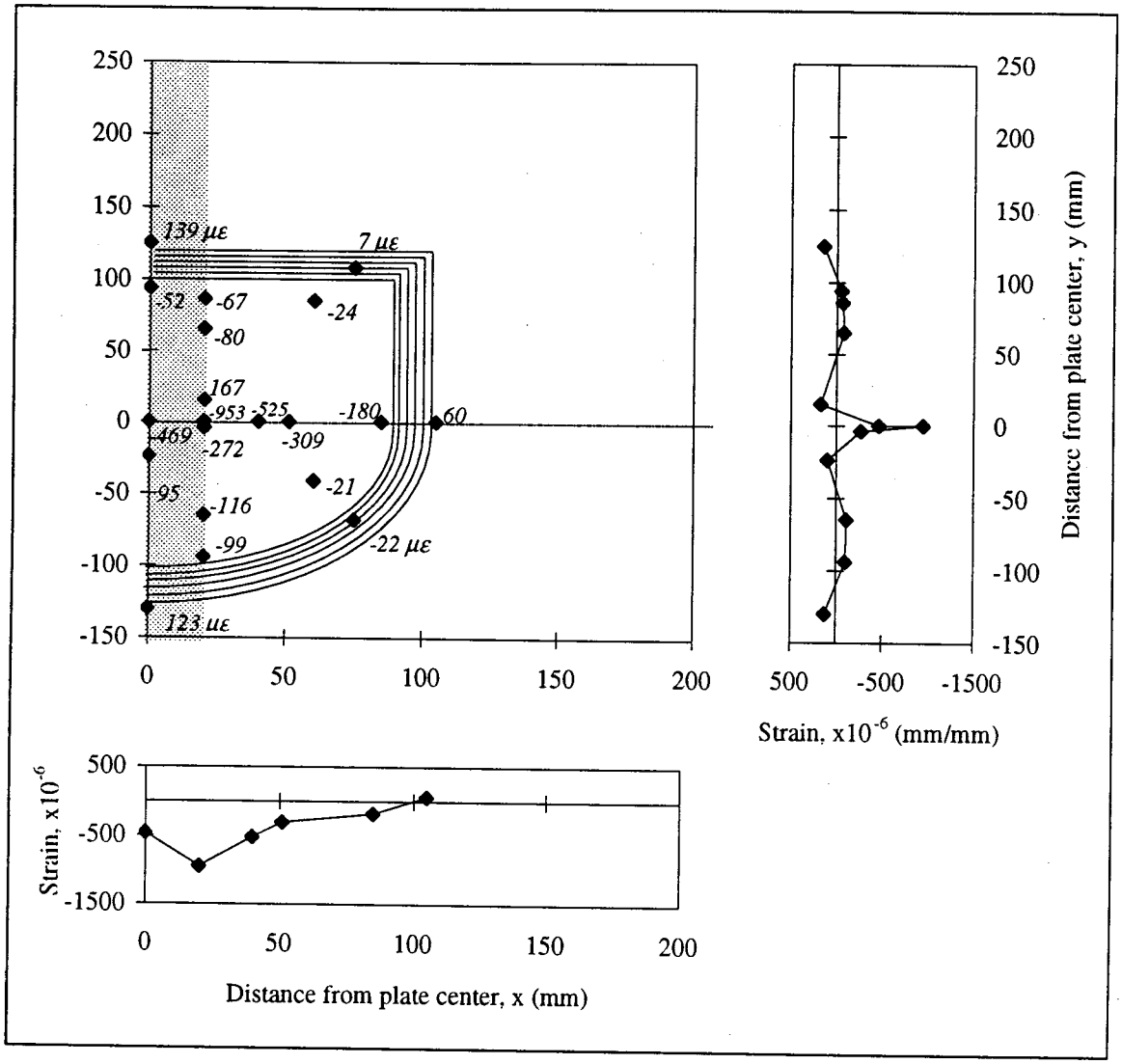

(a) Strain data for patched face

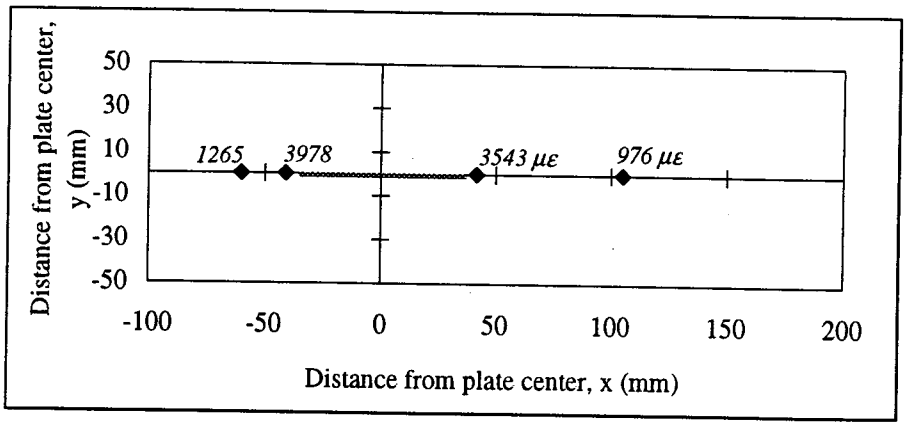

(b) Strain data for unpatched face

Figure 3.9 Experimental strain data for M316 at 100 MPa far field stress

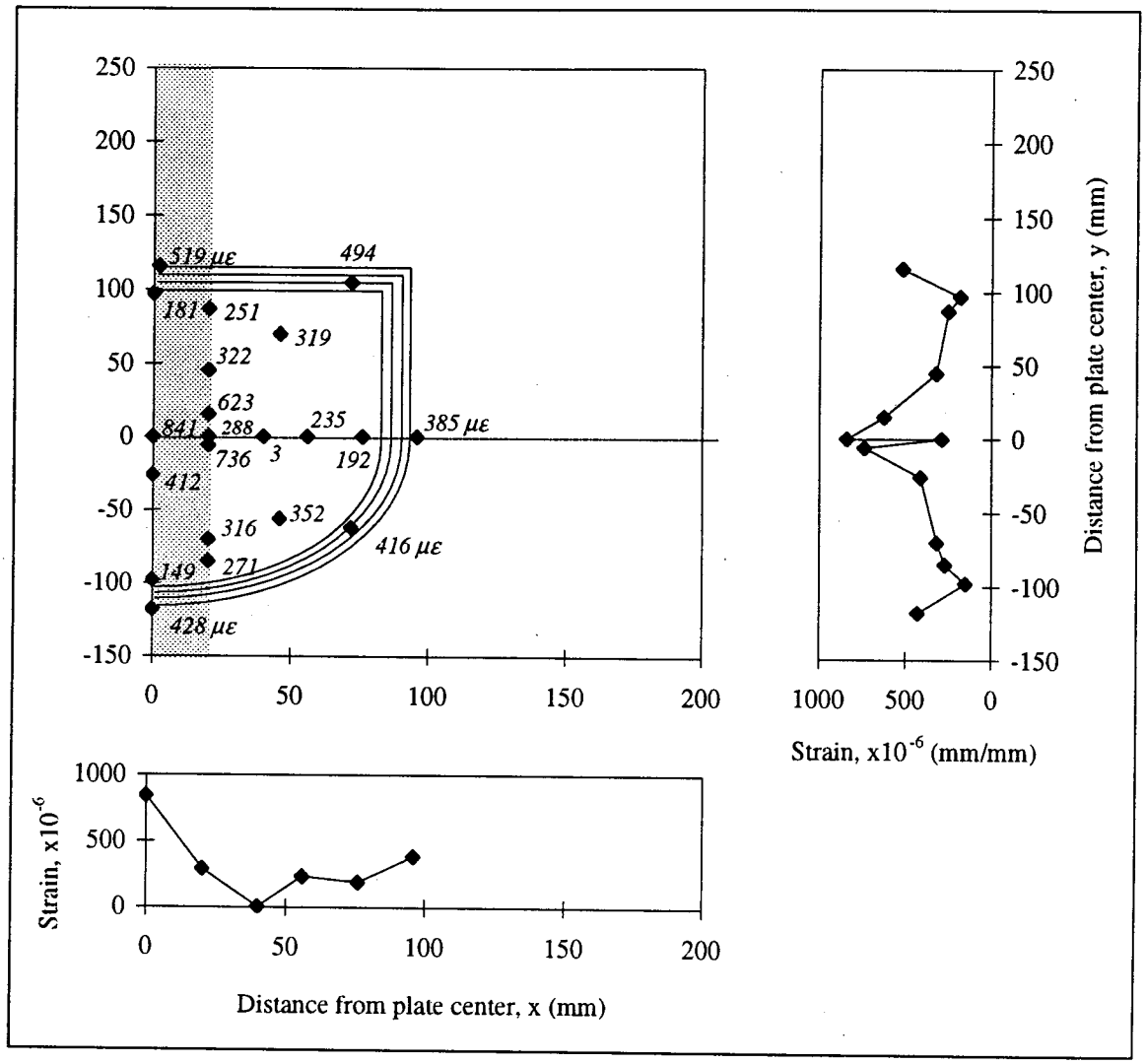

(a) Strain data for patched face

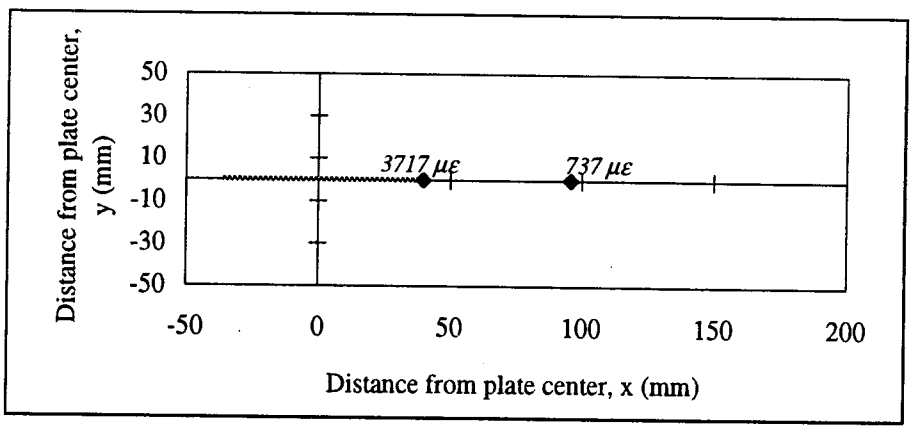

(b) Strain data for unpatched face

Figure 3.10 Experimental strain data for M314 at 100 MPa far field stress

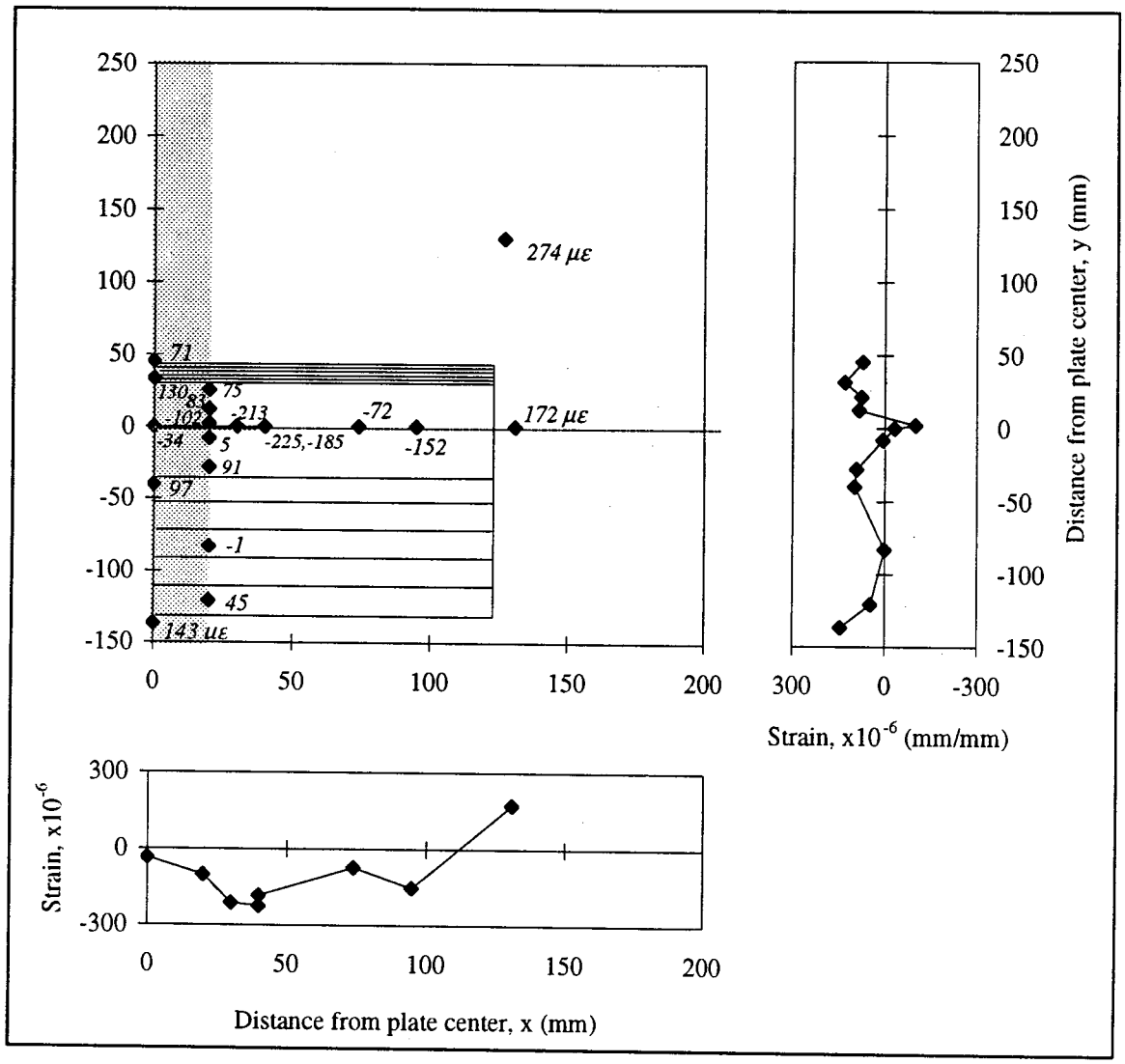

(a) Strain data for patched face

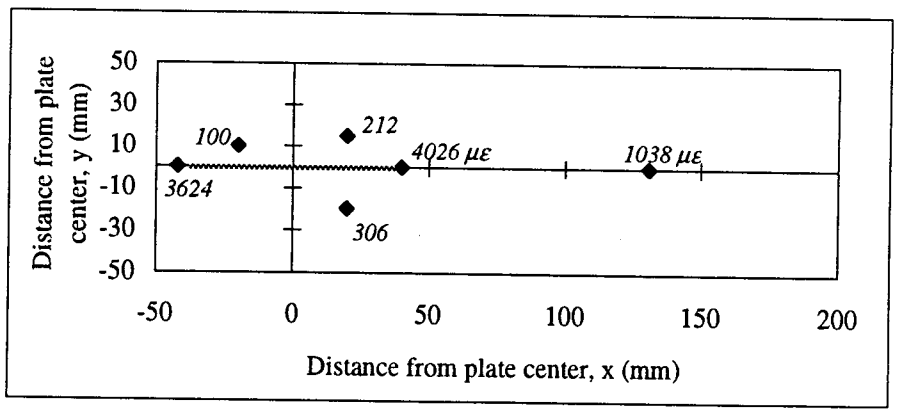

(b) Strain data for unpatched face

Figure 3.11 Experimental strain data for R226 at 100 MPa far field stress

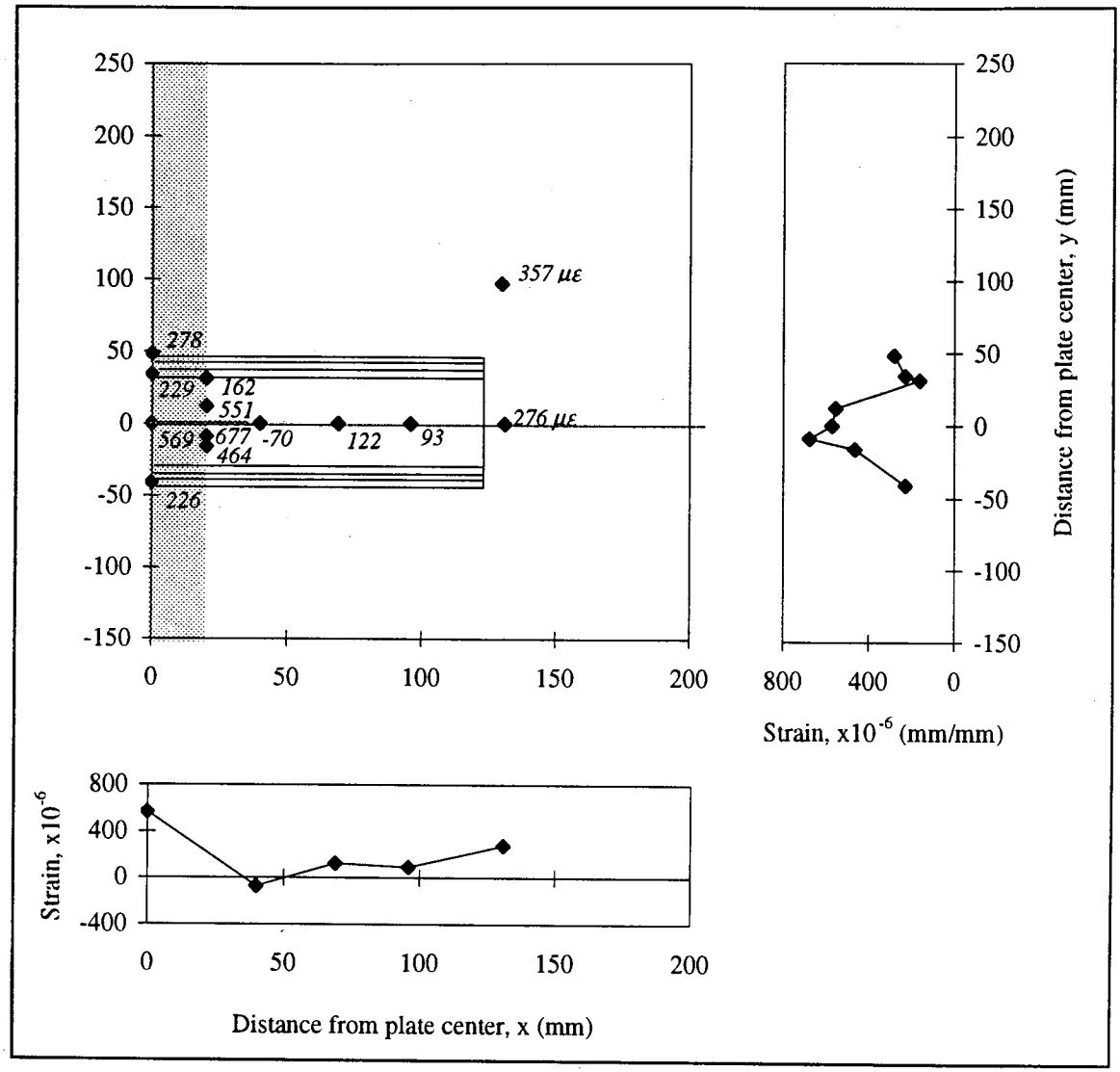

(a) Strain data for patched face

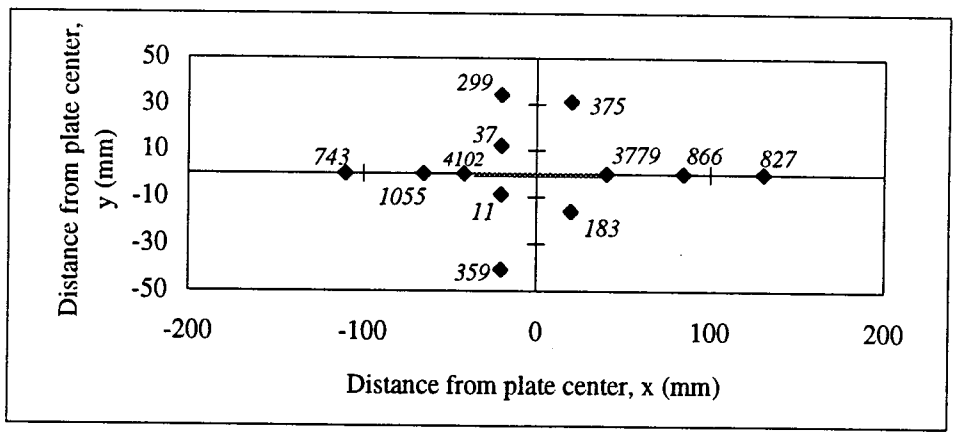

(b) Strain data for unpatched face

Figure 3.12 Experimental strain data for R224 at 100 MPa far field stress

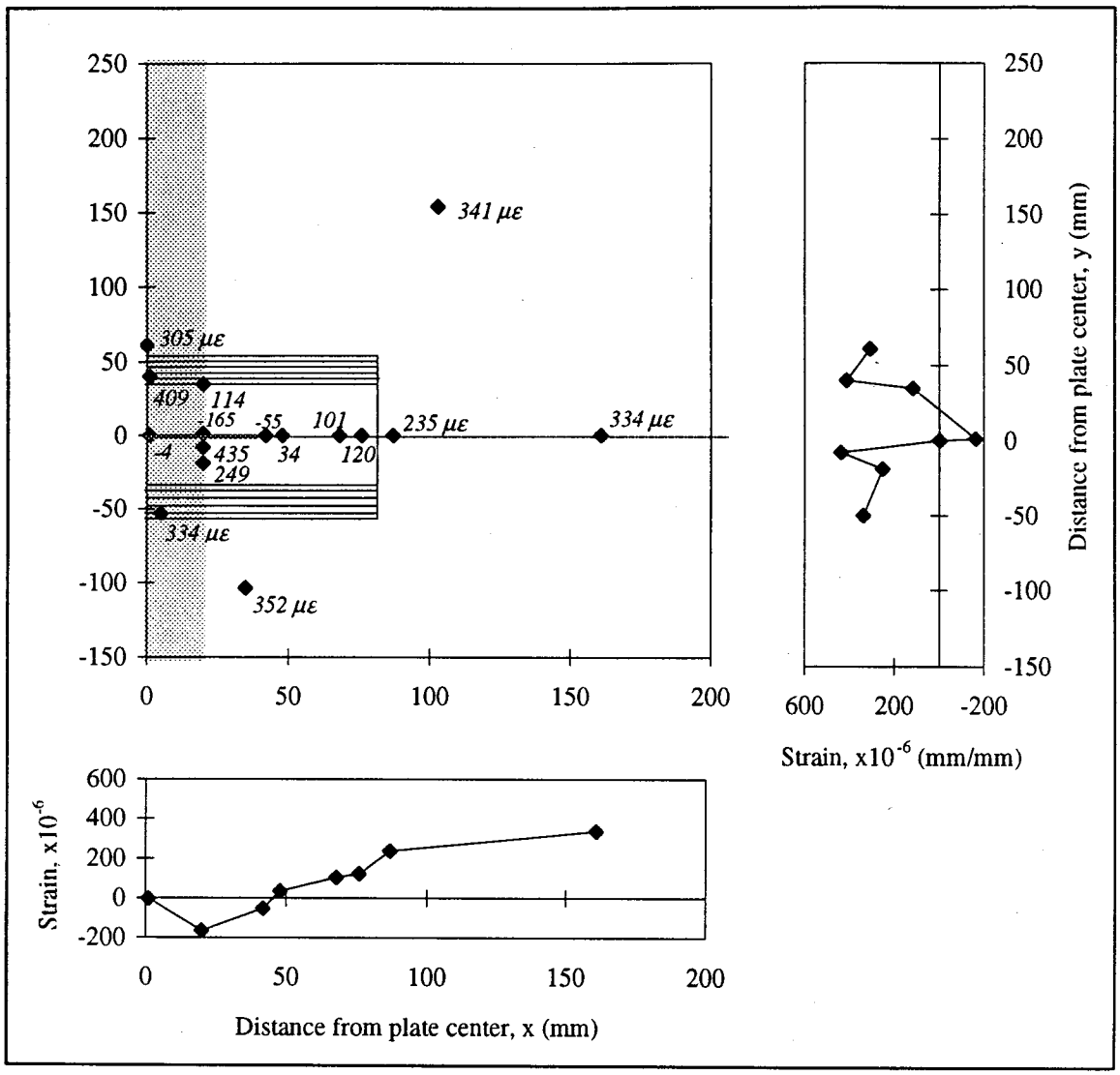

(a) Strain data for patched face

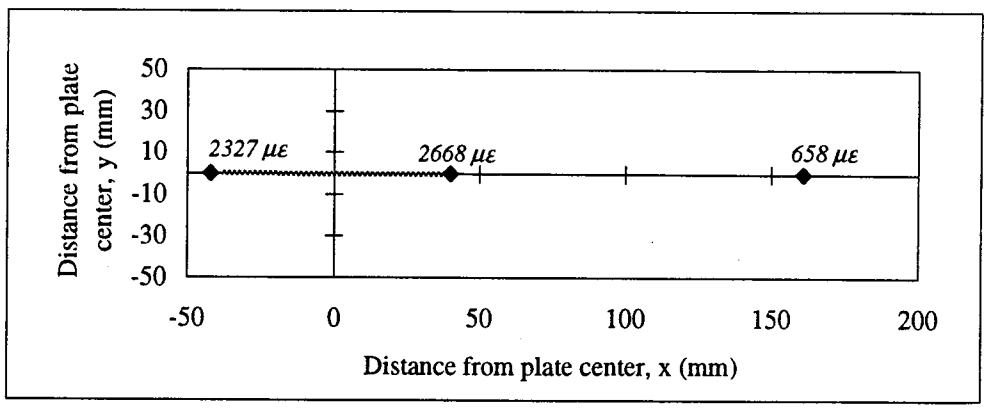

(b) Strain data for unpatched face

Figure 3.13 Experimental strain data for R326 at 100 MPa far field stress

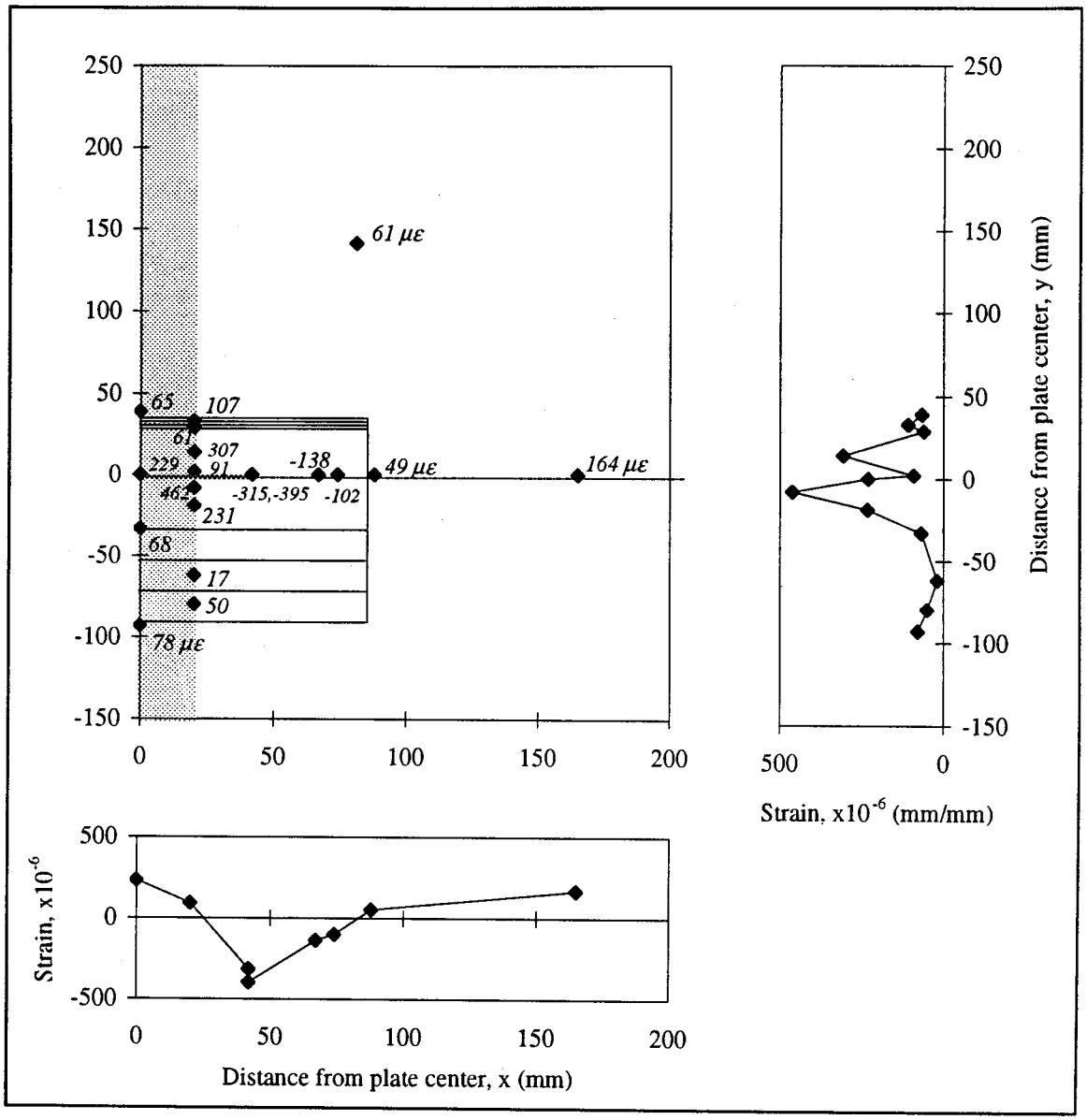

(a) Strain data for patched face

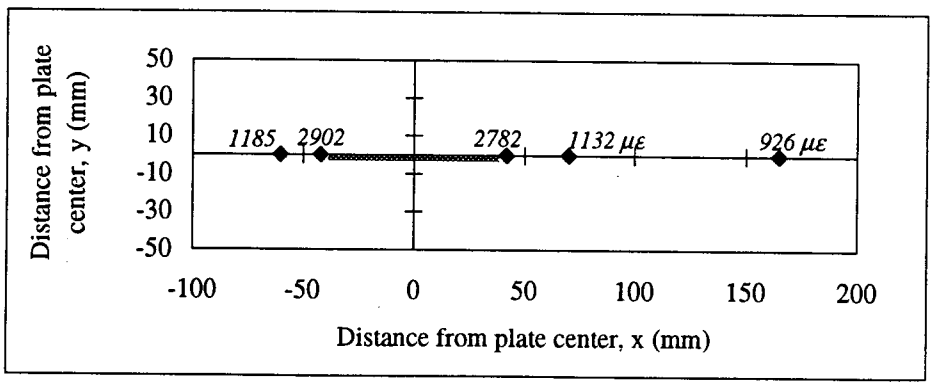

(b) Strain data for unpatched face

Figure 3.14 Experimental strain data for R324 at 100 MPa far field stress

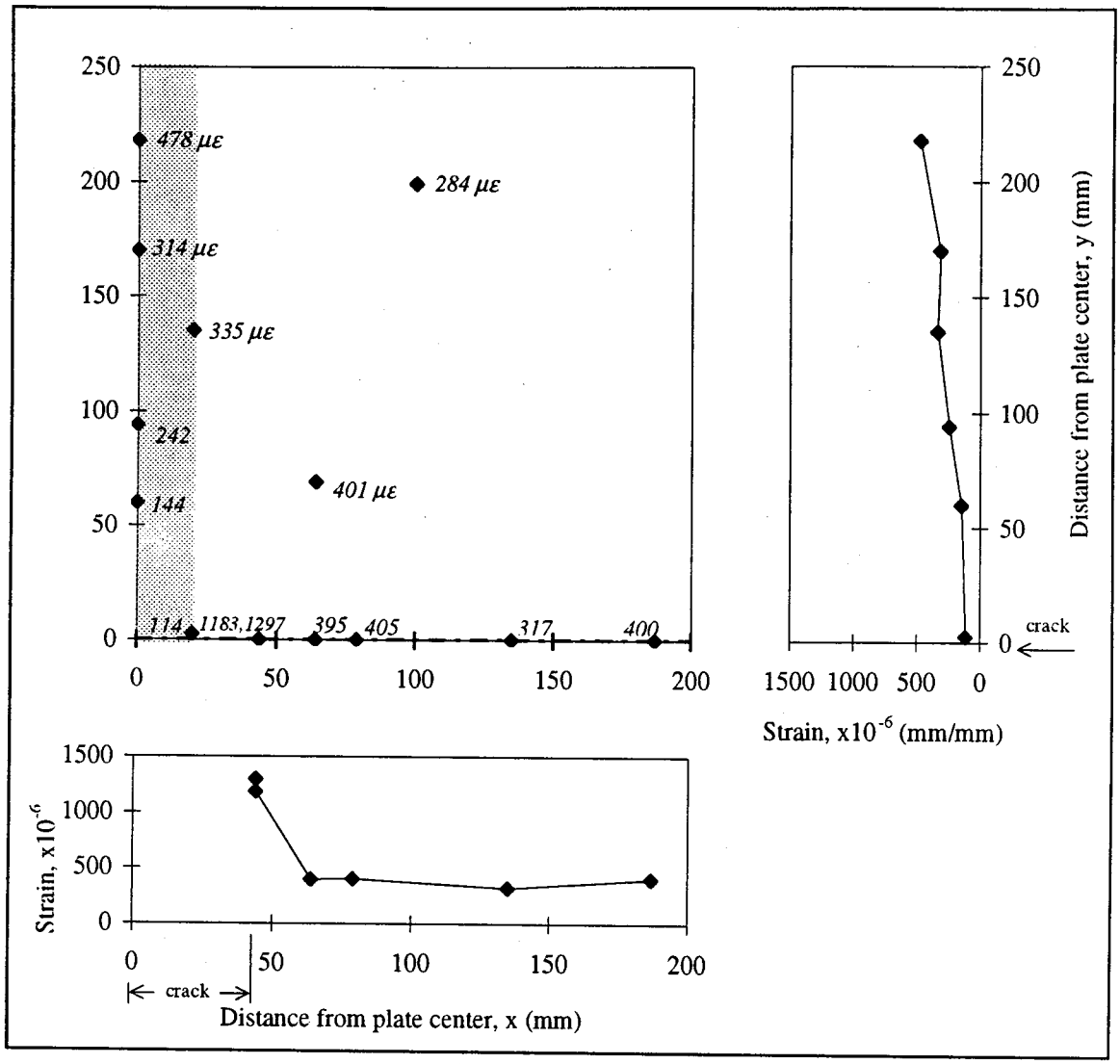

(a) Strain data for front face

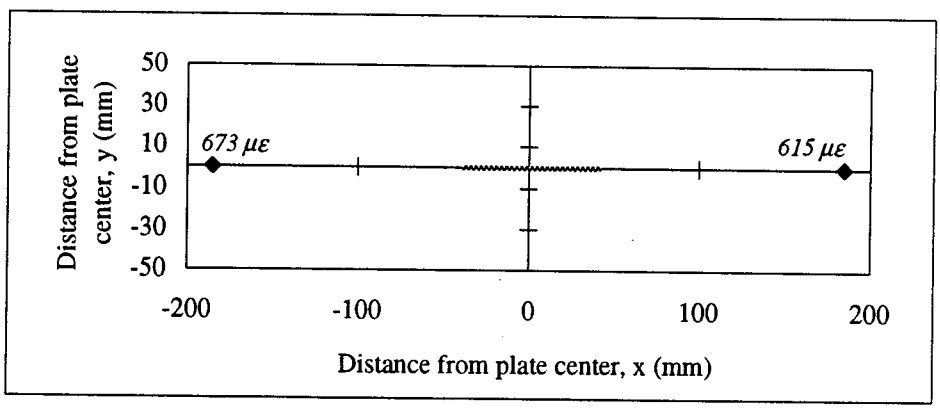

(b) Strain data for back face

Figure 3.15 Experimental strain data for unpatched plate at 100 MPa far field stress

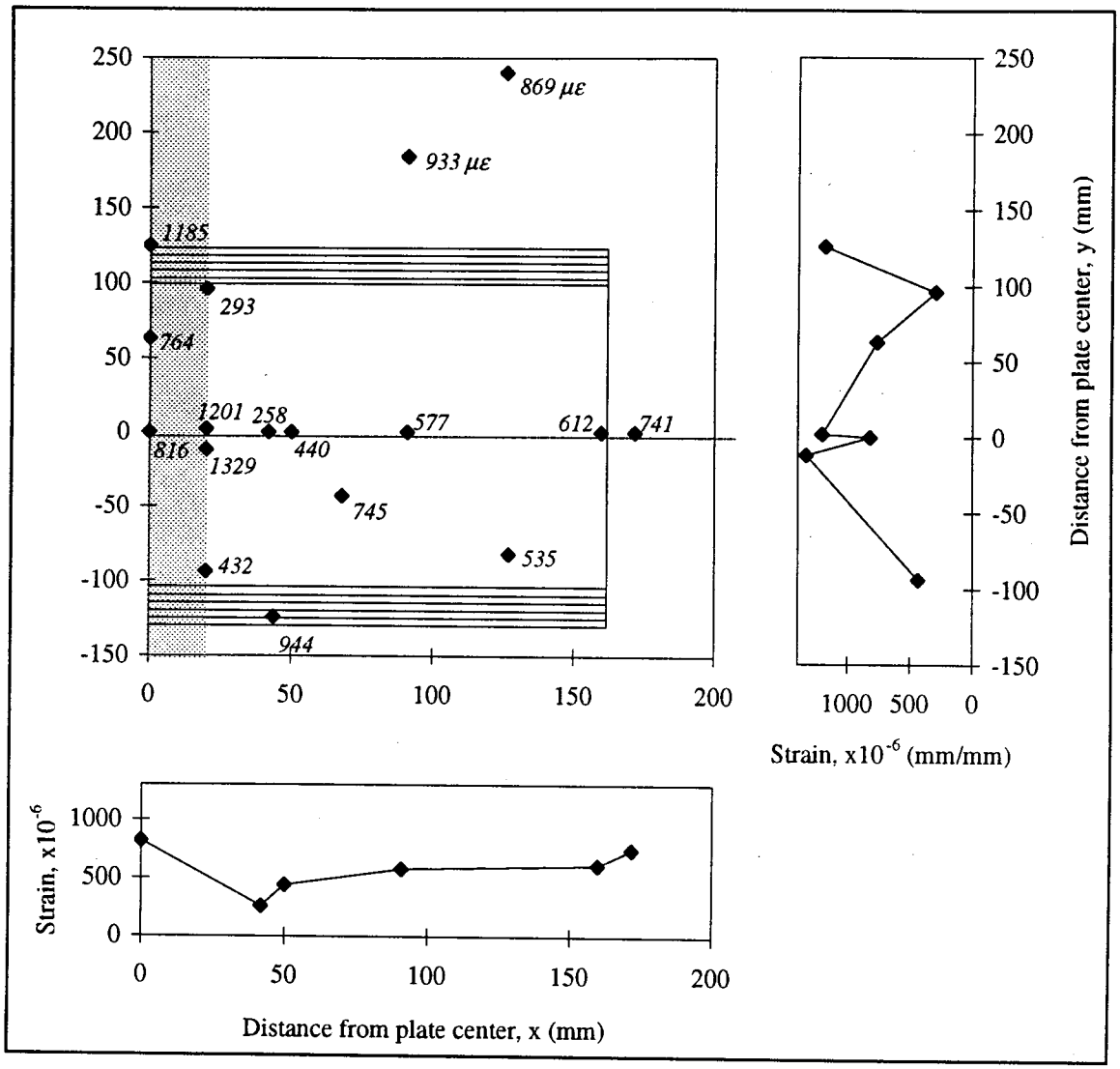

(a) Strain data for patched face

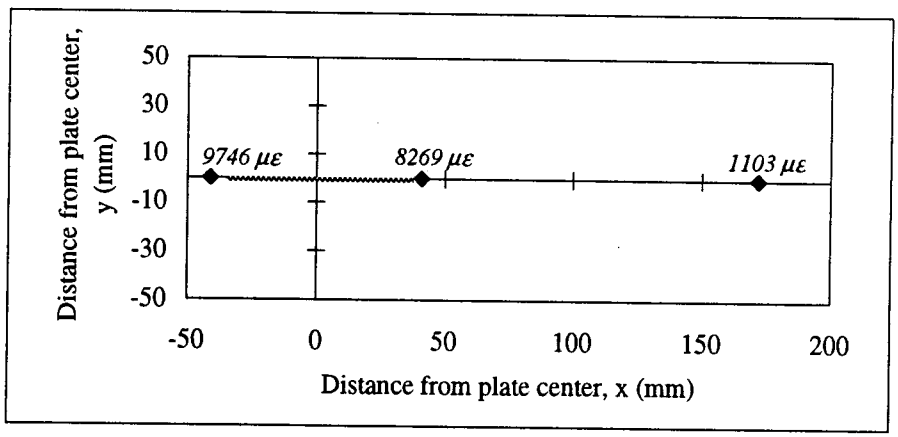

(b) Strain data for unpatched face

Figure 3.16 Experimental strain data for R116 at 200 MPa far field stress

applied stress. One exception to this observation was the substantial increase in strain seen at the gauge in the center of the plate. This discrepancy may be due to the fact that the gauge was located on the patch where it spanned across the crack.

3.2.2 Demec Results

Strains measured across the crack by the electronic demec gauge are shown in Figure 3.17. All tests were referred to by a four-character name, with the first three characters defining the patch dimensions and the fourth the number of layers. Patches for tests with the same first three characters were therefore the same size and shape, and differed only in the number of layers of composite applied. Figure 3.17 categorizes the demec results for different sized patches, identifying each category by the first three characters of the test designation. Different bars within each category show the results for four- and six-layer tests.

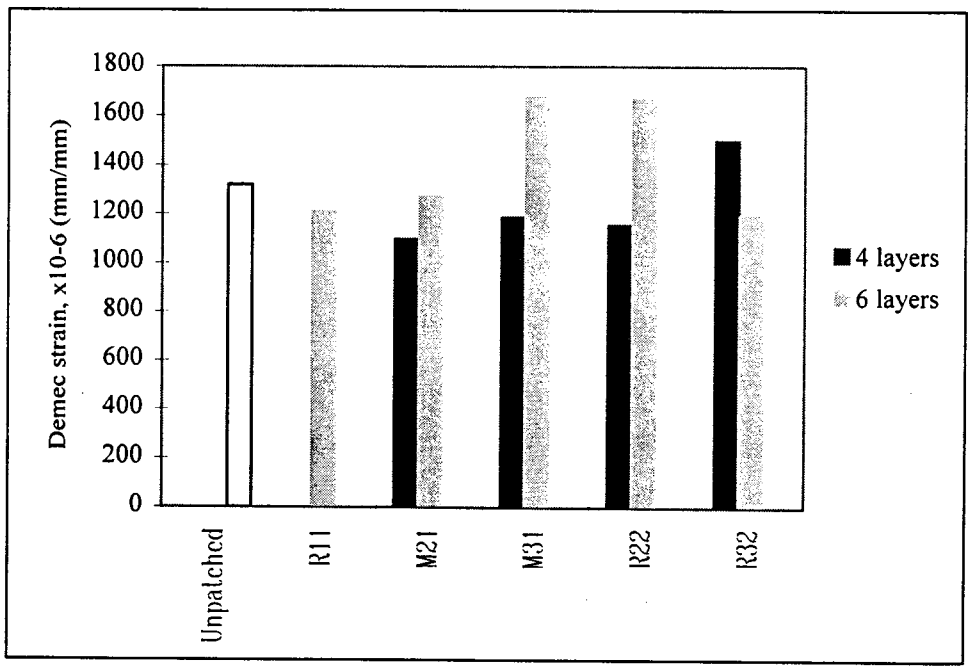

Figure 3.17 Demec strain results for bonded patch tests at 100 MPa far field stress

3.3 Discussion of Test Results

3.3.1 Initial Curvature of Plates

The strain gauge and demec results presented above were corrected to zero at zero loading, but otherwise are the raw data values. It must be noted that the plates were not initially flat - they all had some curvature about the x-axis. The plates were convex towards the patched face, so that tensile loading initially induced compressive stresses on the patched face, and additional tensile stresses on the unpatched face. For the unpatched test, the compressive strains were induced on the front or gauged face, and additional tensile stresses were induced on the back face. The amount of curvature varied among plates and was not measured directly.

3.3.2 Strain Distribution

3.3.2.1 Crack Tip Strains

Strain measurements suggest yielding of the steel plate only occurred at the crack tip, and only on the unpatched face of the patched plates, under 100 MPa loading. It is difficult to compare crack tip strains because of the high strain gradient in the area and undetermined bending effects; however, some qualified conclusions can be drawn.

In an unpatched test, high strains were observed at the crack tip as expected. Patching was expected to lower these strains by restraining the crack from opening and by stiffening the area. The test results showed improvement in strains in the patched face of the repaired plates–crack tip strains were lower than far field strains in all cases. On the unpatched face of the repaired elements however, crack tip strains were higher than for the unpatched plate. In most cases, the patched elements showed more than double the crack tip strain of the unpatched element. Table 3.2 summarizes the measured crack tip strains for all tests. Where two values are shown, gauges were located at both crack tips.

Table 3.2 Summary of crack tip strains, bonded patch tests

	Crack tip strain $X10^{-6}$ (mm/mm)	
Unpatched	1183, 1297	
	Patched face	Unpatched face
R116	102	2899, 3309
M216	65	4573
M214	262	2258, 3390
M316	-525	3543, 3978
M314	3	3717
R226	-225	3624, 4026
R224	-70	3779, 4102
R326	-55	2327, 2668
R324	-315, -395	2782, 2902

There are three factors that may have contributed to this through-thickness strain profile. First, the bending stresses due to the applied load acting on the plates with an initial curvature as discussed in section 3.3.1. Because the crack tip gauges for the unpatched plate were subjected to compression as a result of plate straightening, and the crack tip gauges on the unpatched face of the patched plates were subjected to tension, the patched plate readings should be higher. It is unlikely that this behaviour was responsible for the entire difference, however. Removing the effects of plate curvature from the results is discussed in section 4.3.

The second possible explanation for the higher strains in patched elements is overall bending due to eccentricity of the applied load at the plate edge and the reaction load of the patched cross-section, illustrated in Figure 3.18. The figure shows a portion of a patched plate cross-section along the vertical centerline of the plate. The far field applied load is evenly distributed through the plate thickness, which gives a resultant, P acting through the centroidal axis of the plate. Because of the asymmetry of the patched cross-section, the resultant force in the patched area acts through an axis eccentric to the plate

centroid by a distance e. This results in bending moments of magnitude P·e on the patched cross-section, causing bending of the plate and placing additional tensile stresses on the unpatched face.

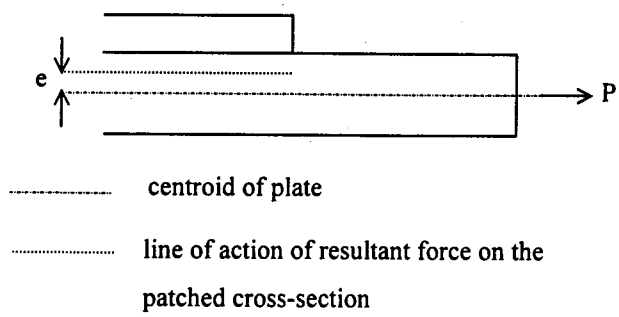

Figure 3.18 Bending due to eccentricity of applied load

The third factor that may contribute to larger strains at the crack tip in the patched element is moment due to a through-thickness strain gradient. For an unpatched element loaded in pure tension, the through-thickness strain distribution is always symmetrical about the through-thickness centerline, and the resultant lies on that through-thickness centerline. Near the crack tip in an element with a one-sided patch, the strains in the patched face are much lower than those in the unpatched face, due to the higher stiffness and restraint on crack opening. Moving away from the crack, however, these strains begin to redistribute themselves through the thickness of the plate. This means the resultant force shifts, and a moment, M_p, is required to keep the element in equilibrium. This local moment causes additional tensile stresses in the unpatched face of the plate. Figure 3.19 illustrates this local bending and why it is particular to asymmetrical elements. The figure shows an elemental cross-section of the plate taken along a vertical axis (in the *y-z* plane), near the crack tip. Bending moments due to other sources have been omitted.

The magnitude of the effects of each of these actions cannot be determined due to the unknown magnitude of initial curvature, the undetermined location of the line of action of

the resultant force in the patched cross-section, and uncertainty of the effect of the crack on local and overall bending. Any or all of these factors may have resulted in the observed increase in tensile stresses at the crack tip in the patched elements. While the idea of increased crack tip stresses suggests increased crack growth rates, it is important to consider that the through-thickness strain distribution changes as a result of asymmetrical patching. The effect this new strain distribution will have on crack growth is unknown.

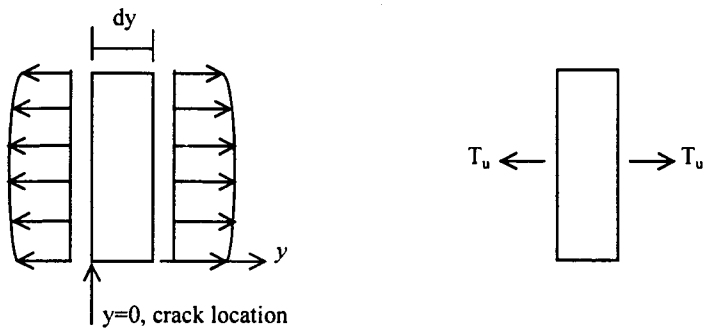

(a) Unpatched element

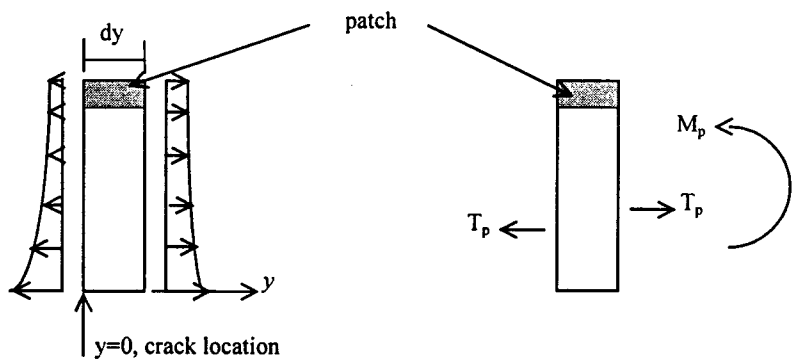

(b) Patched element

Figure 3.19 Local bending due to load transfer through plate thickness, near the crack tip

3.3.2.2 *Strain Distribution Along the Plate Length*

In an unpatched plate, the longitudinal strain is theoretically zero on the plate centerline at the crack edge. Experimental results for the unpatched test (Figure 3.15) showed low strain very close to the crack, and increasing strains along the plate centerline region as the load flowed around the crack and then gradually back towards center to re-establish constant stress distribution. Patched specimens exhibited similar behaviour along the unpatched face, see the output for test M214 in Figure 3.8(b), for example.

Strain measurements for the patched face represent strains in the patch, not strains in the patched face of the steel. Chapter 2 discussed the transfer of load in a bonded joint and similar results are seen here: patch strains are high near the crack, but drop as load is transferred to the steel and strain compatibility is established. Figure 3.10(a) for test M314 is a good example of this behaviour. In one case, for test M316, the strain appeared to plateau and then increase slightly, possibly as the influence of load returning to the plate center became relatively more significant (see Figure 3.9).

In several cases, the strain in gauges on the patch over the crack was lower than for gauges adjacent to the crack. This may have been the result of bending discussed earlier: because the moment of inertia of the cross-section is lower at the horizontal centerline due to the crack, bending stresses in the patch may be much higher. The compressive behaviour of the composite is not known, but the patch may actually have been buckling across the crack due to bending.

3.3.2.3 *Strain Distribution Across the Plate Width*

For the unpatched plate, the strain was high near the crack tip, then decreased quickly and was fairly constant across the remaining plate width. Again the behaviour of the unpatched face of the patched elements was similar, with the exception of higher crack tip strain values as was already discussed.

On the patched face, the strain values recorded by gauges spanning the crack were highly irregular, possibly due to different magnitudes of bending and consequently different behaviour. Strains at the crack tip were typically low on the patched face, and the distribution from the crack tip towards the plate edge tended to increase gradually. This may have been a result of local bending effects close to the crack causing compression stresses in the patch and lowering the net strain value.

3.3.3 Demec Results

The demec gauge, which was attached to the unpatched face of the plates, was intended to monitor the opening of the crack. The results were expected to be highest for the unpatched specimen, lower for the four layer patches, and lower still for the six layer patches, since it was thought a stiffer patch would have an increased ability to hold the crack shut. Figure 3.17 shows the experimental results to be otherwise: while some patches were able to reduce the demec results below the value obtained for the unpatched specimen, the highest strains actually resulted from tests with six layers of composite.

A second plot of the demec results is shown in Figure 3.20. In this figure, the change in demec reading over a 50 MPa increment in applied stress was used in place of the demec reading at 100 MPa used in Figure 3.17. The incremental values allow comparison of demec results without the influence of bending due to initial plate curvature, which was different for each test. It is believed that the plates were virtually flat through the linear portion of the MTS load versus MTS stroke curve (see Figure 3.3), implying bending strains caused by plate curvature were approximately constant. By considering an incremental load in this region, these bending effects are removed.

The use of incremental demec readings reduced the variation in results. In most cases, the patched elements showed lower strain across the crack than the unpatched element. In general, higher strains were still reported from the tests with six-layer patches than

those with the same length and width parameters but only four-layer patches. This suggests that along the demec gauge length, the increase in bending strains caused by a stiffer patch exceeds the decrease in crack opening strains due to a stiffer patch. Bending is increased by a stiffer patch because of greater eccentricity of the applied and resultant loads in the patched area; the same applies for a wider patch.

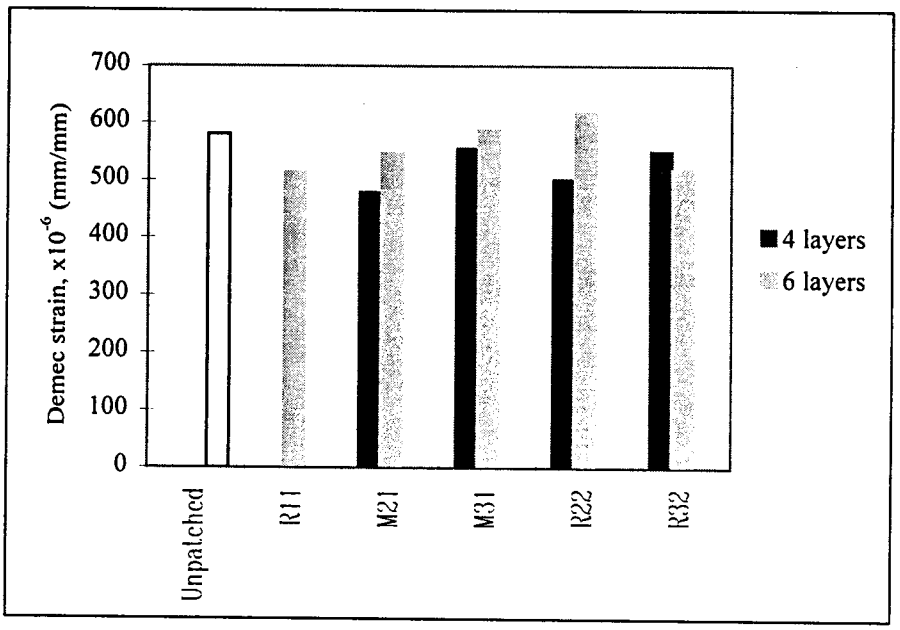

Figure 3.20 Demec strain results for bonded patch tests over 50 MPa incremental far field stress

3.4 References

Baker, A.A. 1987. "*Fibre Composite Repair of Cracked Metallic Aircraft Components - Practical and Basic Aspects.*" Composites, Vol. 18, No. 4, pp. 293-308.

Roberts, Pamela D. 1995. "*Crack Growth Retardation by Carbon Fibre Composite Patching: An Application to Steel Pressure Vessel Repair.*" Master of Science Thesis, University of Alberta, Department of Mechanical Engineering.

Schubbe, J. and S. Mall. 1997. "*Fatigue Crack Growth Behaviour of Thick Aluminum Panels Repaired with Composite Patch.*" 42nd International SAMPE Symposium, pp. 197-207.

4 STRESS DISTRIBUTION IN A BONDED PATCH - NUMERICAL PROGRAM

The study of stress distribution in a bonded patch aimed to define the stress flow patterns resulting from a bonded crack repair. Chapter 3 discusses the experimental program that was conducted, and presented trends identified in the behaviour of plates repaired with different patches. To obtain a more accurate and continuous picture of the strain distribution, a numerical model was developed. General strain distributions obtained from the model are presented here, followed by a comparison of the numerical and experimental results. The effects of changing patch dimensions and stiffness, as determined by a parametric study, are discussed and incorporated into guidelines for basic patch design.

4.1 Numerical Model

A three-dimensional numerical model of the bonded patch specimens was created in ABAQUS 5.6 (Hibbitt, Karlsson & Sorenson, Inc. 1996). The model represented one quarter of a patched plate with an internal, through-thickness crack.

4.1.1 Plate Model

The original ABAQUS 5.6 model of the plate is shown in Figure 4.1. Two layers of 20-node brick elements and 15-node wedge elements defined the plate. Quartic point elements were used around the crack tip to obtain output as close as possible to the crack tip. While a regular brick element has nodes at the corners and at the mid-point of element edges, the mid-side notes in a quartic point element are shifted to the quarter point, as illustrated in Figure 4.2. The integration points are shifted as well, allowing calculation of results closer to a desired point. For a 1 mm cubic brick element, a regular, reduced integration element has integration points 0.2125 mm from each edge; for the same element with quartic points, two integration points will be 0.045 mm from the closest edges.

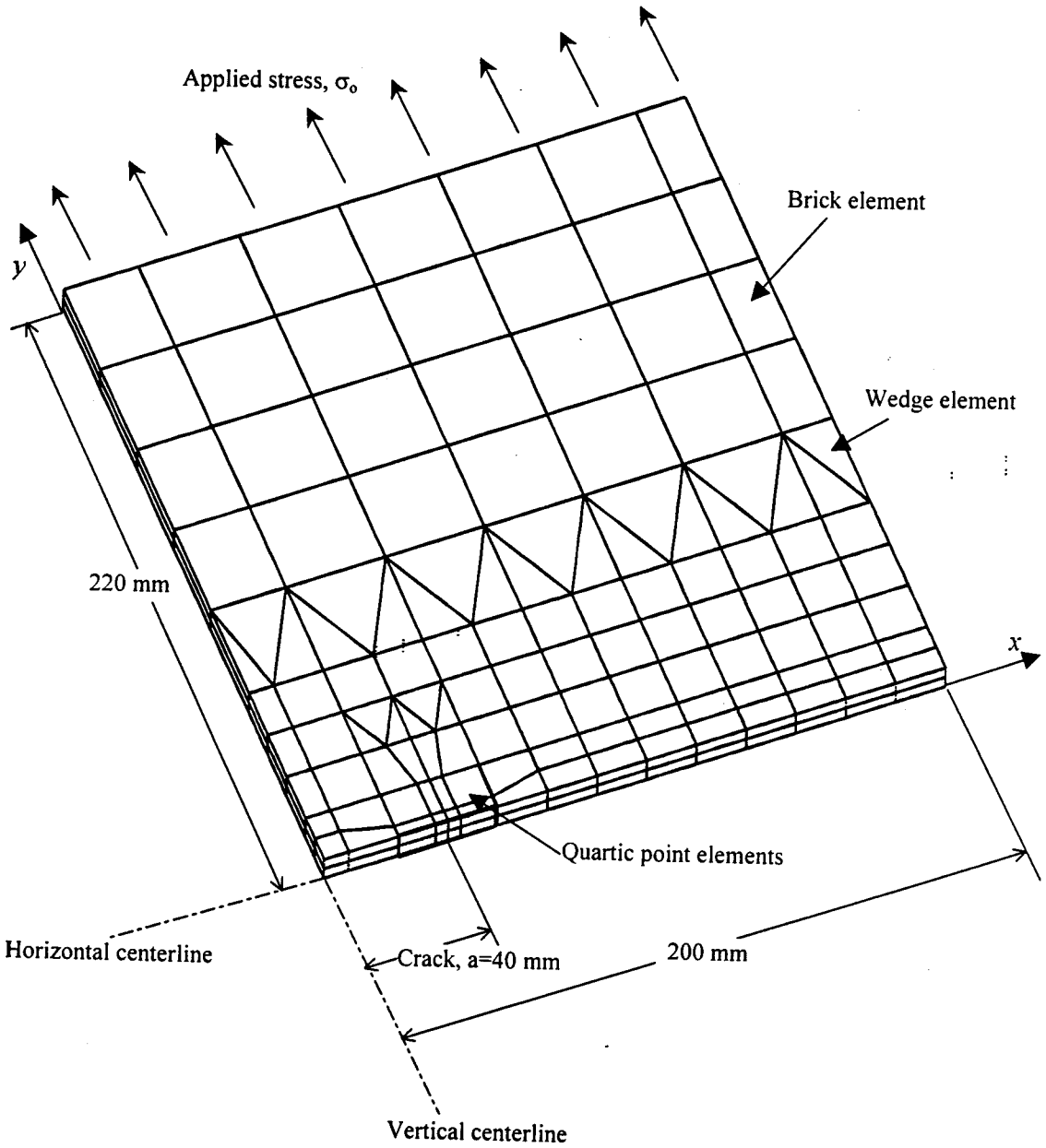

Figure 4.1 Original ABAQUS 5.6 model of cracked plate

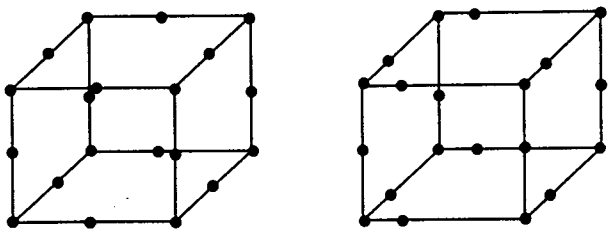

Figure 4.2 Location of nodes on regular and quartic point brick elements

Boundary conditions for the model were dictated by symmetry. The plate was restrained from lateral movement along the vertical (y) axis, and from out-of-plane movement along the loaded edge. Nodes across the horizontal centerline of plate beyond the crack tip were restrained longitudinally, while nodes on the cracked face were not restrained in any direction.

The original model of the plate used 246 elements. A second model, shown in Figure 4.3, was generated by halving the width and length dimensions of the first, and adding

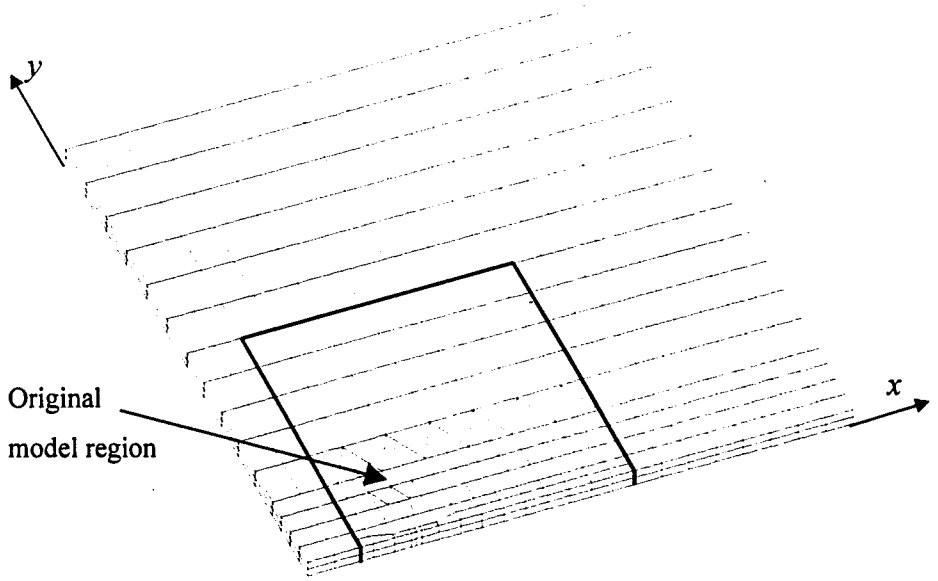

Figure 4.3 Refined ABAQUS 5.6 model of cracked plate

additional elements to the perimeter to restore the original overall dimensions. This second model had 630 elements for 10986 degrees of freedom.

Figure 4.4 shows the through thickness longitudinal strain distribution at the row of integration points closest to the crack tip for both models under 100 MPa far field applied load. Although the integration points were only 0.0275 mm closer to the crack tip in the refined model, the strains were on average 25% higher. Figure 4.5 shows the longitudinal strain distribution across the plate width at the horizontal centerline. The strains shown were at integration points closest to the center of the plate thickness. In the figure, the strain gradient near the crack tip was much steeper (approaching infinite) for the refined plate model than the original. This gradient was believed to be significantly more accurate. The peak strain was nearly 6000 με at 100 MPa far field applied stress; since the model considered elastic behaviour only, it was not deemed necessary to refine the grid further. The refined model was used for further analysis.

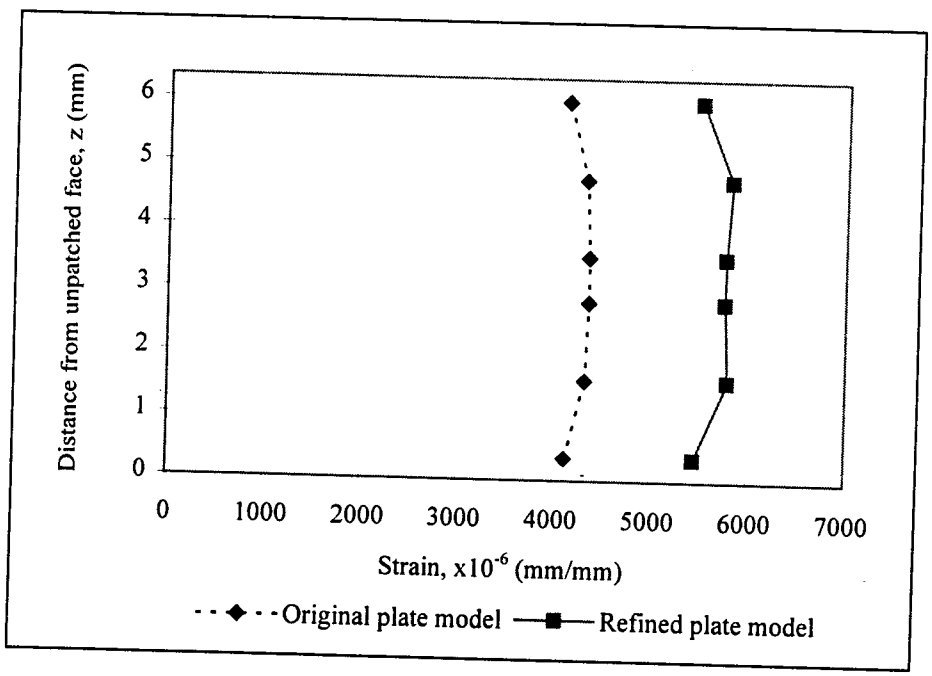

Figure 4.4 Through-thickness strain distribution near the crack tip for two ABAQUS 5.6 plate models

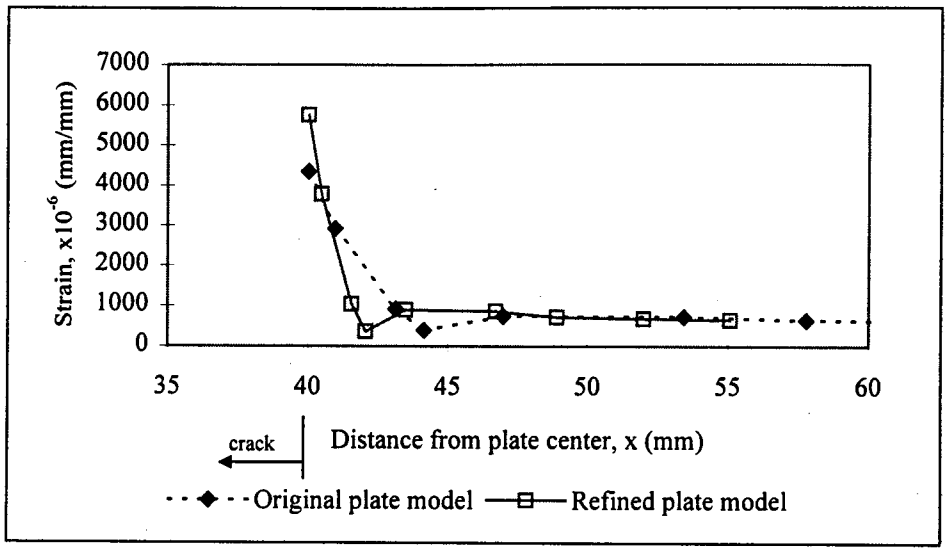

Figure 4.5 Strain distribution across plate width at the horizontal centerline for two ABAQUS 5.6 plate models

Figure 4.5 suggests the longitudinal strain across the plate width decreased then increased again moving away from the crack tip. This was thought to be an anomaly of the numerical model. To try to remove this problem, the model was rerun using reduced integration elements in the high strain gradient area near the crack tip. The resulting strain distribution is shown in Figure 4.6.

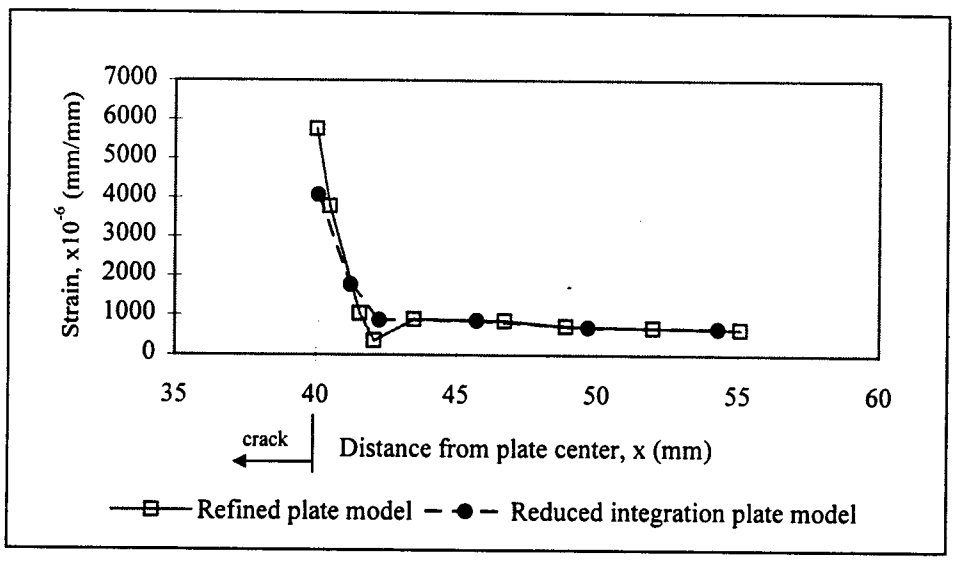

Figure 4.6 Strain distribution across plate width at the horizontal centerline for ABAQUS 5.6 plate models with and without reduced integration elements

The output from the reduced integration model provided a more acceptable strain distribution, while maintaining approximately the same strain gradient as the refined model. The reduced integration model did, however, give a lower peak stress value since the closest integration points to the crack tip were 0.09 mm away (compared to 0.0275 mm in the refined model). Since, in reality, yielding and redistribution of stresses affects the peak stress values in this area, the numerical model results were not expected to return accurate peak stress values regardless of the proximity to the crack tip. The refined model incorporating reduced integration elements was used for all further analyses.

4.1.2 Patch Model

To complete the model, three- and four-node shell elements were added to the plate model to represent the patch, as shown in Figure 4.7. The elements were "bonded" to the plate through the use of common nodes: all patch element nodes were on the surface of the plate. Shell elements were added or removed as necessary to represent changing patch length and width. Figure 4.8 shows the model for a patch with width, w, of 80mm and length, L, of 32 mm. All patch nodes along the horizontal centerline were restrained from longitudinal displacement.

4.1.3 Material Properties

The numerical model represented a unidirectional carbon fibre patch with material properties as discussed in section 2.2.3. Because this model was three-dimensional, additional material properties were required to define behaviour in the lateral direction. The values used are given in Table 4.1.

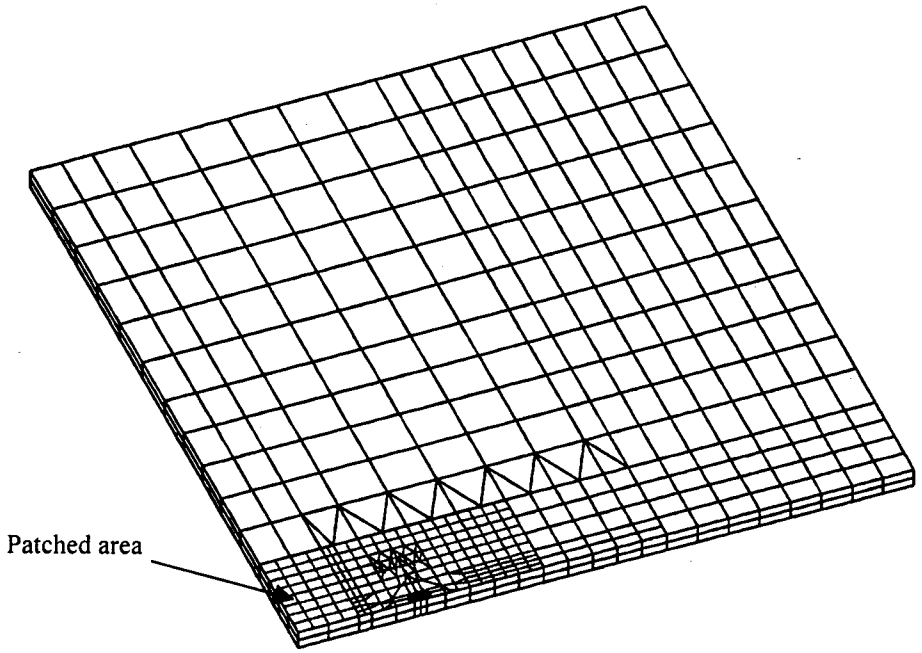

Figure 4.7 ABAQUS 5.6 plate model with bonded patch

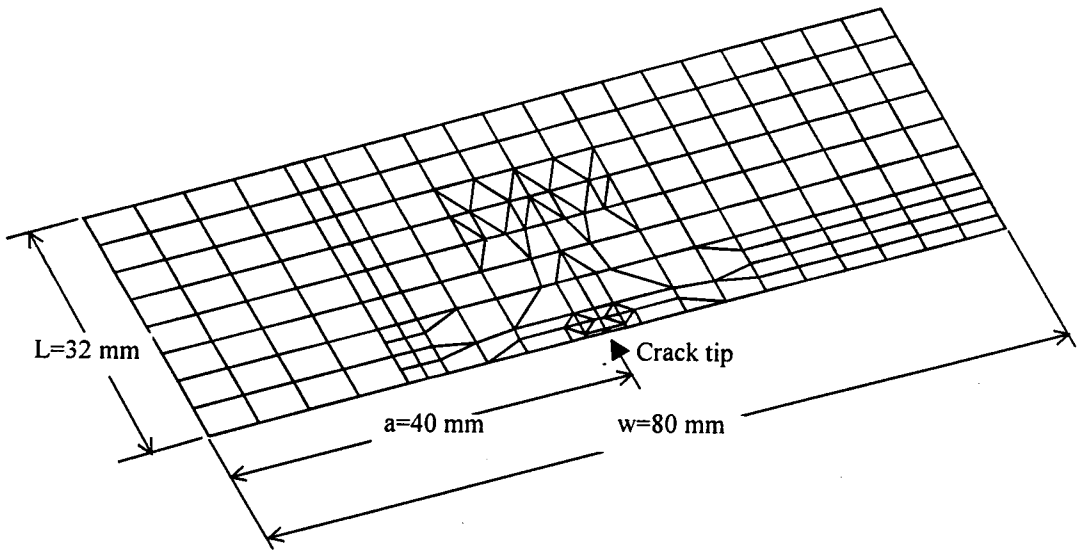

Figure 4.8 ABAQUS 5.6 model of composite patch

Table 4.1 Summary of material properties used in bonded patch model

Summary of	Material Properties
E_1	128 000 MPa
E_2	6 900 MPa *
G	4 480 MPa *
ν_{12}	0.17 †

(* Schwartz 1984; † Schubbe and Mall 1997)

4.2 General Analytical Results

On a macro level, the stress flow patterns can be separated into those of the patched face and the unpatched face. On the patched face, load flows across the crack, transferring from steel to patch and back in a relatively short distance. The unpatched face of the element, however, behaves almost the same after patching as it did before, with the additional influence of some local bending stresses that were not present in the symmetrical, unpatched element. With the exception of the regions immediately surrounding the crack and at the patch edge, the through thickness strain distribution is approximately linear.

This section considers this behaviour on a more micro level, considering strain distributions along horizontal and vertical axes of the plate for a specified patched element under 100 MPa far field applied stress. The basic model used was a 6.35 mm steel plate with an 80 mm internal crack, patched with a 96 mm long by 160 mm wide patch (L = 48 mm, w = 80 mm). To model a four-layer patch, shell elements were 0.92 mm thick.

4.2.1 Crack Tip Strains

Figure 4.9 shows the through-thickness strain distribution 0.09 mm from the crack tip before and after patching. The figure suggests patching reduces crack-tip strains in the

patched face of the plate, and to a lesser degree at the center of the plate. The unpatched face, however, shows an increase in tensile strain, particularly near the crack tip. The changes in strain can be attributed largely to the ability of the patch to restrain the crack from opening on the patched face. Bending also occurs in the patched plate and causes additional tensile stresses on the unpatched face of the plate and compressive stresses on the patched face. There are two main sources of bending:

Overall bending – The applied load, which acts through the centroid of the plate, is not coincident with the reaction load of the patched cross-section. See Figure 3.18.

Local bending - Because of the non-linear strain profile at the crack tip, bending stresses are induced as the load is redistributed through the plate thickness. See Figure 3.19.

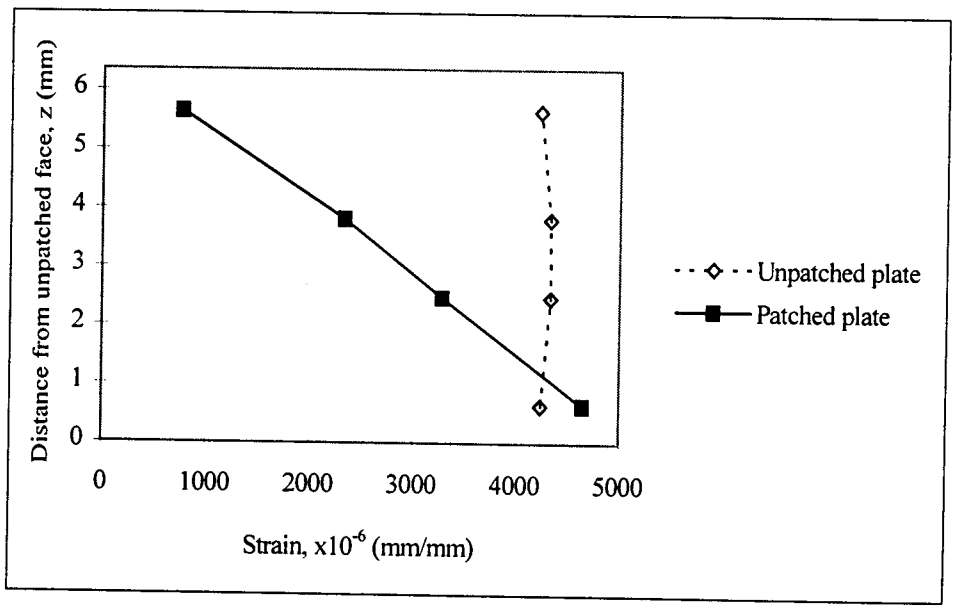

Figure 4.9 Through-thickness strain distribution at the crack tip

Recall that the numerical model did not account for yielding. If the steel yields at approximately 1500 με, some of the load in the unpatched face must be redistributed. This occurs in an unknown combination of load transfer through the plate thickness and through the unpatched face of the plate away from the crack.

4.2.2 Strain Distribution Along the Plate Length

Figure 4.10 shows strain profiles along the vertical centerline of the plate. Results are shown for the patched and unpatched faces of the basic model plate, as well as for an unpatched plate. Numerical results of a two-dimensional bonded joint model (see section 2.3) with the same steel and patch specifications are also shown in the figure.

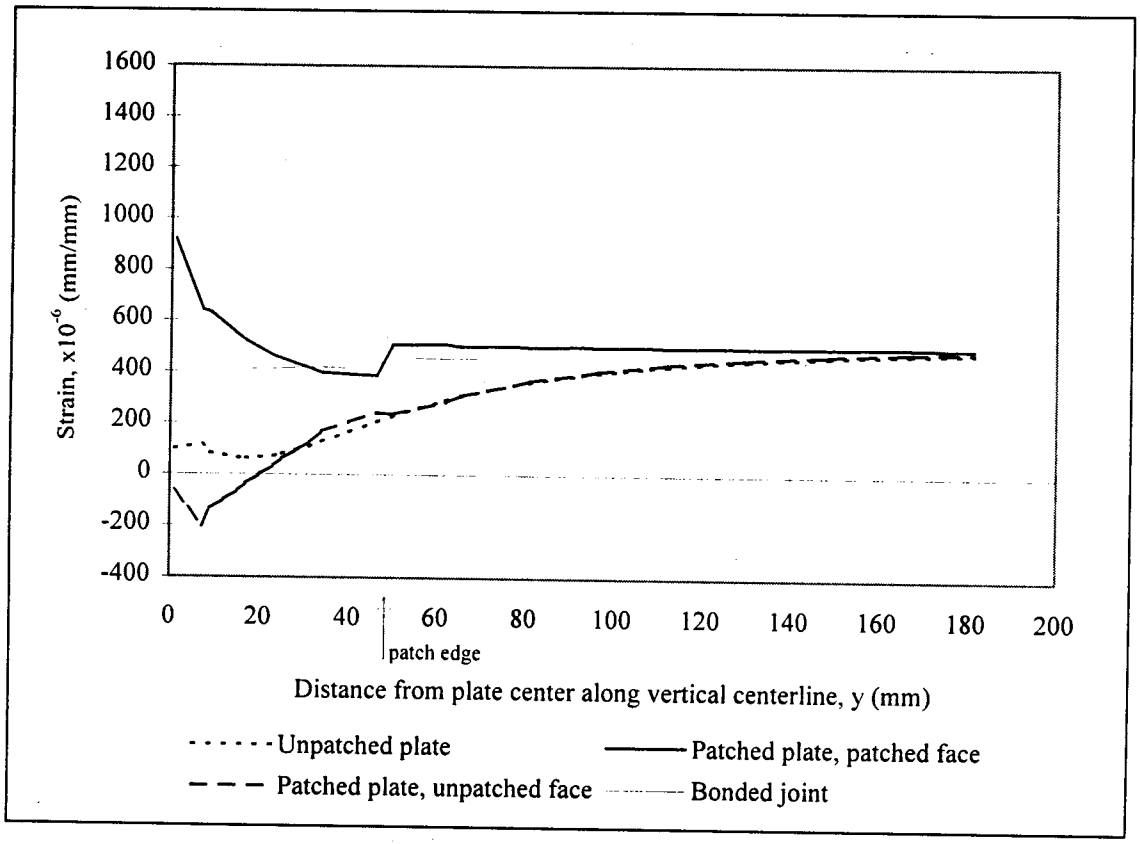

Figure 4.10 Strain distribution along vertical centerline

Because the steel has a free surface at the crack, it should not be able to carry any load; however, the plot suggests high strain in the patched face of the steel at the crack edge. This is due to misrepresentative modeling of boundary conditions. The continuity of the patch across the crack was defined by restraining patch nodes along the boundary from displacement in the vertical direction. The problem arose in that patch boundary nodes were also the steel boundary nodes along the patched face of the plate; thus, the top

surface of the steel was being held shut by the boundary conditions. This was the most accurate representation of the conditions that could be found for the model structure being used. Though not entirely accurate, the boundary conditions are acceptable since a significant portion of the load is believed to transfer from the patch to the steel very quickly, and the patch is believed to restrain the crack from opening to some extent.

Moving away from the crack, the strain profile along the patched face of the steel is similar to that for a bonded joint. The strain is high near the crack, decreasing along the bond to a plateau. There is an increase in strain in the patched face of the steel at the patch edge as the stiffness of the cross-section drops, and the load from the patch transfers to the steel. This stress concentration is discussed further in Chapter 5. Finally, there is a decrease in strain beyond the edge of the patch as the excess load is transferred through the plate thickness and across its width and a constant stress/strain distribution is re-established.

The strain along the unpatched face of the plate tends towards zero strain in the crack face, followed by a region of compression. Compressive strains in the back face of the plate are a result of local bending, similar to that discussed in section 3.3.2.1. Figure 3.19 illustrates how load transfer through the plate thickness results in local bending at the crack tip. At the plate center, the same effect occurs, but in the opposite direction: strains are higher in the patch and the patched face of the plate, and bending is required for equilibrium as these strains distribute through the plate thickness. This bending results in additional tensile stresses on the patched face of the plate, and compressive stresses on the unpatched face.

The strain in the unpatched face increases along the plate length as bending decreases and load flows through the plate thickness and from the crack tip area back towards the center of the plate. In the patched region, load returns to the plate center more quickly than it would in an unpatched element as the stiffness of the patched region attracts more load.

At the patch edge, there is a sudden drop in strain, largely due to the elimination of bending due to the eccentricity of the applied load and the line of action of the resultant force on the patched cross-section, see Figure 3.18. This bending causes additional tensile stresses in the back face of the plate. Beyond the patch edge, the unpatched face strain profile is very close to that of an unpatched plate.

4.2.3 Strain Distribution Across the Plate Width

Distributions of the strain in the steel along the horizontal centerline are shown in Figure 4.11. An unpatched plate has an almost constant through-thickness strain distribution, while a plate patched on one side has variable strain through its thickness, particularly at the crack tip as discussed in section 4.2.1. Strain gradients across the plate width are initially high, particularly in the unpatched face of the plate. The same effect is seen in

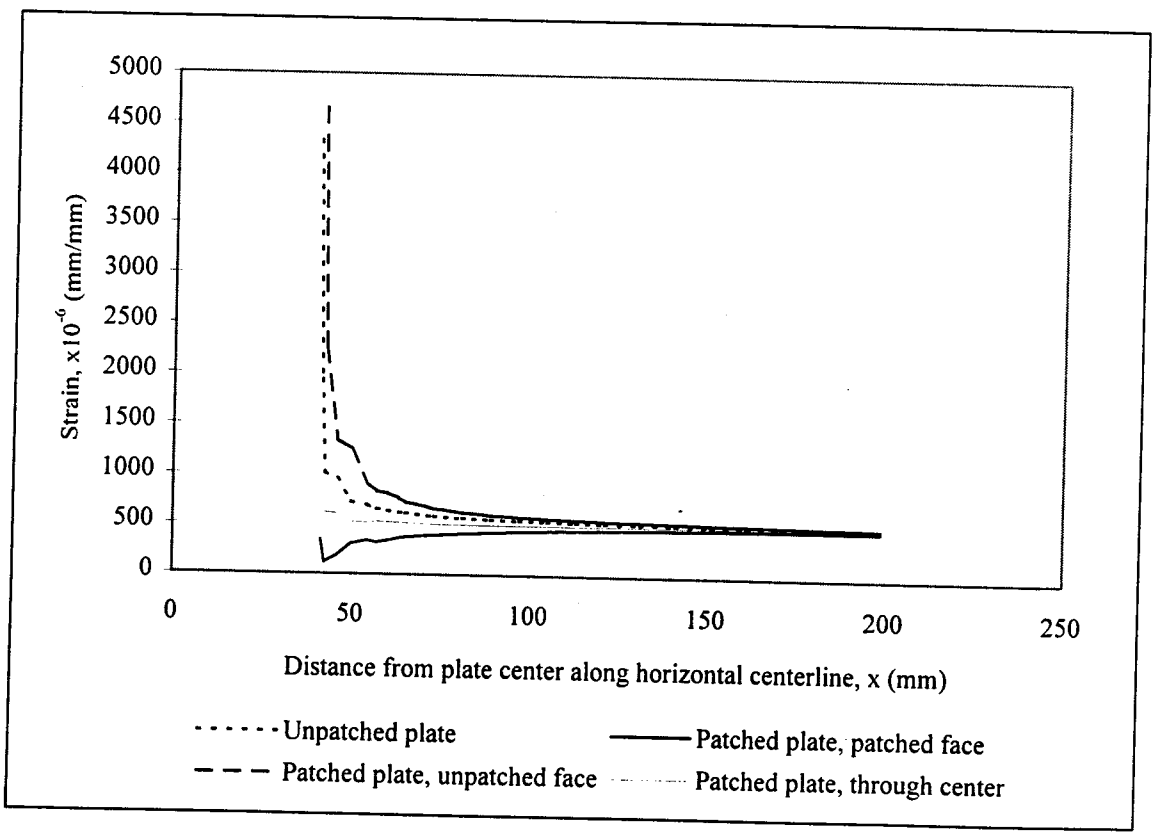

Figure 4.11 Strain distribution across horizontal centerline

the curve for the unpatched plate, showing the localization of crack tip stress concentrations. Following the high initial drop in strains, the distributions show a region of "intermediate" strain gradients, not excessively steep but clearly not zero. This region, from near the crack tip to approximately 30 mm away, is likely the area of the highest local bending effects. Beyond this region, local and overall bending effects decrease, and strains in the front and back faces of the patch approach the far field applied strain at approximately the same rate. There is no discontinuity in the strain profiles at the edge of the patch.

4.2.4 Load Redistribution

After the load flows past the crack tip, it is redistributed across the width and through the thickness of the plate to re-establish constant strain distribution. Figure 4.12 depicts this redistribution for an unpatched plate and the basic patched plate. For each model, strain profiles are given across the width of the plate along four different horizontal axes. All strains are taken at the center of the plate thickness. The axes locations are identified by their vertical distance, y, from the horizontal centerline of the plate. Note that for the patched plate, the profiles at 8.9 mm and 24.9 mm from the horizontal centerline are within the patched region, while the profiles at 65.3 mm and 96.3 mm are beyond the patch edge.

The strain profiles through the center of the plate thickness are generally flatter for the patched element than for the unpatched element, suggesting patching tends to decrease load flow across the plate width, perpendicular to the direction of the applied load. In the unpatched plate, all load must flow around the crack, causing high stress concentrations at the crack tip. In the patched plate, however, the patch is able to carry some load across the crack. It is shown in sections 3.3.2.1 and 4.2.2 that this results in lower stresses at the crack tip on the patched face and through the plate center, and higher stresses due to bending on the unpatched face. Figure 4.12 also shows a reduction in stress concentration at the center of the plate thickness as a result of patching.

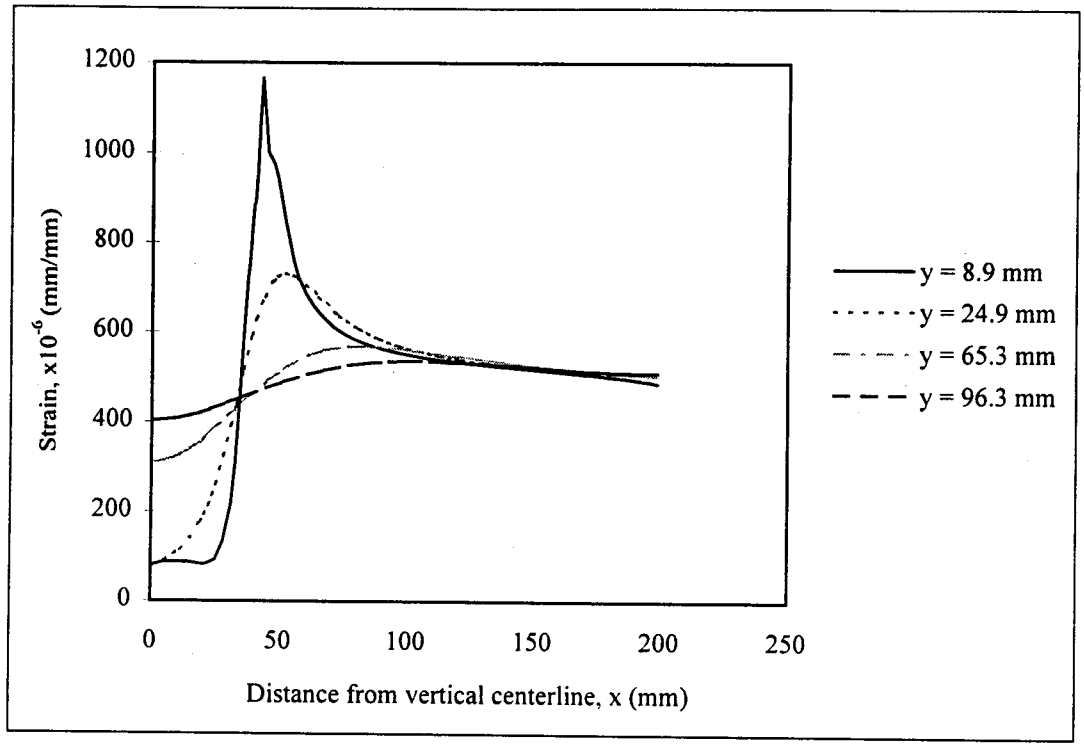

(a) Unpatched plate

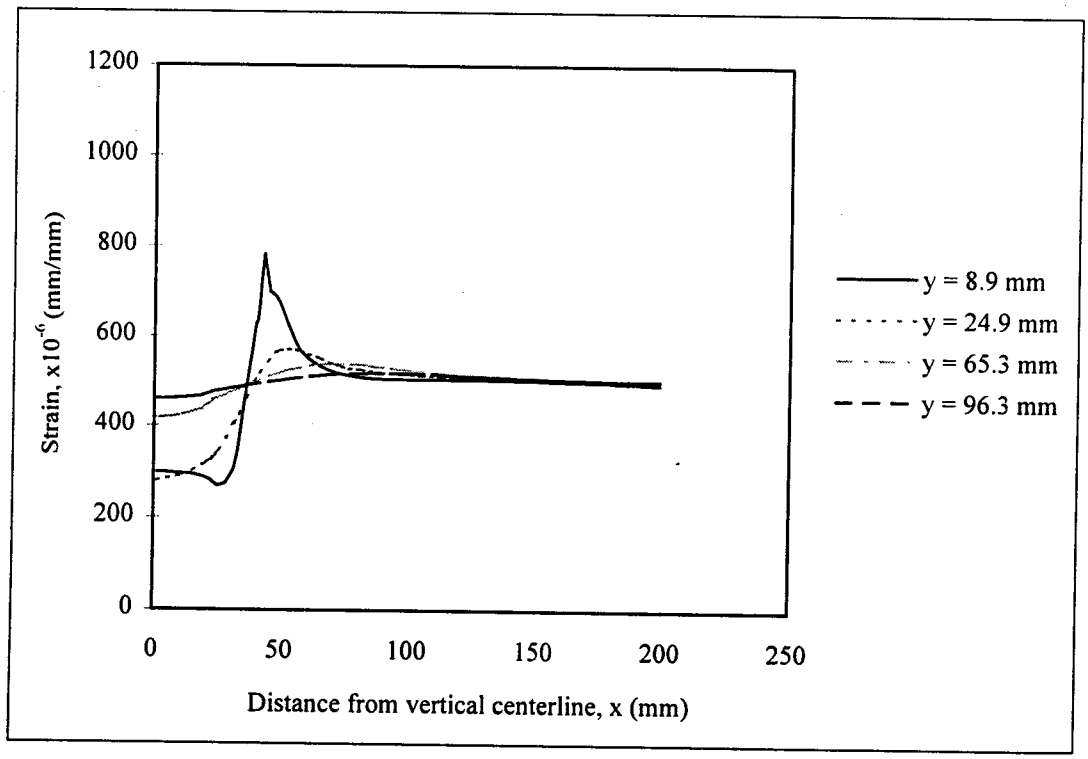

(b) Patched plate

Figure 4.12 Strain distribution across the plate width at different vertical locations

Progressing away from the horizontal centerline, which is the axis of the crack, the load that was forced to flow around the crack gradually returns to the center of the plate to re-establish the uniform state of stress applied at the boundary. In the unpatched plate, this happens very gradually, while in the patched plate, it appears to happen more quickly. This is due in part to the smaller amount of load to be transferred, but there are two other factors that may influence the flow of load. First, the redistribution in a patched plate happens both through the plate thickness and across the plate width, while constant through-thickness strain for an unpatched plate means load can only redistribute across the width. In the patched plate, high loads that flow across the crack through the patch can be distributed towards the unpatched face where the stress is zero on the crack face. High stresses at the crack tip on the unpatched face may transfer towards the patched face where the stress concentration was not as high. The second factor that allows the patched element to regain constant strain distribution more quickly is the increased stiffness of the patched area. For an uncracked plate with a bonded patch, more load would be required in the patched area for strain compatibility across the plate. The same principle applies to the bonded patch in the regions vertically beyond the crack: the patched region is stiffer and thus will draw more load from the areas beyond the edge of the patch. The strain profiles suggest nearly constant strain beyond the patch edge ($x > 80$ mm) in Figure 4.12(b), while there is a more pronounced gradient in the strain profile for the same region of the unpatched plate.

4.3 Comparison of Numerical and Experimental Results

This section discusses the ability of the model to predict experimental results. The implications of the initial curvature of the tested plates are discussed and a correction scheme is applied to the experimental data in attempt to negate the bending effects. Strain distributions along the plate horizontal and vertical centerlines, discussed in the previous section on general analytical results, are the basis for the comparison study. Gauges likely to be affected by edge conditions such as shape or taper are not considered as those conditions were not incorporated into the numerical model for this analysis.

4.3.1 Correction of Experimental Results

Figure 4.13(a) shows the strain distribution along the plate length for an unpatched specimen. Finite element results are for the integration points closest to the vertical centerline and along the surface of the plate; experimental data is from gauges mounted within 20 mm of the vertical centerline ($|x| \leq 20$ mm). This is Zone A discussed in section 3.2.1 and shown in Figure 3.15. Figure 4.13(b) shows the strain distribution across the width of the plate. Finite element results are for the integration points closest to the horizontal centerline, also along the surface of the plate; experimental data is from gauges mounted along the horizontal centerline of the plate.

Because the test plates were not initially flat, tensile loading caused additional tensile strains on one face of the element (the back face), and compressive strains on the other (the front face). This is illustrated in Figure 4.14. Because this bending was not present in the numerical model, the experimental results had to be adjusted for a more accurate comparison of the results.

A correction scheme is presented in Appendix A to eliminate bending effects from the strain gauge readings for patched and unpatched specimens. Corrected data values for the unpatched test are shown relative to the finite element results in Figure 4.15. In general, the corrected values show good agreement with the finite element results.

Another measure of the accuracy of both the numerical model and the correction procedure for the experimental data is the agreement at an arbitrary point away from either axis. In the experimental test of the unpatched specimen, a gauge was located at $x = -64$ mm, $y = -69$ mm. The uncorrected gauge reading at 100 MPa far field applied stress was 401 $\mu\varepsilon$, corrected to a value of 532 $\mu\varepsilon$ using the procedure of Appendix A. The numerical model gave a result of 535 $\mu\varepsilon$. This resulted in a test-to-predicted ratio of 0.75, improved to 0.99 when the correction was applied.

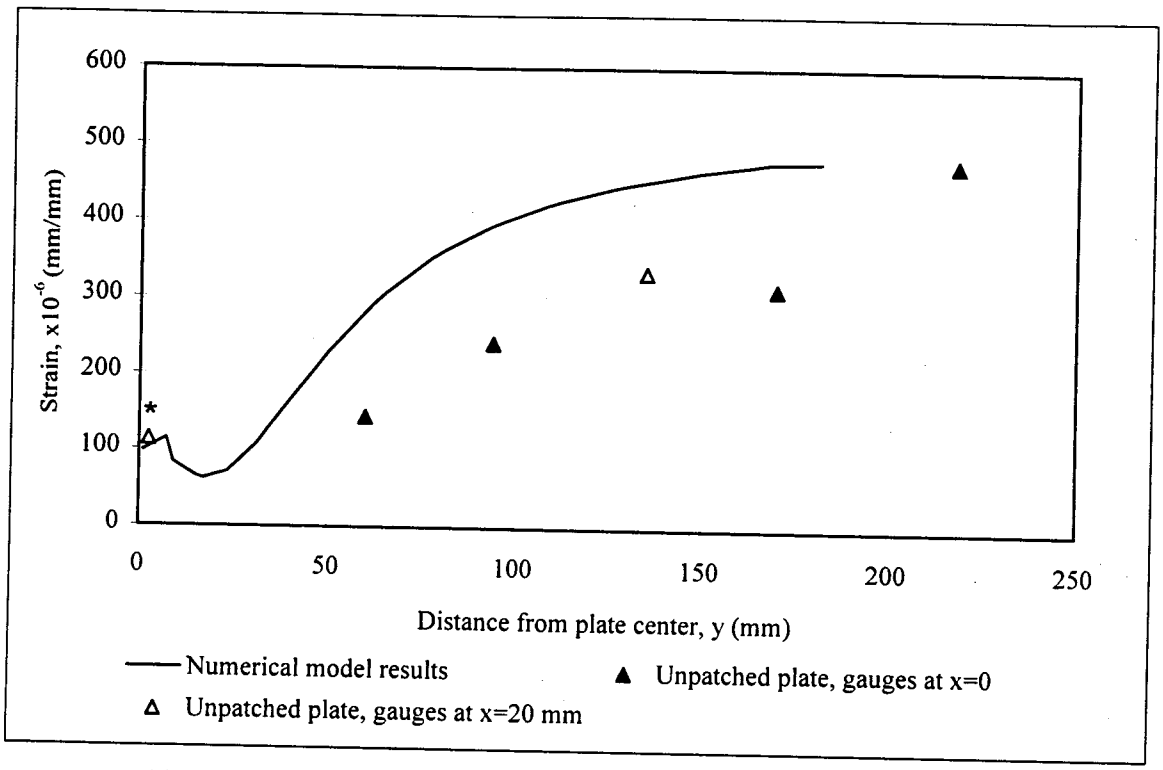

(a) Strain distribution along plate length

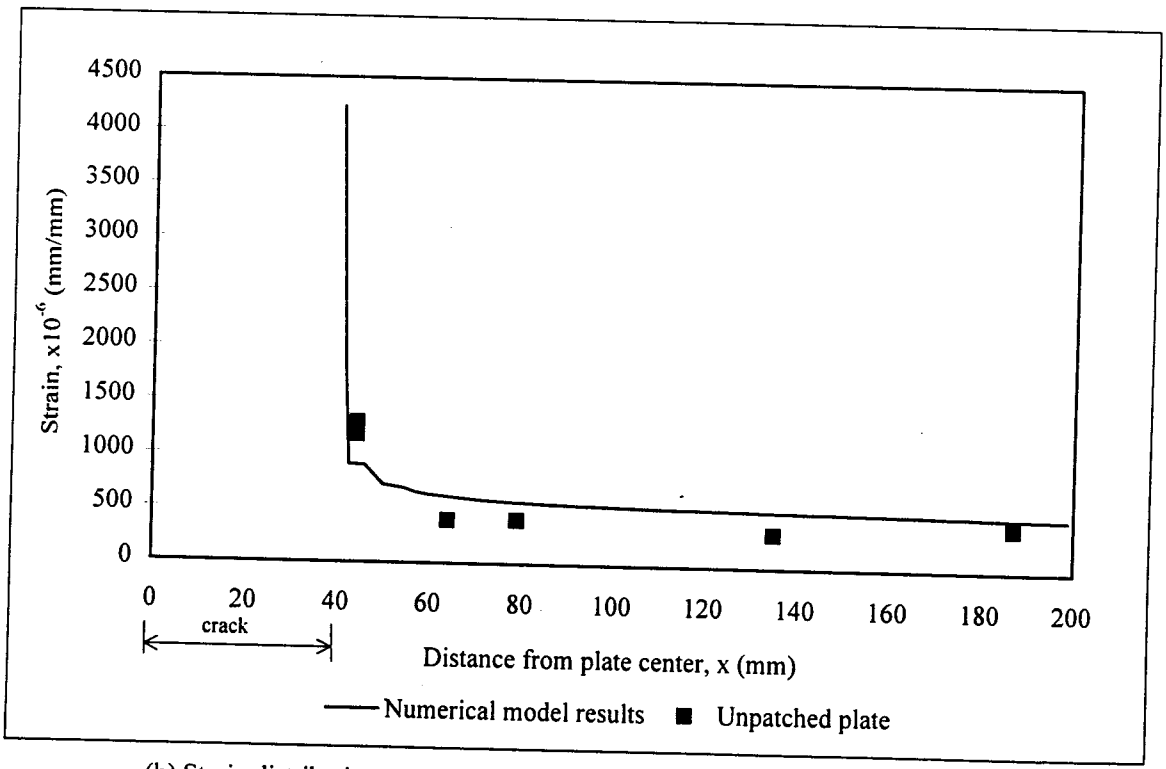

(b) Strain distribution across plate width

Figure 4.13 Comparison of numerical and experimental results for an unpatched plate

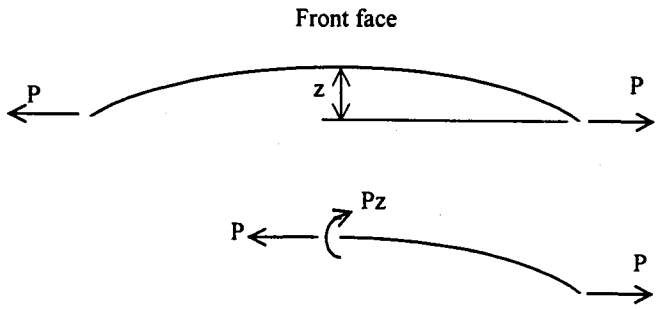

Figure 4.14 Moments induced because plates were not initially flat

While the correction improved agreement for most locations, the gauge immediately adjacent to the crack gave much closer readings prior to correction, as shown by Δ^* in Figure 4.13(a) and Figure 4.15(a). Because the free surfaces of the crack cannot sustain bending stresses, and because the cross-sectional moment of inertia at the crack changes, the bending behaviour of the plate near the crack is difficult to quantify. The results of the comparison suggest bending stresses were minimal immediately adjacent to the crack. Because it is expected that this behaviour existed only in a region very close to the crack, all gauge readings were corrected as outlined and values in the region of the crack should be considered with caution.

The correction of gauge readings for patched elements presented in Appendix A is slightly more involved than the unpatched correction, since patched specimens were subjected to moment due to the asymmetry of the patched cross-section in addition to the effects of plate curvature. Effects of the element asymmetry were present in both the numerical and experimental tests, and are a factor in practical applications, and had to be considered in the results, while effects of plate curvature had to be removed.

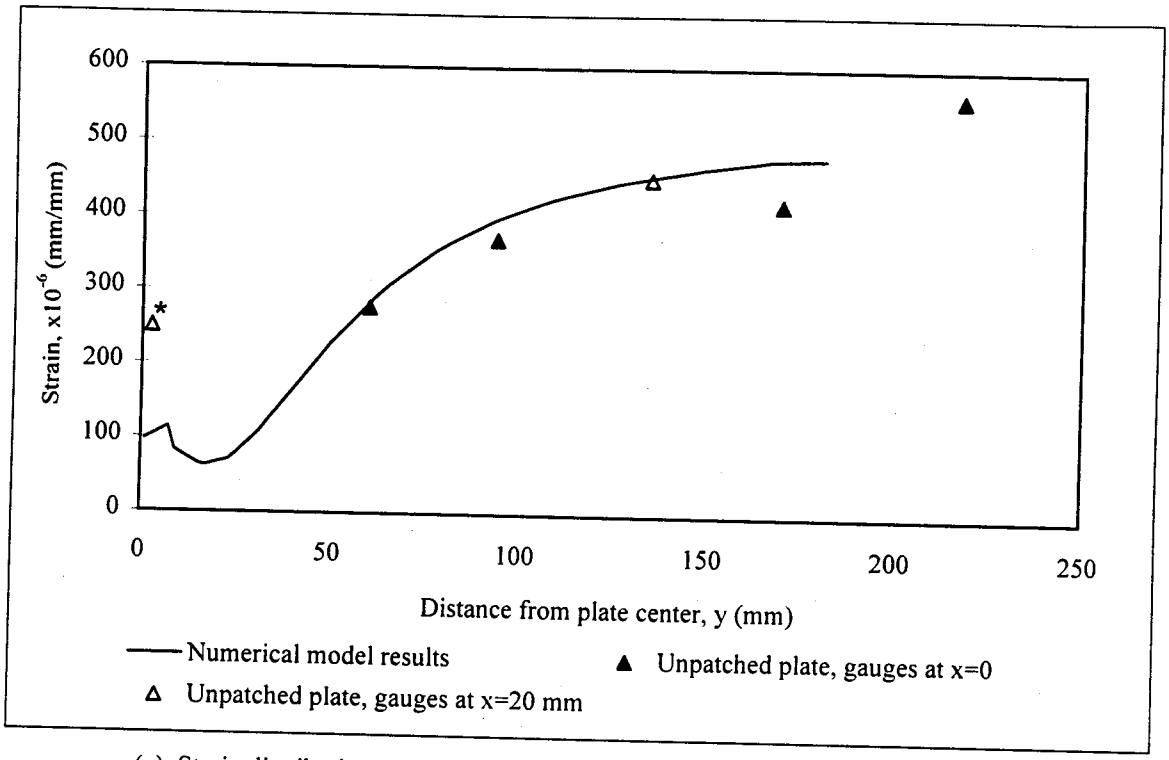

(a) Strain distribution along plate length

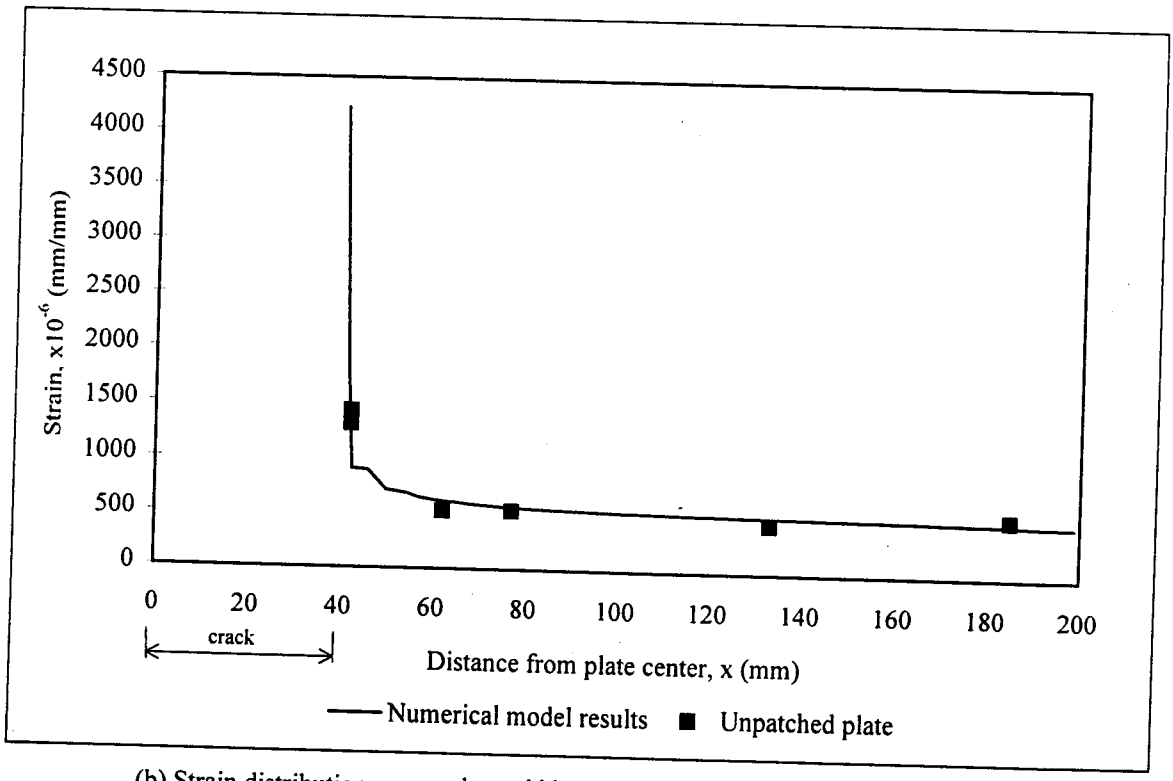

(b) Strain distribution across plate width

Figure 4.15 Comparison of numerical and corrected experimental results for an unpatched plate

4.3.2 Strain Along Plate Length

Figure 4.16 compares numerical and corrected experimental results for strain distributions along the vertical centerline of two patched plates. Experimental data is shown for tests M314 and R324—tests that used patches with four layers of composite and had the same width but different lengths (L = 100 mm and 30 mm respectively). Corrected readings are shown for patched face gauges along the centerline, at x = 0, and at 20 mm away, along the boundary of Zone A identified in Figures 3.10 and 3.14. The numerical results in the figures show strain distributions along the patched face of the steel obtained from models with patches of the same width and thickness parameters as the tests. The length of the numerical patch was restricted by the location of nodes in the model, so the patch lengths used for comparison were L = 95 mm and 32 mm. Because the patch was modeled using shell elements, which shared all nodes with the steel, the strain distribution along the patched face of the steel was virtually the same as the strain distribution in the patch. The edge of the patch can be readily identified in the figures by the sharp increase in strain along the patched face of the plate.

Both tests showed general agreement with the numerically determined profiles. Considering Figure 4.16(a), the strains agreed well along the plateau, but the test results showed slightly higher strains in the higher gradient region towards the crack. This may have been the result of yielding of the bond near the crack, as discussed in section 2.4.1.2, or it may have been due to the inaccurate boundary conditions of the numerical model, as discussed in section 4.2.1.

While the correction procedure removed some of the compressive strain caused by initial out-of-plane curvature of the plate, the test results in Figure 4.16 still show low strains in the patch across the crack. This effect was even more severe for the tests M316 and R326, as shown in Figure 4.17. These six-layer tests had the same patch width and thickness, but different lengths.

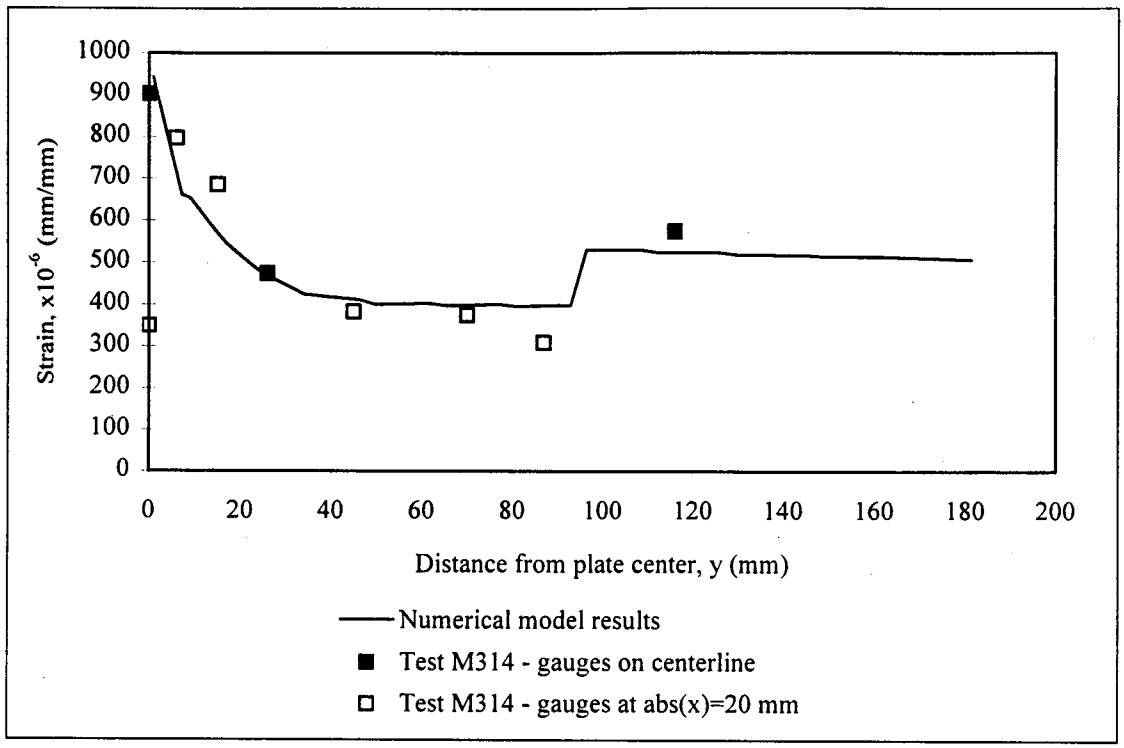

(a)

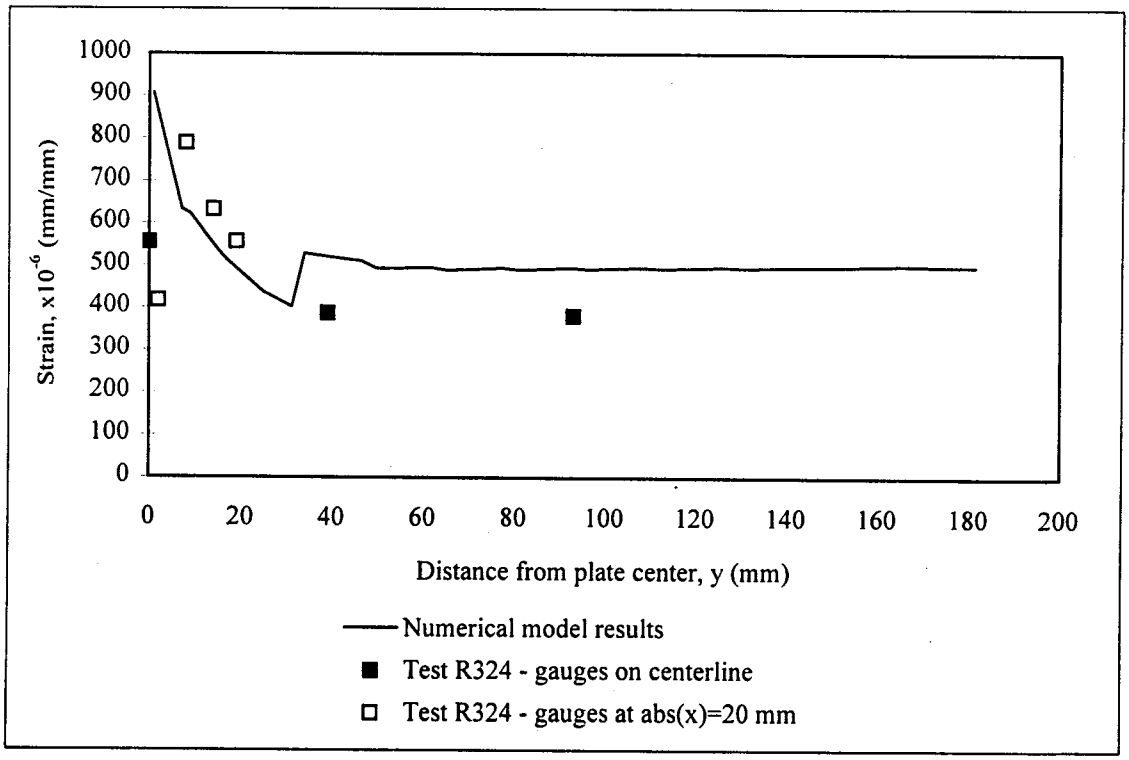

(b)

Figure 4.16 Comparison of numerical and corrected experimental results along plate length for tests M314 and R324

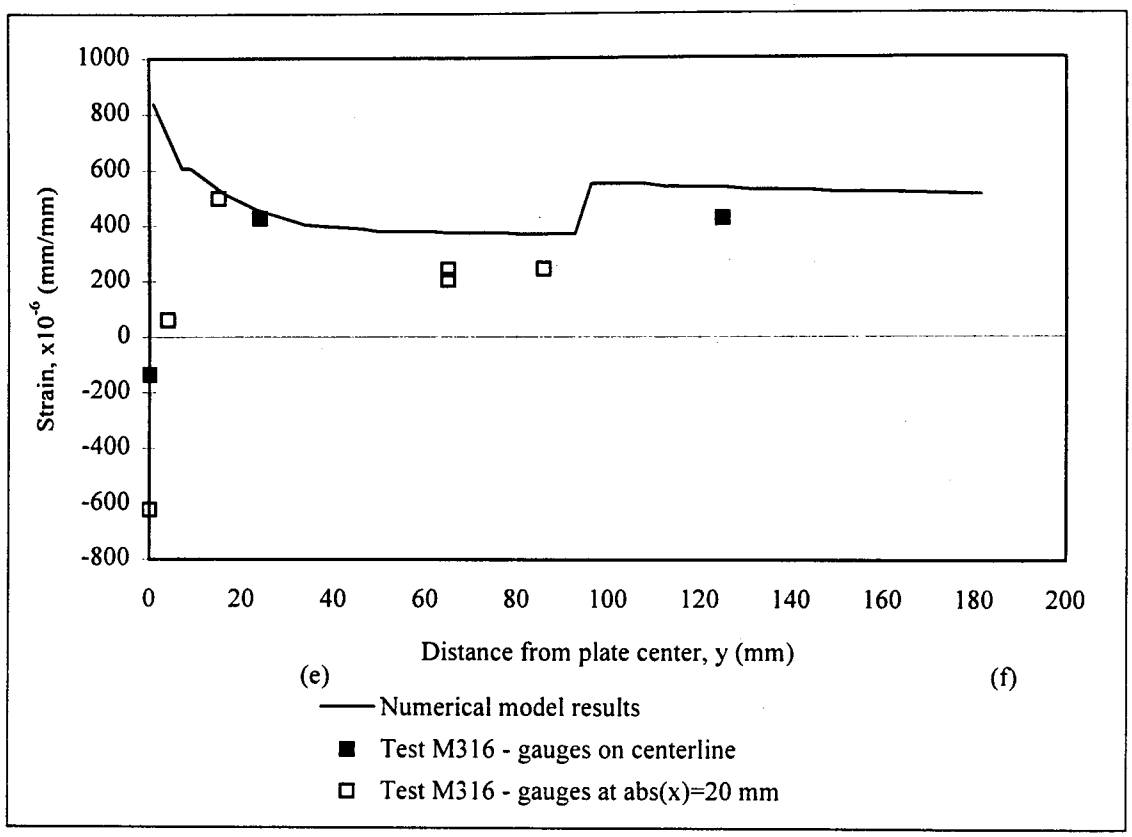

(a)

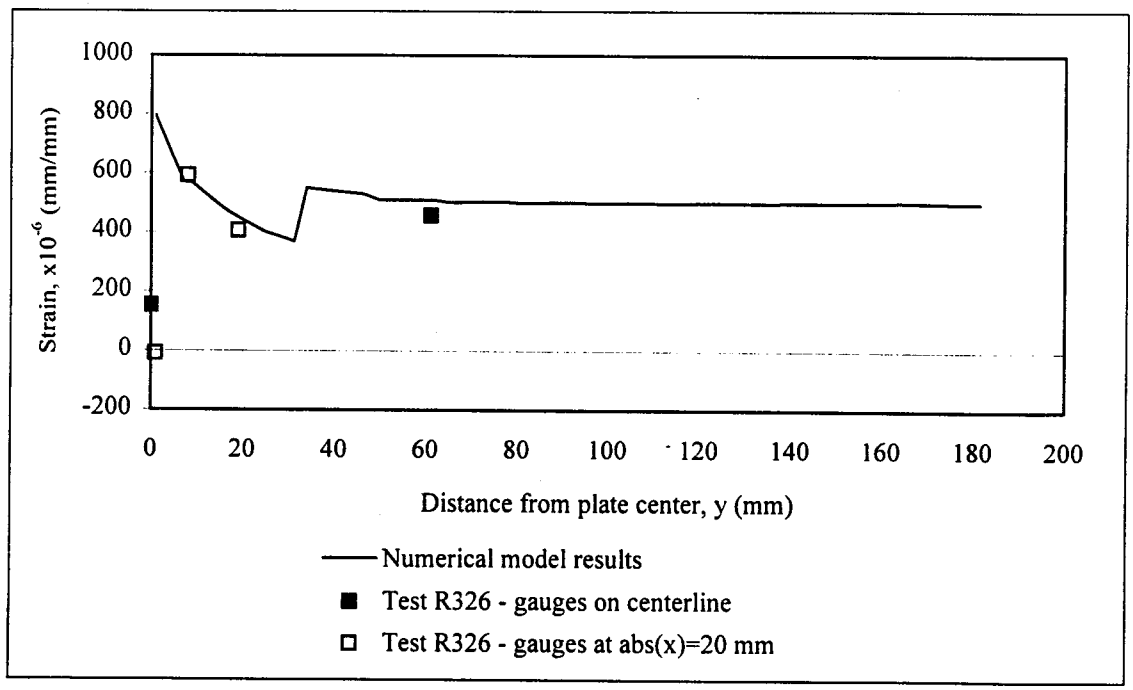

(b)

Figure 4.17 Comparison of numerical and corrected experimental results along plate length for tests M316 and R326

It is believed that compression in the patch across the crack is a result of lower bending resistance of the cross-section along the crack axis. Bending stresses that are resisted by the full cross-section away from the crack must be resisted by the reduced cross-section at the crack location. As discussed in section 4.2.1, the model boundary conditions did not accurately represent the bridging of the crack by the patch. As well, the crack in the model was infinitely narrow, while the test plates used a saw-cut "crack" approximately 2 mm wide. If further study is conducted to predict the response of the test patches to the conditions at the crack, these issues must be dealt with and the compressive behaviour of the composite must be incorporated into the model.

Figure 4.18 and Figure 4.19 show comparisons of the numerical and corrected experimental results for the patched and unpatched faces of tests M214 and R224. The patched face results exhibited similar attributes to Figure 4.16, including higher test than predicted strains between the crack and plateau, and low strains in the test patch across the crack. The unpatched face results showed very good agreement between the predicted and experimental values. The difference in accuracy between the unpatched and patched face results may be attributed to variability in the patch because of the hand lay-up fabrication procedure, or to the accuracy of the strain gauges on each material: it was easier to ensure a complete bond to the steel than to the somewhat irregular surface of the composite.

Results are shown here for six of the nine test plates. The remaining plates showed similar results.

4.3.3 Strain Across Plate Width

Figure 4.20 shows comparisons of numerical and corrected experimental results for strain distributions along the horizontal centerline of three patched plates. All three plates had six layers of composite and the same patch length, L = 100 mm. Numerical strain distributions on the patched and unpatched surfaces of the steel are shown for models

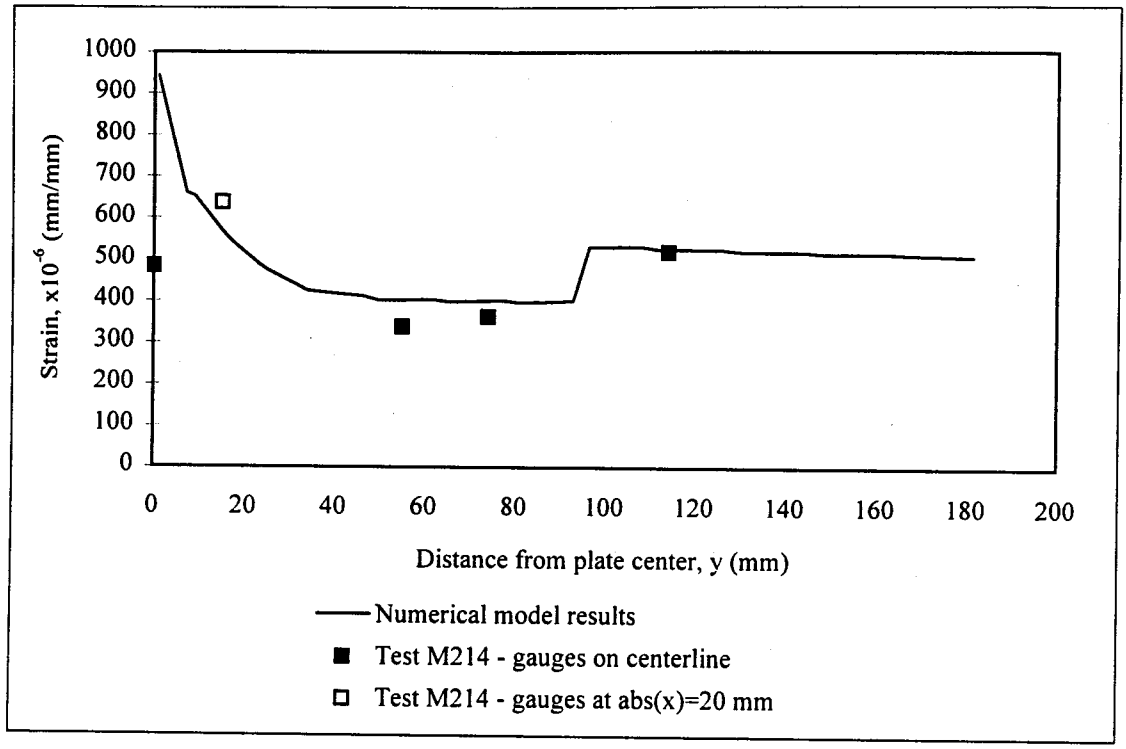

(a) Patched face

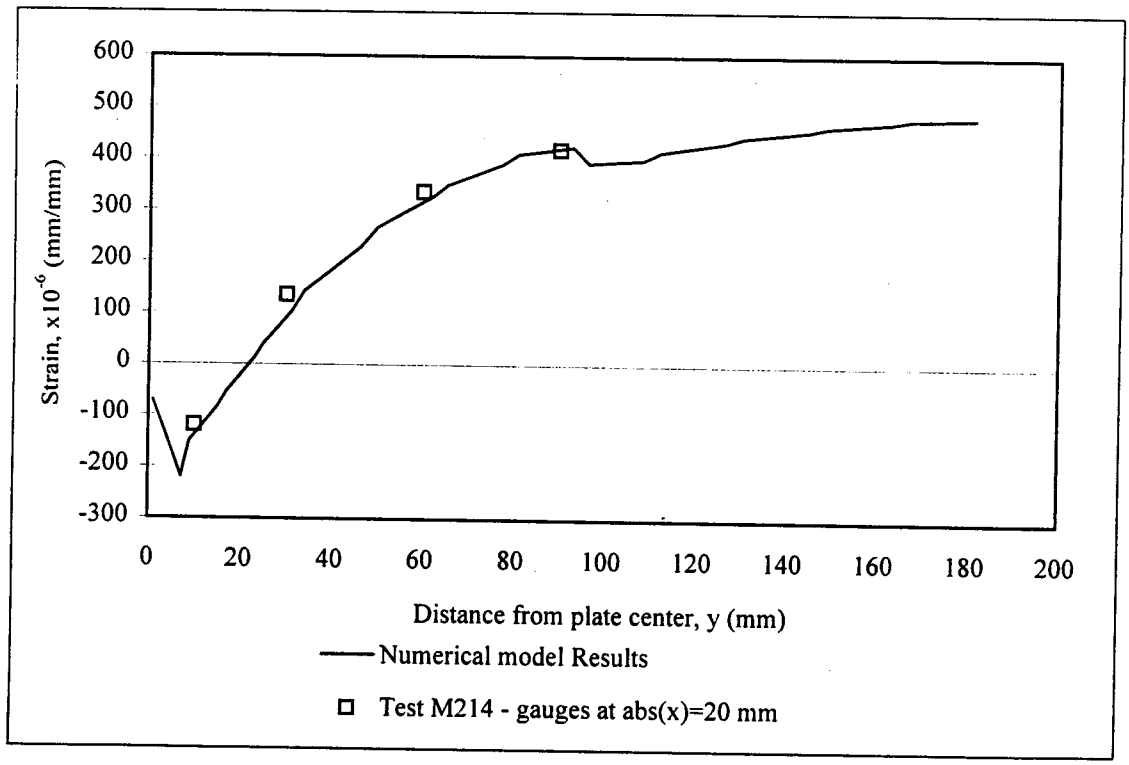

(b) Unpatched face

Figure 4.18 Comparison of numerical and corrected experimental results along plate length for test M214

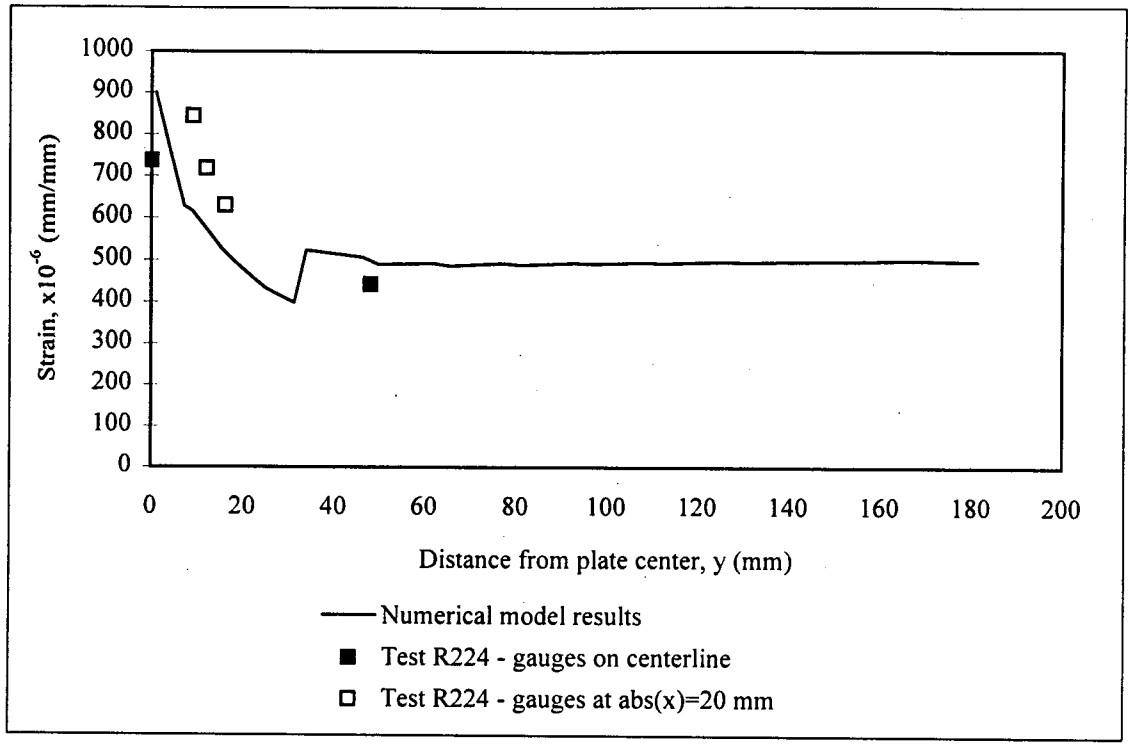

(a) Patched face

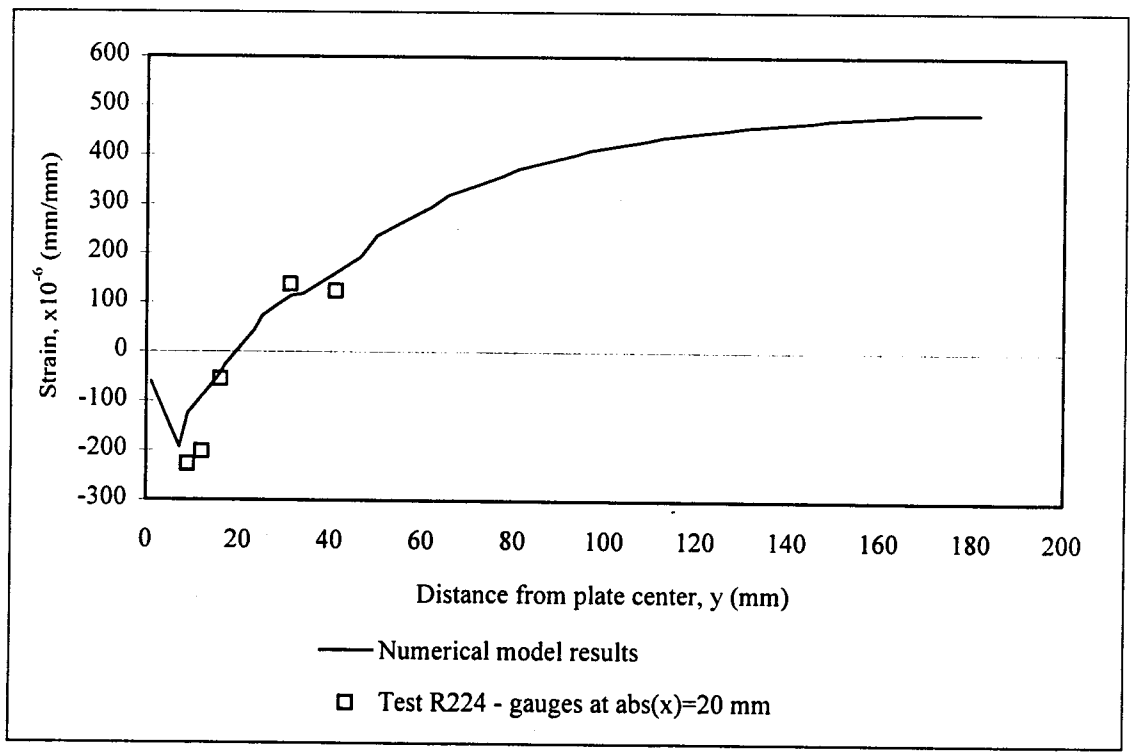

(b) Unpatched face

Figure 4.19 Comparison of numerical and corrected experimental results along plate length for test R224

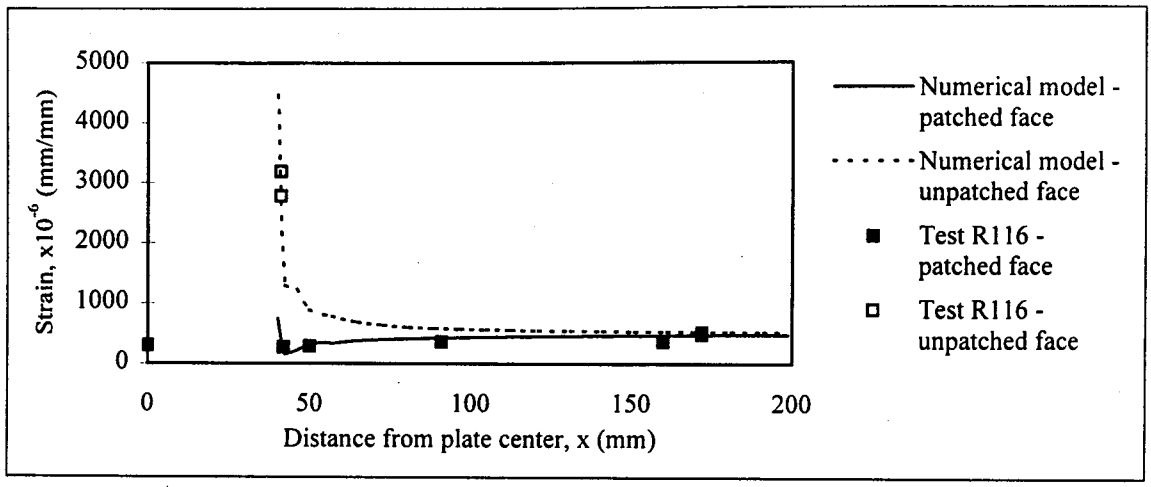

(a) w = 160 mm

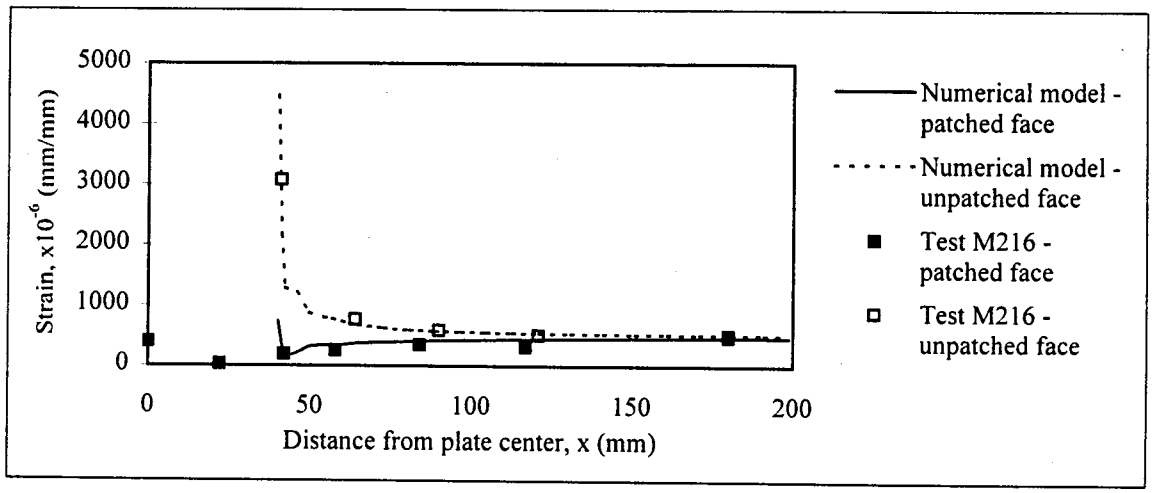

(b) w = 120 mm

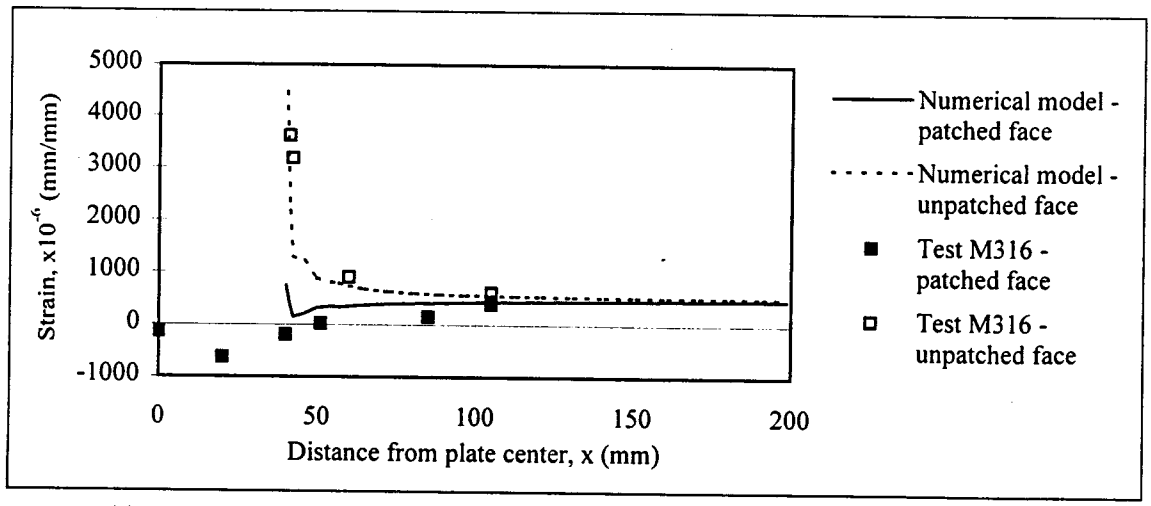

(c) w = 80 mm

Figure 4.20 Comparison of numerical and corrected experimental results across plate width for tests with six layers of composite

with similar patch parameters. Figure 4.21 shows a similar set of comparisons for tests with four layer patches.

In general, the agreement between the numerical and experimental results was good. The test results supported the predicted difference in strain profiles along the patched and unpatched faces of the plate, although again the gauges mounted directly on the steel were more consistent with the numerical results than those mounted on the patch.

In most cases, the experimental results suggested a steady decrease in patched face strains from the edge of the patch towards the center of the plate, including most of the region where the patch bridges the crack. Higher strains were usually recorded right at the plate center, where an 8 mm diameter hole was located to enable the cutting of the crack. These gauges were mounted on the patch with no steel under, while the other gauges along the crack may have overlapped the start of the bond with the steel base material.

There was little difference seen among tests with different patch width, length or thickness. The strain distribution results across the plate width are shown for five of nine tests; the remaining tests showed similar patched face results and did not have a sufficient number of gauges on the unpatched face to allow for comparison with the numerical results.

4.3.4 Demec Readings

Experimental values from the electronic demec gauge were discussed in section 3.3.3. The values showed two trends in the measured strain, which was across the crack on the unpatched face. First, the strain was generally lower in patched plates than in the unpatched plate. Second, strains were generally higher for tests having six layer patches when compared with tests having four layer patches of the same length and width dimensions. The numerical model results showed decreasing vertical displacement of the back face nodes, i.e. lower strain, with increasing patch stiffness. This included lower

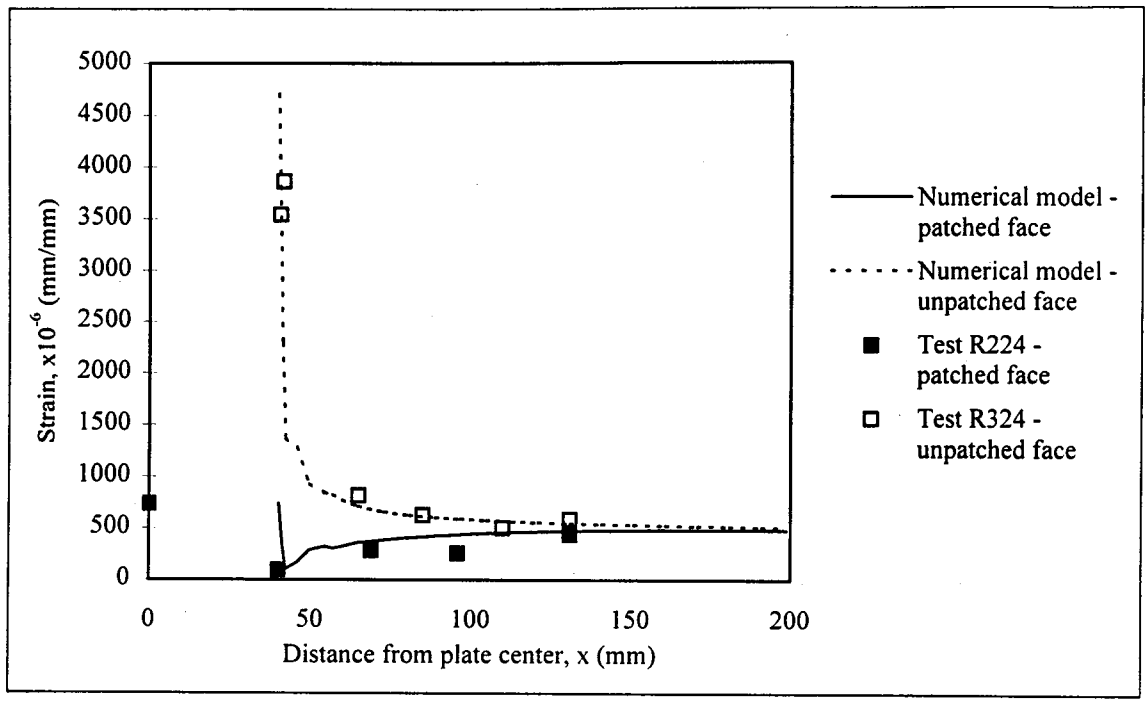

(a) w = 120 mm

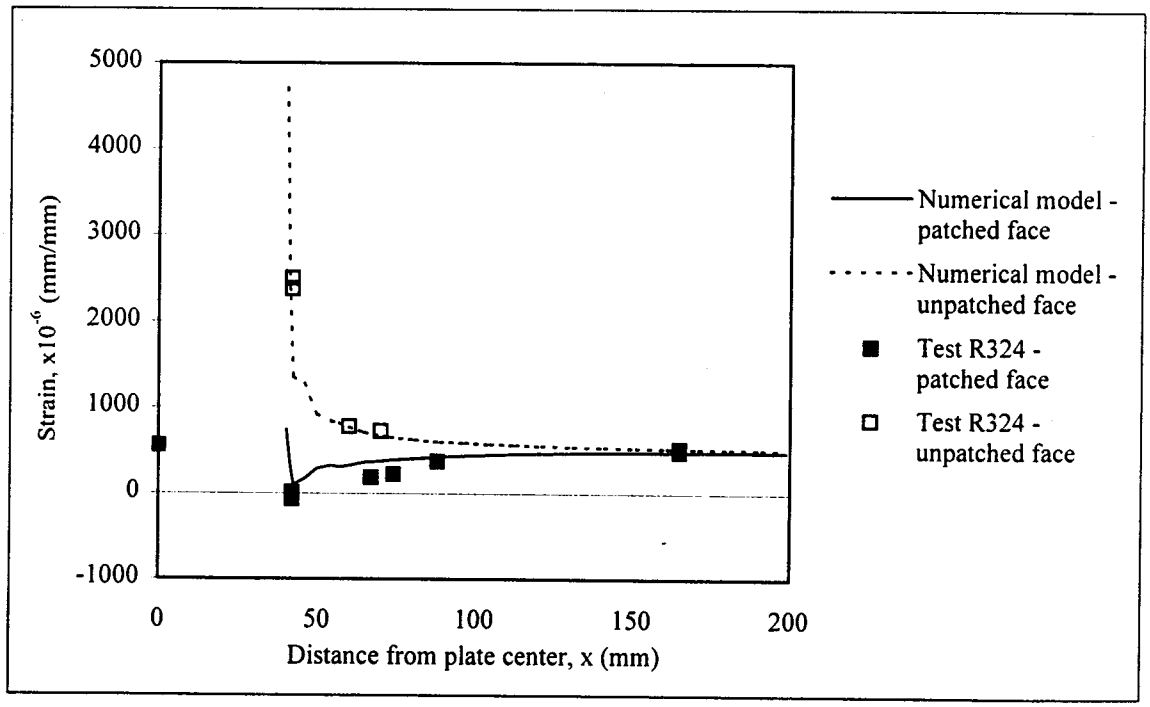

(b) w = 80 mm

Figure 4.21 Comparison of numerical and corrected experimental results across plate width for tests with four layers of composite

strain for any patched plate than for the unpatched plate. The numerical results, therefore, agreed with the first experimental observation, but contradicted the second.

One theory that explains the experimental observations considers two factors that contribute to strains across the demec gauge length: the opening of the crack and the strains due to bending out-of-plane. Crack opening is expected to decrease with increasing patch stiffness; however, stiffer patches may cause higher out-of-plane displacements, which in turn cause increased tension on the unpatched face. Experimentally and numerically, it appears the effects of crack opening were more significant when comparing unpatched and patched plates, as the strain decreased with the application of a patch in both cases. In comparing patches of four and six layers of carbon fibre composite, the experimental results suggest the out-of-plane bending effects governed and the strain increased with increased patch stiffness.

Numerical results suggest that crack opening effects govern the strain along the demec gauge length regardless of patch parameters. This inconsistency with the experimental results may mean that the model underestimated out-of-plane displacements. This underestimate may have been caused by boundary conditions in the model that held the patched face of the crack shut, regardless of the patch stiffness, and increased the stiffness of the cross-section. The modeling of the patch as shell elements may also have resulted in underestimated bending: the center of the patch was perceived as being on the surface of the steel, instead of above it by half of the patch thickness. This would have resulted in lower eccentricity of the resultant loads on the plate and patched cross-section, and therefore lower bending moments.

4.4 Parametric Study

The three primary factors required for patch design are length, width, and number of layers or stiffness. The parametric study considered each factor individually for its effect

on the overall behaviour of a patched element. Analysis was performed at 100 MPa far field applied stress unless otherwise noted.

4.4.1 Patch Length

The parametric study for a bonded patch showed that patch length affects stress concentrations in the steel at the end of the patch, both along the vertical centerline and towards the patch edge. These effects can be divided into the results of load transfer between patch and adherend, and the results of load redistribution across the plate width. To a lesser degree, patch length affects crack tip stresses and local bending near the crack around the vertical centerline.

4.4.1.1 Load Transfer from Patch to Adherend

Figure 4.10 showed the strain along vertical centerline for the patched and unpatched faces of a plate with a four-layer, 96 mm patch (L = 48 mm). Figure 4.22 shows the results for patches with 48 mm, 64 mm, and 190 mm patch lengths (L = 24 mm, 32 mm, and 95 mm respectively). Again the edge of the patch is marked by a sharp increase in strain along the top of the steel.

Comparing the patched face strain results for the 24 and 48 mm patches, it appears that a bond too short results in an increased stress concentration in the steel at the edge of the patch. For the 24 mm patch, no strain plateau is observed and the stress concentration factor, σ_{pk}/σ_o, is 1.085. The plate with the 48 mm patch exhibits a strain plateau of approximately 400 με and has a reduced stress concentration of 1.051. This result is similar to the conclusion of Chapter 2: providing sufficient bond length to allow sufficient load transfer to attain strain compatibility is essential to minimizing the stress concentration in the steel at the end of the joint.

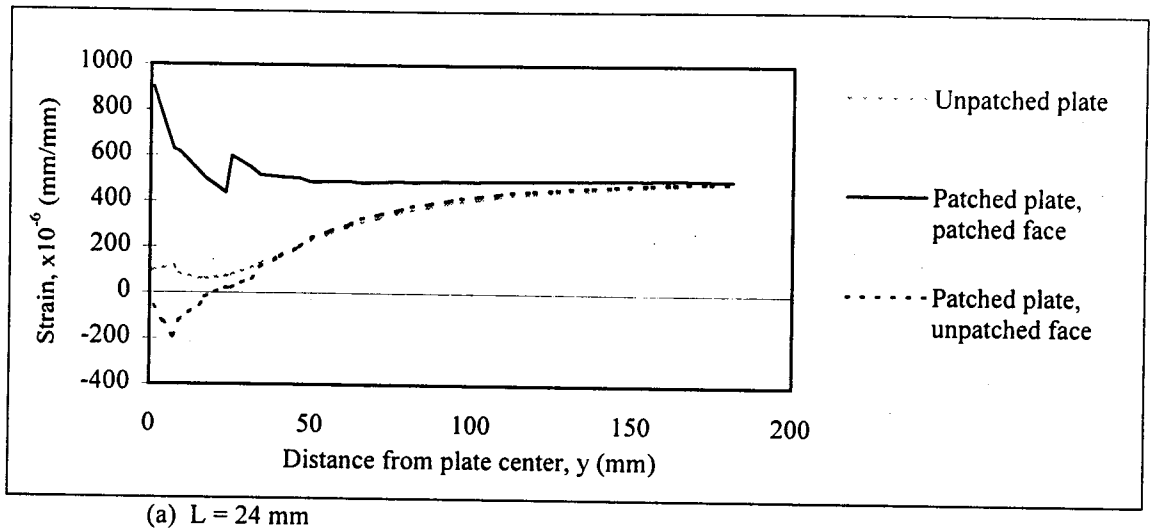

(a) L = 24 mm

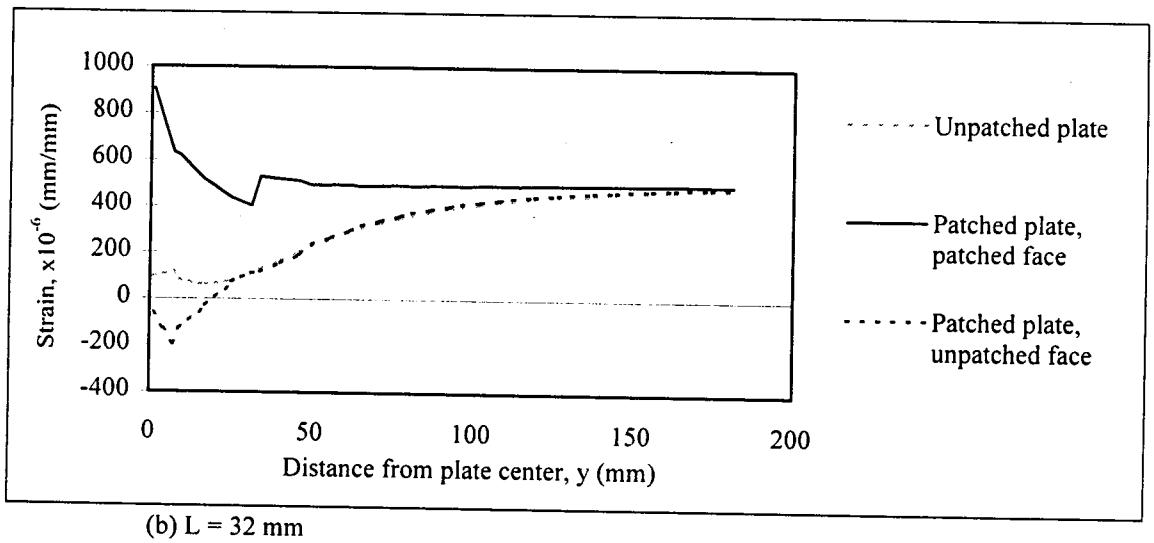

(b) L = 32 mm

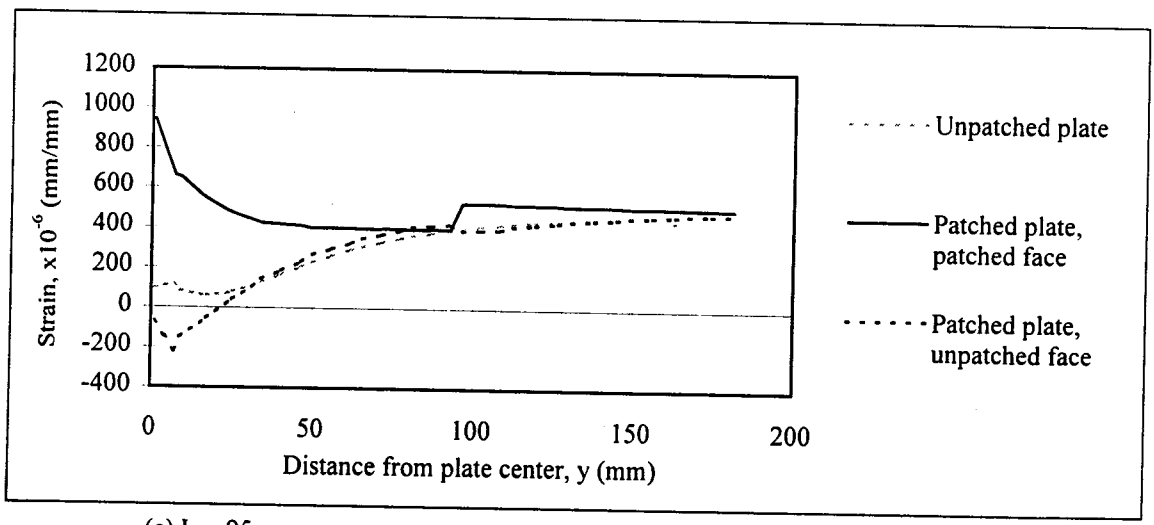

(c) L = 95 mm

Figure 4.22 Strain distribution along vertical centerline for different patch lengths

Applying the minimum bond length calculation method from section 2.4.2.1, minimum bond lengths for various patch configurations were calculated and are presented in Table 4.2. The configurations considered different patch and adherend thickness and two different patch materials, while restricting the stiffness ratio, E_pt_p/E_st_s, to less than 0.25. All calculations were for a 400 mm wide steel plate with an 80 mm (a = 40 mm) internal crack.

Table 4.2 Summary of minimum bond lengths required for load transfer

Thickness of patch, t_p	Elastic Modulus of patch, E_p	Thickness of steel adherend, t_s	E_pt_p/E_st_s	Minimum bond length
(mm)	(GPa)	(mm)		(mm)
2.3	128	6.35	0.232	42.4
1.38	128	5	0.177	42.0
1.38	128	6.35	0.139	29.9
0.92	128	5	0.118	31.3
0.92	128	6.35	0.093	27.7
0.69	128	6.35	0.070	22.2
1.38	35	6.35	0.038	10.7

The results of Table 4.2 are also presented in Figure 4.23. The figure also shows the results for bonded joints, presented in section 2.4.2.3. The bond length required for the patched plate is generally higher than for a joint with the same patch and steel parameters, indicating more gradual load transfer from patch to steel in a patched plate. This transfer rate is influenced by load sharing across the element width and bending that is present in the asymmetrical patched element but not the symmetrical joint. In the patched plate, the bond length is also a function of the amount of load carried by the patch: lower stiffness patches do not carry as much load across the crack and lower bond lengths result.

From Figure 4.23, an estimate of the minimum bond length required for load transfer was determined. Fitting a linear equation to the data, the bond length was estimated as

$$\ell_{min} = 158.25\frac{E_p t_p}{E_s t_s} + 9.89$$

A 95% confidence interval was calculated from the data (Miller et al. 1990), and the equation was rounded for convenience and to reflect the accuracy of the estimate, giving

$$\ell_{min} = 160\frac{E_p t_p}{E_s t_s} + 17 \qquad [4.1]$$

where ℓ_{min} is in mm and the equation is valid for stiffness ratios less than 0.25. The line calculated from this equation is shown in Figure 4.23.

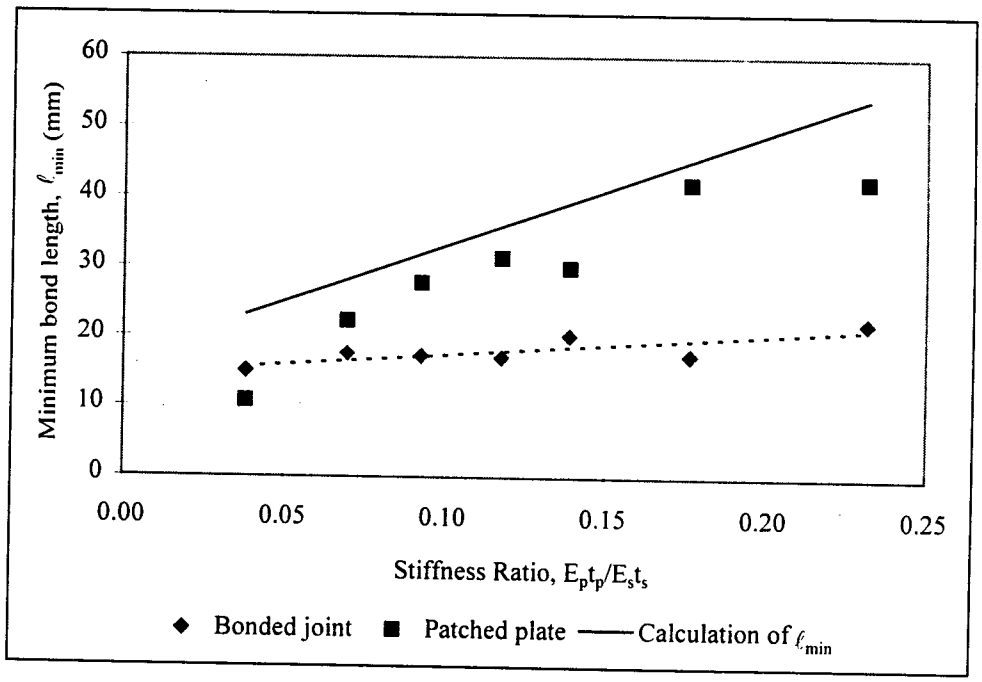

Figure 4.23 Minimum bond length required for load transfer

4.4.1.2 Redistribution of Load Across the Plate Width

Because of the asymmetry of a one-sided patch assembly, and because the patch to adherend stiffness ratio is less than 1.0, a repaired crack still has stress concentrations at the crack tips that result from the flow of load through the base metal around the crack. The return of this load to the plate center takes time, and until it is accomplished the highest stresses in the plate cross-section are at a distance from the centerline of slightly

more than a, half the crack length. Figure 4.11 illustrates the strain profiles across the width of a plate as redistribution of the crack tip stresses occurs.

A longer patch helps to minimize stress concentrations in the steel at the patch edge by allowing more strain redistribution across the plate width before the patch end. This allows dissipation of the high stresses around the crack tip and decreases the peak edge stress concentrations that occur in the steel. To illustrate, consider a 96 mm long patch (L = 48 mm), 160 mm wide (w = 80 mm), fabricated from four layers of unidirectional carbon fibre composite bonded to a 6.35 mm steel plate with an 80 mm internal crack. The stress concentration factor in the steel at the patch edge is 1.051 at the centerline, but is 1.226 towards the patch edge. If instead a 190 mm patch (L = 95 mm) were used, the stress concentrations are 1.098 and 1.155 at the centerline and at the peak stress point near the patch edge respectively. All concentrations are obtained at the nearest integration point to the patch edge, 1.802 mm away, and therefore underestimate the actual stress concentration factor.

To define the minimum bond length with respect to load redistribution, the criteria suggested are:

> *Consider a plate with given crack and plate parameters, and a patch of specified stiffness and excessive length. The minimum patch length is the vertical distance from the crack at which the strain in the plate is less than or equal to the far field applied strain at all points across the width of the patch.*

The minimum bond length predictions from a series of numerical models are shown in Table 4.3. The models considered varied crack length and patch and adherend thickness. All patches were unidirectional carbon fibre, 160 mm wide (w = 80 mm) and 190 mm long (L = 95 mm). Bond length results were restricted to integration point intervals, which were up to 9 mm apart. The effects of crack length and stiffness ratio, $E_p t_p / E_s t_s$, on

Table 4.3 Summary of minimum bond lengths required for load redistribution

Crack length, a	Thickness of Steel Adherend, t_s	Thickness of patch, t_p	Elastic modulus of patch, E_p	E_pt_p/E_st_s	Redistribution length
(mm)	(mm)	(mm)	(GPa)		(mm)
10	6.35	0.92	128	0.093	15.1
20	6.35	0.92	128	0.093	28.0
32	6.35	0.92	128	0.093	51.3
40	6.35	0.92	128	0.093	75.7
40	6.35	1.38	128	0.139	51.3
40	6.35	1.84	128	0.185	35.4
40	6.35	2.30	128	0.232	35.4
40	5.00	0.92	128	0.118	60.2
40	12.7	2.30	128	0.116	66.8

required bond length are summarized in Figure 4.24(a) and (b) respectively. From the first figure, the linear regression relationship between crack length and minimum required bond length for $E_pt_p/E_st_s = 0.093$ was found to be

$$\ell_{min} = 1.722a \qquad [4.2]$$

The linear regression relationship from Figure 4.24(b) was determined to be

$$\ell_{min} = -298.4\frac{E_pt_p}{E_st_s} + 98.031 \qquad [4.3]$$

for ℓ_{min} in mm. If [4.3] was used as a scale factor, so that it equaled 1.0 when $E_pt_p/E_st_s = 0.093$ corresponding to the derivation of [4.2], the equation for minimum bond length was determined to be

$$\ell_{min} = 1.722a\left(-4.246\frac{E_pt_p}{E_st_s} + 1.395\right)$$

So that false accuracy of the estimate was not implied, the equation was rounded to

$$\ell_{min} = 2a\left(-4.2\frac{E_pt_p}{E_st_s} + 1.4\right) \qquad [4.4]$$

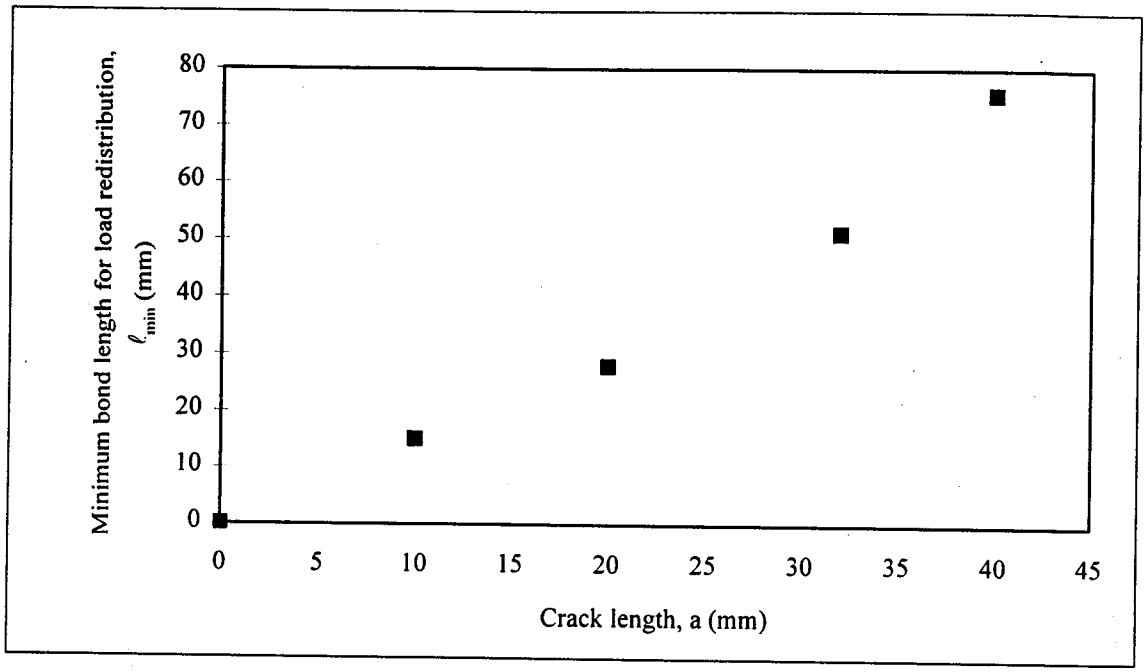

(a) Minimum bond length as a function of crack length. For all tests $E_pt_p/E_st_s = 0.093$.

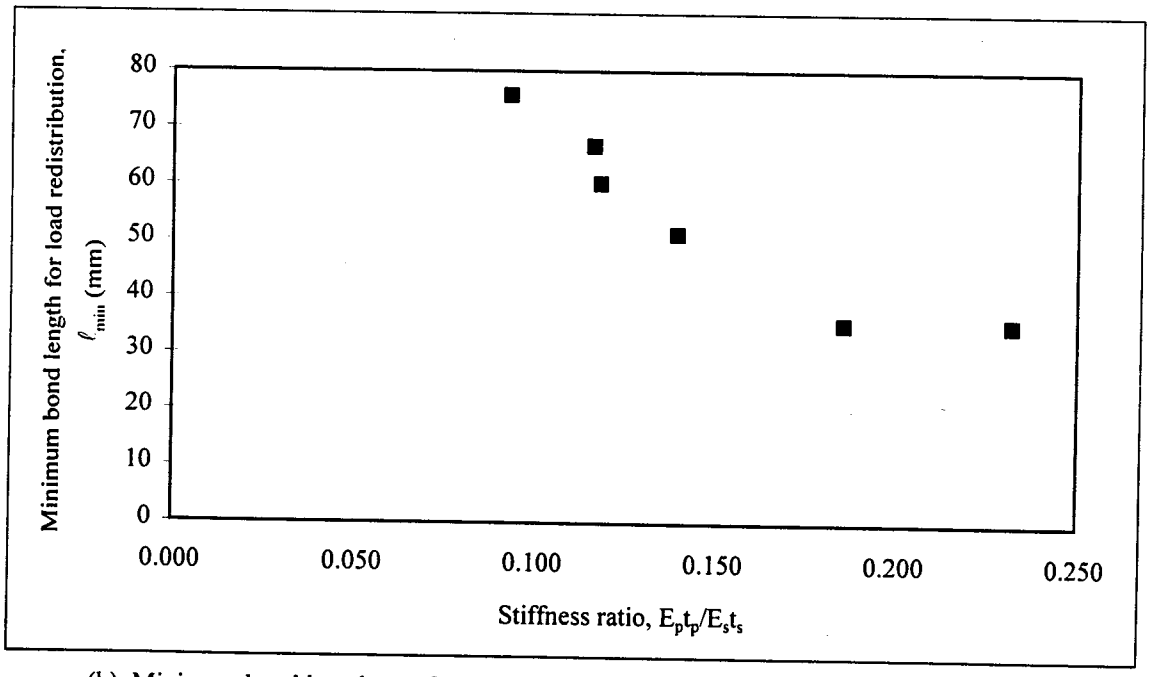

(b) Minimum bond length as a function of element stiffness. For all tests a = 40 mm.

Figure 4.24 Minimum bond length for load redistribution

Considering that the original data points may have been conservative by up to 9 mm, it is difficult to determine a more accurate estimate for the required bond length, or to establish a 95% confidence interval. Based on the low number of data points available, any such estimate would likely be highly conservative. A more comprehensive study, including more refined estimates of bond length for individual test cases, should be used if a more accurate estimate is desired.

4.4.1.3 Crack Tip Strains

Patch length has some effect on the crack tip stress concentration, although it is minimal. Figure 4.25 shows that a plate repaired with a longer patch has higher strains in the patched region of the plate than the same plate repaired with a shorter patch. The strain distributions shown are in the patched face of the plates. There are two implications of this observation. First, crack tip strains increase with an increase in patch length. This is related to increased crack opening as a result of more load acting on a patch of given stiffness. Second, the distance required for load redistribution is a function of patch length. A shorter patch allows more load to flow further outward around the crack towards the edge of the plate; therefore, this load has further to flow back towards the center of the plate and it takes longer to re-establish constant stress distribution. Considering the strain distributions along the unpatched face of the plates in Figure 4.22, it appears load returns to the plate center more quickly in plates repaired with longer patches.

It must be noted that this is a result of elastic analysis only. Yielding of the steel at the crack tip will reduce the effects of the increased stress concentration, which are already minimal. The difference in the rate of load flow back to the plate center for different patch lengths is also minimal. It is therefore assumed that these conditions do not govern minimum patch length requirements.

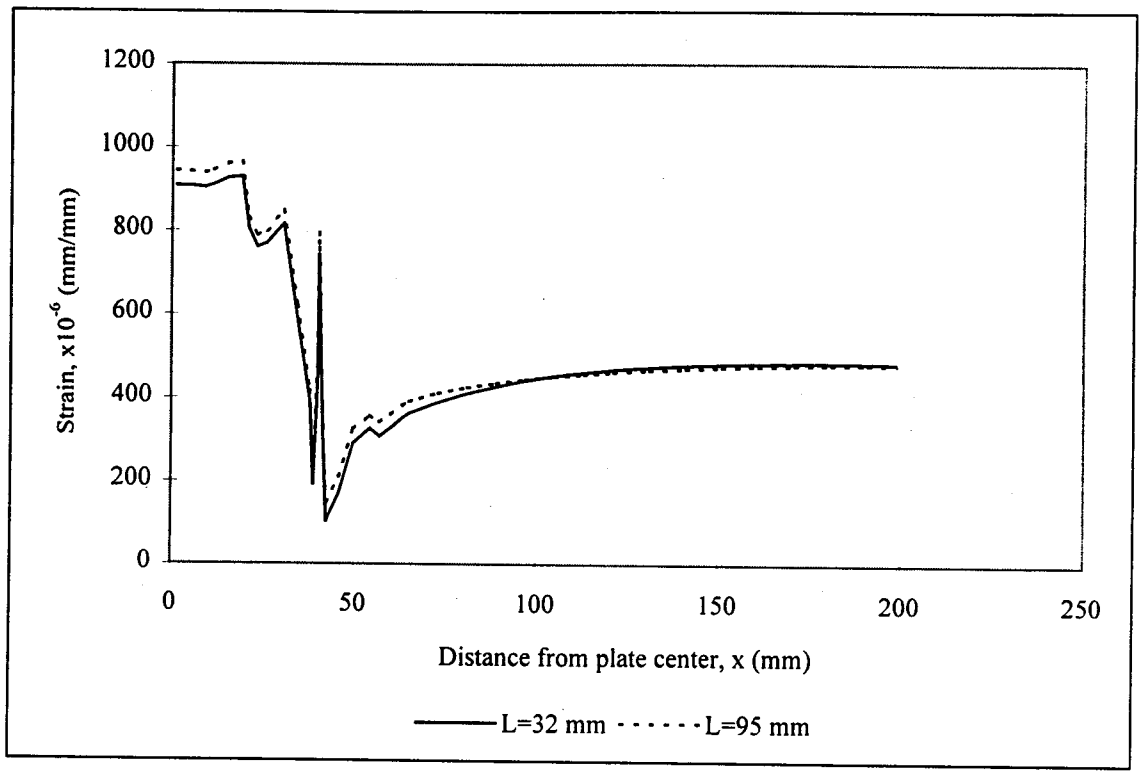

Figure 4.25 Strain distribution across horizontal centerline for different patch lengths

4.4.1.4 Bending

A plate repaired with a longer patch shows slightly higher local bending near the crack than the same plate repaired with a shorter patch. Figure 4.26 shows through-thickness strain profiles at the vertical centerline for elements with L = 32 mm and L = 95 mm patches. The first profile is at y = 0.91 mm, very close to the crack. At this point, the strain distribution is highly non-linear as most of the load is in the patch and the patched face of the plate. Higher strains are seen in the patched face of the plate for the test with the longer patch, as expected from Figure 4.25. Figure 4.26(b) illustrates the through-thickness profile at y = 16.9 mm from the crack. At this point the load distribution is approximately linear in both cases, but the profile for the longer patch shows more bending. It is suspected that bending in this area is due in part to the transfer of stresses away from the patched face of the plate, as discussed in section 4.2.1. Greater load therefore results in greater bending on the same cross-section.

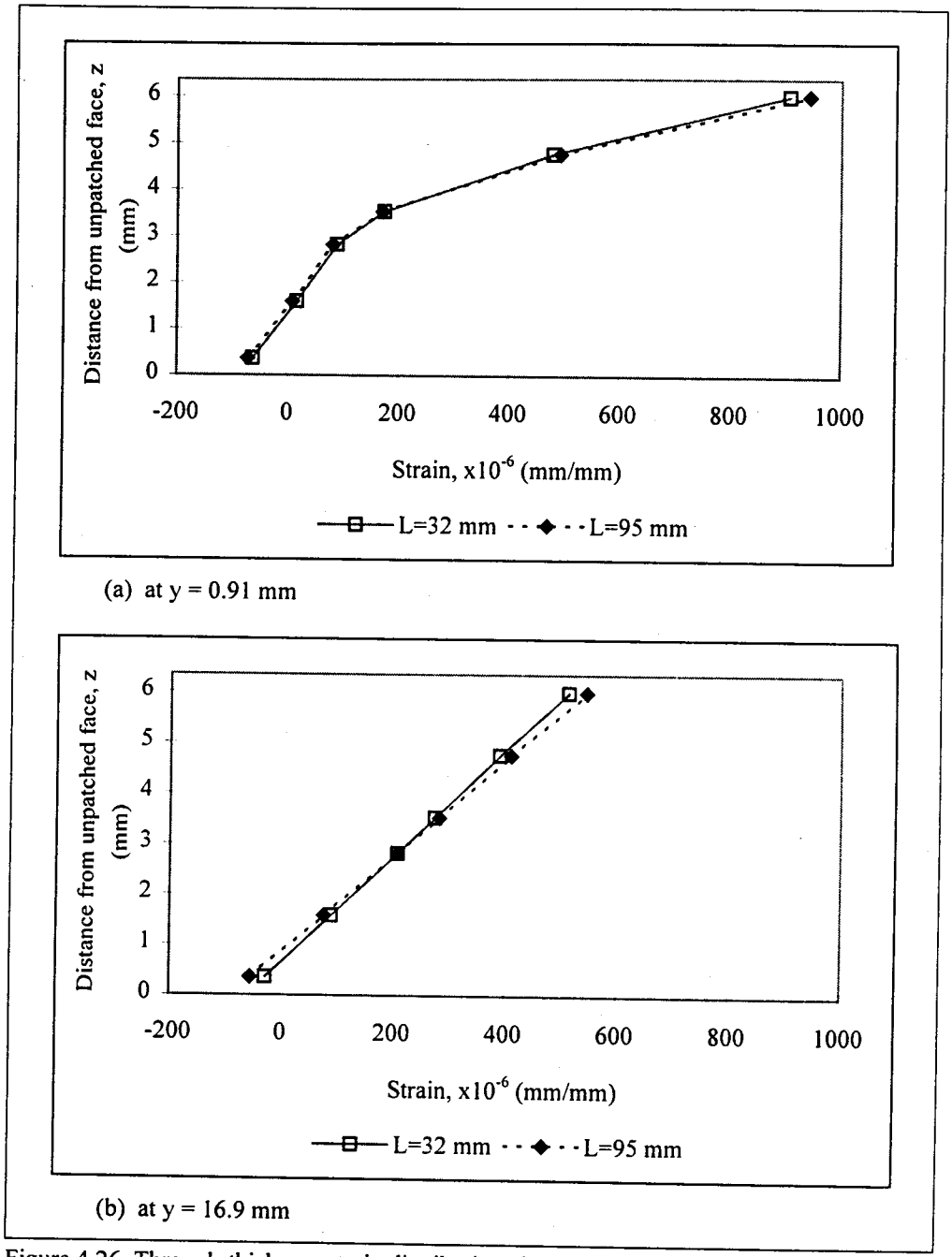

Figure 4.26 Through-thickness strain distribution along the vertical centerline

The influences of bending on the performance of a patch are believed to be minimal compared with load transfer and load redistribution requirements. They were not considered in minimum patch length specifications.

4.4.1.5 Summary

Minimum patch length, L, is governed by the larger of:

1. The length required for load transfer and establishment of a strain compatibility plateau.

$$\ell_{min} = 160\frac{E_p t_p}{E_s t_s} + 17 \qquad [4.1]$$

This criterion governs for small cracks.

2. The length required to allow redistribution of load across the width of the patch.

$$\ell_{min} = 2a\left(-4.2\frac{E_p t_p}{E_s t_s} + 1.4\right) \qquad [4.4]$$

This criterion governs for longer cracks where the area affected by load flow around the crack is larger.

The patch length should not be less than L = 30 mm for practical application.

4.4.2 Patch Width

Figure 4.27 shows the horizontal centerline strain distribution through the center of the plate thickness for an unpatched plate and four patches with different widths. All patches were four layers of unidirectional carbon fibre with L = 32 mm. The plot only extends to x = 140 mm, 100 mm beyond the crack tip, in order to show a maginfied view of the strain profiles near the crack tip. The results show very little change in the strain behaviour with changing patch width.

Strains through the center of the plate width are slightly lower when the crack is repaired with a wider patch, as shown in the patched face strain profiles along the vertical centerline, shown in Figure 4.28. These lower strains may be because of an increase in overall stiffness of the patched plate, or because of an increase in overall bending that

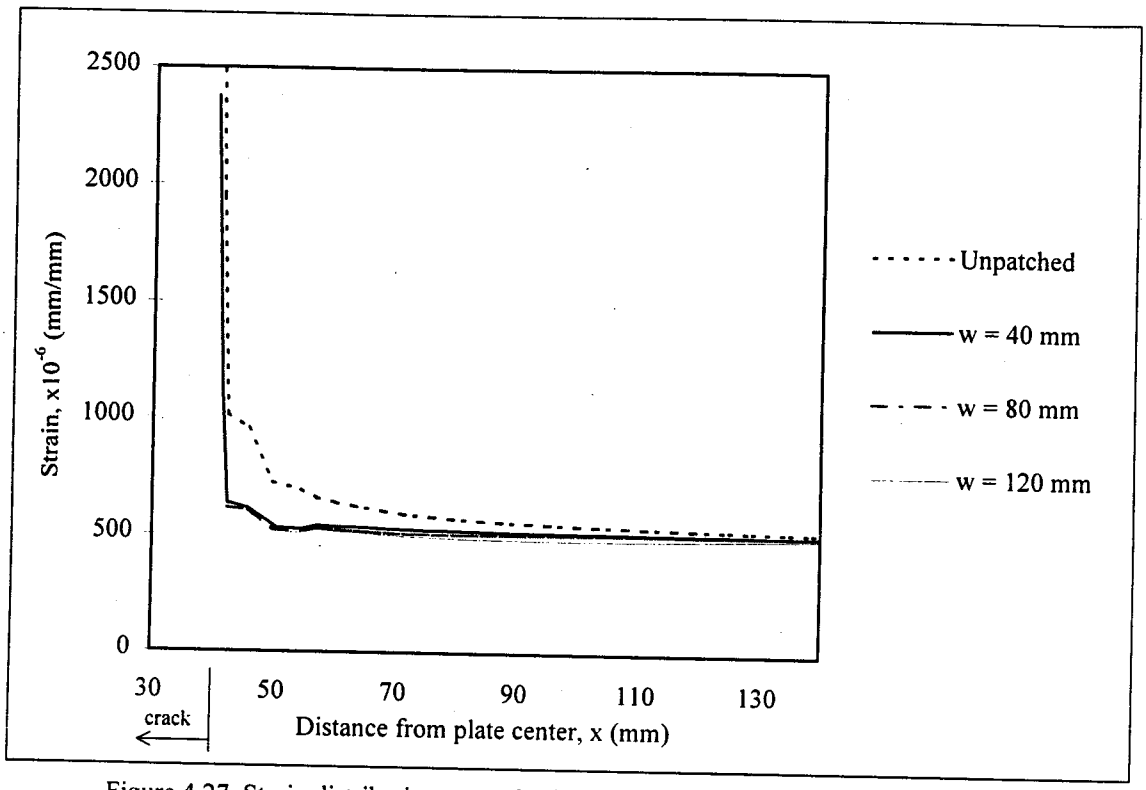

Figure 4.27 Strain distribution across horizontal centerline for different patch widths

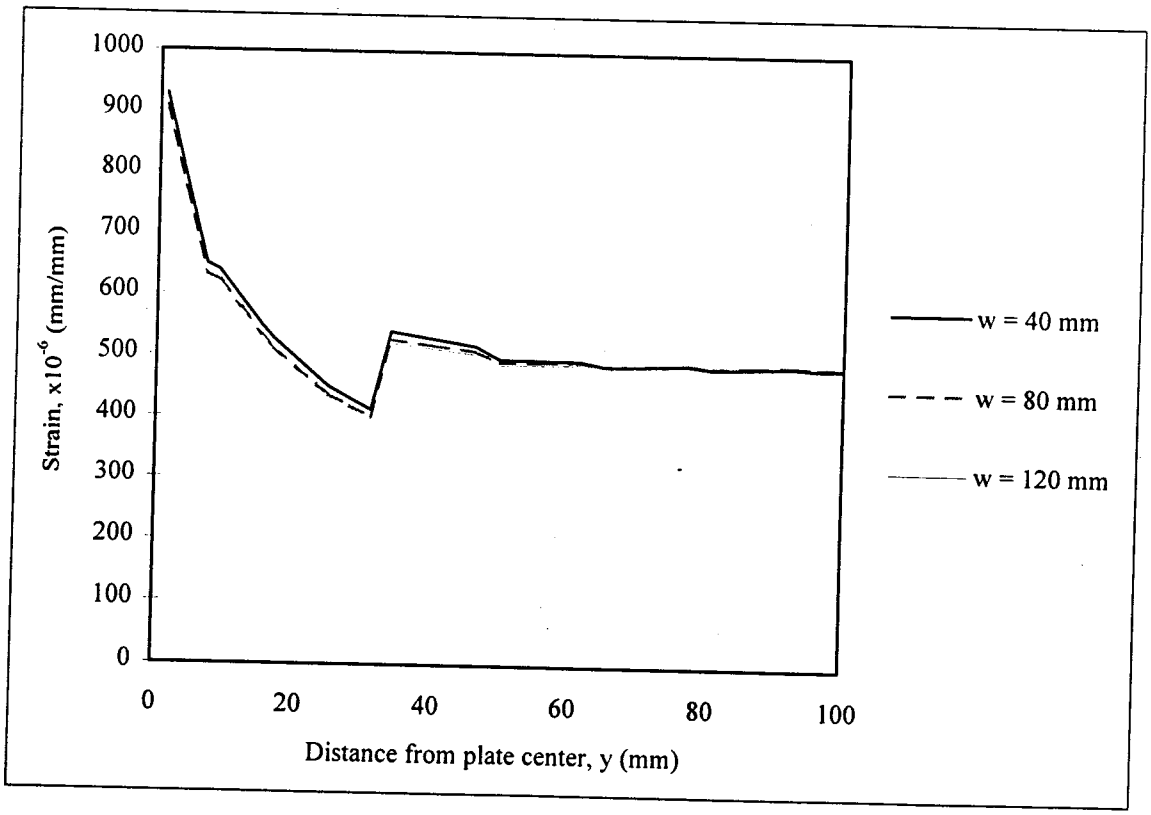

Figure 4.28 Strain distribution along vertical centerline for different patch widths

results from the shift of the centroidal axis further away from the line of action of the applied load.

In considering Figure 4.27 and Figure 4.28, it should be noted that a w = 40 mm patch extends precisely to the crack tip. Although this variation appears to change local bending patterns slightly near the crack tip, the general shape of the strain profile is the same.

The results of this study do not suggest a significant improvement in strain distribution with the use of wider patches. Increasing patch width does, however, allow the patch to remain serviceable with some crack growth. Fatigue testing of patches may help to clarify the effect of patch width, and specifications for patch design will therefore be a function of fatigue test results and crack growth allowed in the repaired plate.

Baker (1987) provided design guidelines for bonded patch repairs based on the stress intensity in the repaired element and the performance of the patch. None of the calculations relied on the patch width parameter, suggesting, as did the results of the study here, that patch width does not significantly affect the response of the repaired element. Baker provided several design examples and typically uses a patch of w = 80 mm for the repair of a crack with a = 25 mm, although no justification for this choice is given.

Rose (1988) provided a theoretical analysis of crack patching based on one-sided elliptical patches applied to aluminum plates. The analysis required that the stiffness of the patch equaled the stiffness of the base metal adherend, $E_p t_p / E_s t_s = 1.0$. While no specific guidelines for dimensional design were given, the patch was required to extend beyond the crack tip, but it was stated that the crack width and the patch width were approximately equal, implying again that excessive width beyond the crack tip is not necessary.

Other analyses have found that patch width does affect repair performance. Numerical analysis by Chue et al. (1996) considered the two-sided patched repair of a crack emanating from a fastener hole in an aluminum plate. For a crack length, a, of 3 mm in 11.2 mm thick plate, boron/epoxy patches were modeled for widths, w, of 6 mm, 12 mm, and 18 mm. No reason was given for the choice of width parameters tested. The results showed that crack tip stress conditions are improved by the use of a wider patch.

Alawi and Saleh (1992) performed fatigue tests on cracked steel specimens repaired with bonded steel patches. The tests compared patches that covered the crack only with patches that extended beyond the crack tip to the edge of the test specimen. It was found that for both one- and two-sided repairs, the wider patches were more effective at reducing crack growth rates. No dimensions were given for the crack size, the test specimens, or steel patches.

4.4.3 Patch Stiffness

The choice of patch stiffness must be based on minimizing edge stress concentrations, while maximizing the ability to arrest crack growth through reduced crack tip stresses.

Figure 4.29 shows the patched face strain profile along the vertical centerline of 6.35 mm plates with four and six layer, L = 48 mm carbon fibre patches. The two conclusions that can be drawn from this data are:

1. A stiffer patch has a slightly longer minimum bond length with respect to load transfer (see section 4.4.1.1). From the data, ℓ_{min} = 28.4 mm for a four layer patch and ℓ_{min} = 29.5 mm for a six layer patch.
2. A stiffer patch results in a higher stress concentration in the steel at the patch edge on the vertical centerline: 1.051 for a four layer patch compared with 1.108 for a six layer patch.

These conclusions were the same for bonded joints.

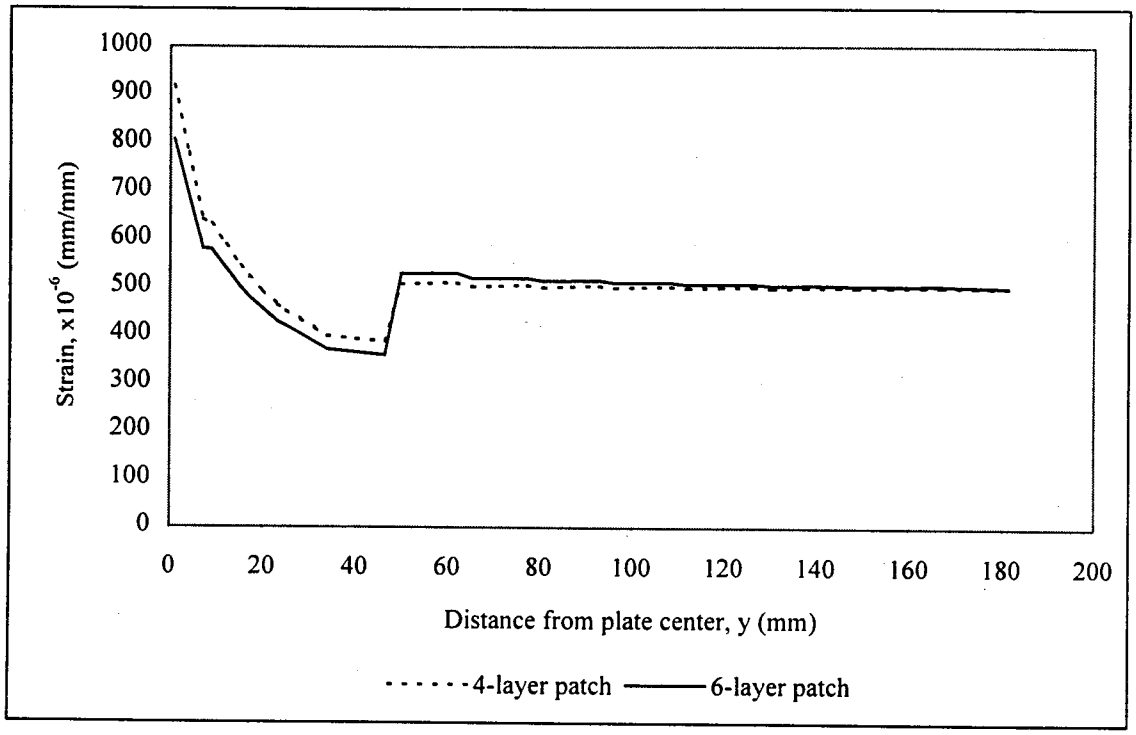

Figure 4.29 Strain distribution along vertical centerline for four- and six-layer patches

The numerical analysis suggested a six-layer patch is able to carry more load across the crack than a four layer patch. Because the patch elements shared all nodes with the steel elements, the strain profile in the patched face of the steel, shown in Figure 4.29, was the same as the strain profile for the patch. Considering the integration points closest to the crack, the strain in the patch was used to approximate the load in the patch by multiplying it by the patch elastic modulus and the patch thickness. This resulted in a load of 1081 N/mm width in the four-layer patch and a load of 1425 N/mm width in the six-layer patch. The same procedure showed higher patch loads in the strain plateau for the stiffer patch, which was necessary for overall plate strain compatibility. It should be noted again that the boundary conditions for this model were such that the crack was restricted from opening on the patched face regardless of the patch stiffness. In reality the response may be different from that discussed here since patch stiffness and load do affect the crack opening.

Because a stiffer patch is able to carry more load across the patch, and because it requires more load for overall strain compatibility, load is held or drawn back to the plate center more quickly than for a lower stiffness patch. This increased rate of load redistribution means a stiffer patch has a lower minimum required bond length for load redistribution, as discussed in section 4.4.1.2.

Bonded composite repairs to aluminum elements, such as aircraft components, are typically designed for $E_pt_p = E_st_s$ (Rose 1988). This is feasible where the stiffness of the base material is low and the elements being repaired are thin; it is not practical when repairing thick steel elements with a material of lower stiffness than the base metal. Alawi and Saleh (1992) performed fatigue tests on thick steel elements repaired with bonded steel patches. The tests found that thicker patches were more effective at increasing the element's fatigue life, based on tests of 1 mm ($E_pt_p/E_st_s = 0.0787$) and 4 mm ($E_pt_p/E_st_s = 0.315$) patches on (assumed) 25.4 mm specimens. The elements were patched on both sides, following earlier tests that showed two-sided patching was more effective than one-sided. Roberts (1995) showed that a two-sided carbon fibre patch, three layers per side, was able to reduce crack growth in a 15.9 mm steel plate ($E_pt_p/E_st_s = 0.0475$). Further fatigue tests are required to better estimate required patch stiffness.

4.5 References

Alawi, H. and I.E. Saleh. 1992. "*Fatigue Crack Growth Retardation by Bonding Patches.*" Engineering Fracture Mechanics, Vol. 42, No. 5, pp. 861-868.

Baker, A.A. 1987. "*Fibre Composite Repair of Cracked Metallic Aircraft Components - Practical and Basic Aspects.*" Composites, Vol. 18, No. 4, pp. 293-308.

Chue, Ch.-H., W.-Ch. Chou, and Th. J.-Ch Liu. 1996. "*The Effects of Size and Stacking Sequence of Composite Laminated Patch on Bonded Repair for Cracked Hole.*" Applied Composite Materials, Vol. 3, No. 6, pp. 335-367.

Hibbitt, Karlsson & Sorenson, Inc. 1996. "*ABAQUS Version 5.6.*" ABAQUS/Standard User's Manual Volumes I and II, Pawtucket, Rhode Island, USA.

Miller, Irwin, John E. Freund, and Richard A. Johnson. 1990. Probability and Statistics for Engineers, Fourth Edition. Prentice-Hall, Inc., Englewood Cliffs, New Jersey.

Roberts, Pamela D. 1995. "*Crack Growth Retardation by Carbon Fibre Composite Patching: An Application to Steel Pressure Vessel Repair.*" Master of Science Thesis, University of Alberta, Department of Mechanical Engineering, pp. 53-85.

Rose, L.R.F. 1988. "*Theoretical Analysis of Crack Patching.*" Bonded Repair of Aircraft Structures, A.A. Baker and R. Jones, Eds., Martinus Nijhoff Publishers, Dordrecht, The Netherlands, pp. 77-106.

Schubbe, J. and S. Mall. 1997. "*Fatigue Crack Growth Behaviour of Thick Aluminum Panels Repaired with Composite Patch.*" 42nd International SAMPE Symposium, pp. 197-207.

Schwartz, M.M. 1984. Composite Materials Handbook. McGraw-Hill, Inc., United States of America, p. 314.

5 PATCH EDGE CONDITIONS

To this point, this report has focused on the flow of stresses around a crack repaired with a bonded patch. Chapter 2 considered the stress distribution in a bonded joint, and Chapters 3 and 4 considered the stress distributions in a one-sided patch repair of a plate with an internal crack. The primary focus has been the stress around the crack, and in particular at the crack tip, as this has the most direct influence on further propagation of the crack. In theory, however, if a stiff enough repair is provided, the crack is held closed on the patched surface and fatigue mechanisms change, possibly losing significance. In this case, boundary mechanisms may become more critical to the performance of the patch, as high stress concentrations in the steel at the patch edge may cause new crack development. These stress concentrations are the focus of this chapter.

The stress concentration factor was used in Chapters 2 and 4 to discuss the effects of patch stiffness and length on stress concentrations in the steel at the patch edge. The causes of these stress concentrations are discussed here in more detail. Two additional design parameters are also considered for the reduction of patch edge stress concentrations: tapering the edge of the patch and using an elliptical patch in place of a rectangular one. The experimental program presented in Chapter 3 incorporated both of these possibilities, and the numerical models developed for bonded joints and a bonded patch were both used to test the effectiveness of these two edge conditions.

5.1 Causes of Stress Conditions in the Steel at the Patch Edge

Load cannot redistribute instantaneously, so stress concentrations are caused when the load acting on the patched cross-section must suddenly be carried by the unpatched cross-section, and in particular the patched face of that cross-section. Consider the two sections in Figure 5.1. If strain compatibility has been established in the patched cross-section and bending is neglected, the strain profile can be approximated as constant with the

resulting stress profile shown in the figure. The total load in this element, P, per unit width, is therefore

$$\begin{aligned} P &= \sigma_1 t_1 + \sigma_2 t_2 \\ P &= \varepsilon E_1 t_1 + \varepsilon E_2 t_2 \\ P &= \varepsilon(E_1 t_1 + E_2 t_2) \end{aligned} \qquad [5.1]$$

At the patch edge, the cross-section changes suddenly, but the total load must stay the same. If for now a constant strain distribution is assumed on this new cross-section,

$$P = \varepsilon' E_2 t_2 \qquad [5.2]$$

Setting [5.1] and [5.2] equal,

$$\varepsilon' = \varepsilon\left(\frac{(E_1 t_1 + E_2 t_2)}{E_2 t_2}\right) \qquad [5.3]$$

For a four-layer carbon fibre/epoxy composite patch on a 6.35 mm thick steel adherend, this results in

$$\varepsilon' = 1.093\varepsilon \qquad [5.4]$$

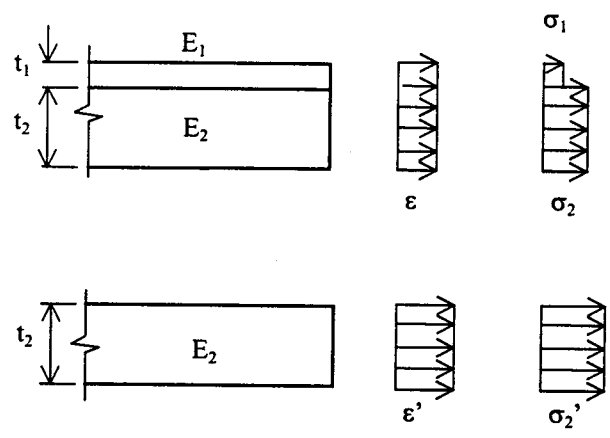

Figure 5.1 Effects of a sudden change of cross-section on magnitude of strain and stress

Now consider the results of a numerical model, developed in section 4.1, of a 6.35 mm steel plate with an 80 mm internal crack. The plate was modeled with a bonded

unidirectional carbon fibre patch, 160 mm wide (w = 80 mm) and 190 mm long (L = 95), as shown schematically in Figure 3.2.

The through-thickness strain profiles in the steel at the integration points before and after the edge of the patch are shown in Figure 5.2 at 100 MPa far field applied stress. Note that these profiles are approximately 1.7 mm away from the end of the patch. Before the patch edge, the strain profile is almost constant, with some bending present due to the eccentricity of the applied load and the reaction force on the patched cross-section. The profile after the patch edge is no longer constant, but can be approximated as linear.

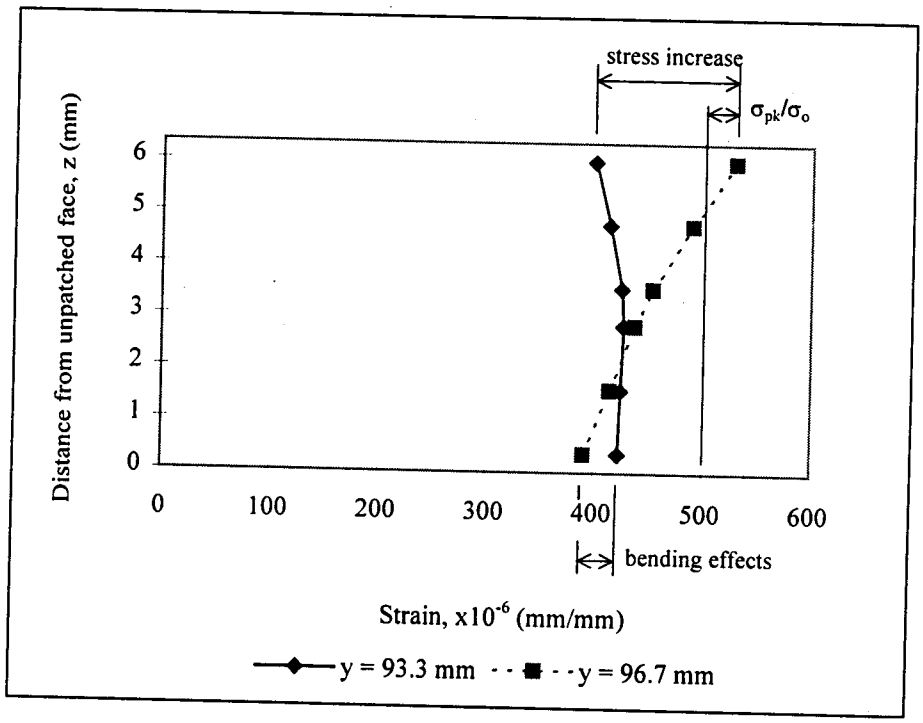

Figure 5.2 Through-thickness strain distribution along the vertical centerline near the patch edge

From the theory of Figure 5.1 and the numerical analysis results shown in Figure 5.2, the stress concentration in the steel at the patch edge can be broken into two components:

1. There is an increase in average strain due to a decrease in stiffness, according to the relationship of [5.3]. From the numerical analysis, the average strain on the

given cross-section before the patch edge was 419 με. By [5.4], this should result in an average strain after the edge of 457 με; numerical results gave an average strain of 453 με. The discrepancy can be attributed to error of integration due to the low number of data points available.

2. As the load transferred from the patch takes some time to travel through the thickness of the metal adherend, it is initially in the patched face of the plate. This results in high strains on the plate surface at the patch edge and accounts for some through-thickness variation in the strain profile following the patch edge (see Figure 5.2). Additional strain variation is caused by bending of the cross-section. A strain of 530 με is shown near the plate surface in Figure 5.2; this profile underestimates the peak strain in the plate surface as it is not immediately adjacent to the patch edge.

5.1.1 Strain Distribution Across the Plate Width

Following the redirection of load around a crack, that load takes a certain distance to be redistributed across the plate width in order to re-establish constant stress distribution. If sufficient bond length is not provided to allow this redistribution, stress concentrations in the steel at the patch edges are higher than necessary near the sides of the patch, as discussed in section 4.4.1.2.

The increased stiffness of the patched area is also responsible for higher stress concentrations in the steel near the sides of the patch, regardless of the patch length used. Figure 5.3 shows the strain distribution in the patched face of a repaired 6.35 mm steel plate under 100 MPa far field applied stress. Distributions are shown before and after the edge of a w = 80 mm, L = 95 mm, four-layer carbon fibre/epoxy composite patch. This patch satisfies the minimum bond length criteria established in section 4.4.1.

The plate is subjected to far field constant stress distribution. Because the patched region is stiffer, the stress causes lower strains near the vertical centerline of the plate than in the

unpatched areas of the plate, towards the edges, where the strain is 500 με under 100 MPa stress. The strain profile must be continuous, however, as shown in Figure 5.3. This requires higher strains near the patch sides, which implies higher loads in the patch, and consequently higher stress concentrations in the steel at the patch edge. Beyond the patch edge, load is redistributed from these areas toward the center of the plate.

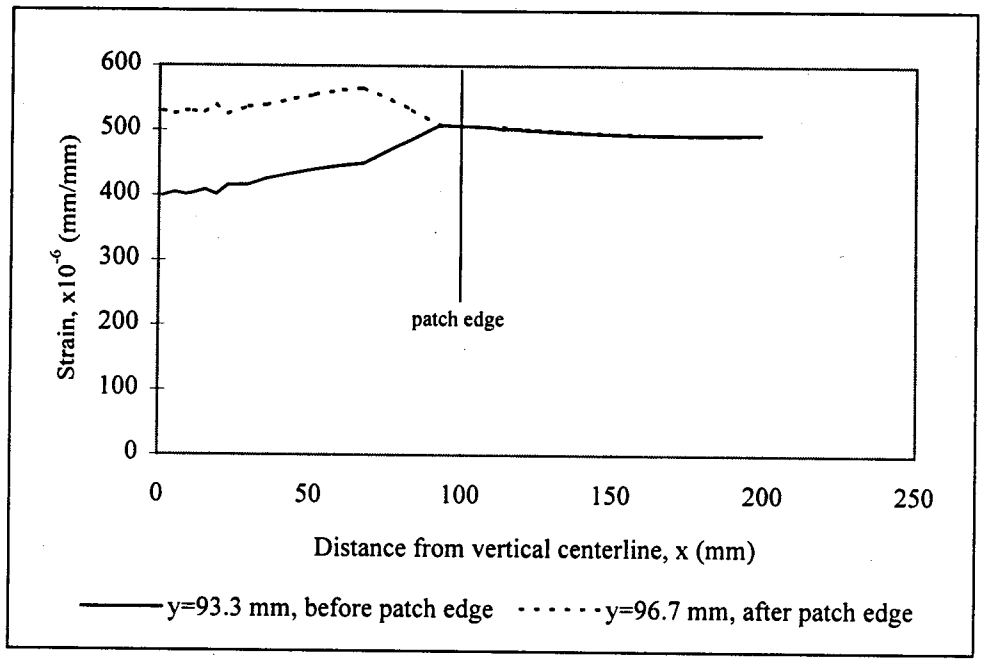

Figure 5.3 Strain in patched face of plate across plate width before and after patch edge

5.1.2 Stress Concentration Factor Versus the Stress Increase

The *stress concentration factor* is commonly used to measure the magnitude of the peak stress at a point. It is calculated as the stress at the point divided by the far field applied stress, σ_{pk}/σ_o. This is a convenient measure to use when performing fatigue analyses, where the stress range is required and the far-field applied stress is known.

Another measure of the effect of discontinuities in the cross-section is the *stress increase*. This value measures the difference in stress before and after the discontinuity. In the case of the patch edge, the stress increase in the patched face of the steel accounts for both the

change in average stress level, see equation [5.3], and the increased strain due to the sudden transfer of load from the patch.

The stress concentration factor and the stress increase are both shown in Figure 5.2 for the patched face of the given plate. Both measures underestimate the peak values at the patch edge as the numerical analysis results are restricted to integration points, which are a short distance from the patch edge. This is also the case for the stress concentration values presented in Chapters 2 and 4 of this report.

The difference in the stress concentration factor and the stress increase can also be illustrated in the patched face strain distributions along the vertical centerline of the plate. Figure 5.4 shows the two values for one such distribution, for a steel plate with a bonded patch 190 mm long (L = 95 mm). It is not known what effect, if any, the stress increase has on fatigue behaviour, as it is not directly related to the stress range typically considered in fatigue analysis.

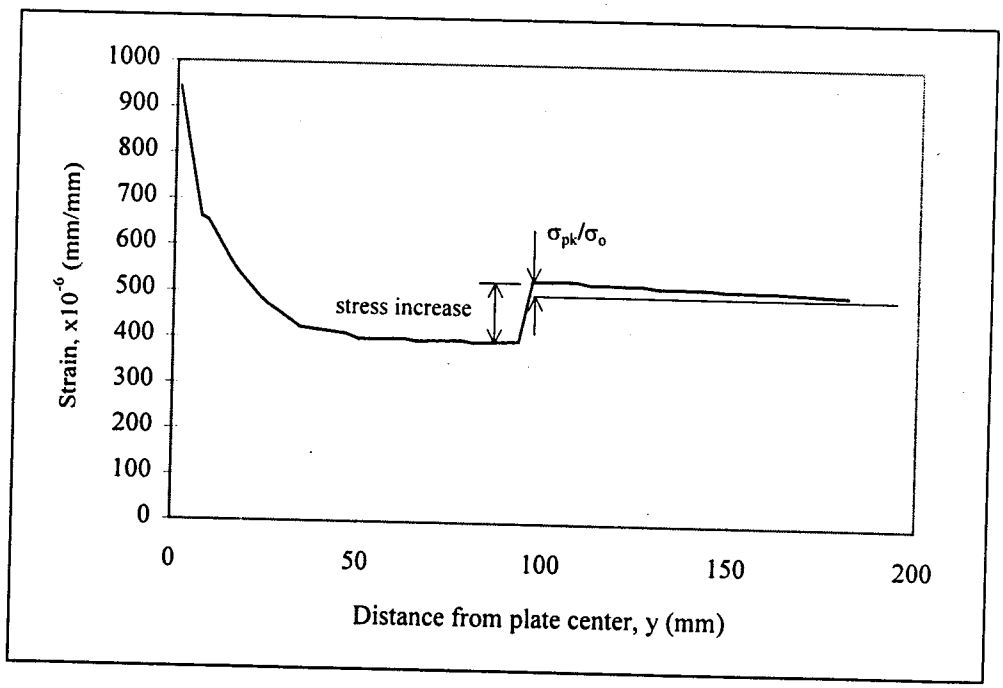

Figure 5.4 Stress concentration factor and stress increase related to patched face strain distribution along the vertical centerline

5.2 Tapered Patch Edges

Tapered edges are commonly used for their contributions to patch durability. Consider the idealized free body diagram of the patch in Figure 5.5. The peel-off stresses shown are necessary for equilibrium. Hart-Smith (1987) suggests that making the patch thinner and more flexible at the end can minimize the effects of these stresses.

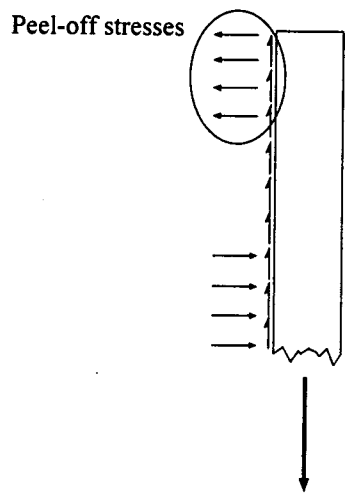

Figure 5.5 Stresses acting on the bonded patch

Tapering the patch edge was investigated here as a possible means of reducing edge stress concentrations in the steel at the patch edge. Experimental tests considered three taper lengths and the bonded lap joint model was used to obtain numerical results. The tapered region of the patch should be completely beyond the minimum required bond length.

5.2.1 Experimental Results

Bonded patch test specimens and procedures were described in section 3.1. Tests R226, R224, R326, and R324 incorporated taper lengths of 3 mm/layer, 5 mm/layer, and 20 mm/layer and were the only tests considered in the taper analysis. The results of these four tests were shown in Figures 3.11-3.14 respectively.

Figure 5.6 shows the results of bonded patch test R224 relevant to the study of edge tapering. The four-layer patch had a 5 mm/layer taper on both ends. On the extreme left of the figure, a sketch shows the area under consideration, and the detail area sketch in the center of the figure shows the locations of strain gauges in that area. The right side of the figure shows the strain measured at each of the gauges when the far field applied stress was 100 MPa. Figure 5.7 shows the results for the remaining tests in a similar way. For tests R226 and R324, a 3 mm/layer taper was used on one end of the patch and a 20 mm/layer taper on the other, so the results of each taper are shown separately.

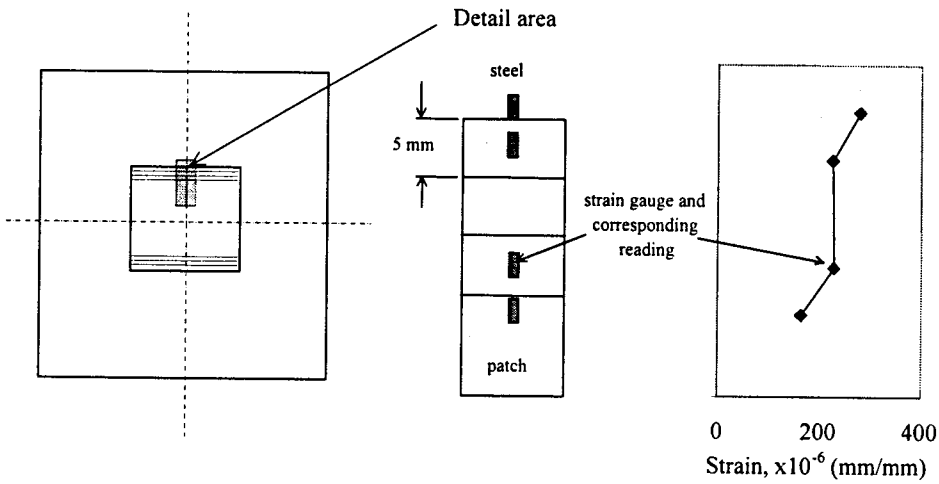

Figure 5.6 Experimental results for taper of bonded patch test R224; 4 layers, 5 mm/layer taper

The long, 20 mm/layer, taper results showed similar behaviour (see Figure 5.7(d) and (e)). In both cases, the gauges on the steel showed the highest strain. This was likely due to low cross-sectional stiffness compared with that of the patched area, and possibly to a stress concentration in the gauged area of the steel as a result of load transferred at the end of the patch. As the number of patch layers increased, the strain decreased, corresponding to increasing cross-sectional stiffness. The center two gauges on both tests were located near the center of the taper layer, and so strains were likely representative of the level of strain compatibility with minimal stress concentration effects due to the

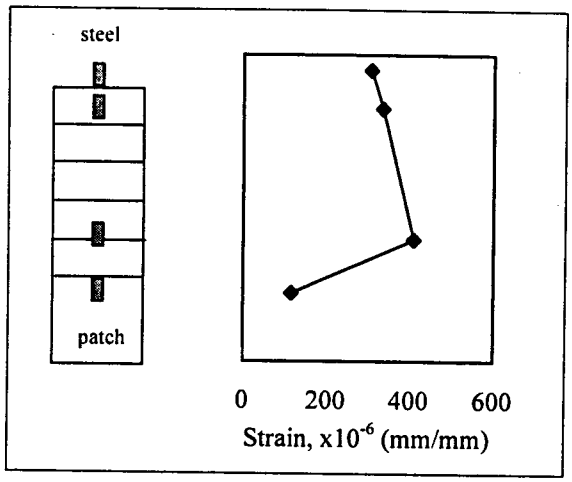

(a) Test R326: 6 layers, 5 mm/layer taper

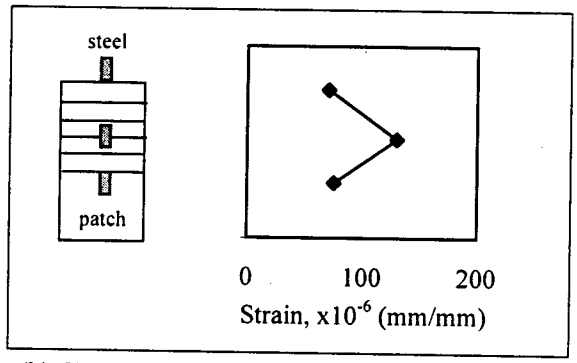

(b) Test R226: 6 layers, 3 mm/layer taper

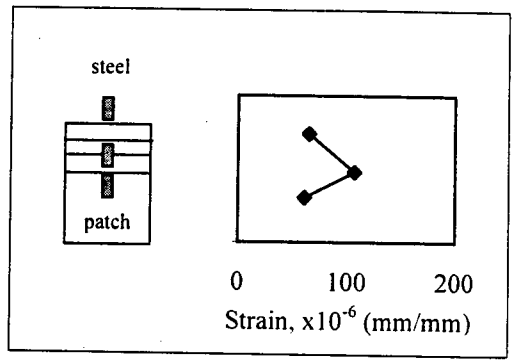

(c) Test R324: 4 layers, 3 mm/layer taper

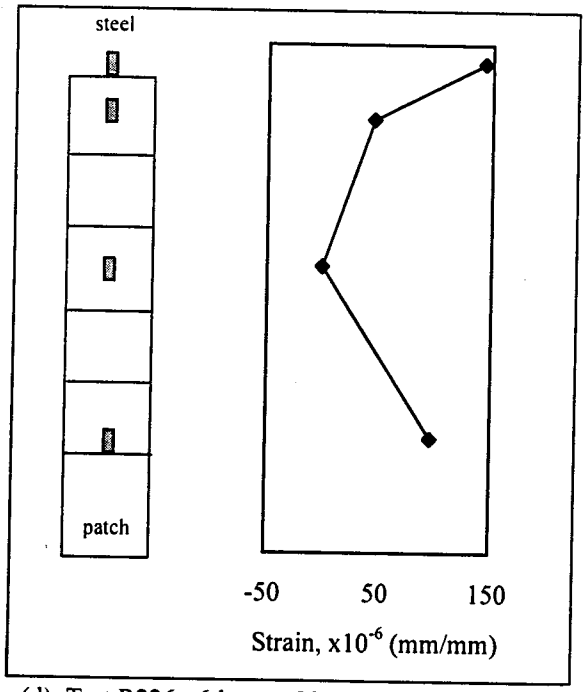

(d) Test R226: 6 layers, 20 mm/layer taper

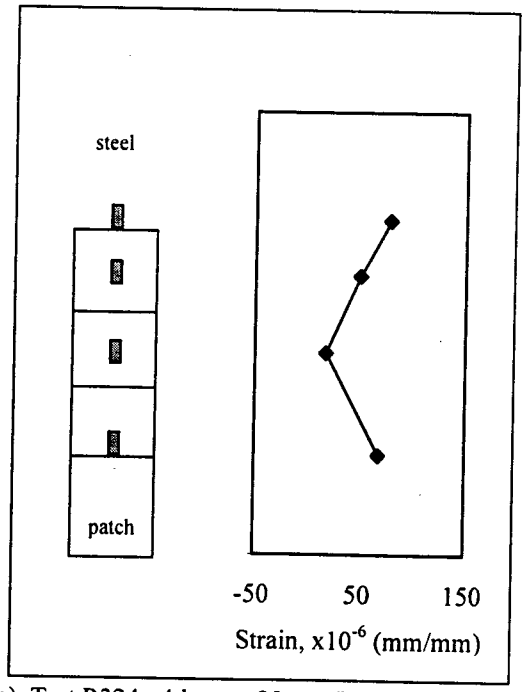

(e) Test R324: 4 layers, 20 mm/layer taper

Figure 5.7 Experimental results for tapered patch edges

transfer of load from the end of the previous patch layer. The gauges located adjacent to the edge of the top patch layer showed higher strains than the gauges through the center of the taper. Because the cross-section was stiffer at this point, this suggests there was a stress concentration due to load transfer from the top patch layer. Some variation in strains along the taper, particularly for the long taper, may have been the result of bending due to initial curvature of the plates. This bending caused higher compressive strains in the gauges closer to the horizontal centerline of the plate, as discussed in Appendix A, and could explain some of the strain gradient observed along the taper length.

Figure 5.6 and Figure 5.7(a) show the results from 5 mm/layer tapers. Gauges on the edge of the full patch thickness reported the lowest strains as they were on the stiffest cross-section. The low strains may also be attributed to the beginning of load transfer out of the top layer of the patch, causing lower strains than in the strain compatibility region for the same number of layers. In test R224, a gradual increase in strains was seen along the taper towards the steel, as was the case for the 20 mm/layer taper. In test R326, one gauge overlapped the edge of a composite layer and reported high strain, suggesting shear stresses were present between the layers of composite.

This interlaminar shearing was also seen in the 3 mm/layer tapers shown in Figure 5.7(b) and (c) – in both cases the gauges mounted across two layers of the patch showed high strains. Baker (1987) suggests the use of an internally stepped patch, where the bottom patch layer is shorter than the next and so on, to reduce interlaminar shear stresses and provide external smoothness. This option may also reduce stress concentrations in the patch layers and should be further investigated.

5.2.2 Numerical Results

A bonded joint model of a four-layer patch applied to a 6.35 mm steel tab was developed in section 2.3.1. By removing some elements from the ends of the patch, the effects of a

tapered patch were tested numerically. An ABAQUS 5.6 model of a bonded joint with a tapered patch is shown in Figure 5.8 (Hibbitt, Karlsson & Sorenson, Inc. 1996).

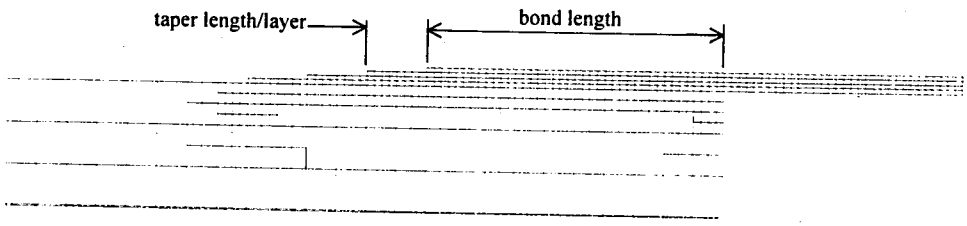

Figure 5.8 ABAQUS 5.6 model for a bonded joint with a tapered patch edge

Figure 5.9 shows the numerically determined strain profiles for a bonded joint between a 6.35 mm steel tab and a unidirectional carbon fibre composite patch with a 3 mm/layer taper. Again all strain distributions are shown at 100 MPa far field applied stress unless otherwise noted. Distributions are shown for the top row of integration points in each patch layer, and for the top row of integration points in the steel. The figure shows that at the end of each patch layer, the load it is carrying for strain compatibility is dumped into the layer below, causing a strain increase in the lower layer. This layer then distributes that load "downward" into the remaining patch layers and the steel, attempting to regain a level of strain compatibility. At its edge, the new "top" layer transfers its load to the layer below it and the cycle repeats.

A tapered model was also studied for a three-dimensional bonded patch. The model, developed in section 4.1, represented a 6.35 mm steel plate with an 80 mm internal crack. The bonded patch was six layers of carbon fibre composite, with a length of L = 63 mm plus two taper steps of 16 mm each, two patch layers ending at each step. Because the model used shell elements to represent the patch, the length of the taper was governed by the size of the elements. The taper was modeled by representing the full patch with 1.38 mm (6 layers x 0.23 mm/layer) thick elements, and reducing the thickness by 0.46 mm at each taper step. The strain distribution in the patched face of the plate along the vertical centerline is shown in Figure 5.10. This distribution shows clearly the increase in the

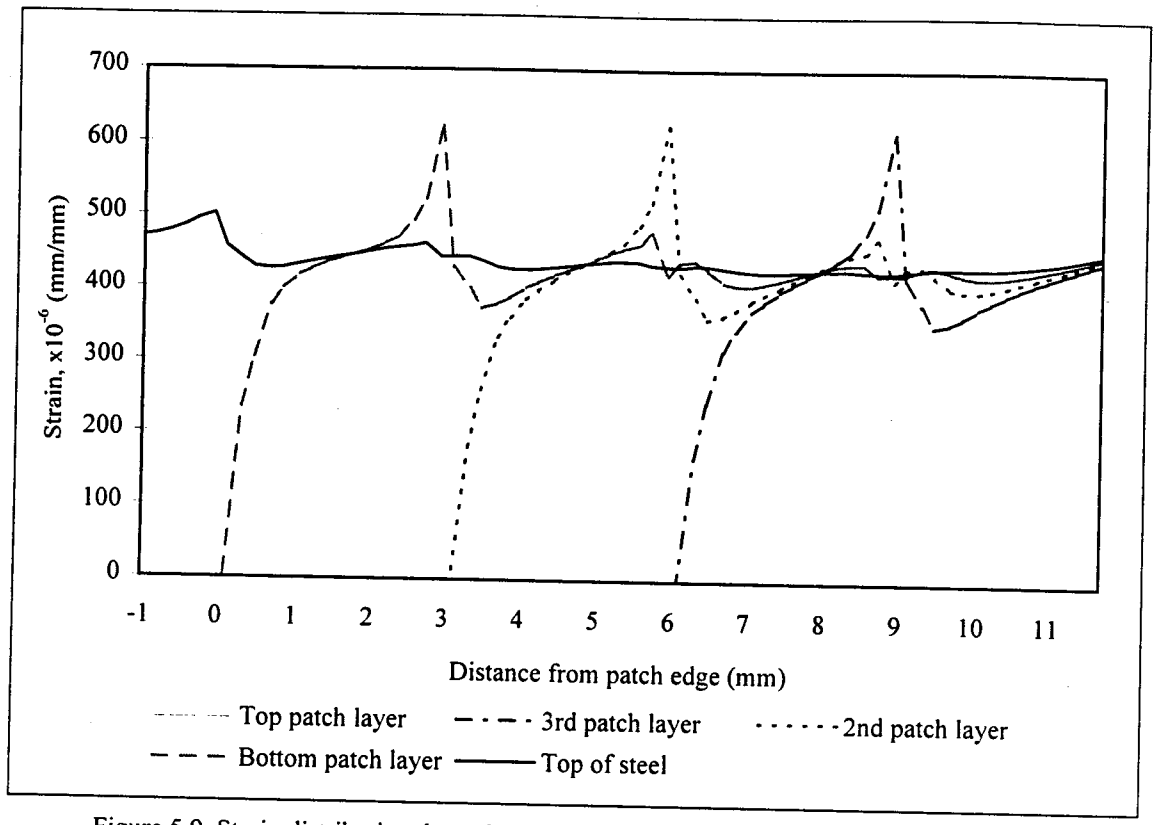

Figure 5.9 Strain distribution through a patch edge with a 3 mm/layer taper

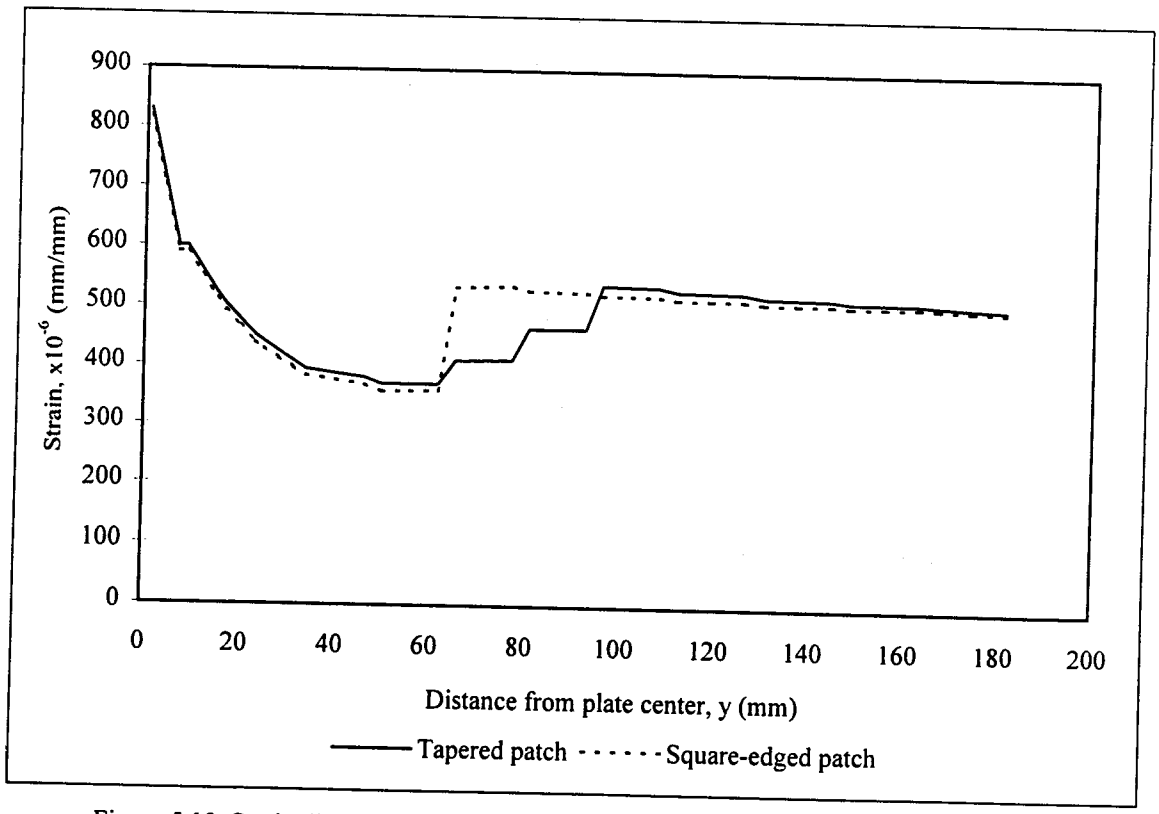

Figure 5.10 Strain distribution along the vertical centerline for a tapered patch

level of the strain compatibility plateau after each taper step. This has the effect of reducing the stress increase, discussed in section 5.1.2, in the steel at the patch edge. An increase in the strain compatibility plateau also occurs in the bonded joint model, but is not as evident in the results shown in Figure 5.9 because of the shorter taper length and the lower stiffness of individual taper layers.

Tapering also reduces the stress concentration factor in the steel at the patch edge. As the patch tapers, its stiffness decreases, and less load is required in the patch to maintain strain compatibility. This leaves less load to be transferred to the steel at the edge of the patch, and consequently a lower stress concentration.

The bonded joint model was used to test the effect of taper length on the stress concentration in the steel at the patch edge. Figure 5.11 suggests that tapering can reduce the stress concentration factor by up to 15 % for a four-layer patch bonded to a 6.35 mm steel tab with sufficient bond length. Again this value underestimates the peak stress concentration because of the distance between integration points and the patch edge.

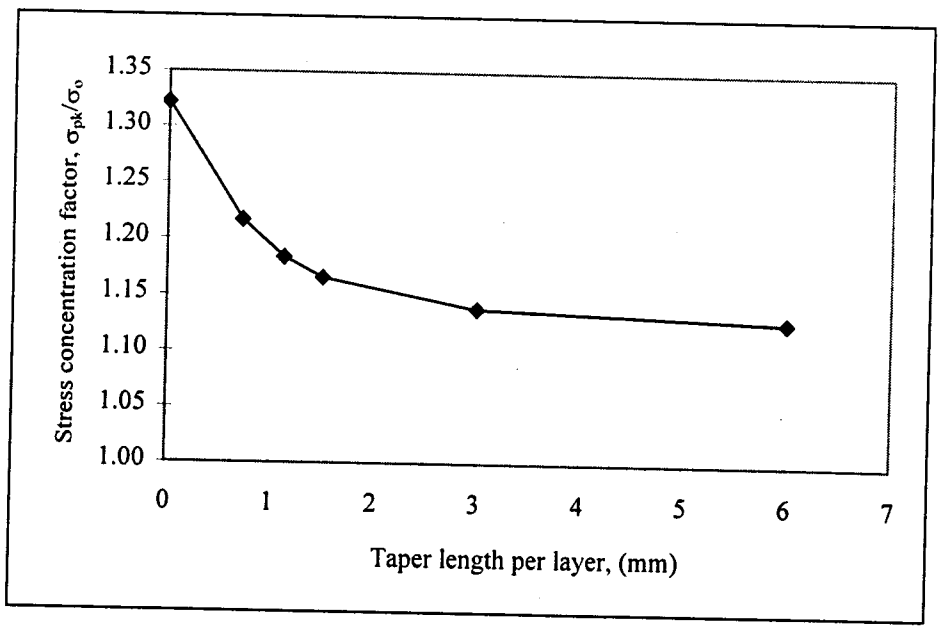

Figure 5.11 Effect of taper length on stress concentration factor in the steel for a bonded joint

The effect of taper length can be better understood if the strain distribution through a 3 mm/layer taper, shown in Figure 5.9, is compared with the strain distribution for a 1.5 mm/layer taper, shown in Figure 5.12. If the taper is long enough, the patch is able to regain a level of strain compatibility after the end of each layer and the magnitude of the stress concentration after each layer ends stays approximately constant. This is the case for the 3 mm/layer taper. If the taper is too short, in the case of the 1.5 mm/layer taper, each layer of the patch has extra load it cannot transfer within its length, and the stress concentration after each layer progressively increases. This remains true at the patch edge, where there is an increased load to be transferred to the steel, and the stress concentration is higher.

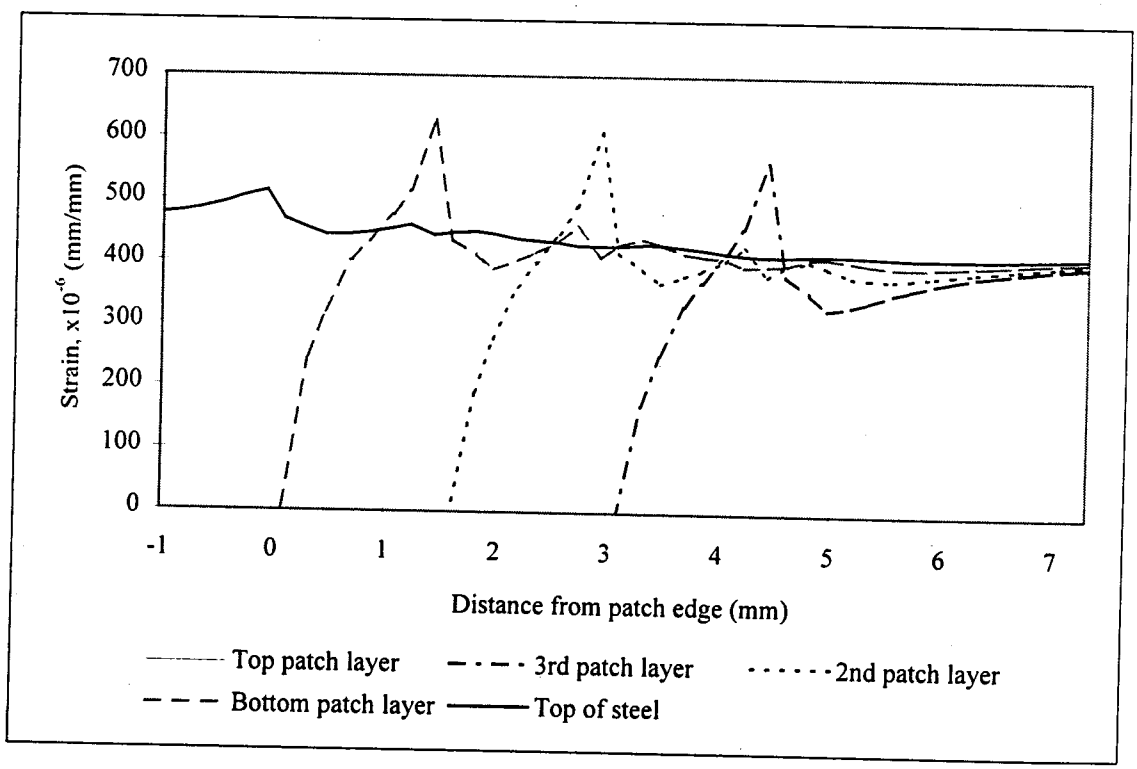

Figure 5.12 Strain distribution through a patch edge with a 1.5 mm/layer taper

Tapering causes a stress concentration in the layers of the patch that is not present in a square-edged patch. These new stress concentrations may cause fatigue problems in the patch when subjected to fatigue loading.

One further concern is the practicality of constructing a multiple-layer patch where each layer must be cut to different dimensions. A bonded lap joint model was run for a four-layer patch where the bottom layer of fibre was 6 mm longer than the next three, shown schematically in Figure 5.13. The solution shows a stress concentration in the steel at the patch edge of 1.131, compared with 1.129 for a 6 mm/layer taper (the primary stress concentration shown in Figure 5.13). The modified 6 mm taper does cause a second stress concentration in the steel at the edge of the top patch layers, shown in Figure 5.13, but with a magnitude of only 1.109. These results suggest this alternative may provide the desired reduction in stress concentration in the steel while making fabrication easier; however, fatigue problems may occur in the bottom layer of fibre. If this layer is cracked, the patch effectively becomes a four-layer patch with no taper. The solution will depend on the fatigue performance of the fibre, which was not investigated here.

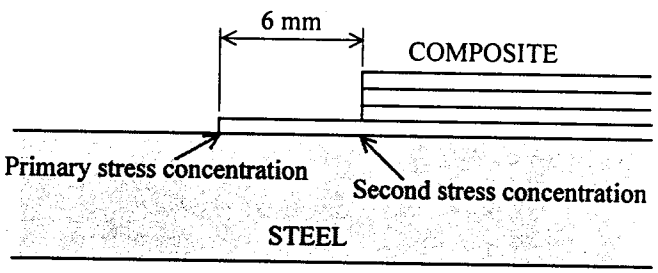

Figure 5.13 Schematic diagram of modified 6 mm taper

5.3 Patch Shape

Composite patching applications in the aircraft industry commonly employ elliptical patches (Baker 1987, Rose 1988), although examples of rectangular patches or irregular

polygon shapes in restrictive areas such as corners can also be found. No documentation has been found, however, regarding the change in stress distributions that result from the different patch shapes. It is possible that an elliptical patch may reduce the potential of stress concentrations in the steel at the patch edge to cause new cracking when subjected to fatigue loading.

The area of an elliptical patch is defined by the equation

$$\left(\frac{x}{w}\right)^2 + \left(\frac{y}{L}\right)^2 \leq 1.0 \qquad [5.1]$$

where (x,y) = (0,0) is at the center of the plate and the crack, and the parameters w and L are the patch width and length "half-dimensions" shown schematically in Figure 3.2 for a rectangular patch.

In the bonded patch tests discussed in section 3, four of the test patches were designed to allow observation of the effects, if any, of patch shape. The results of these tests are discussed here along with an approximate numerical analysis performed using a bonded patch model to estimate the effects of patch shape on stress distribution in the steel.

5.3.1 Experimental results

Tests M216, M214, M316, and M314 had patches that were elliptical below the horizontal centerline and rectangular above in order to study the effects of patch shape. The patch shapes and experimental results were shown in Figures 3.7-3.10 respectively. The elliptical portion of the top patch layer was defined by [5.1] and the length, L, and width, w, parameters specified in Table 3.1. In all cases, a 5 mm/layer taper was used around the patch perimeter, so subsequent patch layers were defined by the parameters L+n5 and w+n5 where n is the number of layers below the top layer of the patch. All results are presented at 100 MPa far field applied stress unless otherwise noted.

Table 5.1 summarizes the strains in the steel adjacent to the patch edge on the vertical centerline for tests with gauges mounted at both the elliptical and rectangular patch edges. No correction was made to the data to account for initial curvature of the plates, so the values for different plates cannot be accurately compared. Gauges on opposite ends of a given patch can however be compared to each other, as bending effects are theoretically the same at both gauge locations. (See section 4.3 for a discussion of the effects of initial plate curvature on experimental results.) The strain results of Table 5.1 are inconclusive.

Table 5.1 Strain in the steel adjacent to patch edges on the vertical centerline, bonded patch tests

Test	Strain at Elliptical Edge $x10^{-6}$ (mm/mm)	Strain at Rectangular Edge $x10^{-6}$ (mm/mm)
M214	475	377
M216	491	493
M316	123	139

Several strain gauges were mounted at the same relative locations on both the rectangular and elliptical sides of the patch: the same distance from the horizontal centerline, the same distance from the patch edge along the same vertical axis, or at the same location relative to a feature of the patch such as the edge of the top layer. The strain results for these gauges are summarized in Table 5.2. The data is inconclusive.

One experimental result that may be of some significance came from test M216. Strains were measured in the steel adjacent to the patch edge at three locations:

- Rectangular edge, vertical centerline: 605 με
- Rectangular edge, near the side of the patch: 671 με
- Elliptical edge, vertical centerline: 603 με

These results confirm that the highest stress concentration in the steel adjacent to a rectangular patch is near the side of the patch, making this the most likely location for new crack formation. Edge stress concentrations around an elliptical patch are on a

curved profile coincident with the patch edge, not aligned perpendicularly to the applied load as is the case for a rectangular patch. Given a curved stress concentration profile, the most likely area for the initiation of a new crack along this profile is at an inflection point, which in this case is at the vertical centerline. If this is the case, the stress concentration that is of concern is significantly lower for the elliptical patch than the rectangular one when measured by relative strains: 603 με compared with 671 με. Fatigue tests should be performed to check for the location of new crack development around an elliptical patch.

Table 5.2 Summary of experimental results for elliptical and rectangular patch shapes, bonded patch tests

	Elliptical Side		Rectangular Side		
Test	Gauge Coordinates	Strain $x10^{-6}$ (mm/mm)	Gauge Coordinates	Strain $x10^{-6}$ (mm/mm)	Notes
M214	(-55,-95)	180	(-55,92)	158	5 mm from edge of top layer
	(-20,-101)	135	(20,95)	111	at edge of top layer
	(87,-84)	337	(-87,104)	217	on bottom patch layer taper
M216	(-58,-83)	208	(-58,85)	238	10 mm from edge of top layer
	(-123,-73)	407	(-123,125)	558	on steel at patch edge
	(113,-86)	236	(-113,112)	129	on 3rd patch layer taper
M314	(0,-98)	157	(0,97)	190	at edge of top layer
	(-72,-57)	437	(-72,105)	519	on 2nd patch layer taper
	(20,-85)	289	(20,87)	267	10 mm from edge of top layer
	(46,-56)	374	(46,70)	339	31 mm from edge of top layer
M316	(-60,-41)	-21	(-60,85)	-24	10 mm from edge of top layer
	(-20,-65)	-116	(-20,65)	-80	65 mm from horizontal centerline
	(20,-94)	-99	(20,86)	-67	10 mm from edge of top layer
	(80,-73)	-22	(80,108)	7	on 3rd and 4th patch layer taper

5.3.2 Numerical Results

An approximate numerical analysis was performed to test the effects of an elliptical patch on strain distribution in the steel. The bonded patch model developed in section 4.1 was run first for the original rectangular patch on a 6.35 mm steel plate, then for the same plate with a patch stepped along the edges to simulate the narrowing effect of an elliptical patch. Both patches were six layers of carbon fibre composite, with a width, w, of 80 mm and length, L, of 95 mm. The models of the two patches are shown in Figure 5.14, and the resulting strain distributions for the patched face of the plate along the vertical centerlines are shown in Figure 5.15.

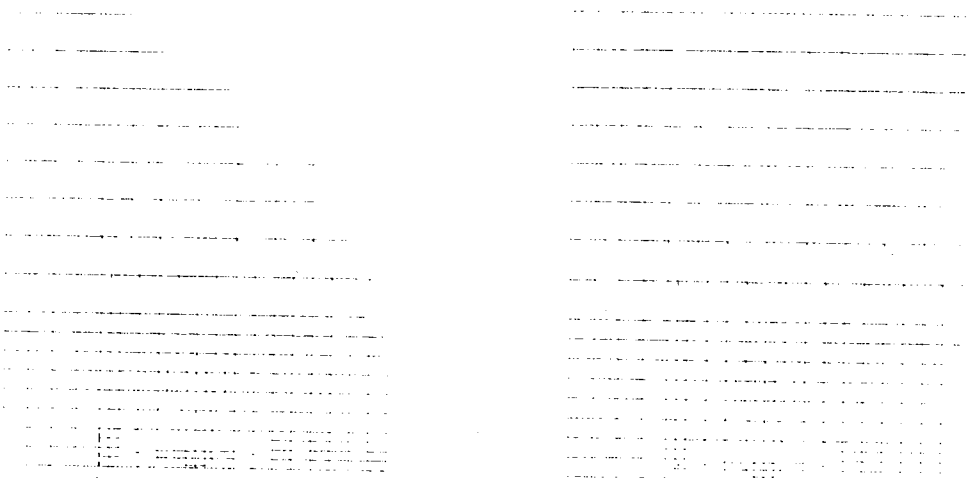

(a) Stepped patch (b) Rectangular patch

Figure 5.14 ABAQUS 5.6 models of stepped and rectangular patches

The results show a slight increase in strain along the center of the narrowing patch, likely a result of a decrease in cross-sectional stiffness. The stress concentration factor in the steel at the patch edge increases from 1.156 for the rectangular patch to 1.203 for the elliptical patch, measured along the vertical centerline.

The increase in stress concentration factor may be a result of load redistribution. In an elliptical patch, the sides of the patch "end" closer to the horizontal centerline where they still carry high loads, according to the load redistribution discussion of section 4.2.3. The

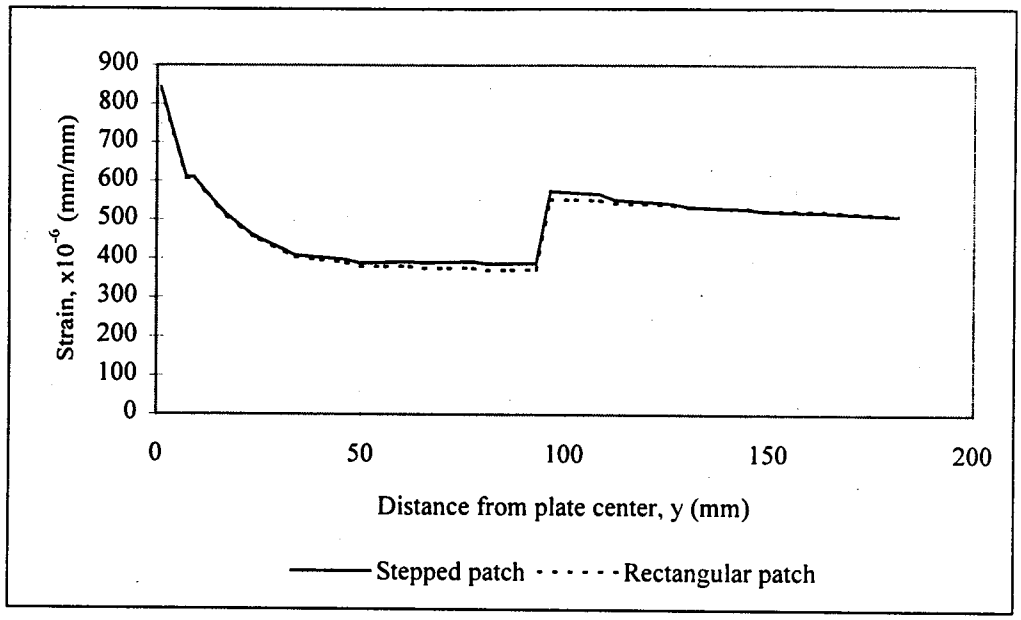

Figure 5.15 Strain distribution along the vertical centerline for stepped and rectangular patches

stress concentrations at these edges are therefore high. Load from the stress concentrations at these outside edges is redistributed to the plate center as the element works to regain overall strain compatibility. If the earlier load transfer out of the elliptical patch causes faster redistribution of the load towards the center of the plate, this may account for the increase in the stress concentration in the steel at the patch edge.

The stress concentration factor in the steel at the edge of the rectangular patch is 1.156 at the vertical centerline and 1.221 near the patch edge. This supports the experimental results of test M216 discussed in section 5.3.1, and emphasizes the idea that new cracks in the steel are most likely to form near the side of a rectangular patch.

5.3.3 Bond Length Considerations

If an elliptical patch is used, further consideration should be given to the specification of minimum bond length. Stress redistribution profiles should be studied to check the relevance of the load redistribution criteria for minimum bond length established in

section 4.4.1.2. It may also be necessary to specify the minimum bond length required at a distance from the vertical centerline, for example between the crack tips and the patch edge.

5.4 References

Baker, A.A. 1987. "*Fibre Composite Repair of Cracked Metallic Aircraft Components - Practical and Basic Aspects.*" Composites, Vol. 18, No. 4, pp. 293-308.

Hart-Smith, L.J. 1987. "*Joints.*" Engineered Materials Handbook, Volume 1: Composites, ASM International, pp. 479-495.

Hibbitt, Karlsson & Sorenson, Inc. 1996. "*ABAQUS Version 5.6.*" ABAQUS/Standard User's Manual Volumes I and II, Pawtucket, Rhode Island, USA.

Rose, L.R.F. 1988. "*Theoretical Analysis of Crack Patching.*" Bonded Repair of Aircraft Structures, A.A. Baker and R. Jones, Eds., Martinus Nijhoff Publishers, Dordrecht, The Netherlands, pp. 77-106.

6 CASE STUDY - FATIGUE CRACKS IN DRAGLINE BOOM

Production at the Syncrude mining site in Fort McMurray, Alberta is reliant on the operational reliability of heavy equipment. Demanding loads, continual use, and a harsh environment lead to cracking in key structural elements of this equipment. Consequently, many possible applications exist for a composite fibre patch, if acceptable performance can be achieved.

The objective of this case study is to design a carbon fibre patch repair for a typical fatigue crack in the boom of a dragline. The design was based primarily on the conclusions of Chapters 4 and 5, and a numerical analysis was performed to study the effects of the repair on the strain distribution in the patched area.

6.1 Background

Draglines used in the Syncrude oil sands mining operations, such as the one shown in Figure 6.1 have been in service since 1978. The use of larger buckets to increase capacity has increased the loading on these structures, and there is continual deterioration due to long-term use and exposure to the harsh climate. Draglines are to remain in service for up to nine more years, but in recent years cracking of boom members has become a leading cause of unscheduled downtime of the equipment. In order to maintain or improve operational reliability throughout the service life of the draglines, efficient and effective crack repair methods must be developed.

Traditional repair by gouging and welding is difficult due to the location of the cracks, and in many locations cracks have already been repaired multiple times. One possible alternative repair procedure is the application of a bonded composite patch.

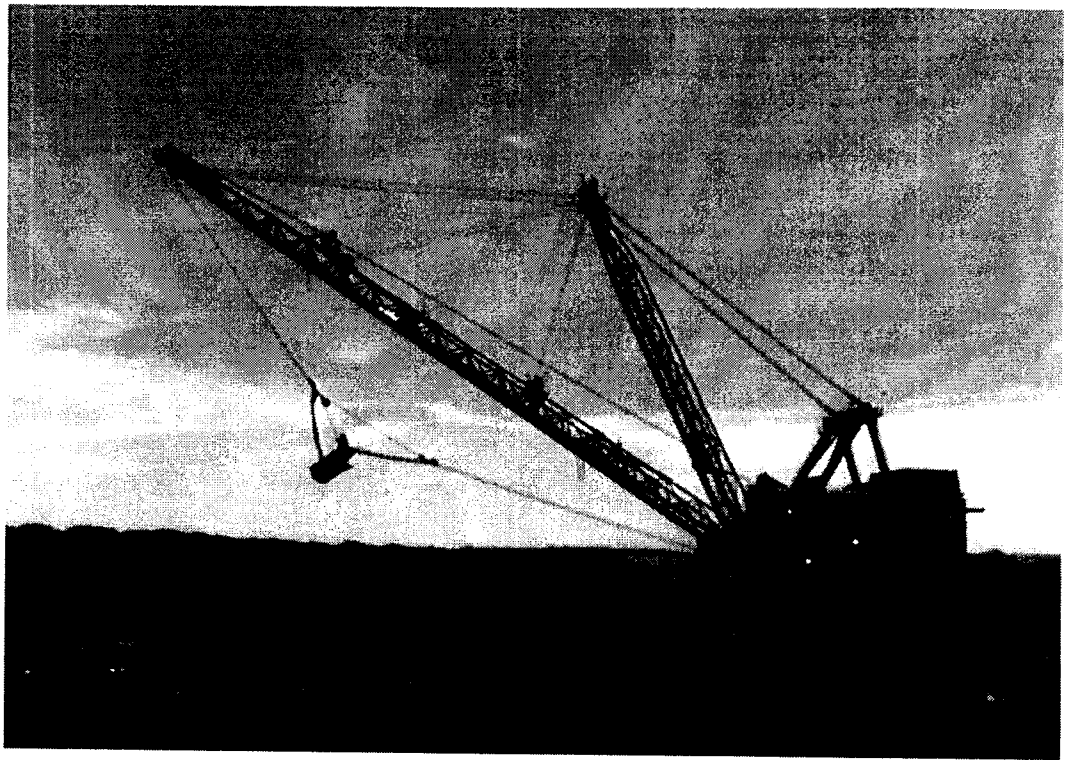

Figure 6.1 Dragline at Syncrude mining site. Courtesy Syncrude Canada Ltd.

Figure 6.2 Cluster in dragline boom, the transition in question is 250 mm away. Courtesy Syncrude Canada Ltd.

6.1.1 Crack Location

The location in question is on draglines with tubular chord members at a distance along the boom of approximately two-thirds the total boom length. A wall-thickness transition occurs 250 mm (10 in.) above the cluster shown in Figure 6.2. There is a stress concentration at this location due to the narrowing of the cross-section and local bending. A diagram of the transition is shown in Figure 6.3.

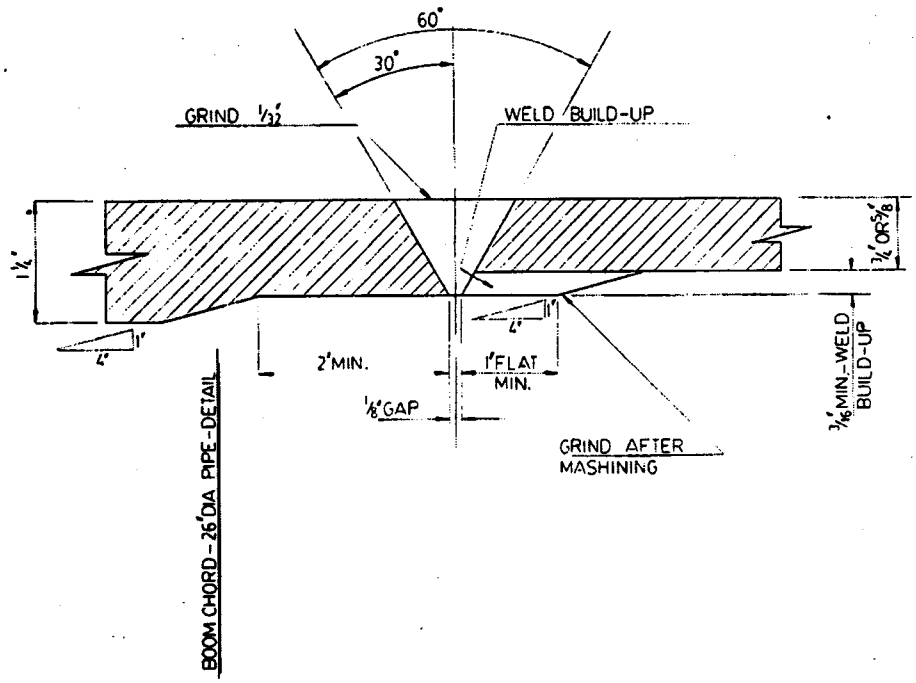

Figure 6.3 Wall-thickness transition in dragline boom chord. Courtesy Syncrude Canada Ltd.

The material properties of the steel at this location are uncertain: previous repairs have required welding in the location without postweld heat treatment, and it is expected that the material is more brittle than would normally be the case. As well, weld repairs are made from the outer side, with no blending on the interior, which aggravates the stress concentration.

6.1.2 Loading

There are two sources of live loading on the member. Hoisting stresses range from zero when there is no payload to high compression when the load is lifted. Swinging stresses cycle between tension and compression with the swing acceleration and deceleration, and are higher when the bucket is full of material. The complete cycle time is approximately 70 seconds.

The total load on a chord member is the sum of the swing stress and the hoist stress. Figure 6.4 shows the individual and total stresses. Hoist stress is the same in both chords at all times. Swing stresses act on the boom as a horizontal beam element with the chords as the tension and compression faces. This results in opposite stresses in the right and left chords of the boom, shown as separate lines in the swing stress plots and total stress plots of Figure 6.4. The set of loads a given chord is subjected to depends on the relative location of excavation and dumping during a given period of operation. Data from 134000 cycles of loading gave an average stress range of 123 MPa, with a standard

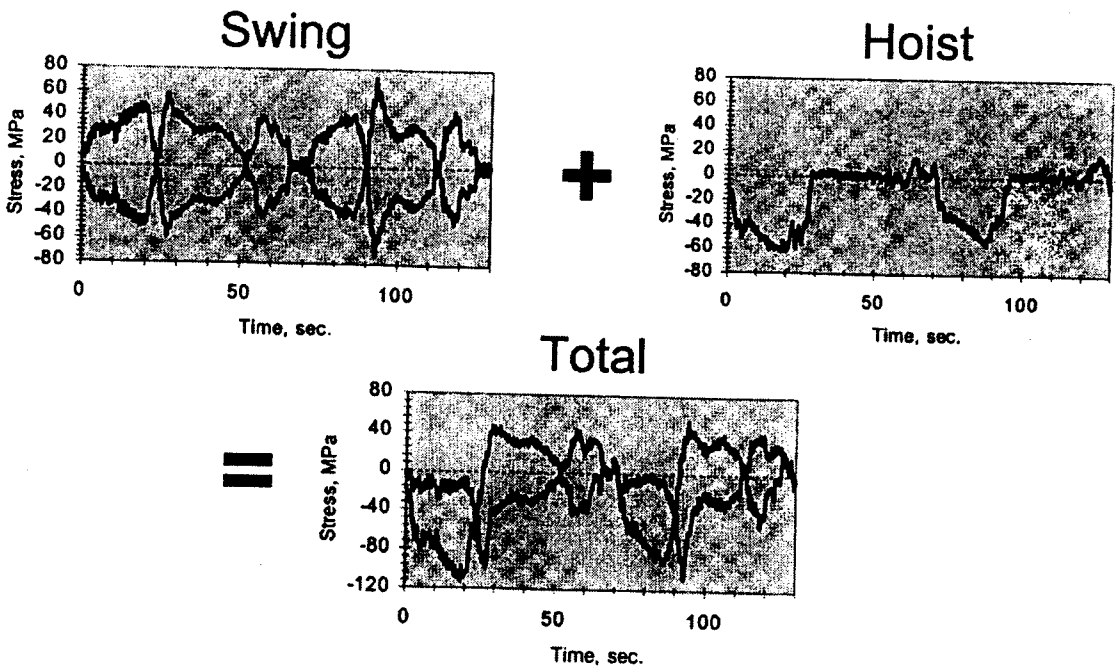

Figure 6.4 Swing and hoist load in dragline boom chords (Carroll 1997)

deviation of 12 MPa. The average peak stress (tensile) is approximately 45 MPa. (Carroll 1997).

6.1.3 Crack Monitoring and Growth

The tube members are constantly pressurized to monitor the chord for through-thickness crack development. Cracks are typically repaired when they are between 180 and 400 mm (7-16 in.).

6.2 Fatigue Life

Using CAN/CSA Standard S16.1-94 (1994), the design life of the transition in question was determined. For a Category b element, and a stress range of 123 MPa, the design life is approximately 2,000,000 cycles. For continual operation at 1230 cycles per day, this is a life of about 4.4 years.

Crack growth rates can be estimated from the Paris equation, [1.1]:

$$\frac{da}{dN} = C(\Delta K_I)^n$$

where da/dN = the crack growth rate in m/cycle

C = a constant, 6.9E-12 for ferrite-pearlite steel

ΔK_I = the stress intensity factor for the pulsating tensile stress, in MPa$\sqrt{}$mm

= $\Delta\sigma\sqrt{\pi a}$

n = a constant, 3.0 for ferrite-pearlite steel

For a 180 mm crack, a = 90 mm, this leads to an estimated crack growth rate of 0.04 mm/day. For a 400 mm crack, the estimated growth rate increases to 0.8 mm/day. Observed crack growth rates are higher than those estimated here, approximately four times higher for a 400 mm crack, suggesting that the material is more brittle than typical structural steel.

6.3 Patch Design

It is assumed the crack is being repaired at a length of 180 mm (7 in.). From Figure 6.3, the thickness of the steel, t_s, is 15.9 mm (5/8 in.) above the transition and 31.8 mm (1¼ in.) below. The Elastic Modulus of the steel, E_s, is assumed to be 200 000 MPa. Unidirectional carbon fibre composite is used, with a patch thickness, t_p, of 0.23 mm/layer and an Elastic Modulus, E_p, of 128 000 MPa.

6.3.1 Thickness

In order to apply the equations developed in this report, the stiffness ratio must be less than 0.25. For 22 layers of composite, the stiffness ratios are

$$\frac{E_p t_p}{E_s t_s} = .204$$

above the transition and

$$\frac{E_p t_p}{E_s t_s} = .102$$

below.

The patch can only be applied on one side of the element, but the section will receive some support for out-of plane bending because it is a tube. Thus the bending stresses are expected to be lower than those seen in the unsupported analyses of Sections 4 and 5.

6.3.2 Length

From section 4.4.1.1, for load transfer:

$$\ell_{min} = 160\left(\frac{E_p t_p}{E_s t_s}\right) + 17$$

this is governed by the higher stiffness ratio so that

$$\ell_{min} = 160(0.204) + 17 = 49.6\text{mm}$$

For load redistribution (see section 4.4.1.2), the result is governed by the lower stiffness ratio and

$$\ell_{min} = 2a\left(-4.2\frac{E_p t_p}{E_s t_s} + 1.4\right) = 2(90)\left(-4.2(0.102) + 1.4\right) = 175\text{mm}$$

The longer length governs; the patch length should be at least 175 mm on either side of the crack.

It should be noted that if the crack were any longer, it would require a longer bond length than what is allowed by the geometry of the example, since there is a lacing crotch 250 mm (10 in.) below the crack location. Possible alternatives would be changing the thickness of the patch. If necessary, the patch could be made shorter on one side than the other, but this would not solve the problem of higher stress concentrations.

6.3.3 Width

The crack will not be visible following application of the patch, and the method of crack detection through a leak in the pressurized pipe will not work as long as the crack is under the patch. Thus, until suitable monitoring methods for crack growth under a composite patch repair are established, a critical crack length will govern the width of the patch. In this case, crack growth must be apparent before the crack reaches 400 mm (16 in.) so the total patch width (2w) is restricted to 380 mm (15 in.)

6.3.4 Taper

From the analysis, a minimum of 3 mm/layer taper should be provided at the patch edge. For a 22-layer patch, it is not necessary to cut each layer a different size. The proposed design uses five-layer steps, with a seven-layer step on the top of the patch. Each step should be 15 mm. This allows for some error in alignment during fabrication.

The taper makes the total patch length (L + taper length) a minimum of 220 mm, slightly lower than the specified allowable length of 250 mm. The location should be checked to confirm that application of this patch is feasible.

6.3.5 Shape

Without fatigue test results, merits of different patch shapes are questionable. Rectangular patches were shown to produce high stress concentrations in the steel near the corners of a patch on a flat plate; however, in this application, the patch is being applied to a tube section under bending loads. This implies that the stresses along the vertical centerline of the patch exceed the stresses near the sides of the patch, since the sides of the patch approach the neutral axis of the member. It is therefore not anticipated that new cracks will form near the sides of the patch, and a rectangular patch is recommended. A rectangular patch is also easier to fabricate.

The suggested patch design is shown in Figure 6.5.

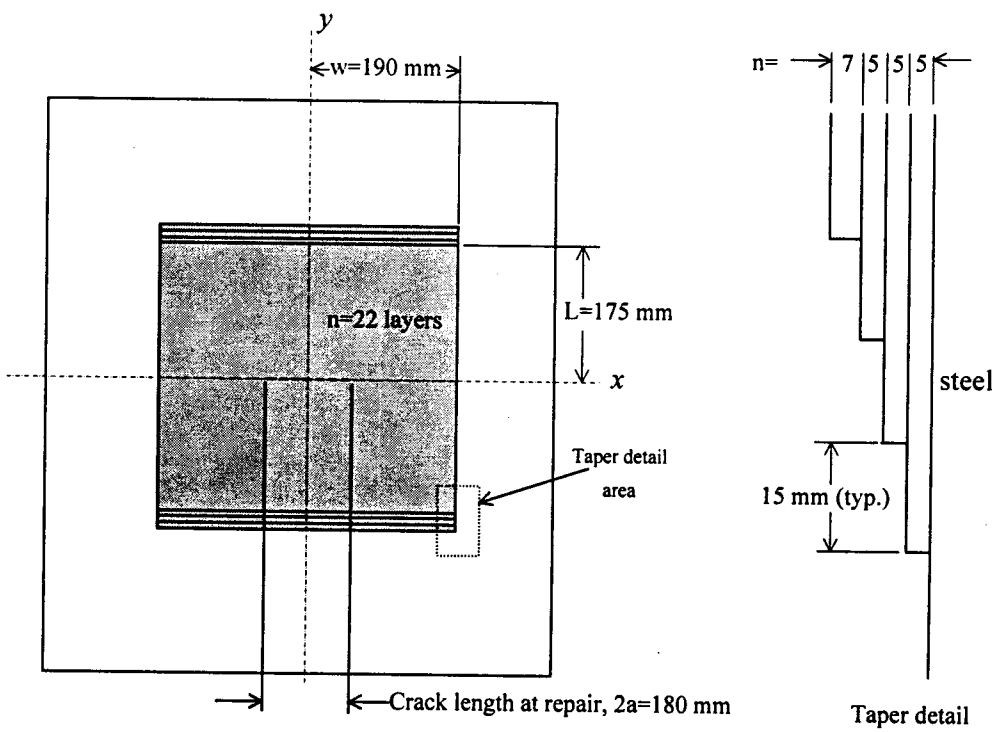

Figure 6.5 Suggested patch design

6.4 Anticipated Stresses

A cracked plate was modeled numerically to simulate the chord member before and after patching. The three-dimensional, elastic model developed in section 4.1 was modified to represent the parameters of this application. The new model was a uniform thickness of 15.9 mm, corresponding to the region above the transition, and was 410 mm wide by 400 mm long, representing one quarter of a plate with the specified internal crack. The carbon fibre/epoxy composite patch was modeled according to the suggested design.

Figure 6.6 shows the theoretical change in crack tip strains due to application of the patch. The strains are taken at the closest integration points to the crack tip, 0.18 mm away. The results show a decrease in strains on the patched face of the plate, and very little change in the strains on the unpatched face. According to the figure, yielding occurs through most of the plate thickness at the crack tip of the patched element.

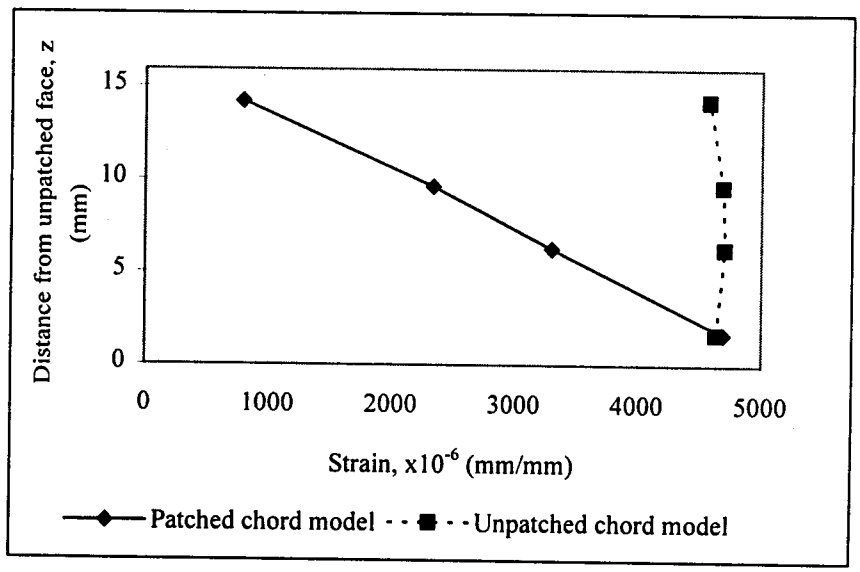

Figure 6.6 Strain distribution at the crack tip of the chord model

Figure 6.7 shows the strain distributions along the horizontal and vertical centerlines of the model plate, which correspond to the axis of the crack and the axis perpendicular to the crack through its center respectively. The results are typical of those discussed in

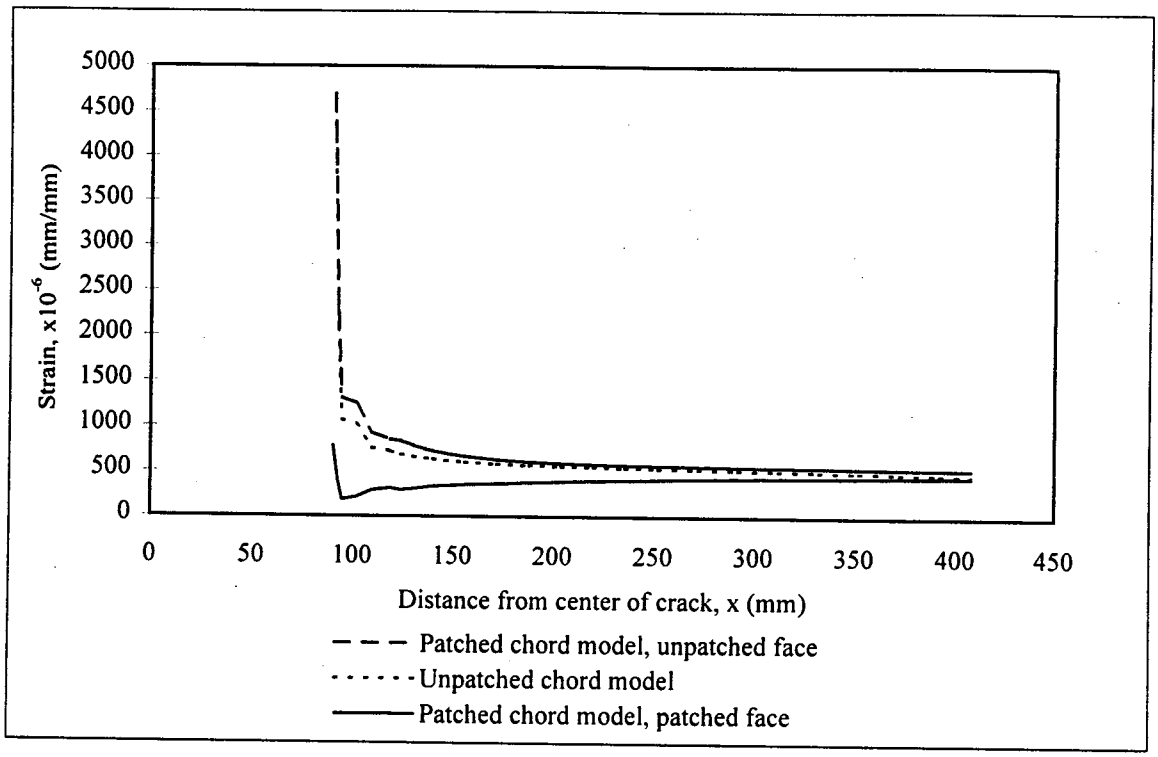

(a) Strain distribution across horizontal centerline, the axis of the crack

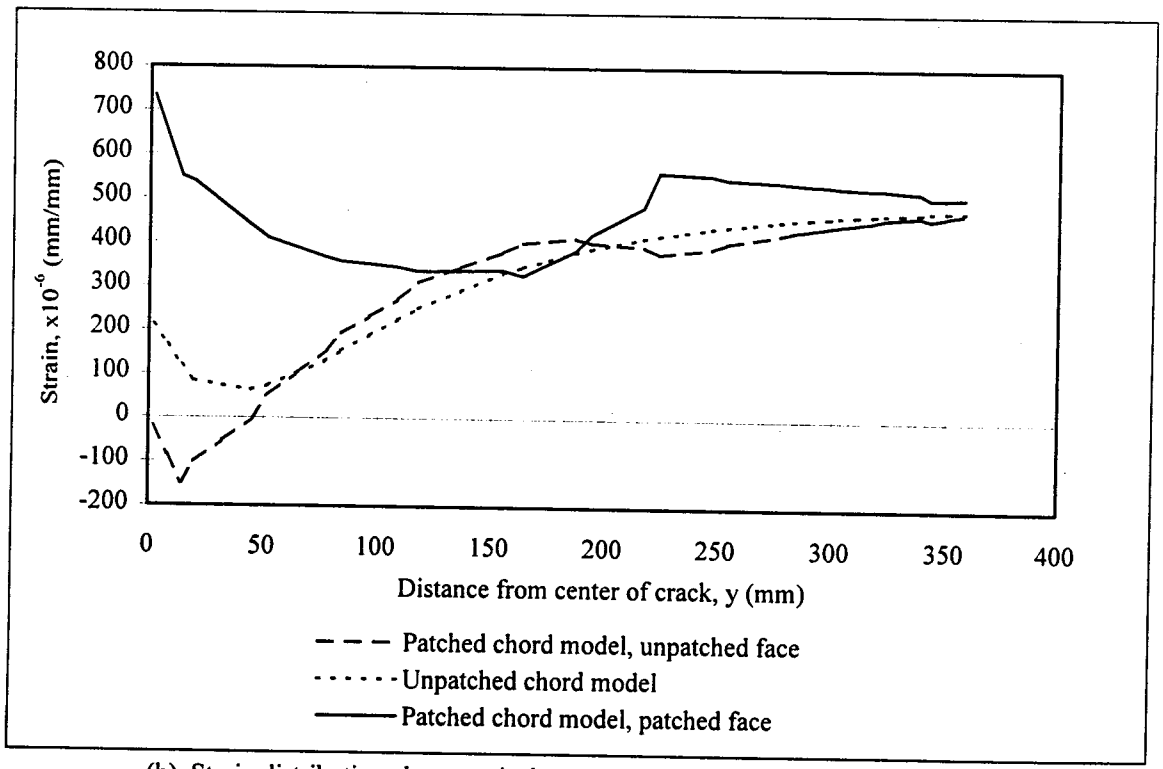

(b) Strain distribution along vertical centerline, perpendicular to the axis of the crack

Figure 6.7 Strain distributions along the horizontal and vertical centerlines of the chord model

sections 4.2 and 4.4. The stress concentration factor was 1.152 at the plate centerline, although this result is 3.4 mm from the end of the patch and is believed to severely underestimate the actual value.

The model is intended to give an approximation of the patching effects only; there were some assumptions made in the determination of the results. First, the boundary conditions of the model hold the patched face of the steel shut regardless of the patch stiffness or applied load. This likely results in low estimates of crack tip stresses on the patched face, and may cause an increase in local bending around the crack tip. Second, the model considers elastic behaviour only. From the strain results through the entire plate, this is only expected to affect the behaviour at the crack tip, where strains exceed the yield strain of the steel before and after patching. Finally, the model allows unrestrained bending in the out-of plane direction. Section 4.3.4 suggests the model underestimates out-of-plane bending in the bonded plates tested, which may also be the case here. Alternatively, because the chord members are tubes, they may provide internal support against out-of-plane bending and the model may overestimate the actual bending in the chord. Bending in the model is especially apparent in Figure 6.7(b) near the ends of the patch, where strains in the unpatched face exceed those in the patched face. This bending is a product of the eccentricity of the applied load and the reaction force on the patched cross-section.

6.5 References

Barsom, John M., and Stanley T. Rolfe. 1987. Fracture and Fatigue Control in Structures. Prentice-Hall, Inc., New Jersey.

CAN/CSA Standard S16.1-94. 1994. Limit States Design of Steel Structures. Canadian Standards Association, Ontario, Canada.

Carroll, Mal. 1997. "*Mining Equipment Monitoring at Syncrude.*" 7th Canadian Symposium on Mining Automation, pp. 169-193.

7 SUMMARY, CONCLUSIONS, AND RECOMMENDATIONS

7.1 Summary

Experimental and numerical testing was used to study the effects of a bonded, one-sided composite patch repair on the flow of load through a steel plate with an internal, through-thickness crack.

The first objective of the program was to determine the changes in strain distribution that occur when a bonded patch is applied to one face of a cracked plate subjected to tensile loading. From these strain distributions, future study may investigate the effects of patching on crack propagation. The second objective of the program was to determine basic guidelines for patch design. The design parameters considered were patch length and width, patch stiffness, tapering of patch edges, and patch shape.

Five bonded joint specimens were tested to study the transfer of load between a steel adherend and a unidirectional carbon fibre/epoxy composite patch. Strain distributions and joint strength were analyzed to determine the effects of bond length and material properties on joint behaviour. A numerical model was developed to supplement the experimental results. A second experimental program tested ten 6.35 mm steel plates with simulated internal cracks, nine of which were patched on one side with carbon fibre/epoxy composite patches of varying size, thickness, and edge conditions. A three-dimensional, elastic numerical model representative of the test plates was developed and the results compared with the experimental findings. The model was then used to conduct a parametric study of the effects of patch design parameters on stress concentrations in the steel at the crack tip and at the patch edge. This lead to the development of patch design guidelines, which were applied to a case study as an example.

7.2 Conclusions

With respect to strain distribution in a patched plate:

1. On the patched face of a cracked steel element, load flows through the patch across the crack and transfers quickly back into the steel. Through the thickness of the element, load must flow around the crack, then gradually back towards the plate center, so that load flow in the unpatched face is much the same after patching as before.

2. One-sided patching decreases crack tip strains significantly in the patched face, and increases them slightly in the unpatched face. The decrease in strains is largely a result of the crack being held shut and of the increased stiffness of the area. Bending due to asymmetry of the patched element causes additional reduction of strains in the patched face of the plate, and is responsible for the increased strains in the unpatched face.

3. Compared with an unpatched plate, the strain distribution for a patched plate through the center of the plate thickness along an axis parallel and close to the axis of an internal crack shows lower extremes and smoother gradients – strains near the centerline of the crack are higher, and near the crack tip are lower. Loads are also drawn back to the low strain area around the crack centerline more quickly in a patched plate. These two factors enable constant stress distribution across the width of the patched plate to be re-established in a shorter distance than for an unpatched plate.

With respect to guidelines for patch design:

4. The minimum patch length is governed by two factors. First, a sufficient bond length must be provided so the load carried across the crack by the patch may be transferred to the steel and a level of strain compatibility between the patch and adherend established. This is required to maximize the strength of the bond, and to minimize

stress concentrations in the steel at the edge of the patch. Second, sufficient length must be provided for the high stress at the crack tip to redistribute across the plate width. This is required to minimize the peak stress concentration in the steel at the patch edge.

5. Patch width has little effect on strain distribution in the plate; therefore, until fatigue test results are available, patch width is governed by crack length. The patch should be as wide as the crack being repaired, but should not exceed the width the crack may safely be allowed to grow to before further action must be taken. The latter requirement may be relaxed if means of monitoring crack growth beneath the patch are in place.

6. Higher stiffness patches reduce crack tip stresses while lower stiffness patches reduce stress concentrations in the steel at the patch edge. Fatigue test results are required to determine patch stiffness design guidelines.
   - A patch with a material of lower elastic modulus under a material of higher elastic modulus may provide necessary stiffness for crack repair while reducing stress concentrations in the steel at the patch edge. This is accomplished by slowing the rate of load transfer from patch to adherend. The lower modulus material may be a thick adhesive layer or a lower stiffness composite such as glass fibre/epoxy.

7. Tapering the patch edge can greatly reduce the stress concentration in the steel at the edge of the patch. Sufficient taper length should be provided to allow strain compatibility between the adherend and the patch to be re-established after each taper step.

8. The use of an elliptical patch in place of a rectangular one has little effect on stress concentrations in the steel at the patch edge or the crack tip.

7.3 Recommendations

To determine the effectiveness of composite patching for the repair of fatigue cracks in steel elements, and to further develop guidelines for patch design:

1. Fatigue testing and fracture mechanics analysis should be performed to study the effect of one-sided patching on crack propagation. This analysis should consider the effects of yielding at the crack tip on the through-thickness strain distribution. Patch width and stiffness requirements may be derived from fatigue test results.

2. Fatigue testing and fracture mechanics analysis should be performed to study the potential for crack formation in the base metal at the patch edge as a result of stress concentrations introduced by patching. Consideration should be given to the use of elliptical patches in place of rectangular ones as they may provide a stress concentration profile that is less prone to crack initiation.

Towards optimization of patch design and improved field applications and monitoring:

3. The use of alternative patching materials, or combinations of materials, should be considered as a means of providing effective crack repair while minimizing stress concentrations in the steel at the patch edge. This study should consider bonded steel patches, hybrid patches, and patches with varying fibre orientations.

4. Durability of patch repairs should be studied, including the potential for corrosion in the base metal and bond durability under harsh environmental conditions.

5. Methods of monitoring of crack growth beneath a patch should be considered.

APPENDIX A – CORRECTION OF EXPERIMENTAL RESULTS, BONDED PATCH TESTS

A.1 Unpatched Plate

An unpatched cross-section is symmetrical; therefore, strain due to uniform applied tensile stress is constant through the plate thickness at any point away from the crack (neglecting any shear lag). Also because of symmetry, bending stresses on the plate faces are equal and opposite. As a result, the average of strains on the front and back faces of the plate at any location equals the value of the pure tensile strain at that point. This is illustrated in Figure A.1.

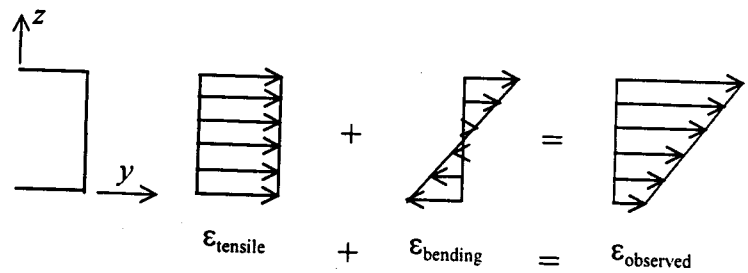

Figure A.1 Tensile and bending strains in an unpatched test plate

Because the plate was not restrained out-of-plane, the bending is believed to be about an axis parallel to the horizontal (x) axis. If this is the case, the bending stresses at a given vertical (y-coordinate) location are constant across the width of the plate, i.e. for any x-coordinate location. The one exception is the region immediately surrounding the crack, where the influence of the crack on bending is not known.

For each experimental test, a pair of gauges was mounted on opposite faces of the plate at the same coordinate location, always along the horizontal centerline (x-axis). For the unpatched plate, readings from the two gauges were averaged for each loading increment to determine the average tensile strain at the given coordinate location.

For gauges along the horizontal centerline, the absolute difference between the average strain and the strain at the front or back is the magnitude of the correction factor. For a gauge on the front face of the specimen, the correction is added to the gauge reading; for a gauge on the back face of the specimen, the correction is subtracted from the gauge reading.

The induced moment is a function of the out-of-plane displacement of the plate at any location. If the displaced shape of the plate can be approximated by a quadratic function,

$$z(y) = ay^2 + by + c \qquad [A.1]$$

and the boundary conditions are

$$z'(0) = 0$$
$$z(350) = 0$$

then

$$z(0) = c$$

which is the displacement from plane of the horizontal centerline. Applying the boundary conditions,

$$z(y) = c\left(1 - \left(\frac{y}{350}\right)^2\right) \qquad [A.2]$$

The moment at any location y is equal to the moment at the plate horizontal centerline, y=0, multiplied by a scale factor, s.f.. This scale factor is the ratio of the displacement at y to the displacement at the horizontal centerline:

$$s.f. = \frac{z(y)}{z(0)} = \frac{z(y)}{c}$$

$$s.f. = 1 - \left(\frac{y}{350}\right)^2 \qquad [A.3]$$

Thus the correction for the unpatched plate is calculated from the average strain as discussed above, and the scale factor is calculated at each gauge location. The product of the correction and the scale factor is then added to or subtracted from the original gauge readings.

A.2 Patched Plates

In the unpatched test specimen, the only bending was due to the plates not being initially flat; this is referred to as M_1 moment. Patched specimens, however, are subjected to additional moment, M_2, due to the asymmetry of the patched cross-section. M_1 effects should be removed while retaining M_2 effects.

M_1 moments are due to plate out-of-straightness and increase at initial loading but approach a constant value as the plate approaches plane. M_2 moments are a function of the applied load and constant plate parameters and will continue to increase proportionally with the applied load. Figure A.2 illustrates the theoretical effects of these relationships on the overall bending moments in the patched element.

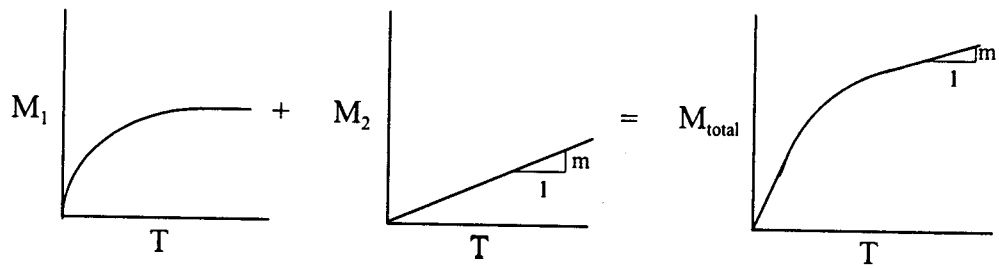

Figure A.2 Relationship between applied load and M_1 and M_2 moments

As for the unpatched plate, two gauges were mounted at the same coordinate location on opposite faces of each patched test plate. The magnitude of the moment in a cross-section is directly proportional to the difference in the strains on opposite faces of the plate, assuming a linear strain distribution. Plots of this difference in strain versus applied load are shown in Figure A.3 for patched and unpatched tests at 100 MPa far field applied load. Note the unpatched test appeared to exhibit only M_1 moments while the patched test, in this case R324, exhibited M_1 and M_2 bending.

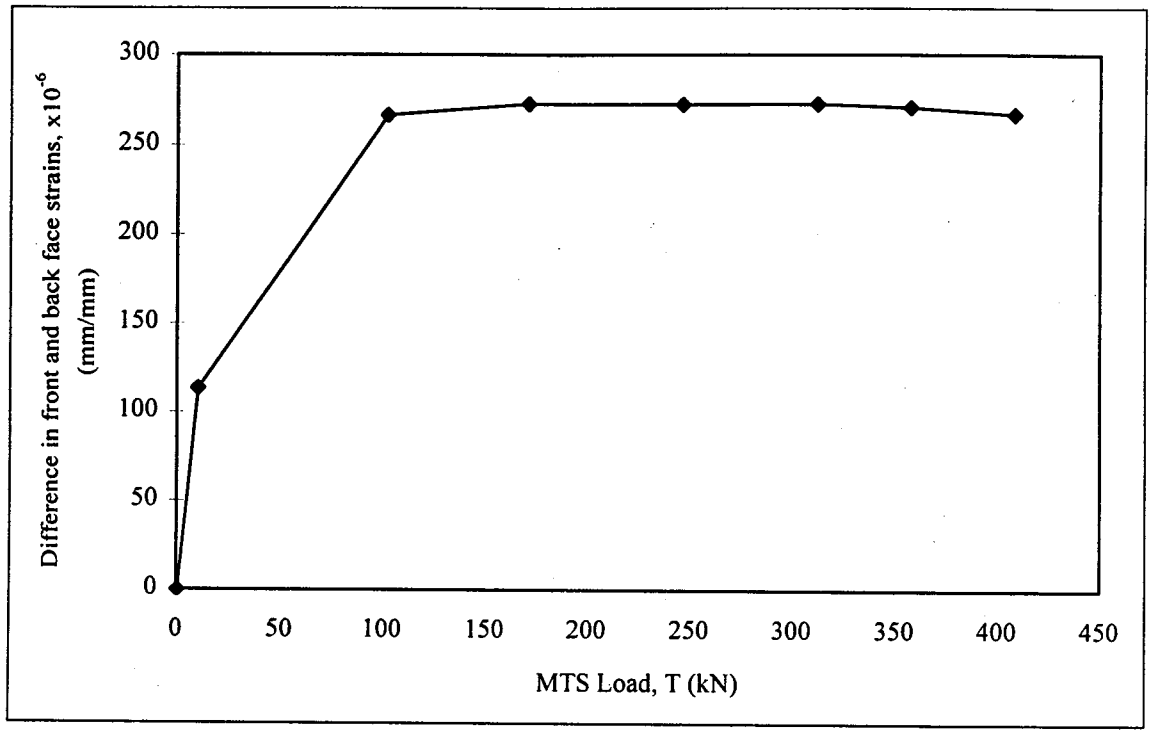

(a) Unpatched plate

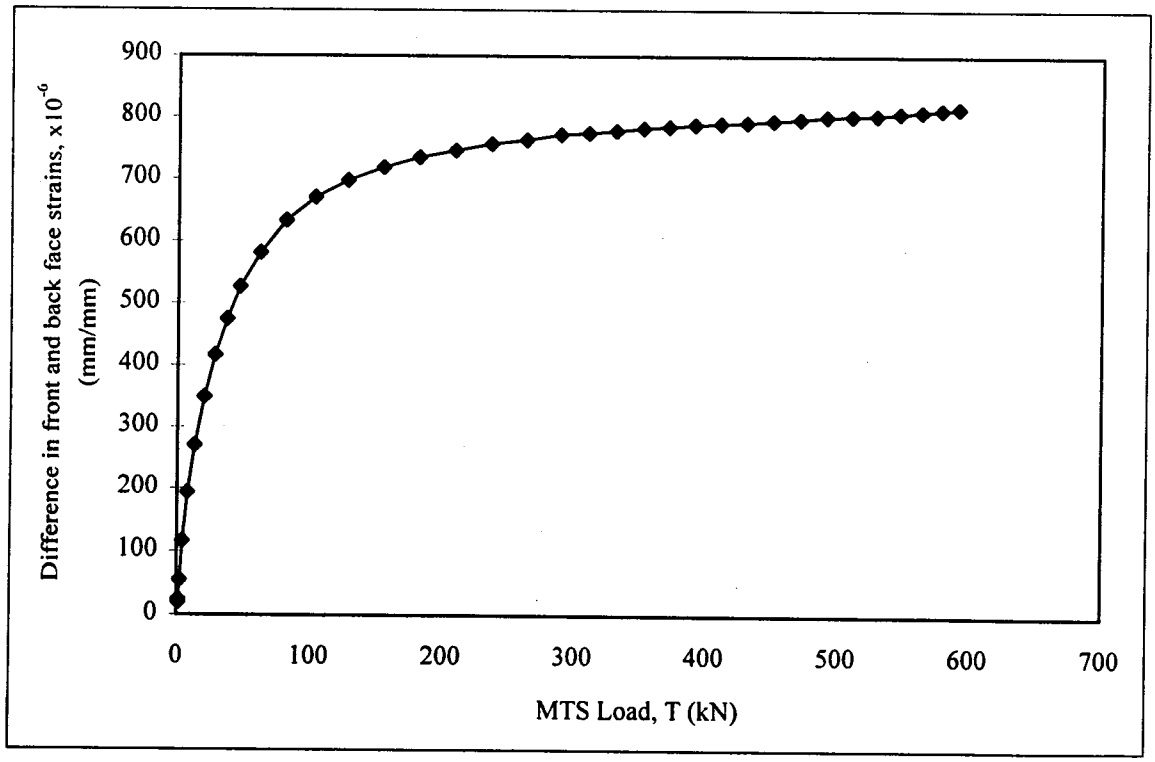

(b) Patched plate, test R324

Figure A.3 Difference in front and back face strains as a function of applied load

In order to remove only the M_1 bending strains from the test data, the effects of the two bending sources must be isolated. From Figure A.2, the slope of the final linear portion of the overall bending curve is approximately equal the slope of the M_2 curve. The corrected difference (c.d.), the portion due to M_1 bending, is then

$$c.d. = (\varepsilon_{back} - \varepsilon_{front})_{M_1} = (\varepsilon_{back} - \varepsilon_{front}) - mT \qquad [A.4]$$

where ε_{back} = strain reading from the back face gauge

ε_{front} = strain reading from the front face gauge

m = slope of the difference in strain versus applied load plot (1/kN)

T = applied tensile load (kN).

Figure A.4 shows the relationship between the corrected difference and the applied tensile load, which appears to be the same shape as the M_1 curve in Figure A.2. Results of test R324 has been used as an example.

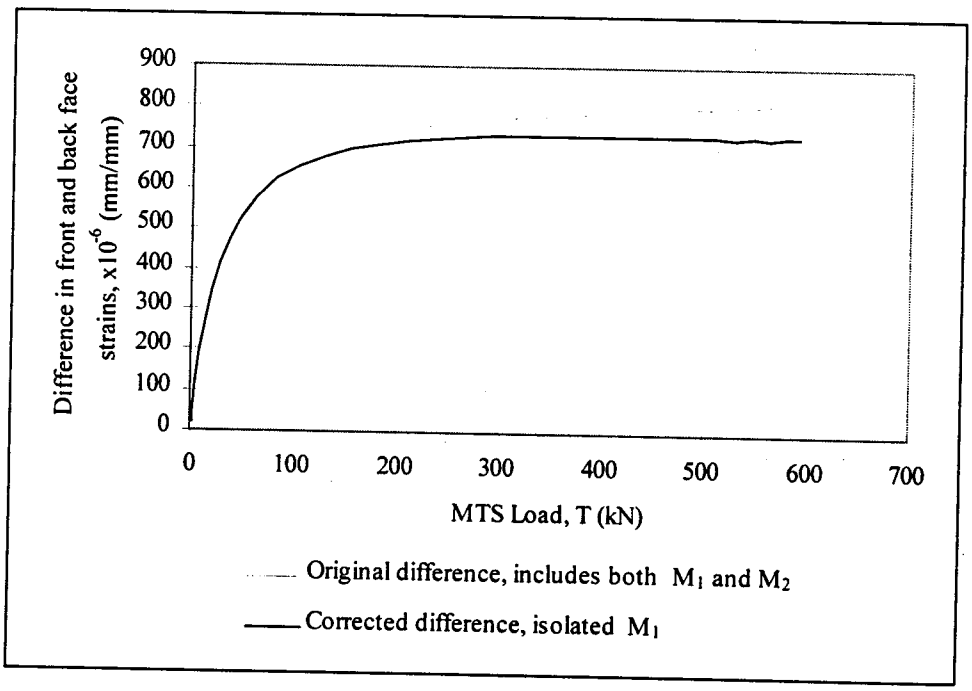

Figure A.4 Corrected difference in strains to isolate effects of M_1 moments

Finally, the value of the correction for front and back strain gauge readings is determined. Since the pair of gauges was located in the far field stress range, it is assumed that the tensile strain at that location is equal to the far field applied strain:

$$\varepsilon_{tensile} = \frac{1000T}{A_g E_s} \qquad [A.5]$$

where A_g = gross area of the steel plate (mm^2)

E_s = Young's Modulus for steel, assumed 200 000 MPa.

The corrected strain distribution remains linear and has the same neutral axis as the overall strain measurement; therefore,

$$\frac{\varepsilon_{tensile} - \varepsilon_{front}}{\varepsilon_{back} - \varepsilon_{tensile}} = \frac{\varepsilon_{fc}}{\varepsilon_{bc}}. \qquad [A.6]$$

If

$$\varepsilon_{fc} + \varepsilon_{bc} = c.d. \qquad [A.7]$$

Then rearranging [A.6] and combining with [A.7],

$$\varepsilon_{fc} = \frac{c.d.}{1 + \frac{\varepsilon_{back} - \varepsilon_{tensile}}{\varepsilon_{tensile} - \varepsilon_{front}}} \qquad [A.8]$$

$$\varepsilon_{bc} = c.d. - \varepsilon_{fc} \qquad [A.9]$$

where ε_{fc} = correction to be applied to front strain gauges

ε_{bc} = correction to be applied to back strain gauges.

Again the front correction is added to the gauge reading, while the back correction is subtracted.

Three deficiencies exist within this correction scheme. First, there is uncertainty in the quantification of behaviour near the crack for both patched and unpatched plates. The moment of inertia of the cross-section is different at the crack than other areas of the plate, and the free surface of the steel at the crack is unable to sustain any bending stresses. The region of these influences could not be defined using the data available.

The second deficiency is the assumption that all front gauges are the same distance from the neutral axis. This is not the case for patched elements with gauges being on the patch, the tapered edges, the epoxy surrounding the patch, or the steel. Because it is difficult to determine the exact location of the neutral axis, and to quantify the exact distance of each gauge from the axis, these effects were not incorporated.

Finally, for patched elements, the relationship between M_2 moments and applied load was approximated as linear. These moments are a product of the applied load acting along the neutral axis of the plate, eccentric to the neutral axis of the patched cross-section. In reality, M_2 moments tends to bend the plate so that the eccentricity of the axes is reduced, and the relationship between the applied load and the induced moment should show a decreasing slope, similar to that of M_1 moments as the plate is straightened. The magnitude of M_2 moments was found to be small, since the eccentricity causing the bending is small, relative to both M_1 moments and the stiffness of the cross-section. The approximation of the relationship as linear is therefore believed to be acceptable for low loads as are being considered here.

Recent Structural Engineering Reports

Department of Civil & Environmental Engineering

University of Alberta

195. *Some Behavioural Aspects of Composite Trusses* by Berhanu Woldegiorgis and D.J. Laurie Kennedy, January 1994.

196. *Flexural Behavior of High Strength Concrete Columns* by Hisham H.H. Ibrahim and James G. MacGregor, March 1994.

197. *Prediction of Wrinkling Behavior of Girth-Welded Line Pipe* by Luis T. Souza, Alaa E. Elwi, and David W. Murray, April 1994.

198. *Assessment of Concrete Strength in Existing Structures* by F. Michael Bartlett and James G. MacGregor, May 1994.

199. *The Flexural Creep Behavior of OSB Panels Under Various Climatic Conditions* by Naiwen Zhao, J.J. Roger Cheng, and Lars Bach, June 1994.

200. *High Performance Concrete Under High Sustained Compressive Stresses* by Said Iravani and James G. MacGregor, June 1994.

201. *Strength and Installation Characteristics of Tension–Control Bolts* by Scott T. Undershute and Geoffrey L. Kulak, August 1994.

202. *Deformational Behavior of Line Pipe* by Magdi Mohareb, Alaa E. Elwi, Geoffrey L. Kulak and David W. Murray, September 1994.

203. *Behavior of Girth-Welded Line Pipe* by Nader Yoosef-Ghodsi, Geoffrey L. Kulak and David W. Murray, September 1994.

204. *Numerical Investigation of Eccentrically Loaded Tied High Strength Concrete Columns* by Jueren Xie, Alaa E. Elwi, and James G. MacGregor, October 1994.

205. *Shear Strengthening of Concrete Girders Using Carbon Fibre Reinforced Plastic Sheets* by Efrosini H. Drimoussis and J.J. Roger Cheng, October 1994.

206. *Shrinkage and Flexural Tests of a Full-Scale Composite Truss* by Michael B. Maurer and D.J. Laurie Kennedy, December 1994.

207. *Analytical Investigation of the Compressive Behavior and Strength of Steel Gusset Plate Connections* by Michael C.H. Yam and J.J. Roger Cheng, December 1994.

208. *The Effect of Tension Flange Movement on the Strength of Point Loaded I-Beams* by Dean Mullin and J.J. Roger Cheng, January 1995.

209. *Experimental Study of Transversely Loaded Continuous Steel Plates* by Kurt P. Ratzlaff and D.J. Laurie Kennedy, May 1995.

210. *Fatigue Tests of Riveted Bridge Girders* by Daniel Adamson and Geoffrey L. Kulak, July 1995.

211. *Fatigue of Riveted Tension Members* by Jeffery DiBattista and Geoffrey L. Kulak, November 1995.

212. *Behaviour of Masonry Cavity Walls Subjected to Vertical Eccentric Loads* by Ru Wang, Alaa E. Elwi, Michael A. Hatzinikolas and Joseph Warwaruk, February 1996.

213. *Thermal Ice Loads on Structures* by Azita Azarnejad and Terry M. Hrudey, November 1996.

214. *Transmission of High Strength Concrete Column Loads Through Concrete Slabs* by Carlos E. Ospina and Scott D.B. Alexander, January 1997.

215. *Seismic Behaviour of Steel Plate Shear Walls* by Robert G. Driver, Geoffrey L. Kulak, D.J. Laurie Kennedy and Alaa E. Elwi, February 1997.

216. *Extended End Plate Moment Connections under Cyclic Loading* by Bryan T. Adey, Gilbert Y. Grondin and J.J. Roger Cheng, June 1997.

217. *Connection on Infill Panels in Steel Plate Shear Walls* by A. Schumacher, Gilbert Y. Grondin and Geoffrey L. Kulak, August 1997.

218. *Shear Rehabilitation of G-Girder Bridges using CFRP Sheets* by John G.S. Alexander and J.J. Roger Cheng, October 1997.

219. *Seismic Evaluation of Steel Buildings with Concentrically Braced Frames* by Manoj S. Medhekar and D.J. Laurie Kennedy, October 1997.

220. *Rational Design of Prestressed and Reinforced Concrete Tanks* by Abdelaziz A. Rashed, David M. Rogowsky and Alaa E. Elwi, December 1997.

221. *Repair of Cracked Steel Elements using Composite Fibre Patching* by Gaylene D. Kennedy and J.J. Roger Cheng, May 1998.